UNIVERSITY OF STRATHCLYDE

Department of Biomedical engineering


# Combining a microfluidic platform with LC-MS for the detection of induced hepatotoxicity using primary hepatic spheroids

Myndert P. Claasen

A thesis presented in partial fulfilment of the requirements for the degree of Doctor of Engineering

2020

# Declaration of Authorship

This thesis is the result of the author's original research. It has been composed by the author and has not been previously submitted for examination which has led to the award of a degree.



Signed:

Date: 28 / 01 / 2020

# Abstract

The success rate of bringing a new drug from conception to market is extremely low as well as time consuming and very costly. Simple sub-cellular models can provide high throughput data allowing early detection of many drugs doomed to fail, but do not encompass the complexity found in whole cell-based models, which provide more in-depth data. Cell culture models have evolved from simple 2-dimensional cultures on hard substrates i.e. plastic dishes, to 3 dimensional cultures that promote and enhance *in vivo*-like function and architecture. The liver is the main organ of interest during the drug development stages, as it is the organ that metabolizes xenobiotics. Drug metabolism entails converting a compound into a more hydrophilic state that can be actively excreted. However, the process of metabolism does sometimes result in the creation of a toxic intermediate metabolite that can lead to drug-induced liver injury. Thus to increase the efficacy of drug development the models, which are often scare and / or costly, and screening methods employed would need to be optimized. Microfluidics enables miniaturization through the control and manipulation of fluids n the nano – to millilitre range. Combining microfluidics with appropriate 2 dimensional / 3 dimensional cell culture systems can lead to higher throughput data production using far less resources compared to conventional culturing methods; and when combined with a screening modality that allows collection of detailed information it could be used to improve the efficacy of the preclinical drug-development process. One such modality is liquid chromatography-mass spectrometry. The chromatography technology allows separation of

compounds from a mixed sample based on the interactions between the compounds of interest and the mobile and stationary phase. This enables quantitative analysis based on the retention time and absorbance measured by the detector. Mass spectrometry allows identification of the chemical composition of a component based on the mass-to-charge ratio. Both technologies are highly-sensitive and specific, which is ideally suited for metabolic analysis. In this thesis the effects of a miniaturisation process on cell culture environment are investigated, specifically the effect of using far less cells to form functional, metabolically active 3-dimensional liver spheroids, compared with conventional methods. HepG2 and primary rat hepatocyte spheroids were cultured in a microfluidic platform and exposed to drugs known to induce toxicity. The cells were cultured for 4 days before being exposed to each drug for 24 hours. Half the cultures were analyzed the following day and the other half were allowed to recover for an additional 24 hours. The platforms were compared to a gold standard culture model, a collagen sandwich culture. Cell supernatant and lysate samples were analyzed using liquid chromatography-mass spectrometry. The results showed that similar data could be obtained from the microfluidic platforms compared to collagen sandwich configurations when screening phase I and phase II metabolites, using far less cells and culture media. In conclusion, metabolically active liver spheroids can be generated using far less cell than previously thought. Information about metabolism can be extracted when combining the microfluidic cell culture system with liquid chromatography-mass spectrometry

Acknowledgements

Firstly, I would like to thank the EPSRC and the Department of Biomedical engineering for providing me with this wonderful opportunity.

Many people have helped me along the way, and I would like to mention a few. For always helping me in the lab and providing me with training I am grateful to my colleagues Kay, Theresa and Graham.
I especially would like to thank Katie from the BME and Dr Watson from SIPBS for their wisdom, help and expertise.
For keeping me smiling and making the difficult times less so I want to thank my fellow EngD researchers Jon, Scot, Audrey, Pretheepan, Josh and Jacob.

I would also like to thank my family and my partner Danielle from the bottom of my heart for all their love and support during this research.

Finally, I must thank my supervisors Michele and Helen for their guidance and endless patience.

# Contents

**Declaration of Authorship** ..... **i**

**Abstract** ..... **ii**

**Contents** ..... **v**

**Figures, Tables and Equations** ..... **xi**

**Abbreviations** ..... **xv**

**Chapter 1. Thesis overview** ..... **1**

1.1 Motivation ..... 1

1.2 Aims and Objectives ..... 3

1.3 Novelty ..... 3

1.4 Thesis outline ..... 4

1.5 Presentations and publications ..... 4

**Chapter 2. Background and literature review** ..... **6**

2.1 The Human Liver ..... 6

2.1.1 The structure of the liver ..... 6

2.1.2 The cell types and functions of the liver ..... 7

2.1.3 The implications of liver-related metabolism on drug development ..... 11

2.2 Pharmaceutical industry ..... 15

2.2.1 ADME parameters ..... 16

2.2.2 *In vitro* models for drug induced toxicity ..... 18

2.2.3 Culturing hepatocytes into spheroids ..... 24

2.3 Microfluidics platforms ..... 31

2.3.1 Droplets and microwells for generating spheroids ..... 32

2.3.2 Three-dimensional liver cultures in microfluidic platforms ..... 38

2.4 Liquid chromatography-mass spectrometry ..... 48

2.4.1 Principles and fundamentals ..... 48

2.5 Three-dimensional liver cultures in microfluidic platform combined with LC-MS ..... 53

2.6 Objectives ..... 58

**Chapter 3. Methods and Materials ..... 59**

3.1 Introduction ..... 59

3.2 Device fabrication ..... 59

3.2.1 Droplet-based platform ..... 59

3.2.2 Microwell array platforms ..... 64

3.3 HepG2 and Primary Rat Hepatocyte culture ..... 66

3.3.1 HepG2 culture ..... 67

3.3.2 Perfusion and isolation of primary rat hepatocytes ..... 68

3.4 Loading and maintenance of the microfluidic platforms ..... 72

3.4.1 Droplet-based microfluidic platform (HepG2 cells only) ..... 72

3.4.2 The multi-array microfluidic platform ..... 76

3.5 Culturing of primary rat hepatocytes in a collagen sandwich configuration in 24 – and 6 well-plates ..... 78

3.6 Immunofluorescence of hepatic cultures in the microfluidic platforms and collagen sandwich configurations ..... 79

3.6.1 Hepatic spheroids..... 80

3.6.2 Collagen sandwich configurations..... 83

3.7 Induced hepatotoxicity in the microfluidic platforms and collagen sandwich configurations..... 85

3.8 Preparation of solutions for LC-MS analysis of primary rat hepatocyte supernatant and cell lysate ..... 86

3.8.1 LC-MS Solutions..... 86

3.8.2 Collection and storage of primary rat hepatocyte samples for LC-MS analysis..... 86

3.9 Separation and identification of components using LC-MS..... 90

3.9.1 Data processing..... 90

**Chapter 4. Cultured HepG2 and Primary rat hepatocytes in the microfluidic platform and the collagen sandwich configuration. ..... 92**

4.1 Preliminary results of culturing HepG2 cells in a droplet-based microfluidic platform ..... 92

4.1.1 Cellular aggregation and spheroid formation ..... 94

4.1.2 Diclofenac induced hepatotoxicity in HepG2 spheroids in the microfluidic platforms..... 100

4.2 Results of culturing primary rat hepatocytes ..... 104

4.2.1 Preliminary results of the primary rat hepatocytes cultured in the microfluidic platforms and on the collagen sandwich configurations ... 105

4.2.2 Viability of primary rat hepatocytes cultured in the microfluidic platform ..... 108

4.2.3 Induced hepatotoxicity in primary rat hepatocytes cultured in the collagen sandwich configuration versus the microfluidic platform ..... 110

4.2.4 Viability of the single array microfluidic platform after Diclofenac exposure ..... 123

4.3 Discussion and conclusion on the droplet-based vs multi-array platforms using the HepG2 cell line ..... 126

4.3.1 Platform operation and maintenance ..... 126

4.3.2 Culturing HepG2 spheroids in the droplet-based and multi-array microfluidic platforms ..... 127

4.3.3 Conclusion ..... 129

4.4 Discussion of primary rat hepatocytes toxicity experiments ..... 130

4.4.1 Functional assessment of microfluidic platform ..... 131

4.4.2 Drug-induced toxicity in collagen sandwich configuration versus the microfluidic platform ..... 132

4.4.3 Toxicity of the Phase I metabolite, Hydroxy-diclofenac ..... 138

4.4.4 Drug-induced toxicity of primary rat hepatocytes in the single array platform ..... 138

**Chapter 5. Liquid chromatography-mass spectroscopy analysis of primary rat hepatocytes cultured in the microfluidic platform ..... 140**

5.1 Introduction – detection of metabolites ..... 140

5.2 LC-MS experiment results ..... 143

5.2.1 LC-MS raw data ..... 144

5.2.2 Collagen sandwich configuration vs Microfluidic Platform ..... 146

5.2.3 Single array platform ..... 164

5.3 Discussion ..... 168

5.3.1 Drug metabolism ..... 168

5.3.2 Single array platform ..... 174

5.3.3 Sample preparation and LC-MS considerations ..... 176

**Chapter 6. Conclusion for the use of microfluidics and LC-MS for detection of drug induced hepatotoxicity ..... 179**

6.1 Introduction ..... 179

6.2 HepG2 spheroids in a microfluidic platform ..... 179

6.3 Drug-induced response in primary hepatic spheroids and a collagen sandwich configuration ..... 181

6.4 Intra- and extracellular metabolic analysis of primary hepatic spheroids and collagen sandwich configurations using LC-MS ..... 183

6.5 Conclusions ..... 185

6.6 Future work ..... 188

**References..... 189**

**Appendix..... 211**

Reagents and Equipment ..... 211

Chemicals and reagents..... 211

Equipment ..... 213

LC-MS representative figures ..... 214

# Figures, Tables and Equations


| | | |
|---|---|---|
| Figure 2.1 | The micro-architecture of the liver | 7 |
| Figure 2.2 (a and b) | The metabolic pathway of paracetamol at therapeutic and supratherapeutic concentrations | 13-14 |
| Figure 2.3 | The drug development pipeline | 16 |
| Figure 2.4 | A sandwich configuration | 21 |
| Figure 2.5 | Regenemed co-culture trans-well system | 22 |
| Figure 2.6 | C3A spheroids generated using different starting cell numbers | 26 |
| Figure 2.7 | CYP450 activity of hepatocytes in 2D sandwich cultures vs spheroids | 28 |
| Figure 2.8 | Diagram of a hanging drop system | 30 |
| Figure 2.9 | T-junction used to generate droplets | 33 |
| Figure 2.10 | Flow focusing junction to generate droplets | 34 |
| Figure 2.11 | Droplet storage and coalescence | 35 |
| Figure 2.12 | Microwell-based microfluidic platform | 38 |
| Figure 2.13 | Droplet-based production of collagen particles | 40 |
| Figure 2.14 | Hepatic "pucks" cultured on collagen islands | 41 |
| Figure 2.15 | Co-cultured Hepatocytes and Stellate cells in microwells | 42 |
| Figure 2.16 | Co-cultured Hepatocytes and Stellate cells in separated compartments | 44 |
| Figure 2.17 | Microfluidic platform with gradient generator | 45 |
| Figure 2.18 | Microfluidic platform simulating the endothelial barrier | 46 |
| Figure 2.19 | Diagram of the components in HPLC | 49 |
| Figure 2.20 | Diagram of the components in an Orbitrap mass analyzer | 53 |
| Figure 2.21 | Microfluidic platform with cells in layers | 54 |
| Figure 2.22 | Hepatic spheroids constrained between a glass slide and a porous membrane | 56 |
| Figure 2.23 | Graph of the formation of OH-chlorzoxazone | 57 |
| Figure 3.1 | Diagram of the droplet-based platform | 60 |
| Figure 3.2 | Diagram of the fabrication process | 63 |
| Figure 3.3 | Diagram of the multi-array platform | 65 |
| Figure 3.4 | Diagram of the single array platform | 66 |
| Figure 3.5 | Equipment used during isolation of rat hepatocytes | 70 |
| Figure 3.6 | Sequential trapping of droplets | 73 |
| Figure 3.7 | HepG2 cells in droplets | 74 |
| Figure 3.8 | Diagram of trapping cells using the multi-array platform | 75 |
| Figure 3.9 | Segmented image of interface used to monitor spheroids | 80 |
| Figure 3.10 | Brightfield, FDA / PI image of hepatic spheroid | 81 |

| | | |
|---|---|---|
| Figure 3.11 | Timeline of experimental protocol | 88 |
| Figure 4.1 | HepG2 spheroids development in droplet | 94 |
| Figure 4.2 | Graph of the change in mean area of HepG2 spheroids in the droplet-based platform during culture | 95 |
| Figure 4.3 | Viability of HepG2 spheroids in the droplet-based platform after 9 days in vitro | 95 |
| Figure 4.4 | Aggregation and spheroid formation of HepG2 cells in the multi-array platform | 97 |
| Figure 4.5 | Size distribution of HepG2 spheroids in the multi-array platform | 97 |
| Figure 4.6 | Mean starting cell number versus area of HepG2 cells in the multi-array platform | 98 |
| Figure 4.7 | Graph of the change in mean area of HepG2 spheroids in the multi-array platform during culture | 99 |
| Figure 4.8 | HepG2 spheroids after drug exposure | 100 |
| Figure 4.9 | Mean viable fraction of HepG2 spheroids after drug exposure | 102 |
| Figure 4.10 | Primary rat hepatocytes in multi-array platform | 105 |
| Figure 4.11 | Seeding density of primary rat hepatocytes in multi-array | 106 |
| Figure 4.12 | Primary rat hepatocytes cultured in a collagen sandwich configuration | 107 |
| Figure 4.13 | Mean viable fraction of primary rat spheroids during culture | 108 |
| Figure 4.14 | ZO-1 staining of hepatic spheroid | 109 |
| Figure 4.15 | Primary rat hepatocytes in a collagen sandwich configuration after drug exposure | 111 |
| Figure 4.16 | Primary rat spheroids after drug exposure | 112 |
| Figure 4.17 (a and b) | Viability after Diclofenac exposure | 113 |
| Figure 4.18 | Primary rat spheroids after Hydroxydiclofenac exposure | 115 |
| Figure 4.19 | Normalised viability after Hydroxydiclofenac exposure | 116 |
| Figure 4.20 (a and b) | Viability after Paracetamol exposure | 118 |
| Figure 4.21 (a and b) | Normalised viability after Diclofenac exposure | 120 |
| Figure 4.22 (a and b) | Normalised viability after Paracetamol exposure | 121 |
| Figure 4.23 | Variable viability between neighbouring spheroids | 122 |
| Figure 4.24 | Viability after Diclofenac exposure in the single array platform | 123 |
| Figure 4.25 | Viable fraction of single array platform | 124 |
| Figure 5.1 | Diclofenac and metabolites | 141 |
| Figure 5.2 | Paracetamol and metabolites | 142 |

| | | |
|---|---|---|
| Figure 5.3 | Total ion chromatogram and mass spectra of Diclofenac | 144 |
| Figure 5.4 | Concentration of Diclofenac detected | 146 |
| Figure 5.5 | Relative abundance of Hydroxydiclofenac detected | 147 |
| Figure 5.6 | Relative abundance of Acryl Glucuronide Diclofenac detected | 148 |
| Figure 5.7 | Concentration of Diclofenac detected in cell lysate | 150 |
| Figure 5.8 | Relative abundance of Hydroxydiclofenac detected in cell lysate | 151 |
| Figure 5.9 | Relative abundance of Acryl Glucuronide Diclofenac detected in cell lysate | 152 |
| Figure 5.10 | Concentration of Paracetamol detected | 153 |
| Figure 5.11 | Relative abundance of Sulfated Paracetamol detected | 154 |
| Figure 5.12 | Relative abundance of Glucuronidated Paracetamol detected | 155 |
| Figure 5.13 | Relative abundance of GSH conjugated metabolite detected | 156 |
| Figure 5.14 | Concentration of Paracetamol detected in cell lysate | 157 |
| Figure 5.15 | Relative abundance of Sulfated Paracetamol detected in cell lysate | 158 |
| Figure 5.16 | Relative abundance of Glucuronidated Paracetamol detected in cell lysate | 159 |
| Figure 5.17 | Relative abundance of GSH conjugated metabolite detected in cell lysate | 160 |
| Figure 5.18 | Concentration of Paracetamol detected after 48 hours | 161 |
| Figure 5.19 | Relative abundance of Sulfated Paracetamol detected after 48 hours | 162 |
| Figure 5.20 | Relative abundance of Glucuronidated Paracetamol detected after 48 hours | 163 |
| Figure 5.21 | Concentration of Diclofenac detected in single array platform | 164 |
| Figure 5.22 (a and b) | Relative abundance of Hydroxy diclofenac and Acyl Glucuronide detected in single array platform | 165-166 |
| Figure A.1 | LC-MS (TIC and mass spectra) of APAP-SULF | 213 |
| Figure A.2 | LC-MS (TIC and mass spectra) of APAP-GLUC | 214 |
| Figure A.3 | LC-MS (TIC and mass spectra) of APAP-GSH | 215 |
| Figure A.4 | LC-MS (TIC and mass spectra) of APAP and metabolites | 216 |

| | | |
|---|---|---|
| Table 2.1 | Liver models for toxicity detection | 24 |
| Table 2.2 | Droplet and microwell based microfluidic platforms | 47 |
| Table 5.1 | m/z ratios for compounds and metabolites | 143 |

| | | |
|---|---|---|
| Equation 2.1 | The oxidative reaction equation | 10 |
| Equation 2.2 | GHS conjugation equation | 11 |

| | | |
|---|---|---|
| Equation 2.3 | The Reynolds number | 31 |
| Equation 2.4 | The Capillary number | 33 |
| Equation 2.5 | Calculating the fluidic resistance in a channel | 35 |
| Equation 2.6 | Calculating the hydrostatic pressure | 37 |
| Equation 3.1 | Calculating percentage viability of isolated hepatocytes | 71 |
| Equation 3.2 | Calculating the number of viable isolated hepatocytes | 71 |
| Equation 3.3 | Calculating the viable fraction | 79 |
| Equation 3.4 | Calculating the mean viable fraction | 82 |
| Equation 3.5 | Calculating the viable ratio | 83 |
| Equation 3.6 | Calculating the normalised viability | 84 |
| Equation 4.1 | The 4-PL model | 128 |
| Equation 5.1 | Ion intensity ratio | 145 |
| Equation 5.2 | Relative abundance | 145 |

# Abbreviations

| | |
|---|---|
| ADME | Absorption, Distribution, Metabolism and Excretion |
| AGDIC | Diclofenac acyl glucuronide |
| APAP | Paracetamol (Acetaminophen) |
| APAP-GLUC | Paracetamol-glucuronide |
| APAP-GSH | Paracetamol-glutathione |
| APAP-SULF | Paracetamol-sulfate |
| CMFDA | 5-chloromethylfluorescein diacetate |
| CSC | Collagen Sandwich Configuration |
| CYP450 | Cytochrome P450 |
| dH2O | De-ionised water |
| DIC | Diclofenac |
| DILI | Drug-Induced Liver Injury |
| DMEM | Dulbecco’s Modified Eagle Medium |
| DMSO | Dimethyl sulfoxide |
| ECM | Extra-cellular Matrix |
| FBS | Foetal Bovine Serum |
| FDA | Fluorescein diacetate |
| GSH | Glutathione |
| ITS | Insulin-transferrin-selenium solution |
| KA | Krebs-Albumin buffer |
| KH | Krebs-HEPES buffer |
| LC | Liquid Chromatography |
| LDH | Lactate Dehydrogenase |

| | |
|---|---|
| LSECs | Liver Sinusoidal Endothelial Cells |
| m/z | Mass-to-charge ratio |
| MFP | Microfluidic Platform |
| MRP | Multidrug resistance protein |
| MS | Mass Spectrometry |
| NADPH | Dihydro-nicotinamide-adenine Dinucleotide Phosphate |
| NAPQI | N-acetyl-p-benzoquinone imine |
| NDE | New Drug Entity |
| NEAA | Non-essential amino acids |
| NPCs | Non-parenchymal Cells |
| OHDIC | ‘-Hydroxydiclofenac |
| PBS | Phosphate Buffered Saline |
| PCR | Polymerase chain reaction |
| PDMS | Poly(dimethyl siloxane) |
| PHHs | Primary Human Hepatocytes |
| PI | Propidium Iodide |
| PRHs | Primary Rat Hepatocytes |
| SULTs | Sulfotransferases |
| TIC | Total Ion Chromatogram |
| UGTs | UDP-glucuronosyltransferases |

# Chapter 1. Thesis overview

Chapter 1 briefly introduces the context and motivation behind the work presented in this thesis, followed by the aims and objectives and the structure of the thesis.

## 1.1 Motivation

The process of developing a new drug entity (NDE) for the treatment of a disease / illness is costly and time consuming, producing only low numbers of successful drug candidates that are approved for market [1] [2]. There is a large demand to develop robust *in vitro* models to test drug efficacy while reducing the number of animal-based experiments by using cultured hepatocytes. Hepatocytes are the main cells used to evaluate metabolism-related toxicity, as the liver is the primary organ responsible for first-pass drug metabolism (from drugs taken orally). Current preclinical drug screening practices provide us with valuable information, but still fail to predict many compounds that ultimately lead to drug-induced liver injury (DILI), post-market release. The limitations of current models that are used in toxicity detection may arise from multiple factors, such as lack of complexity compared to the *in vivo* situation, or limited availability of suitable *in vitro* model systems such as primary human hepatocytes (PHH) and their stability in culture, to mention a few. Many fluorescent-based screening assays rely on end-point indicators of toxicity alone [3] [4] which provide limited information on the metabolic pathway of the NDE, which is critical for our understanding of the biochemical

interactions in the cells. This provides an opportunity to explore other technologies that enable more complex models that provide better physiological relevance and in-depth analysis, while increasing throughput of information. There are many methods for prolonging the viability and function of primary cells in cultures. A widely-employed method is to sandwich cells between two layers of an extra-cellular matrix (ECM) that re-establishes an *in-vivo* like architecture. An alternative method is to allow cells to adhere to each other without an ECM, promoting the formation of spheroids or cord-like (rope-like) structures made of compacted cells. Both methods have unique advantages, as well as disadvantages when used for toxicity assays.

Microfluidics is the controlled manipulation of a fluidic environment on the millilitre to nanolitre scale, usually in an enclosed system. Applications in using microfluidic platforms for bioassays or 3D cell culture have increased as the miniaturization process can provide many advantages (e.g. reduction of resources needed to complete an experiment, high throughput potential and small footprint for ease of storage).

Liquid chromatography (LC) is a technique used to separate compounds of interest from a complex mixture using a small sample volume. Mass spectrometry (MS) is used to analyse the chemical composition of molecules, isotopes and molecular fragments by ionisation, at very high resolution.

Combining LC-MS analysis with a microfluidic platform enables large-throughput screening to be obtained using a reduced number of resources (i.e. cells and reagents) and enables the miniaturization of 3D micro-liver structures and their function to be studied. Metabolically active spheroids can act as a model of the liver and are a good candidate for increasing the physiological relevance of assays.

## 1.2 Aims and Objectives

The aim of this project was to develop:

A microfluidic platform, enabling:

a) Formation and culture of primary liver cells into 3D structures;

b) Controlled exposure of 3D cultures to a range of concentrations of drugs;

c) Analysis of the metabolizing capabilities of the 3D structures

This was combined with a screening method, allowing:

a) Extraction of individual spheroid viability data;

b) Analysis of supernatant and intra-cellular content (cell lysate) after drug exposure using LC-MS.

## 1.3 Novelty

The novelty of the research is to generate metabolically functional, 3D primary hepatic spheroids in a microfluidic format and to test their metabolic response to compounds by LC-MS, and demonstrating proof-of-concept results (of a miniaturised platform) for the analysis of metabolic activity and drug response.

The metabolites were detected using far less (a decrease of up to 50%) cells than is currently being used in literature. Results obtained showed the same metabolites could be detected in the collagen sandwich configuration and the microfluidic platforms. A further reduction in resources (using the “single array platform”) also allowed positive identification of metabolites.

## 1.4 Thesis outline

Chapter 2 presents relevant background to justify the research project, the rationale for the project, including a review of current literature. Chapter 3 presents the methods and materials employed to culture the cells into spheroids in the microfluidic platform(s) and LC-MS prep. Chapter 4 describes the preliminary results using an immortalised human hepatic cell line (HepG2) and primary rat hepatocytes in the microfluidic platform(s). Chapter 5 presents and discusses the metabolic capabilities of the cultures in the microfluidic platform(s) and the collagen sandwich configurations measured using LC-MS. Lastly, Chapter 6 presents a summary of this thesis and conclusion.

## 1.5 Presentations and publications

*Conference presentations*

09/2018 BioMedEng18 (Imperial College London, London) – “Combining a microfluidic platform with LC-MS for hepatoxicity detection” (Poster)

12/2018 Scottish Toxicology Interest Group (University of Strathclyde, Glasgow) – “Miniaturized microfluidic device for detection of Hepatocyte-induced toxicity” (Oral presentation)

*Publications*

M Claasen, M Zagnoni “Detection of induced hepatotoxicity in a single array microfluidic platform using micro-tissue structures and liquid chromatography-mass spectrometry” (in progress)

# Chapter 2. Background and literature review

## 2.1 The Human Liver

### 2.1.1 The structure of the liver

The liver is a complex, multi-cellular, multi-functional organ and one of the largest internal organs in the body [5]. The liver (Figure 2.1) is located just below the diaphragm in the abdominal cavity. It is perfused by two separate blood supplies; the portal vein, which brings de-oxygenated blood rich in nutrients from the digestive tract, the spleen and the gall bladder; and the hepatic artery, containing oxygen-rich blood from the pulmonary circulation. Branches of these two vessels, along with the bile duct, form what is known as the portal triad. The hepatic artery and portal vein divide into smaller capillaries that feed the liver sinusoid, where the de-oxygenated, nutrient-rich blood mixes with the oxygen-rich blood in an approximate 3:1 ratio [6]. The sinusoid is lined with specialized endothelial cells called liver sinusoidal endothelial cells (LSECs), which are fenestrated, through which tiny microvilli protrude from the hepatocytes which enables direct blood contact [7]. The liver acinus (smallest functioning unit of the liver) is the tissue served by a terminal branch of the hepatic artery consisting of the portal triad lined with chords of hepatocytes on either side, separated from the capillaries by the Space of Disse.

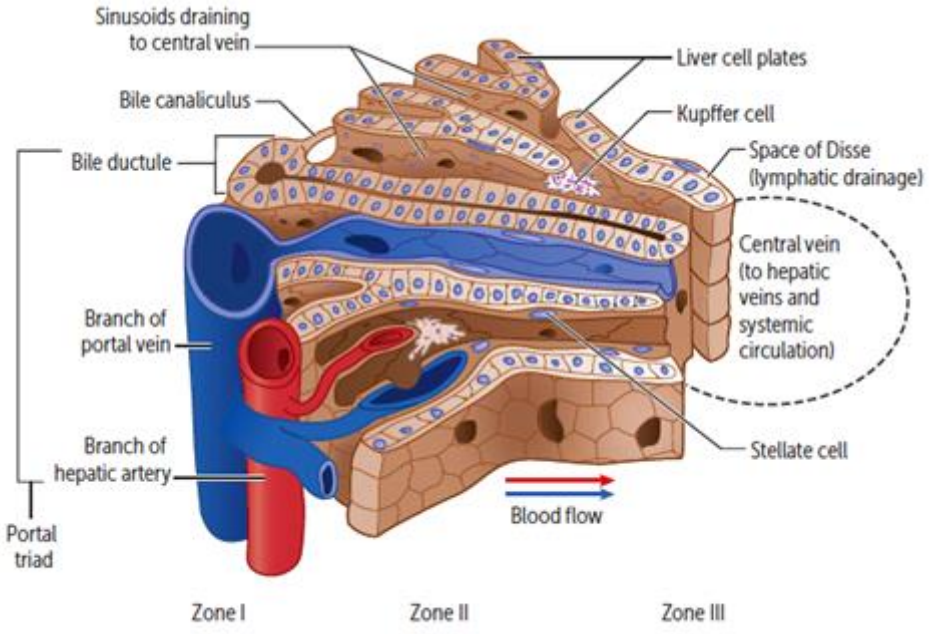


*Figure 2.1 The micro architecture of the liver acinus. Hepatocytes are arranged in plates with the capillaries in between to allow nutrient and waste exchange. Oxygen rich blood from the hepatic artery (red) and de-oxygenated blood from the portal vein (blue). Stellate cells reside in the Space of Disse.* [5]

### 2.1.2 The cell types and functions of the liver

The liver is contains numerous parenchymal (hepatocytes) and non-parenchymal cells (NPCs) types, of which the most know are the Stellate cells, Kupffer cells and liver sinusoidal endothelial cells (LSEC's).

Hepatocytes are highly differentiated epithelial cells that make up the largest population of cells (approximately 60%) in the liver by mass/volume or number. These cells are polarized (specific orientation) *in vivo* with adjacent cells forming tight junctions on the apical face, where bile can be excreted into the bile duct [13]. They are also one of the most metabolically active cells in the body. Ideally all cells present *in vivo* should be included when attempting to

culture an *in vitro* model of the liver, as these cells consistently communicate with and affect each other.

The Stellate cells, first discovered by Kupffer in 1871 , are responsible for storing vitamin A and fat droplets in a healthy liver, and deposition of extra-cellular matrix proteins, like collagen type I, III and IV [8]. There is some evidence that suggests they help regulate blood flow with the endothelial cells thought cytokines and physical contraction / relaxation [9]. Because of their ability to produce ECM components when activated, they have an active role in the development of liver fibrosis following prolonged or extensive liver injury. By volume they account for less than 2% of the liver cells [10].

Kupffer cells are the native macrophages of the liver and are primarily involved in scavenging pathogens and inflammation mediation and thus in the pathogenesis of various liver related diseases. They have been shown *in vivo* to activate stellate cells by eliciting expression of the platelet-derived growth factor receptors, leading to the increased production of ECM and stiffening of the liver [11]. Liver sinusoidal endothelial cells (LSECs) line arteries and veins and aid in the transfer of nutrients to the hepatocytes [12].

The liver has many functions, such as production and excretion of bile which aids in lipid digestion, synthesis of plasma proteins (e.g. albumin), storage of glycogen and metabolism of food and xenobiotics. Metabolism of xenobiotics can be divided into two phases: Phase I metabolism is carried out by a large family of proteins called cytochrome P450 (CYP450). These proteins are involved in the addition or uncovering of a functional group on the foreign compound through reduction, oxidation or hydrolysis. Oxidation (addition of an

oxygen or removal of a hydrogen molecule) catalyzed through the CYP450 proteins require oxygen and nicotinamide adenine dinucleotide phosphate (NADPH), a cofactor in anabolic reactions. An example of CYP450-mediated oxidation is hydroxylation, which is common for drugs containing an aromatic ring. Reductive (addition of a hydrogen or removal of an oxygen molecule) metabolism also requires NADPH but not oxygen. The types of compounds that are generally reduced are epoxides (an ether containing a three-atom ring), Azo- (aryl or alkyl bearing a diazinyl functional group) and Nitro-compounds (containing a nitro functional group) [14]. Lastly, hydrolysis, is a chemical reaction that uses water to break down the compound. Compounds that can readily be hydrolysed are esters (compound derived from an acid with an -OH group replaced with an O-alkyl group) and amides (carboxylic acid derived where -OH group is replaced with an amine or ammonia) [15]. This list in not complete as virtually every compound can be catalysed by the Phase I drug metabolizing enzymes. Mostly, the end metabolite will contain a chemically reactive functional group such as -OH, -$NH_2$, -SH or -COOH, which makes the compound more hydrophilic and enables excretion. The enzymes involved in Phase I metabolism have been extensively studied due to their major role in xenobiotic metabolism. Over 50 CYP450 genes have been isolated and identified in humans. Of interest are the xenobiotic drug metabolizing enzymes, such as the CYP1A2, CYP2A6, CYP2C8/9, CYP2E1, CYP2D6 and (arguably most important) CYP3A4/5/7. CYP3A7 plays an important role during the foetal development stage, but “switches off” after birth allowing CYP3A4 to be the more predominantly expressed enzyme [16]. In

general, the oxidative reactions (Equation 2.1) catalysed by the CYP450 enzymes can be expressed below:

$$NADPH_2 + O_2 + RH \xrightarrow{CYP450} NADP^+ + H_2O + ROH$$

*Equation 2.1 NADPHH$^+$, oxygen and a compound with a hydrogen group (RH) is metabolized by CYP450 resulting in the reduced form NADP$^+$, water and the compound now containing a function -OH group.*

Where RH is an oxidizable compound and ROH is the hydroxylated product. Phase I metabolism may produce a toxic intermediate metabolite and can be detoxified through Phase II metabolism, usually referred to as conjugation. Phase II metabolism mostly involves the “transferase” enzymes, which conjugate the electrophilic Phase I metabolite with a nucleophilic species to reduce toxicity and make the compound more hydrophilic for excretion. These reactions include methylation (mostly endogenous compounds), acetylation, glutathione conjugation, glucuronidation and sulfation, with the UDP-glucuronosyltransferases (UGTs) and sulfotransferases (SULTs) being the most predominant enzymes [17]. Glucuronidation can occur with compounds such as alcohols, carboxylic acids, amines and thiols. Sulfation occurs primarily with phenols, but SULTs can also conjugate with alcohols, amines and thiols. Since most drugs can either undergo glucuronidation or sulfation, there may be competition between the two pathways, however, in general sulfation dominates at low concentrations, while more glucuronidation occurs at high concentrations. Glutathione (GSH) conjugation (Equation 2.2) is also very important as it has been shown to have protective anti-oxidative properties, specifically for electrophilic compounds [18]. This is due to the

nucleophilic cysteinyl thiol group on the reduced GSH form [19]. GSH conjugation is a vital protection mechanism which detoxifies reactive electrophilic intermediate metabolites produced in the liver during intermediate metabolism of several xenobiotics, e.g. Paracetamol (PAR) [20], Aflatoxins [21] and many more [22] [23] [24].

$$R - CH_2 - X \xrightarrow{GSH} R - CH_2 - SG$$

*Equation 2.2 Compound (R) conjugated with glutathione (GSH).*

Where R-$CH_2$-X represents any number of electrophilic compounds and R-$CH_2$-SG represents the glutathione conjugate.

### 2.1.3 The implications of liver-related metabolism on drug development

Considering the major role the liver has in xenobiotic drug metabolism it is no surprise that it is one of the main organs targeted during safety testing of a new drug entity for market. Some drugs are known to elicit a toxic response without metabolism (doxorubicin), however it has clearly been shown that intermediate metabolites produced through Phase I metabolism can elicit toxicity and interfere with the life-sustaining processes of the cells [14]. An example of this is paracetamol (APAP), one of the most widely used analgesic drugs obtainable without prescription. At low to therapeutic levels (Figure 2.2 (a)), the majority of APAP is metabolized by the Phase II SULF and GLUC pathways that are readily excreted by the ATP-binding cassette (ABC) transporters in the cell membrane. A small percentage is metabolized into N-

acetyl-p-benzoquinone imine (NAPQI) by the CYP450 proteins, predominantly the CYP2E1 and CYP1A2; however CYP2D6 [25] and CYP3A4 [26] have also been implicated in the bioactivation of APAP. Under normal circumstances NAPQI is detoxified through conjugation with GSH which is excreted through the bile. At supra-therapeutic levels (Figure 2.2 (b)) the SULF pathway gets saturated leading to excessive production of NAPQI that depletes the stored GSH. NAPQI reacts with the sulfhydryl groups on proteins forming adducts that can target DNA in the mitochondria through excessive oxidative stress [27]. Generation of reactive oxygen species (ROS) is a by-product during normal metabolism but becomes problematic when it starts to accumulate inside the cell as it can oxidize important cellular components. The generation of excessive oxidative stress along with the activation of a group of proteins known as the mitogen-activated protein kinases (MAPKs) leads to mitochondrial dysfunction and eventual cellular necrosis [28].

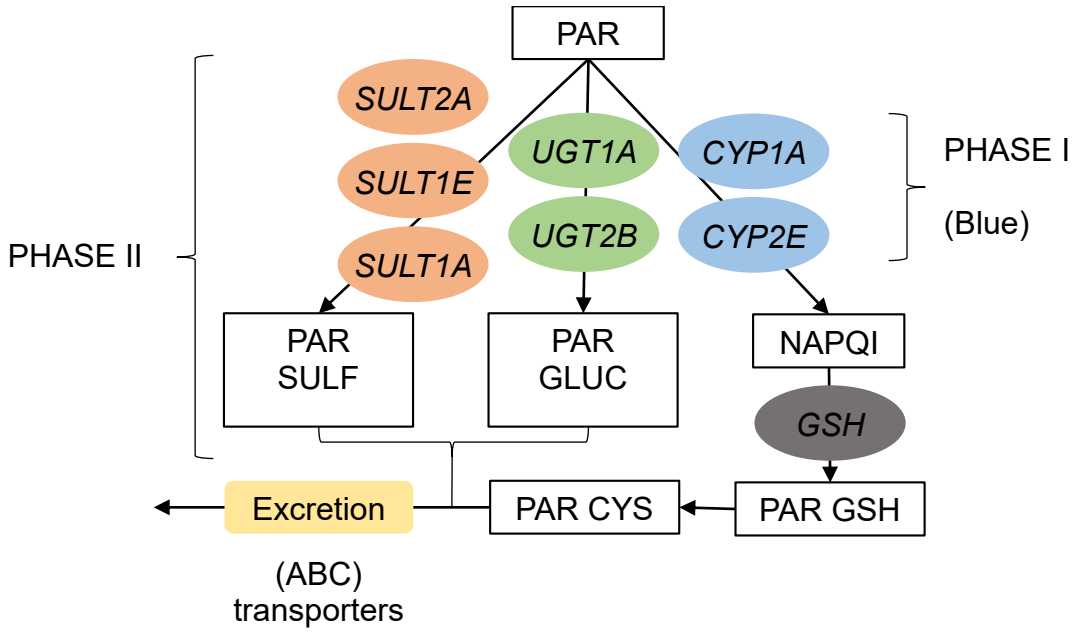


*Figure 2.2 (a) Metabolic pathway of Paracetamol at therapeutic concentrations. Most of the parent drug gets metabolized through sulfation and glucuronidation, with a small percentage metabolized into NAPQI through the CYP enzymes (Phase I metabolism). NAPQI gets detoxified through GSH conjugation (Phase II metabolism) and excreted by active membrane-bound transporters.*

*Figure 2.2 (b) Metabolic pathway of Paracetamol at supra-therapeutic concentrations. The sulfation pathway gets saturated, leading to an increase in NAPQI production through mainly CYP2E1 metabolism. Excessive NAPQI depletes GSH reserves resulting in injury through excessive generation of reactive oxygen species (ROS), combined with MAPKs activation, leading to mitochondrial membrane permeability transition, mitochondrial dysfunction and eventual cell necrosis.*

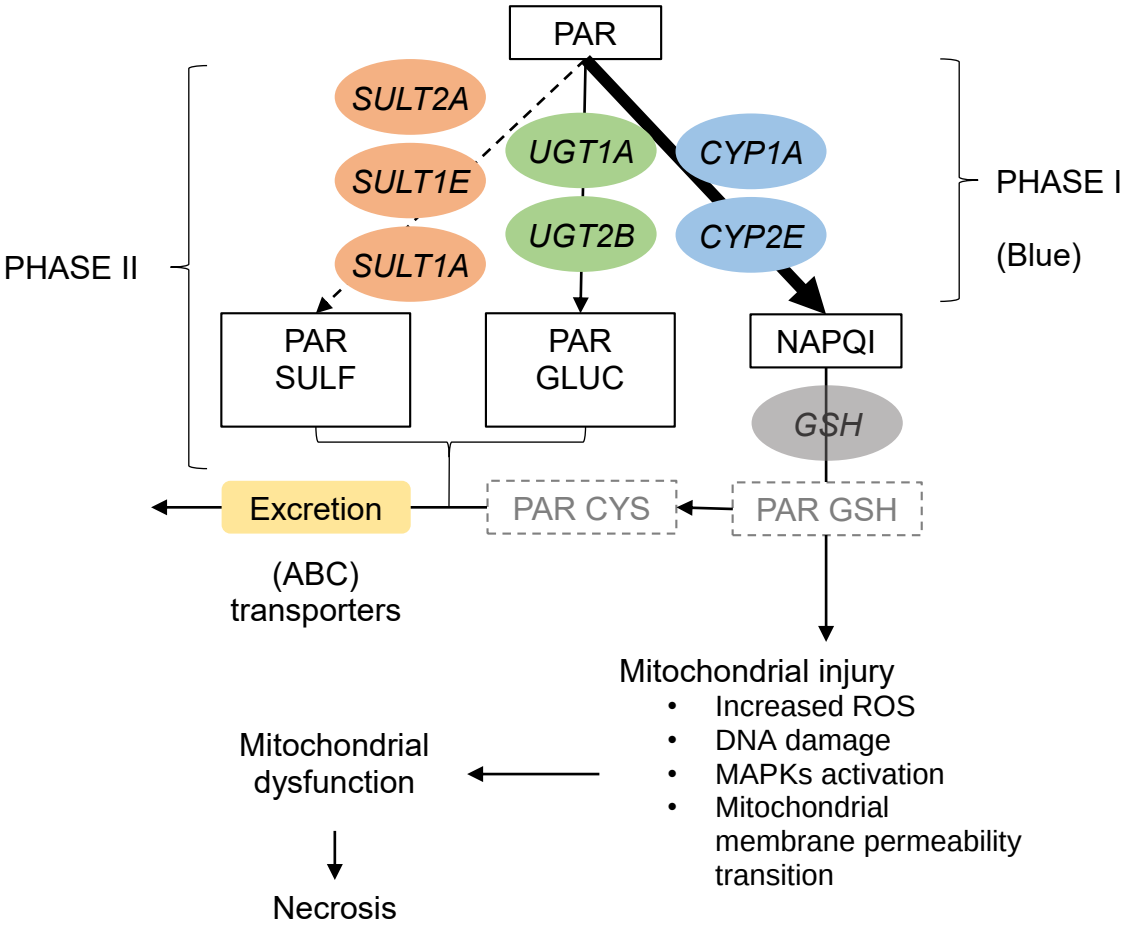


Another drug extensively researched is Diclofenac [29]. Diclofenac is metabolized by CYP2C9 (and a lesser extend other CYPs [30]) into various oxidized metabolites (3'-OHDIC, 4'-OHDIC, 5'-OHDIC etc.). Additionally, secondary activation of these oxidized metabolites results in the formation of highly reactive *p*-benzoquinone imines [29]. These metabolites can inhibit important hepatic functions, such as gluconeogenesis and albumin synthesis [31], increase oxidative stress and reduce production of ATP (if not detoxified through GSH conjugation). This is followed by mitochondrial permeability transition and dysfunction. Metabolic activation of DIC also results in an acyl glucuronide, which can from protein adducts. The eventual result is apoptosis through activation of caspases 8 and 9, ending with caspase 3 activation [32].

Once caspase 3 has been initiated there is no way to stop the cell undergoing apoptosis.

A drug (or its metabolites) could also induce or inhibit other metabolizing enzymes. For example, Rifampicin is a potent inducer of CYP3A4, thus co-administration with another drug substrate (e.g. Midazolam [33]) will alter the rate of that drugs metabolism [34]. This could lead to a reduction in the overall efficacy of the drug (due to the increased rate of clearance) or the production of more reactive metabolites that depletes the reserves of Phase II enzymes. The next section will briefly detail some key parameters evaluated when developing a new drug entity for market.

## 2.2 Pharmaceutical industry

Development of a new drug from concept to market is a costly and time-consuming process, with a very low number of drugs successfully reaching market. On average it takes 10 – 15 years and at a cost of over a £1 billion [35]. The reason for this huge expense and time is due to the number of stages (Figure 2.3) needed to evaluate the efficacy and safety of the drug. These stages are broadly divided into the discovery, preclinical and clinical stages [36]. In the discovery stage, thousands of potential candidates are rapidly screened to eliminate those compounds that have obvious unwanted characteristics (e.g. off-target binding), thus reducing the number progressing down the development process. Throughout all stages the absorption, distribution, metabolism and excretion (ADME) of a new drug is analyzed [12].

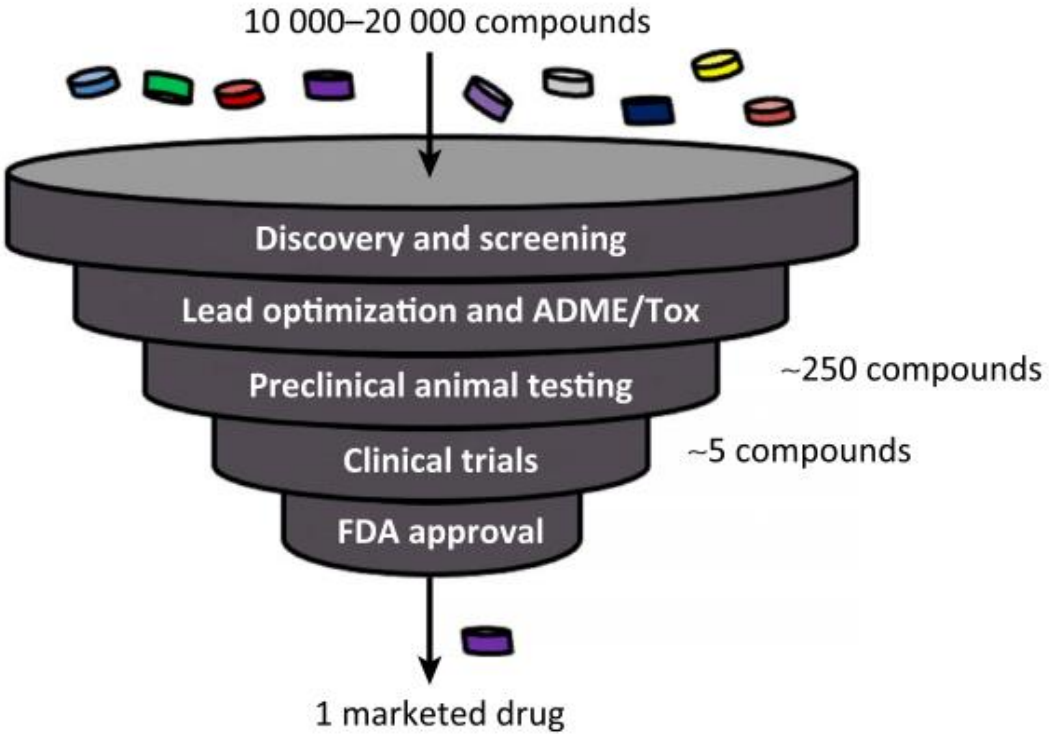


*Figure 2.3 The different stages of the drug development pipeline. The discovery stage starts with thousands of potential candidates. The number of chemical entities reduces significantly as the pipeline progresses, with only a single candidate making it to market.* [36]

### 2.2.1 ADME parameters

The development process of new drugs has seen many changes over the years to increase the success rates of bringing them to market. Important parameters that are evaluated are grouped into what is commonly referred to as the ADMET (absorption, distribution, metabolism and excretion) characteristics of the drug which are examined throughout the whole development process [37]. Absorption can broadly be described as the measure of passage of the drug from the administration site into the bloodstream [38]. Factors such as chemical stability of the drug, permeability through the cell membrane or solubility influence absorption, which in turn

affects the bioavailability of the drug. Bioavailability refers to the amount of unchanged (considered active) drug reaching the circulatory system. Distribution and Excretion characteristics can in most circumstances be evaluated simultaneously, usually by analysing the concentration of the drug and its metabolites in specific tissue samples at regular time intervals [39]. The distribution parameter is the study of movement of the drug between the different “compartments” in the body, either through passive or active mechanisms (cell membrane transporters). Xenobiotics can be designed to passively diffuse across the cell membrane but can also be actively transported via membrane bound drug transporters, such as the ATP binding cassette (ABC) transporter family. A xenobiotic compound will eventually need to be excreted (cleared) as accumulation of a foreign compound can have detrimental effects on normal cellular function and health. The major elimination pathways are excretion through the kidneys (urinary), biliary (and eventually faecal) excretion though the liver and excretion through the lungs (exhalation). There are many biochemical factors that can influence the distribution and excretion of a drug such as the size of the molecule, polarity or extent of protein-binding. **The last parameter, and the focus of this project, is metabolism of the administered drug**. Many xenobiotics are lipophilic in nature, meaning they can passively pass through the cell membrane to reach their specific receptor. Metabolism converts these lipophilic compounds into hydrophilic ones that can be eliminated from the body, however some metabolites are toxic and need to be detoxified through further metabolism (usually Phase II). Experiments to determine metabolism-

related toxicity early would eliminate potentially toxic candidates reaching later stages in the development process. To explore metabolism-related toxicity scientists have made significant improvements to *in vitro* models that mimic the *in vivo* liver, focusing on functions such as albumin and urea production, and metabolism. Some parameters can be evaluated early on using relatively "simple" *in vitro* models, while others require more complex and ideally *in vivo-like* models.

### 2.2.2 *In vitro* models for drug induced toxicity

The use of 2D *in vitro* models has been very widely adopted in both industry and academia. Although animal or humans would provide more accurate data regarding the pharmacokinetic and pharmacodynamic properties of a drug, cost, limited availability and ethical considerations are the main concerns. *In vitro* models offer the advantages of being relatively cheap, quick and can provide more data in a shorter time (high throughput). Even "simplistic" models can be valuable in drug development at the early stages. Liver-derived enzymes can be used to identify the involvement of particular CYPs in metabolism (referred to as CYP mapping) [40], or their potential for drug-drug-interaction; a consideration in induction / inhibition studies [37]. Sub-cellular fractions are a step up in complexity compared to derived enzymes and can be broadly classified into the cytosol, microsomal – and S-9 fractions. The cytosol can be used to study mechanistic (conjugation reactions) characteristics after a drug has undergone Phase I metabolism. The microsomal fraction contains mainly the Phase I metabolizing enzymes and

primary conjugation enzymes (e.g. UGT) that are together responsible for metabolizing roughly 90 % of all marketed drugs. Microsomal fractions can be used to gather information on Phase I action, while the cytosol provides information from further down the metabolic pathway. S-9 fractions contains both the microsomal and cytosol content and thus provides a more complete picture of the metabolism of a drug, but it has been reported that co-factors that mediate Phase I and Phase II metabolism can be lost during the isolation procedure (e.g. NAPDH or UDP-glucuronic acid) [41]. These models are valuable as they allow researchers to exclude many parameters that would need to be considered when using (e.g.) *in vivo* models, such as distribution across different tissue / organs, which would complicate data collection and analysis. As advantageous using these sub-cellular fractions as models for metabolism related toxicity are, they still lack characteristics that play an important role in drug development. Excretion of a drug also needs to be evaluated, which implies that active membrane bound transporters (e.g. human multidrug resistance-associated proteins) needs to be included in the model. This suggests using whole cells with intact cellular membranes would lead to more accurate *in vivo* correlation. Intact cells possess all the cytosolic and microsomal enzymes as well as the membrane bound transporters that actively move compounds across the cell membrane. By having a complete system (whole organism), information regarding the effect of the drug on the physiological processes of the cells can be acquired.

Isolated primary human hepatocytes contain most of the co-factors and enzymes at physiological levels, however, are limited in their use, due to low

availability and short functional life span *in vitro*. In fact, it has been shown that primary hepatocytes plated in 2D monolayers (historically on a rigid polystyrene petri dish) dedifferentiate after only a few hours. Seeding the hepatocytes onto a layer of ECM promotes the re-establishment of polarization and increases the time the cells are viable and metabolically functional [42]. Hepatocyte suspension cultures are also employed to investigate drug metabolism, but experiments are limited to only a few hours [43], as cells rapidly lose viability [44]. Additionally, hepatocytes are a relatively "dense" cell, resulting in the cells settling on the bottom forming a layer. This affects the transfer of oxygen, nutrients and waste between the circulating medium and the cells on the very bottom. In attempts to improve longevity and functionality of primary hepatocytes, scientists have focussed on mimicking the *in vivo* environment using a variety of strategies, such as continuous perfusion, co-culturing cells with NPCs and establishing a 3D structure (with or without ECM).

The sandwich configuration (Figure 2.4), where cells are "sandwiched" between a bottom ECM layer (normally collagen) and a top layer (collagen or more recently Matrigel) [13] is an example of one of these advances. This configuration has been shown to allow cells to retain more *in-vivo* like properties, for example, the restoration of polarity leading to tight-junction formation between neighbouring cells; and is one of the most widely employed methods of culturing primary hepatocytes for hepatotoxicity assays [45].

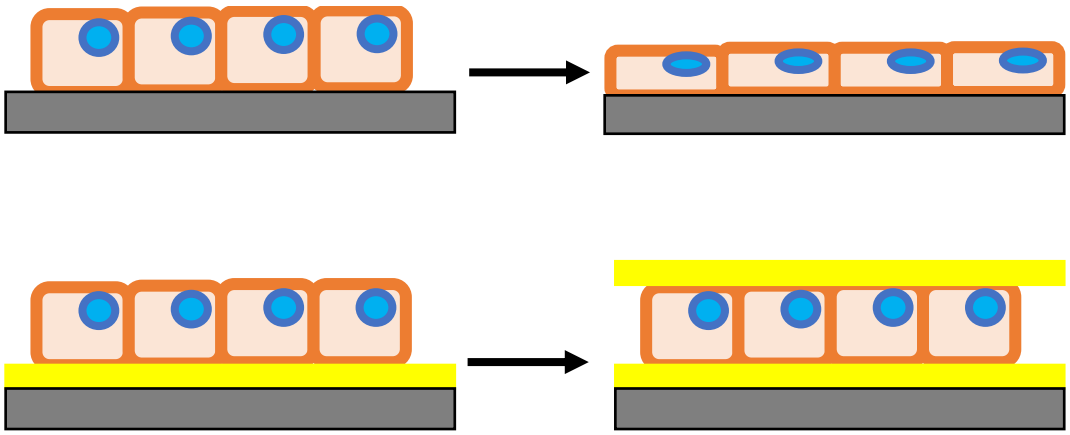

*Figure 2.4 Diagram of cells cultured in monolayer (top) resulting in a change in shape due to lack of ECM and (bottom) cells cultured between two ECM layers, allowing retention of shape and prolonged function.*

Although sandwich configurations are a valuable tool in maintaining hepatic function, the micro-environment can be further improved by including, for example, NPCs. Layering to mimic the *in vivo* architecture is still a challenge, however Kostadinova and coworkers [46] attempted to address this problem by using multiwell inserts in a 24 well-plate format (Figure 2.5) to enable cell-cell communication. NPCs (Kupffer, hepatic stellate cells and endothelial cells) were seeded onto a nylon scaffold a week before human or rat hepatocytes were introduced. They compared albumin and urea secretions between their trans-well system and monolayers, cultured on a collagen-coated 24 well-plate, using 3 x$10^5$ cells/well. Additionally, they compared the toxicity of Paracetamol and Trovafloxacin on human hepatocytes in their “3D model” to monolayers by monitoring the release of lactate dehydrogenase (LDH) release into the medium. Cultures in the multi-well system displayed a concentration-dependent decline in viability after chronic exposure to either compound over 15 days, but the monolayered cultures showed no response after acute treatment (2 days). The reason for the difference in exposure times was not

mentioned in the publication, however it is likely due to the fact that monolayered cultures could not maintain their metabolizing capabilities for as long as the 3D cultures. Unfortunately, no comparison was made to a collagen sandwich configuration, so it is difficult to conclude whether this multi-well approach is significantly better. Although layering of the cell types was achieved, this configuration does not fully represent the architecture that is found *in vivo*.

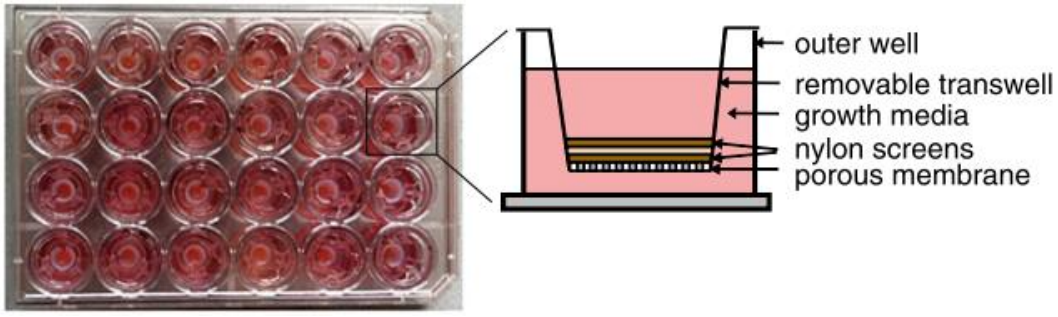


*Figure 2.5 Top down view of Regenemed co-culture platform and a side view of the layered insert. NPCs were seeded and allowed to proliferate to cover the top nylon screen for a week before hepatocytes were seeded on the bottom of the well. The porous membrane on the bottom allows access to medium.* [46]

Methods for manipulating cells into aggregates and eventually spheroids have increased in use over the last 20 years. A matrix-based method is encapsulation of cells inside ECM, restoring and prolonging cellular function through establishment of a 3D environment. Liu T and coworkers [47] demonstrated the advantages of embedding human induced pluripotent stem cells (hiPSCs) in a hydrogel made from self-assembling polypeptides; which differentiated into hepatocyte-like cells. They also compared morphology, albumin and urea production and CYP activity with 2D cultures in plastic plates.

Their results showed that the 3D cultured cells (which aggregated into spheroids in the gel) had significantly higher basal CYP450 gene expression. Induction and inhibition of CYP3A4 and CYP2C9 was evaluated using a P450-Glo™ CYP2C9 and 3A4 assay kit (Promega). Rifampicin was used for induction of both CYP3A4 and CYP2C9, and Ketoconazole for inhibition as these proteins are involved in a large portion of xenobiotic metabolism. Ramaiahgari and co-workers [48] also demonstrated improved metabolic capabilities of HepG2 spheroids cultured in Matrigel™ (gelatinous protein mixture produced by Corning Life Sciences). They compared the difference in Phase I enzyme expression between monolayered HepG2 cells and spheroids (day 21 and day 28) using real time-polymerase chain reaction assays.

An alternative method for generating spheroids that do not rely on an ECM component utilises a non-adherent surface that promotes cell-cell contact [49] [50]. Well established methods are ultra-low adherent well-plates, the hanging drop configuration [51] and microarrays [52] (with geometric constraints) to trap cells. Finally, even more complex *in vitro* models have been used. Liver slices contain the relevant cell types, retain their structure and may reduce the risk of damaging cells during the isolation process. Phase I and II enzyme expression remains stable during use, however, these tests usually only last between 30 minutes to a few days maximum [53]. This is due to the reduction in metabolic capability and the development of necrosis after a couple of days in culture. Additionally, the rate of metabolism and clearance is lower compared to isolated primary cells [54]. It is suggested that this may be due to a chemical gradient of exposure across the slice, meaning that not all

hepatocytes are exposed to the compound of interest. A short summary of different models can be found below in Table 2.1 [36] [55].

*Table 2.1 Summary of different in-vitro liver models used for the detection of metabolism related toxicity.*

| Model | Advantages | Disadvantages |
|---|---|---|
| Subcellular fraction [41] | -Contain most proteins;<br>-Relatively inexpensive. | -Only provides partial information on metabolism.<br>-Cofactors required for activation. |
| Hepatic cell lines [56] | -Some liver-specific functions.<br>-High availability. | -Lower relevant metabolizing proteins. |
| iPS-derived hepatic cells [57] | -Patient specific. | -Variable results.<br>-Potential tumour formation (potentially affecting function). |
| Primary hepatocytes (monolayer) [58] | -Some cell-cell interactions.<br>-Relatively high throughput. | -Only applicable for short term studies due to rapid reduction in functionality. |
| Primary hepatocyte (suspension) [59] [55] [60] | -Relatively high throughput.<br>-Maintains expression of enzymes levels close to *in vivo.* | -Short term applications only (hours).<br>-No / limited cell-cell interactions. |
| Primary hepatocytes (Sandwich configuration) [61] [62] | -Restores some *in vivo* morphology.<br>-Functional establishment of bile canaliculi. | -Decline / alterations in CYP activity in long term culture. |
| Liver slices [63] [64] | -Contains all cells.<br>-Maintains liver structure.<br>-Intact bile canaliculi. | -Short viability – necrosis.<br>-Gradient of exposure Diffusion-limited.<br>-Limited availability. |

### 2.2.3 Culturing hepatocytes into spheroids

Spheroids are defined as a collection of cells that aggregate (either passively or through an external mechanism), with or without using ECM. There are numerous general methods available to generate spheroids, with several

relying on the concept of culturing the cells in a non-adherent environment - promoting cell-cell adhesion.

*Liquid overlay method*

Spheroids can also be created using a liquid over-lay method which forms a concave non-adherent surface for cells, promoting cell-cell aggregation. Gaskell and coworkers [65] characterized the spatiotemporal structure (Figure 2.6) and functions of the hepatoma cell like C3A in spheroids and compared them to monolayer cultures. The spheroids were more sensitive to Paracetamol than the monolayer cultures during exposure for 24 hours (repeated doses). Formation of bile canaliculi was assessed by inhibiting the multidrug resistance-associated protein 2 (MRP2) and permeability-glycoprotein (Pgp) transporters. These transporters are responsible for the efflux of organic anions and lipophilic cations from the cell and thus play a function in biliary transport. The cultures were exposed to 5-chloromethylfluorescein diacetate (CMFDA) which is membrane permeable dye which is converted inside the cells into glutathione-methylfluorescein (GSMF), a substrate for MRP. Their results showed retention of CMFDA inside the cells in the monolayer culture, compared to limited retention and localisation of CMFDA between cells in the spheroids, suggesting the membrane transporters are functional in the spheroids.

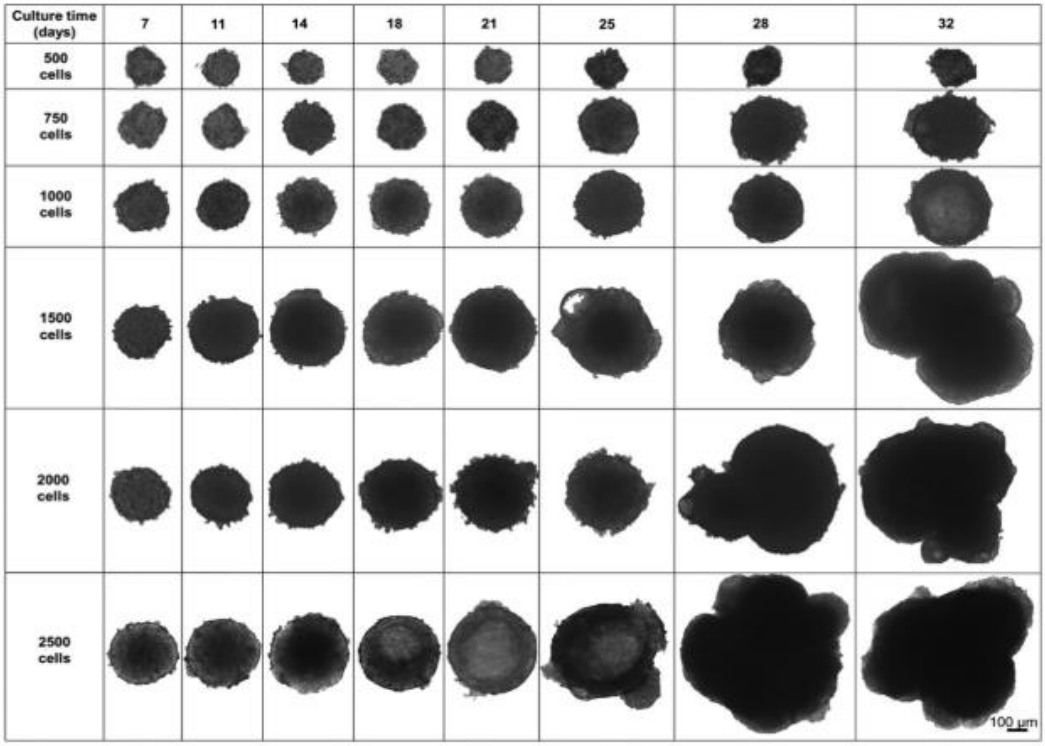


*Figure 2.6 C3A cells aggregated into spheroids over 32 days with different starting numbers of cells used in a 96 well-plate. The spheroids were generated using the liquid overlay technique.* [65]

*Ultra-low attachment plates*

Bell and coworkers [66] cultured primary human hepatic spheroids by seeding 1500 cells / well in ultra-low attachment 96 well-plates. The hepatocytes were centrifuged at 100 x g for 2 minutes and allowed to aggregate into spheroids (averaging 200 µm in diameter). These spheroids were cultured for 35 days and characterized as a suitable model for liver disease (cholestasis and steatosis), liver specific function and hepatotoxicity testing. LC-MS/MS analysis of five different CYP450 enzyme substrates were carried out, and the results showed stable expression of CYP1A2, CYP3A4 and CYP2D6 from day 8 to 35, but not CYP2C8 (reason unclear).

In a following paper Bell and coworkers [67] again compared primary human hepatocytes, in the widely used collagen sandwich configuration to spheroids over 14 days. Cryopreserved PHHs were thawed and seeded at 7 x $10^4$ cells / well in 96 well-plates for cytotoxicity and LC-MS analysis and 4 x $10^5$ cells / well in 24 well-plates for Proteomics assessment. Spheroids were generated by seeding 1500 cells / well in ultra-low attachment 96 well-plates followed by centrifugation for 2 minutes. Spheroids formed over 7 days. Proteomics data showed that overall many proteins were significantly downregulated in the monolayers (including important proteins produced through Phase I enzymatic activity, like CYP3A4) and the spheroids remained more phenotypically stable compared to the collagen sandwich configurations. The spheroids expressed higher activity of these Phase I enzymes throughout the entire culture (Figure 2.7). They concluded that spheroids are more functionally stable during the 14 days of culture (compared to the sandwich configurations) and illustrated the culture method-induced differences between spheroids and collagen sandwich configurations.

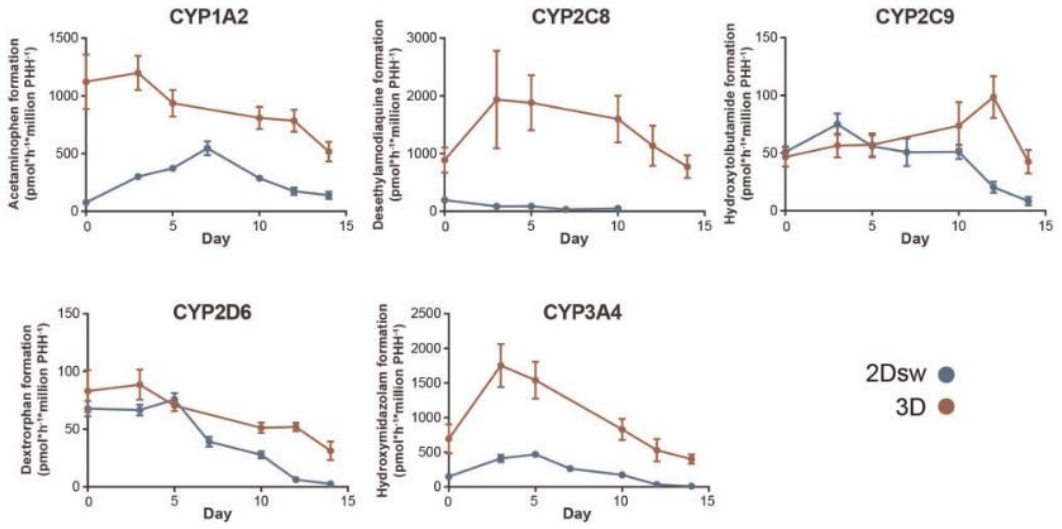


*Figure 2.7 Expression of Phase I metabolizing enzymes in primary human hepatocytes (single donor) between spheroids generated in ultra-low adherent 96 well-plates (red) and 2D sandwich cultures (blue). The activity was quantified through LC-MS/MS using specific substrates for each CYP of interest.* [67]

*Micro-moulding*

Although non-adherent well plates provide an effective method for generating spheroids, micro-moulding techniques have improved on throughput.

Nakazawa and coworkers [68] fabricated a PDMS chip (24 mm x 20 mm) containing approximately 2500 cylindrical microwells. Primary rat hepatocytes were harvested, then seeded and cultured for 10 days. Liver-specific functions such as Albumin secretion and CYP450 activity was monitored and compared to hepatocytes cultured on a collagen monolayer configuration and a flat PDMS chip. The conversion of Ethoxyresorufin to Resorufin is catalyzed by the CYP450 activity (CYP1A) [69]. Their results showed the spheroids had higher albumin secretion, ammonia removal and EROD activity compared to the monolayer cultures.

*Hanging-drop method*

Another method for generating spheroids by providing a non-adherent surface is referred to as the hanging drop method. Murayama and coworkers [70] utilised this method using the profile of a 96 well-plate (Figure 2.8). HepaRG cells were cultured at different seeding densities, ranging from 0.2 – 7.2 x $10^4$ cells / drop and induction studies were performed on CYP1A2, CYP2B6 AND CYP3A4. Interestingly, their data showed no significant difference between the levels of the metabolized Midazolam (a CYP3A4 substrate) when decreasing the number of starting cells / drop. This indicated that the metabolizing capabilities of spheroids made from lower starting cell numbers are similar to those with high starting cell numbers. Unfortunately, no data were given on the amount of unmetabolized midazolam in the cultures, so it is unclear whether the cells in the higher or lower starting number spheroids achieved different rates of metabolism. This does demonstrate that spheroids generated using low starting cell numbers can be metabolically active. In this study the lowest concentration was still relatively large at 2.3 x $10^3$ cells / spheroid. A drawback of using this method is that cells in the spheroids are not able to communicate with other spheroids.

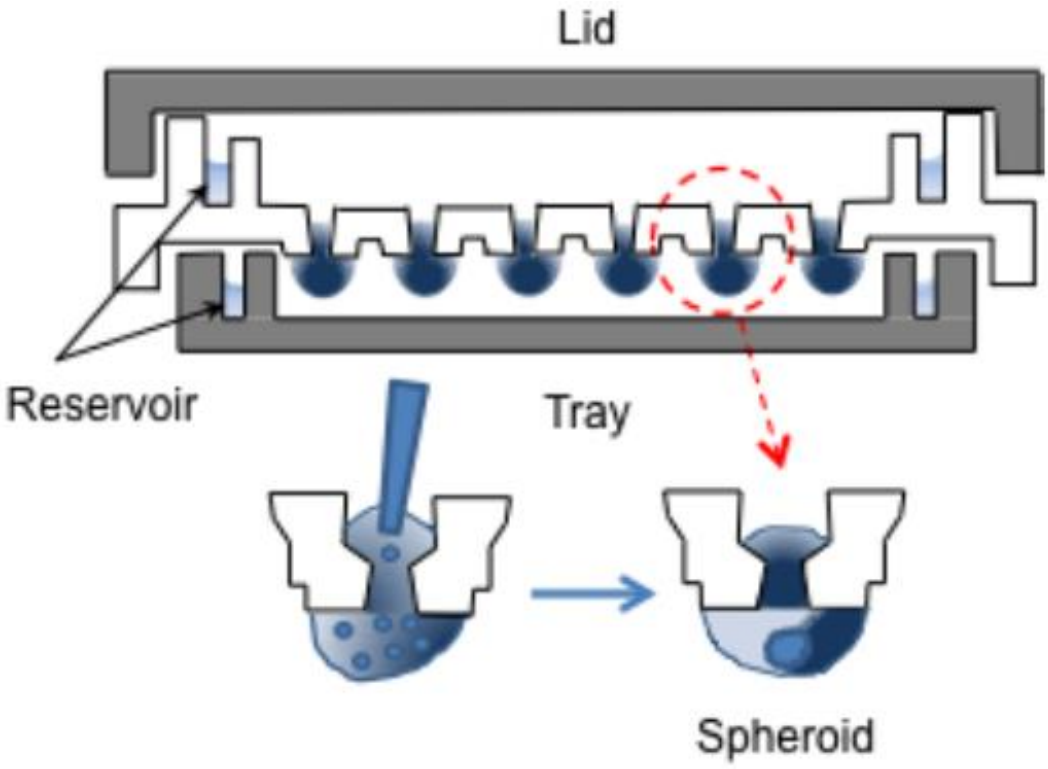


*Figure 2.8 Diagram of a hanging drop system used to provide a non-adherent surface for cells to aggregate into spheroids.* [70]

These systems can be used to provide valuable information on the differences between 3D (sandwich configuration and spheroids) and monolayered cultures. A limitation is that these systems are relatively low throughput (apart from micro-moulding). This can be improved through the implementation of microfluidics. Microfluidic platforms could provide a significant advantage, as thousands of data points can be collected using a platform with a smaller footprint compared to commercially available well-plates.

## 2.3 Microfluidics platforms

Microfluidics involves the manipulation of fluid on the microlitre to picolitre range, using small (sub-millimetre) channels. The Reynolds number (Equation 2.3) is a qualitative descriptor of how a fluid behaves and is an important parameter to understand when designing most microfluidic platforms.

$$Reynolds\ number = \frac{\rho v L}{\mu}$$

*Equation 2.3 The Reynolds number equation, where ρ is the density of the fluid, $v$ is the velocity of the fluid, $L$ is the length of the channel and μ is the dynamic viscosity of the fluid.*

If the Reynolds number is below 1 the flow is considered laminar, meaning it is more easily controlled, which is a desirable characteristic when designing microfluidic platforms. Microfluidics can offer several advantages for bio-applications, such as using less resources (which may be expensive or rare), rapid prototyping and high-throughput potential. Polydimethylsiloxane (PDMS) is commonly used to manufacture microfluidic platforms, as this material allows diffusion of oxygen, is inexpensive and allows rapid prototyping [71]. The PDMS surface may need to be functionalised to prevent adhesion of the fluid being manipulated or the (if used in biological applications) cell cultures.

### 2.3.1 Droplets and microwells for generating spheroids

Various methods can be employed to generate 3D structures in microfluidic platforms.

*T-junctions*

A well-established method is using two immiscible fluids, a continuous phase (usually oil-based) and an aqueous phase (water-based) to generate and store droplets containing cells. This can be achieved using a T-junction [72] (Figure 2.9) or a flow focussing [73] approach (Figure 2.10). The T-junction involves one channel meeting another perpendicularly. The phases meet at the junction and when the tip of the aqueous phase enters the channel carrying the continuous phase the channel gets blocked [74]. This causes the pressure upstream from the junction to increase, resulting in the “neck” of the aqueous phase thinning and breaking off to form a droplet [75]. One of the important parameters in determining the generation of droplets is the Capillary number (Equation 2.4)

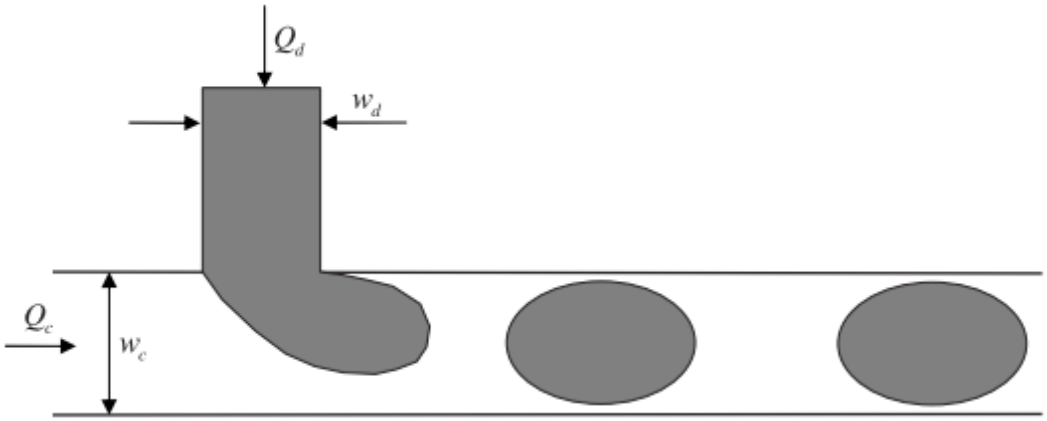


*Figure 2.9 A diagram of a T-junction used to generate droplets. $Q_d$ and $W_d$ are the volumetric flowrate (of the aqueous phase) and width of the dispensing channel, respectively. $Q_c$ and $W_c$ is the volumetric flowrate (of the continuous phase) and width of the continuous channel, respectively.* [72]

$$Ca = \frac{\mu v}{\gamma}$$

*Equation 2.4 Calculating the dimensionless Capillary number, where μ is the dynamic viscosity of the continuous phase, $v$ is the velocity of the continuous phase and $\gamma$ is the interfacial tension between the two phases*

The Capillary number influences the size of the droplets generated as it is related to the deformity of the droplet interface. The smaller the Capillary number the larger the droplets that are generated.

*Flow focussing*

The flow focussing method (Figure 2.10) uses the aqueous phase flowing through a middle channel, while the continuous phase flows through two other outer channels. These two outer channels meet resulting in the aqueous phase breaking up into droplets.

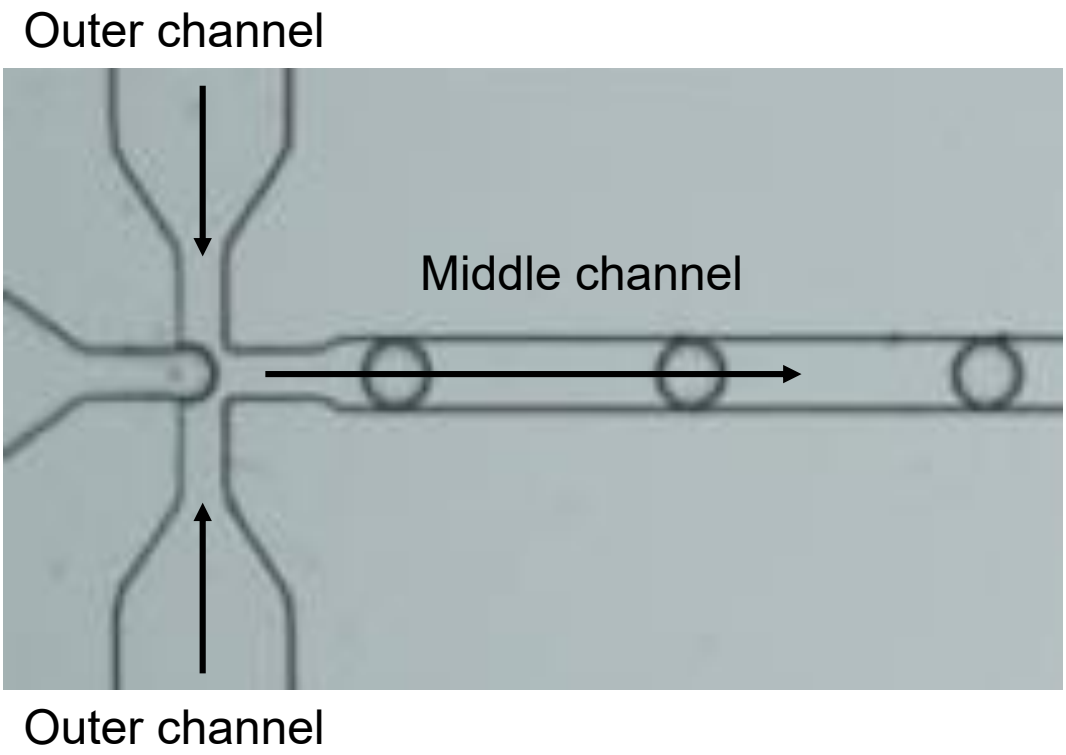


*Figure 2.10 The flow focussing method for generating droplets. The aqueous phase flows through the middle channel while the continuous phase meets from the two outer channels, breaking the aqueous phase into droplets.* [76]

*Microfluidic parking networks*

The droplets are stored (or trapped), either off-chip (e.g. using a well-plate) or on-chip. A method for on-chip storage is to use the geometry and configuration of the downstream channels to manipulate the droplet down a path that ends in being blocked by the droplet, while allowing flow to continue through another channel [77]. This is easily achieved using a structure [68] seen in Figure 2.11 (Top). The droplet will follow the path of least resistance which can be calculated using Equation 2.5; once the droplet is trapped and the path is essentially closed, the next droplet will follow the only other path available, this design is sometimes referred to as a microfluidic parking network.

$$R = \frac{12\mu L}{wh^3}\left(1 - \frac{192}{\pi^5}\left(\frac{h}{w}\right)\right)^{-1}$$

*Equation 2.5 To calculate the resistance (R) of a channel, where μ is the dynamic viscosity, $L$ is the length, $w$ is the width and $h$ is the height of the channel.*

Due to the low volume in the droplet (nl – μl), cells cannot be stored for an extended amount of time, due to depletion of nutrients and accumulation of waste. To extend the culturing time the droplets need to coalesce with fresh medium which is achieved by displacing the continuous phase (Figure 2.10 - bottom).

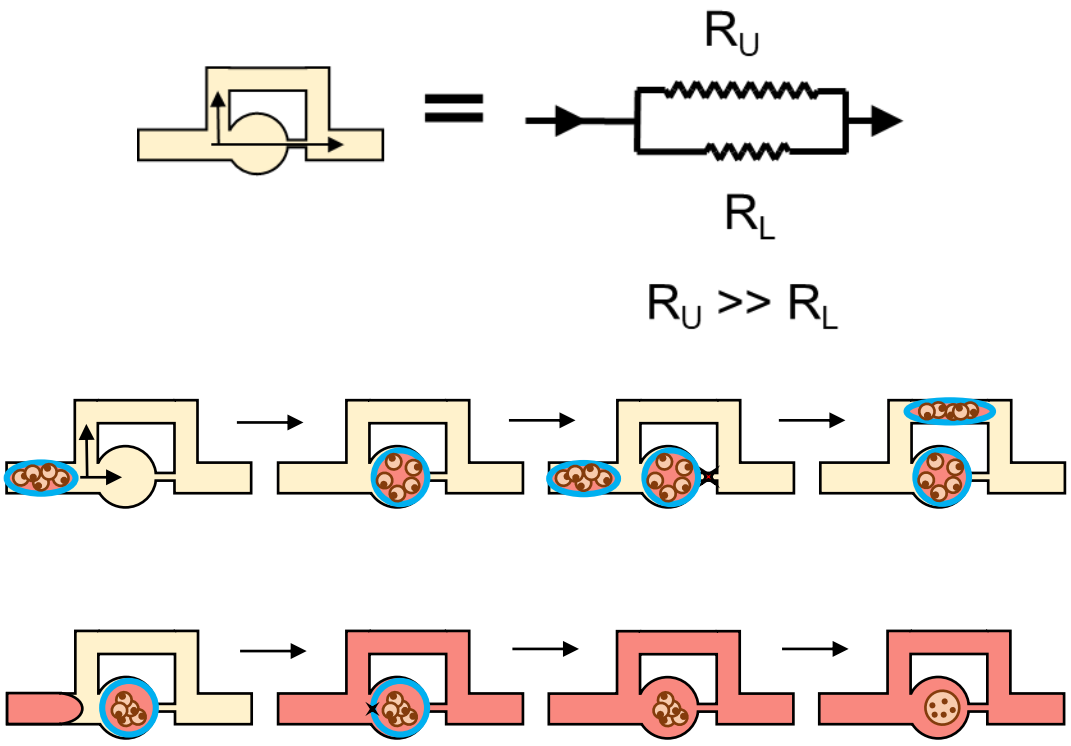


*Figure 2.11 (Top) A single droplet trap in a microfluidic parking network and the electrical equivalent where the resistance of the upper channel ($R_U$) is larger than the resistance of the lower channel ($R_L$). (Bottom) Diagram of how droplets are sequentially trapped, and the continuous phase displaced by medium.*

*T-junction and microfluidic parking network platform*

The first microfluidic platform used in this thesis was based on the work done by Bithi et al. [78] and McMillan et al. [79] who used a T-junction and microfluidic parking network to culture the human carcinoma cell line (UVW) for 28 days. This design proved useful by allowing the exchange of nutrient and waste and provided relatively high-throughput, considering the small amounts of cells and culture medium needed to operate and maintain the platform.

Alternatively, cells can also be trapped using microwells, a concept that has previously been employed without using microfluidic platforms, either using a micro-milling [80] technique or micro-moulding (stamping) [81]. These approaches significantly increase the throughput compared to their conventional well-plate counterparts. By enclosing the system in a channel and manipulating the dimensions or geometry of the channel, more control over the flow of medium can be achieved. This could be beneficial as a means to induce perfusion [82] to more accurately mimic the *in vivo* micro-environment; or generate a concentration gradient [83] in a single channel, increasing throughput.

A fluid (containing cells) is introduced into a channel with microwells patterned on the bottom. Cells flow through from the inlet over the microwells and drop due to gravity and the declining flowrate. This flow rate can be controlled passively by the volume of fluid added to the inlet. If the added volume is large enough to increase the height of the fluid in the reservoirs above the threshold

needed to overcome the resistance of the channel, the flow is then generated by hydrostatic pressure (Equation 2.6) between the reservoirs.

$$P = \rho g H$$

*Equation 2.6 Calculating the hydrostatic pressure (P), where ρ is the density, g is gravity, H is the height of the fluid in the reservoir.*

If the volume in the reservoir is low (µl) so that the difference in hydrostatic pressure is negligible, the flow is driven by Capillary forces and surface tension. As with the active method the flow-rate inside the channels can be controlled by manipulating the geometry of the channels and the volume of the aqueous phase introduced. Careful consideration needs to be taken when using this method as spheroids could be pulled out of the microwells if the flowrate is too high. For example, increasing the width of the channel or reducing the height [84] can limit the number of spheroids escaping.

Chen and coworkers [85] fabricated a PDMS chip (Figure 2.12) consisting of a top layer with four channels and a bottom layer of 300 microwells (diameter 500 µm, depth 200 µm). They cultured three carcinoma cell lines (Human colon carcinoma cell line - HCT116, Human breast cancer cell line – T47D, and HepG2) and exposed them to anti-cancer drugs. Their results suggested that the size of the spheroid has an impact on how deeply the drug penetrates the spheroid, thus affecting their response. They hypothesized that the penetration of the drug is limited in larger (diameter) spheroids compared to smaller ones. This needs to be taken into consideration when designing the geometry of the microwells. In turn, smaller spheroids may be more susceptible to the drugs.

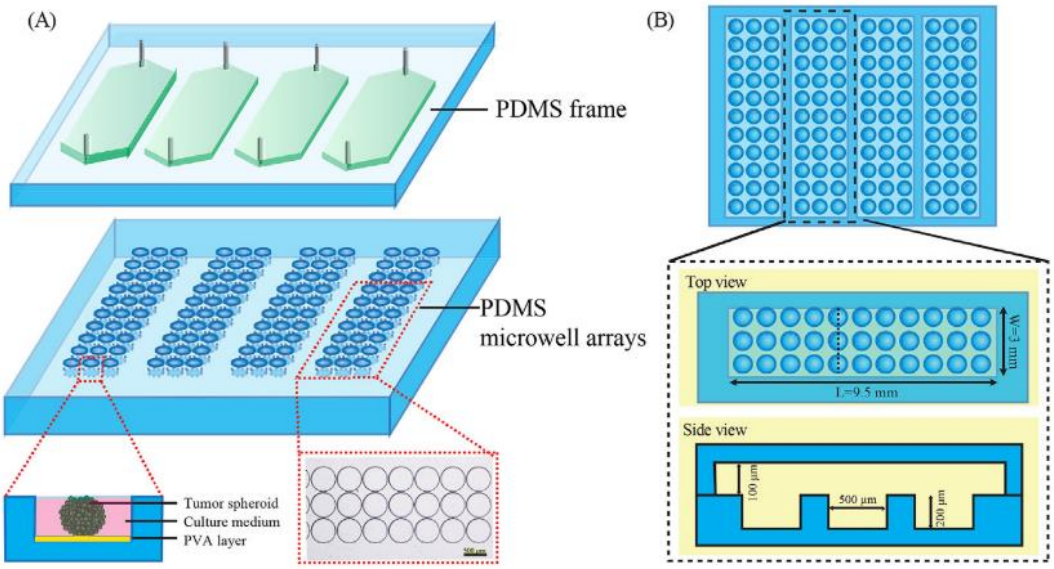


*Figure 2.12 (A) The top and bottom layer of the microfluidic platform with inserts showing the microwells with a layer of PVA to prevent cell adhesion and (B) the bottom layer of the platform with a top and side view indicating the dimensions used.* [85]

### 2.3.2 Three-dimensional liver cultures in microfluidic platforms

A variety of methods have been used to successfully culture hepatic spheroids in microfluidic platforms. This section will focus on platforms that used either of the two methods mentioned above (Droplets and Microwells). During the writing of this thesis the literature on generating (specifically) hepatic spheroids using droplet-based platforms was limited. In most of the papers reviewed, spheroids were either generated off-chip and stored in a microfluidic platform or generated using a microfluidic platform and stored off-chip. This may be related to droplet-based platform generally requiring additional equipment to operate (such as highly precise pumps) or the method producing relatively low throughput compared to (e.g.) microwell-based platforms. Alternatively, droplet-based platforms are difficult to culture for an extended time unless a

method to exchange nutrients / waste is implemented, which increases complexity, cost, time to culture, or a combination of all these factors.

Corrado and coworkers [86] used a double emulsion method to generate porous-gelatin microbeads. They seeded HepG2 cells into a spinner flask to create what they termed as HepG2-microtissue precursors (HepG2 µTP) and compared Albumin secretion to that of spheroids generated in a round-bottom 96 well-plate. Their results showed that the HepG2 µTP spheroids produced significantly more Albumin on day 7 and day 14 of culture. Based on these results they transferred their HepG2 µTP spheroids to a platform that artificially mimics the endothelial barrier found *in vivo*. Exposure to ethanol was investigated to simulate alcohol abuse. Albumin production, Urea synthesis and LDH leakage was significantly affected using an ethanol concentration of 100 or 300 mM. No further analysis was performed to confirm the decline of the cultures were due to the ethanol. This platform is also limited in that no droplets were generated on chip.

Yamada et al [87] combined droplet-generation of hepatic cells with extra-cellular matrix (ECM) microparticle production on a microfluidic platform. The collagen particles were produced on-chip (Figure 2.13) and stored with hepatocytes in a non-adherent culture dish (35 mm) to allow cells to aggregate onto the particles. Their results demonstrated a difference in gene expression, determined by PCR, between different particle to cell seeding densities and compared their results to spheroids cultured without ECM. Albumin production was significantly increased in the spheroids formed using the collagen particles, however there was no significant difference in the gene expression

of CYP3A1. This may suggest that incorporating an ECM component improves some hepatic functions, but not necessarily metabolism-related function. Unfortunately, the particles containing cells were not exposed to any xenobiotic compounds.

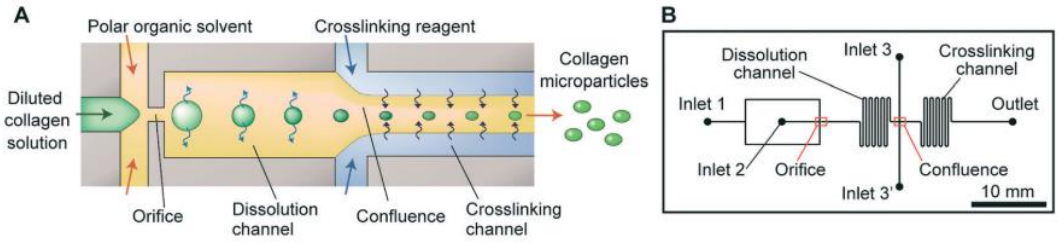


*Figure 2.13 (A) Collagen microparticles are generated on-chip, (B) diagram of the platform.* [87]

An interesting method was employed by Li and coworkers [88], who used collagen micropatterning of 6 well-plates to culture primary rat hepatic spheroids, using collagen islands (Figure 2.14) as a method to control spheroid size. Freshly isolated hepatocytes were allowed to adhere onto 50, 75 and 100 µm diameter islands for 2 hours before the unattached cells were removed. These cells formed what the author referred to as “pucks”, which were later introduced into an emulsion based microfluidic platform that encapsulated these “pucks” in a polyethylene glycol (PEG) hydrogel, presumably to prevent further aggregation during exposure. This hydrogel is relatively inert [89] and has been used in other culture application [90] [91]. One thousand of these microtissues (per condition) were exposed to Paracetamol for 24 hours and viability assessed using calcein AM (live) and ethidium homodimer (dead) fluorescent staining. Individual microtissue viability was assessed using flow cytometry. A large decline in viability was observed at the highest

concentration (40 mM), but not at 10 or 20 mM. Of interest was that these “pucks” contained between 6 to 12 cells / island, which is far below the number of cells considered needed to form functioning hepatic units (worth noting 1000 pucks were used equalling between 6000 to 12000 cells in total). However, no analytical measurements were performed to conclusively confirm the presence of metabolites.

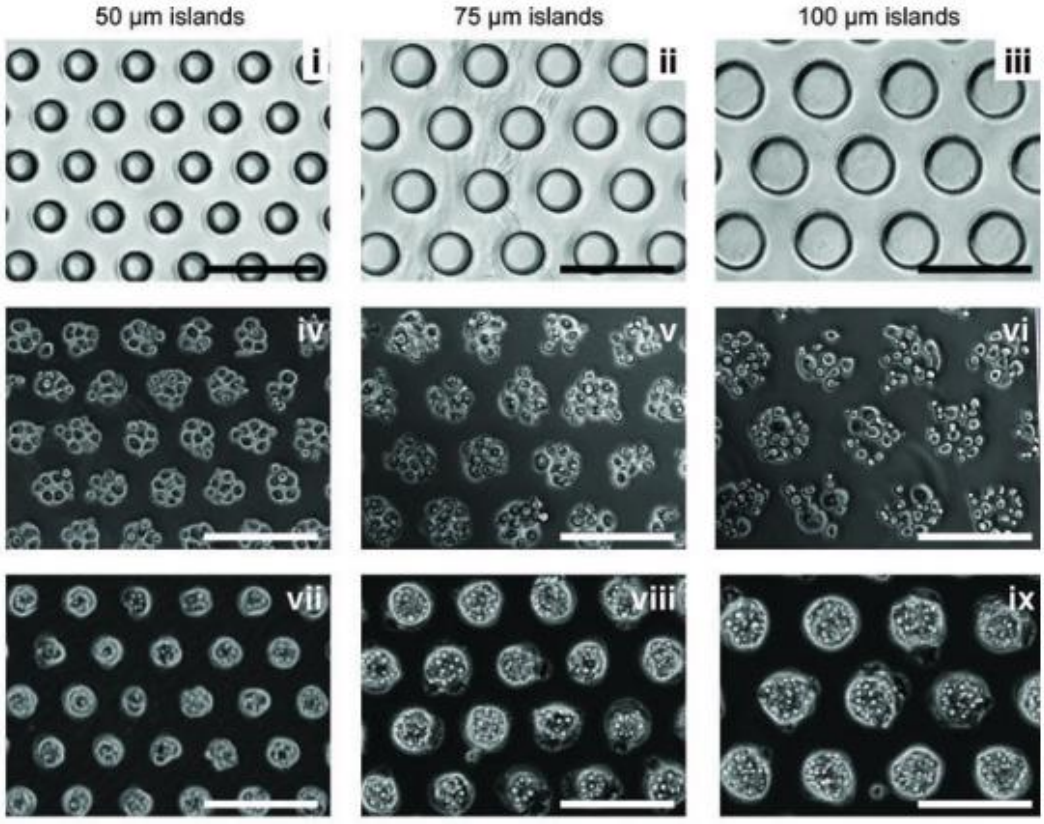


*Figure 2.14 (i – iii) Image of PDMS mould to define collagen islands, (iv – vi) Seeding of hepatocytes and (vii – ix) Aggregation into spheroids after 24 hours culture (Scalebar = 200 µm).* [88]

Wong and coworkers [92] employed concave microwells (Figure 2.15) to co-culture primary rat hepatocytes and primary rat hepatic stellate cells into spheroids. Albumin and urea secretion was monitored over 9 days. CYP3A4

activity was measured using a substrate (Luciferin-PFBE) which showed increased CYP3A4 activity and albumin secretion in the co-cultured spheroids compared with the mono-cultured spheroids. They also performed immunochemistry staining to confirm the presence of bile canaliculi and these appeared more obvious in the co-cultured spheroids.

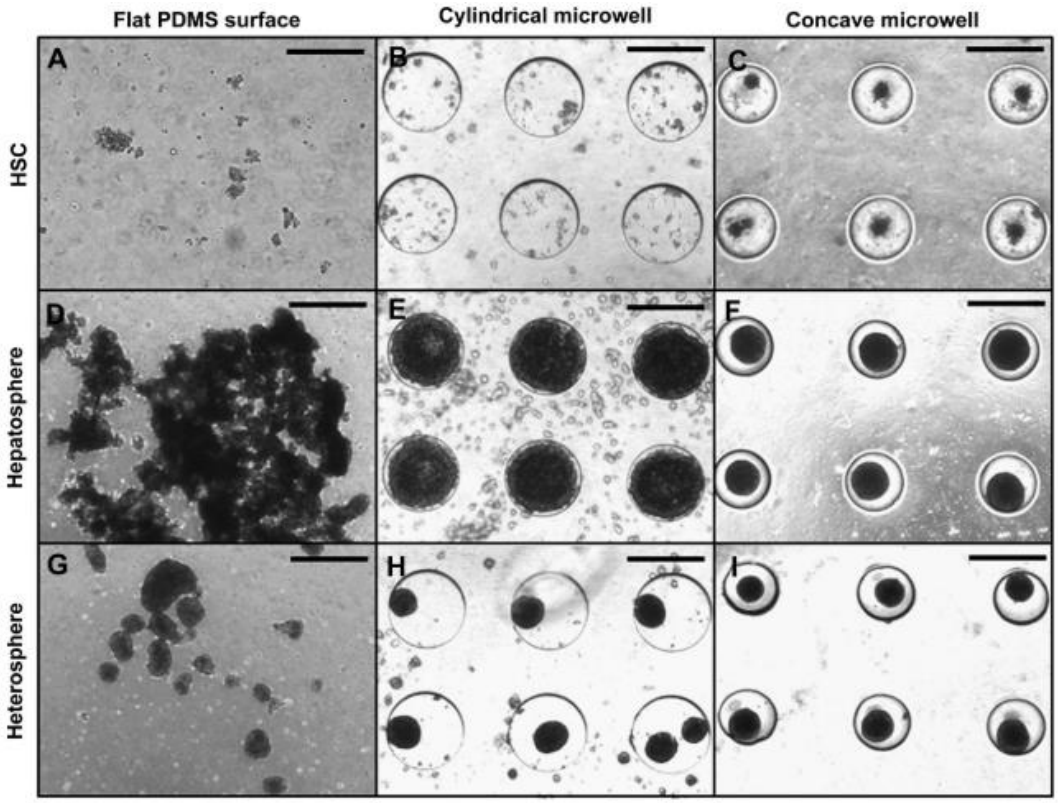


*Figure 2.15 Hepatic stellate cells cultured on a (A) flat surface, (B) in the microwells and (C) in the concave wells; Primary rat hepatocytes cultured on a (D) flat surface, (E) in the microwells and (F) concave wells; Co-cultured hepatocytes and stellate cells on a (G) flat surface, (H) in the microwells and (I) concave wells after 3 days (Scalebars = 50 µm).* [92]

Yoon et al [93] fabricated a PDMS chip with concave microwells and seeded primary rat hepatocytes at a density of 1 x $10^5$ cells / chip. These cells were trapped in the wells and perfusion was produced using an osmosis-driven

pump and compared to cells seeded in a flat chamber. Albumin and Urea was measured every 2 days in culture and their results demonstrated that spheroids produced significantly more during culture. Next, they measured gene expression, specifically UGT1A5 (Phase II) and CYP1A2 (Phase I). Their results indicated increased expression of these genes in the spheroids cultured under perfusion, compared to static spheroids and monolayer cultures.

Lee and coworkers [94] demonstrated that primary rat hepatic spheroids and rat stellate cells were able to communicate without direct cell-cell contact by culturing the cells in separate (but connected) compartments on a microfluidic platform (Figure 2.16) under perfusion. For the hepatocytes, $2 \times 10^5$ cells were introduced into the concave chamber and the same amount was introduced into the flat chamber coated with collagen type I. Afterwards flow was induced to remove any un-trapped hepatocytes and unadhered stellate cells. Scanning electron microscopy revealed differences in the surface characteristics between the mono and co-cultured platforms, indicated by the smooth surface of the co-cultures compared to the monocultures. The authors suggested this may be due to the cell-cell junctions being tighter in the co-cultures. The co-cultures produced significantly more albumin from day 3 to day 8 *in vitro* compared to the monocultures. These results demonstrated that cellular communication (likely via cytokines) can occur *in vitro* without direct cell-cell contact.

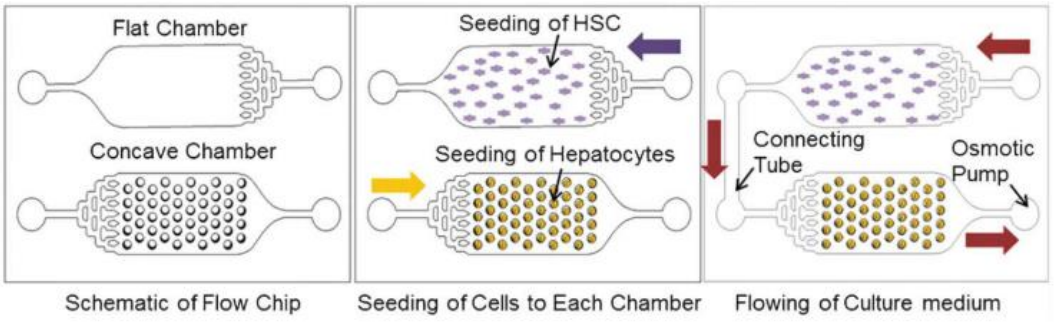


*Figure 2.16 Diagram of the different culturing chambers for the hepatic stellate cells (HSC) and the hepatocytes, the seeding protocol and the final connected platform.* [94]

Apart from spheroids, hepatic cord-like structures can also be cultured in microfluidic platforms. Toh and coworkers [95] cultured hepatocytes on a microfluidic platform (Figure 2.17) in this configuration. Eight channels (length x width x height: 1000 x 200 x 100 µm) were seeded with 3 x $10^6$ cell / ml of primary rat hepatocytes (suspended in methylated collagen to provide an ECM) into a central channel with two adjacent channels used for perfusion. The functionality of the platform was compared to that of a collagen-coated monolayer of primary rat hepatocytes after 72 hours of culture. A gradient generator was part of a second layer to the platform which was used to expose each channel to a different concentration of five drugs known to induce hepatotoxicity at high concentrations. They found that the platform performed similarly to a collagen sandwich culture with regards to drug induced toxicity and outperformed the monolayer culture significantly.

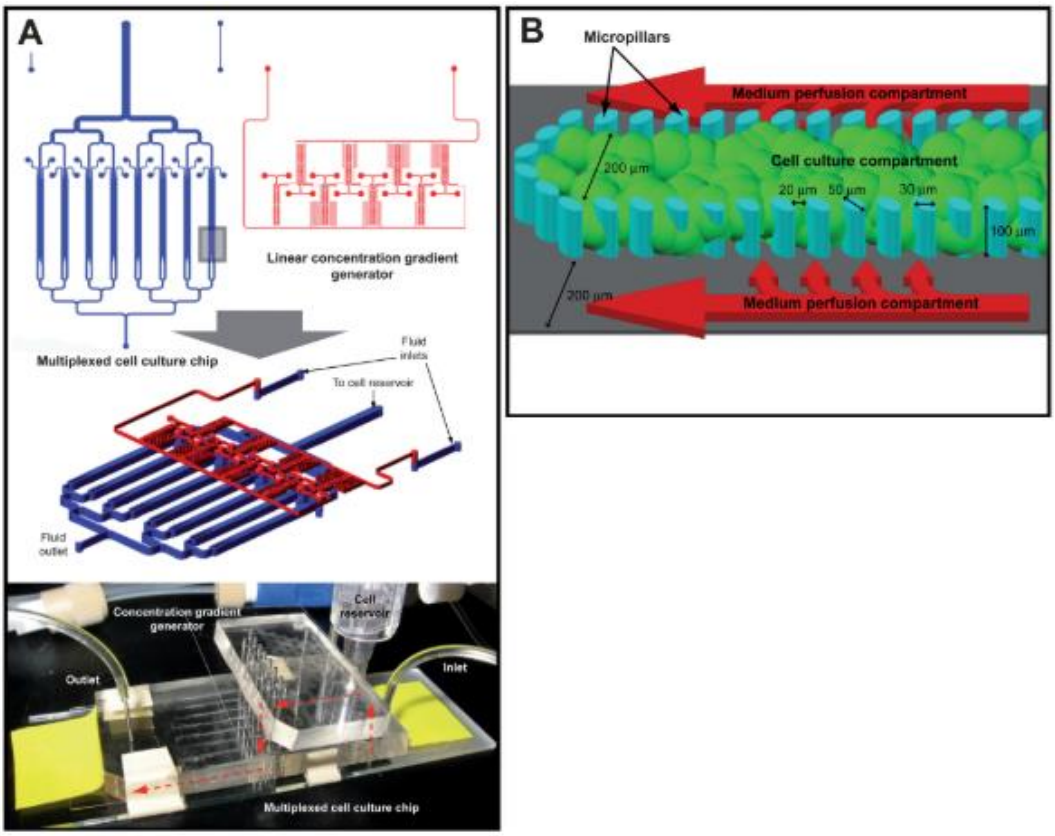


*Figure 2.17 (A) Diagram and image of the microfluidic platform with (B) a diagram detailing the dimensions of the micropillars that simulate the endothelial barrier found in vivo.* [95]

Nakao et al [96] also cultured primary rat hepatocytes into a cord-like structure. Their aim was to design the microfluidic platform (Figure 2.18) to allow cells to arrange in two rows under perfusion to encourage the formation of bile canaliculi. A concentration of 1 x $10^7$ cells was introduced into a chamber coated with collagen to aid in cell attachment; then after 1 hour a Matrigel solution was perfused into the culture channel. Their results indicated the formation of bile canaliculi, through the fluorescent substrate 5-(and-6)-carboxy-2',7'-dichloro-fluorescein (CDFDA) that is transported into the canaliculi via the multidrug-resistance protein 2 (MRP2) transporter. Although no hepatotoxicity assays were performed, the authors suggested that due to

the establishment of polarity in the cords, it is likely the cells retained other liver-specific functions that can be used for investigating hepatotoxicity. Future experiments would need to be conducted to confirm that the hepatocytes in the cord are capable of Phase I and Phase II metabolism though the addition of drugs which cause DILI.

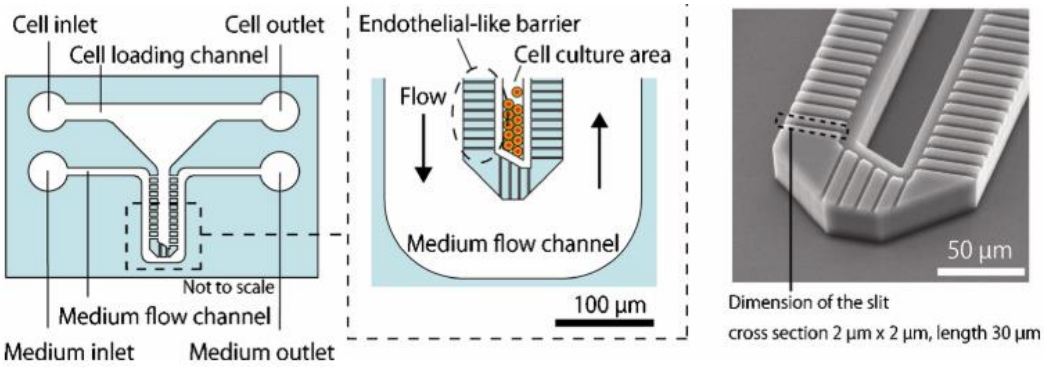


*Figure 2.18 (Left and middle) Diagram of the microfluidic platform and (Right) an image taken using scanning electron microscopy.* [96]

Although both these platforms are not compatible with high-throughput capabilities, they are important to mention, as they demonstrate the versatility of microfluidic platforms. Culturing hepatocytes into this cord-like structure without using a microfluidic platform would be extremely difficult if an ECM was not employed.

It is clear that microfluidic platforms have huge potential in generating large number of 3D structures that can be used for hepatotoxicity testing.

Several types of droplet-based and microwell platforms found in literature are shown in Table 2.2 (that have been specifically used to culture 3D hepatic structures):

*Table 2.2 A comparison of other microfluidic platforms capable of culturing 3D hepatic structures.*

| Author (Year) | Cell type | Seeding density | Tests | Disadvantages | Ref |
|---|---|---|---|---|---|
| *Droplets* | | | | | |
| Chen et al (2016) | HepG2 and NIH-3T3 fibroblasts | 1 x $10^8$ cells / ml | Albumin Urea | No on-chip storage | [97] |
| Siltanen et al (2017) | Primary rat hepatocytes | 20 – 40 x $10^6$ cells / ml | Albumin Urea CYP3A4 induction | No toxicity assays performed | [98] |
| *Microwells* | | | | | |
| Okuyama et al (2010) | Fibroblast and HepG2 | 2 x $10^7$ cells | Concentration gradient of fluorescein | No toxicity assays performed | [99] |
| Patra et al (2016) | HepG2 | 3.4 x $10^6$ | Cisplatin Resveratrol TPZ | Short culture length (3 days) | [100] |
| Choi et al (2016) | Primary rat hepatocytes | 1 x $10^5$ | Albumin Urea RT-PCR Optimal flow | No toxicity assays performed | [93] |

Acquisition of data from these platforms is important, and many methods are employed. Fluorescent assays are useful for structure related information, but a growing field of data acquisition is using chromatography and spectrometry. Chromatography and spectrometry allows more in-dept data acquisition on the biochemical processes that are going on within cell cultures. The second part of the chapter will introduce both analytical techniques.

## 2.4 Liquid chromatography-mass spectrometry

Liquid chromatography-mass spectrometry is a widely used method for identifying chemical components in a sample. This technology is highly sensitive, specific and different modes can be employed depending on the level of data required or the type of sample available. This section will briefly explain the principles of liquid chromatography and mass spectral identification. It will end with a subsection on biological applications and some specific examples in literature.

### 2.4.1 Principles and fundamentals

Liquid chromatography (Figure 2.19), in its simplest form, is a technique used to separate a sample into its individual components based on the interaction of said components with the mobile – and stationary phase. The mobile phase is the liquid used to drive the sample through the solid stationary phase. Once the components are separated, the relative abundance can be determined based on the amount of absorbance (or other response) measured by a detector.

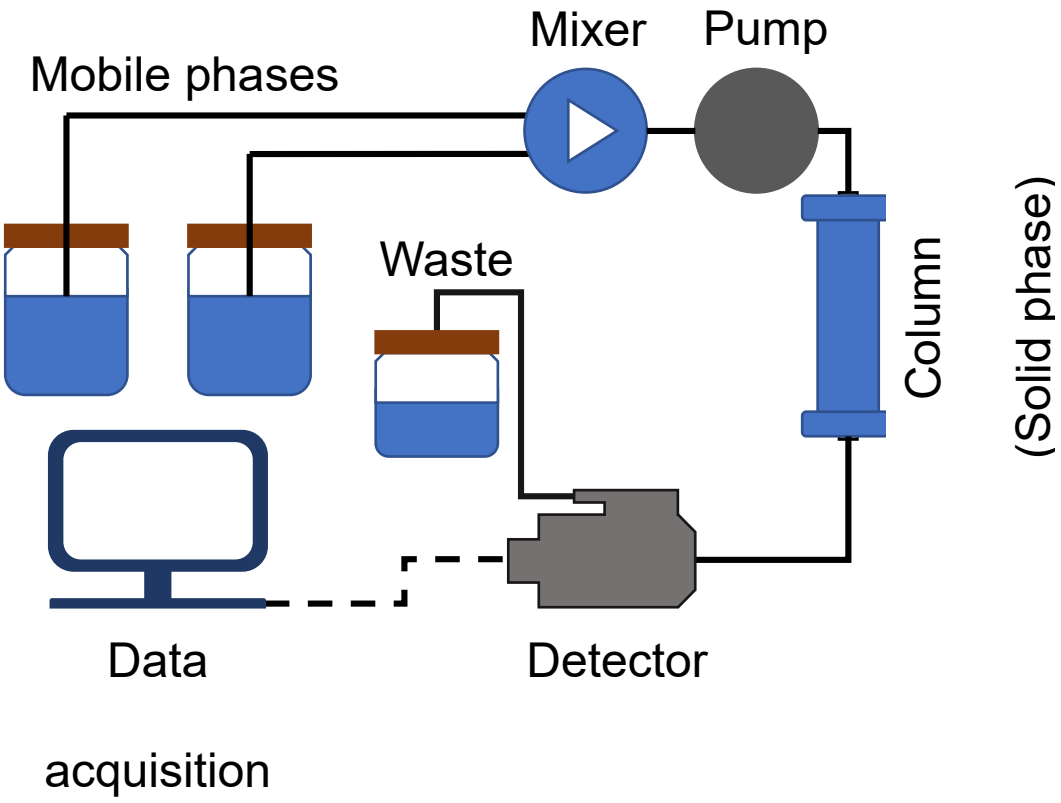


*Figure 2.19 A diagram of the main components that make up an HPLC. Two different liquids make up the mobile phase, which is used to drive the sample through the column (stationary phase). As the components exit the column at different times a detector can measure the absorbance (or other chosen parameter) and determine the relative abundance of the component of interest.*

In the last few decades high performance liquid chromatography (HPLC) has been combined with mass spectrometry acting as an additional, powerful detection method, referred to as LC-MS. The separating capabilities of liquid chromatography compliments mass spectrometry and allows more accurate data acquisition from complex samples. In fact, consecutive mass spectrometry-mass spectrometry (MS/MS) analysis is employed in both the pharmaceutical industry and academic field. This tandem analysis allows for increased sensitivity and more accurate identification of the molecular

structure of the components of interest [101]. Some principles of mass spectrometry will be discussed and how the two technologies complement each other.

*Mass spectrometry*

Mass spectrometry (MS) is an extremely powerful analytical technique used to identify and quantify unknown components in a sample, based on structural and chemical properties of different molecules present in the sample. The process involves ionising the component, which could lead to fragmentation of the compound and characterizing these structures by their mass-to-charge (m/z) ratio. The output is referred to as the mass spectra, which is a plot of the relative abundance and the m/z ratio of the ions (or fragments). The components of a mass spectrometer (in brief) are: the ion source, a mass analyzer and a detector. The ion source (e.g. electrospray ionization or chemical ionisation) is used to ionise the sample (e.g. by bombarding the components with electrons) resulting in charged fragments (through loss of an electron or addition of a proton which results in positively or negatively charged fragments). These fragments are typically separated by the m/z ratio by accelerating and deflecting them past a magnetic field. The energy required and time taken to reach the detector is used to calculate the m/z ratio, which can be compared to known masses of molecular standards.

The type of sample will determine the type of ionisation method used. For example, electrospray ionisation (ESI) is convenient for samples with

components with large masses (macromolecules) as the lower fragmented m/z ratios tend to fall in the range of masses that can be detected by the detector.

*Matrix-assisted laser desorption*

Another widely used ionisation method is matrix-assisted laser desorption ionisation (MALDI). The main difference between these two methods is the state of the sample when ionised. In MALDI the sample is dissolved in a matrix before ionisation. This technique also has an advantage of (generally) producing less fragmentation than ESI, making interpretation of the mass spectral data easier.

The mass analyzer component is the part of the instrument that separates the different components based on their m/z ratio and is usually driven by an electrical or a magnetic component. There are different types of analyzers, each with their own advantages and disadvantages.

Three widely employed analyzers that function based on different methods of separation will be briefly introduced.

*Time of Flight*

The first type is the Time of Flight (ToF) analyzer that separates the m/z ratio based on the time for an ion of specific mass to reach the detector [102]. An advantage of this type of analyzer is that almost all the ionised components will eventually reach the detector. However, this type of analyzer is not widely used in the pharmaceutical industry, likely due to its limited application of tandem (consecutive) MS experiments (LC-MS/MS). MS/MS analysis leads to

more detailed analysis of a sample by focussing on m/z ratio's that fall within a set range.

*Quadrupole analyzer*

The next mass analyzer is a Quadrupole analyzer consisting of 4 symmetrically placed rods. Two rods are negatively charged (and the other two positively charged), influencing the direction of the incoming ions based on their charge. The charges switch the current in these rods, effectively changing the path the charged ion was originally travelling on. By manipulating the frequency of the changing charges on the rods only components within a specific m/z range would reach the detector, while others would simply "crash" into these rods. The advantage of using this type of analyzer is the relatively low cost and robustness of the equipment, however, only a small mass range can be effectively analyzed.

*Ion Trap analyzer*

Finally, the Ion Trap analyzer (Figure 2.20). These provide high resolution data in terms of accurate m/z ratios and the ability to be combined with additional MS experiments. The relative abundance of the ions that reach the detector can then be converted into a signal known as a mass spectrum. Signals grouped closely together can be used to identify the compound, based on the fragmentation pattern. For example, carbon has two naturally occurring isotopes ($^{12}C$ and $^{13}C$) that occur in a 98.9 to 0.1 ratio, so a second smaller ion will be detected 1 m/z unit heavier next to the parent ion, but at a 98.9:0.1 ratio.

Similarly, chlorine also has two naturally occurring isotopes ($^{35}Cl$ and $^{37}Cl$) at a 75.8 to 24.2 ratio, thus when a compound contains 2 Cl atoms, the fragmentation pattern will display 3 grouped peaks in a 9:6:1 ratio at 2 and 4 m/z units 2 higher.

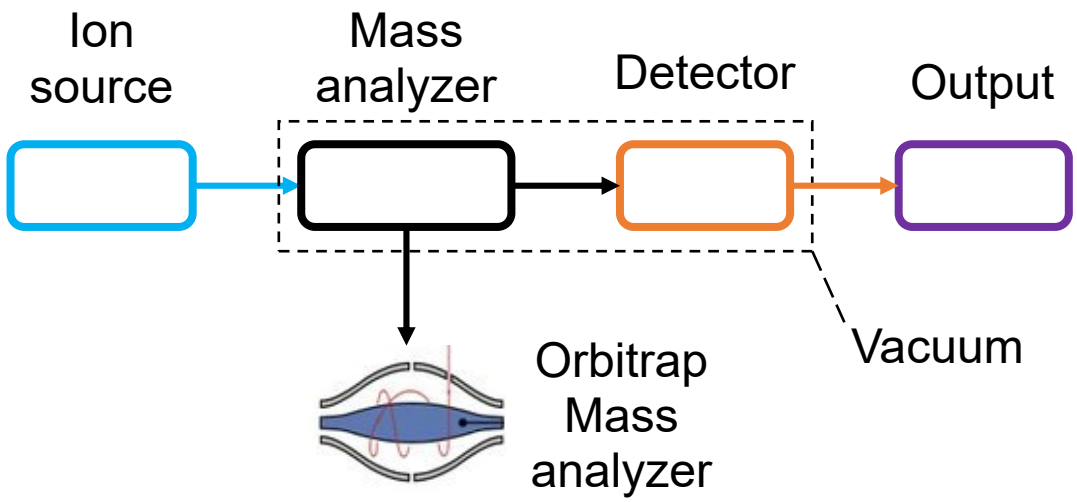


*Figure 2.20 A diagram showing the components that make up a Ion trap Mass spectrometer.* [103]

## 2.5 Three-dimensional liver cultures in microfluidic platform combined with LC-MS

Combining microfluidic platforms with LC-MS to determine the potential hepatoxicity of a drug may provide advantages compared to conventional methods, as this technology is highly-sensitive and specific. The high-throughput capabilities of microfluidic platforms and inherent miniaturisation could lead to a reduction of resources needed to carry out multiple assays.

Rennert and coworkers [104] tried to more closely mimic the *in vivo* architecture of the human liver sinusoid by culturing hepatocytes along with NPCs in a layered assembly (Figure 2.21) *in vitro*. A mixture of HepaRG (3

x$10^5$) and LX-2 stellate (4 x$10^4$) cells were cultured on the bottom of a PET membrane (pore size and density: 8 µm and 1 x $10^5$ pores/$cm^2$) opposite to a mixture of the Human umbilical cord vein endothelial cells(HUVECs) (3 x $10^5$) and Peripheral blood mononuclear cells (1 x $10^5$). The difference in metabolic capabilities between a static and continuously perfused platform was determined by using Midazolam as a substrate for CYP3A4 and measuring the formation of the hydroxylated metabolite (1-hydroxy-midazolam) after 6 hours incubation, confirmed using LC-MS/MS. Results indicated enhanced metabolism for the perfused cultures through higher detected levels of the hydroxylated metabolite. Although this platform mimics the in-vivo architecture of the liver, it provides lower throughput compared to platforms that culture spheroids.

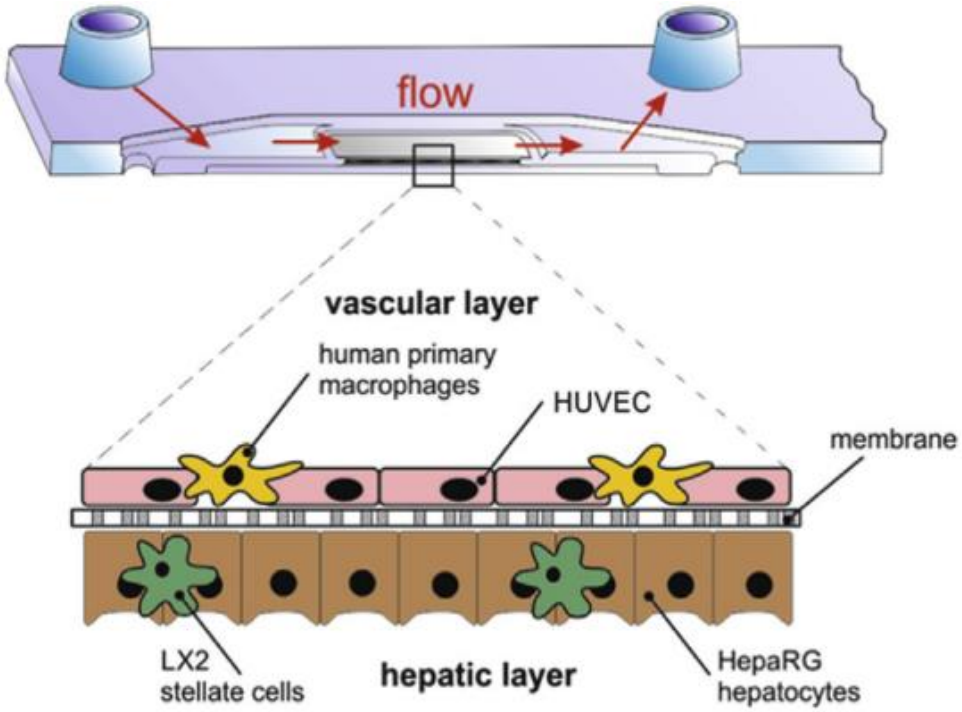


*Figure 2.21 Diagram of the (Top) microfluidic platform and (Bottom) layering of the hepatocytes along with NPCs.* [104]

Yu et al [105] developed a “liver-on-chip” platform that perfused rat hepatocyte spheroids between a porous membrane (Parylene C) and a glass cover (Figure 2.22) for 24 days, while assessing their ability to metabolize five model drugs. They approached some issues encountered using microfluidic platforms for chronic hepatotoxicity testing, namely contamination, clogging and bubbling, by integrating electronic components (heater and debubbler). They measured the expression of Phase I metabolizing enzymes (CYP1A2, CYP1B1/2 and CYP3A2) through the production of metabolites after acute exposure either Acetaminophen (APAP), Bupropion or Midazolam. They detected larger concentrations of the metabolites produced in the spheroids compared to the collagen sandwich cultures. Viability after acute and chronic exposure to Diclofenac and Paracetamol were also monitored. Acute toxicity cultures were exposed to a range of concentrations (0 – 1000 µM for Diclofenac and 0 – 40 mM for Paracetamol) for 24 hours while the chronic toxicity cultures were exposed every 2 days over a 14-day period. The viability was calculated on day 1 and day 14. While this study provides great details of how versatile microfluidic platforms are by allowing prolonged culture and high-throughput, the spheroids were formed off-chip in 48 well-plates. A method to constrain the size of the spheroids and to form them on chip would be more advantageous, as large spheroids (> 500 µm diameter) may develop a necrotic core.

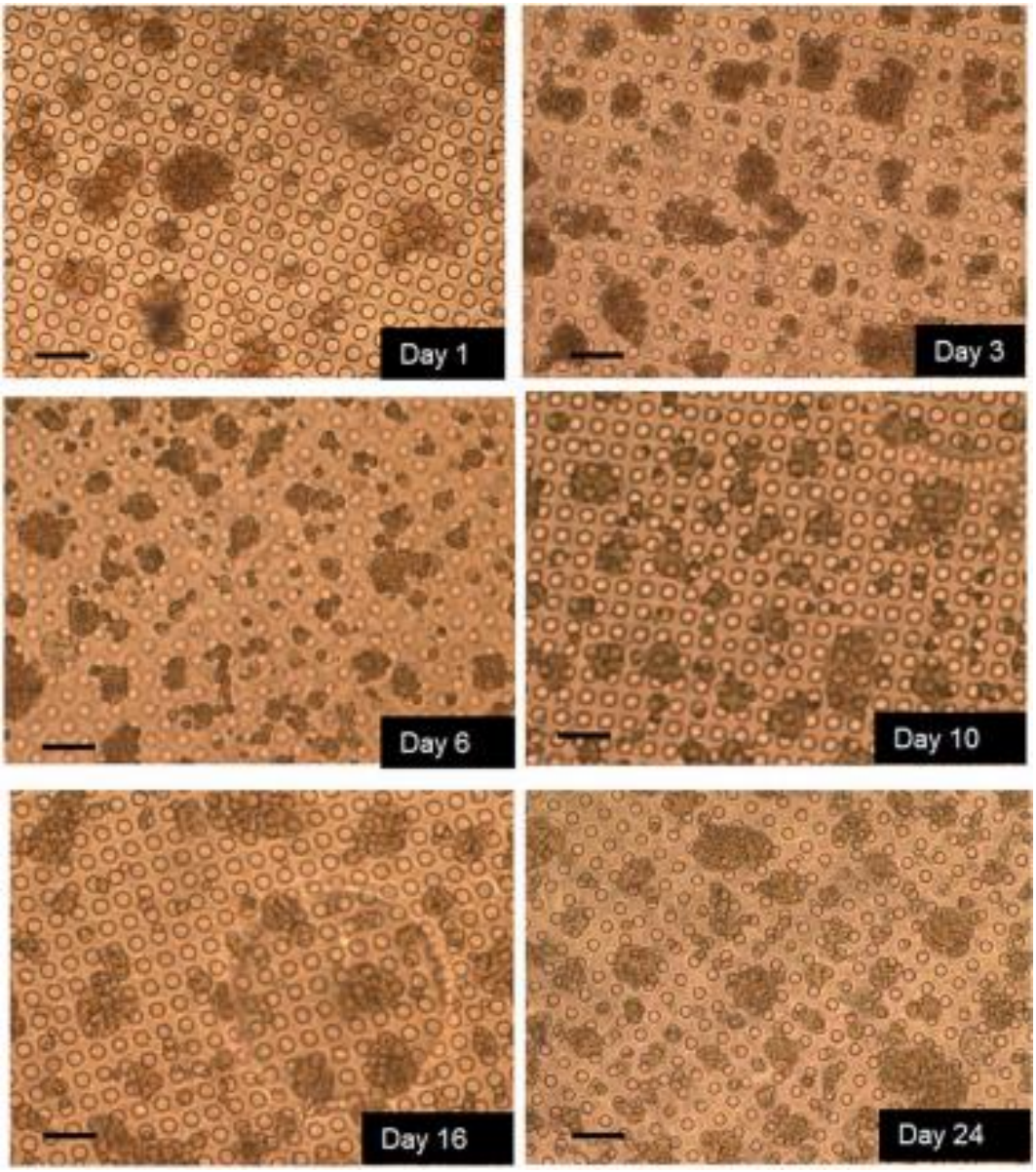


*Figure 2.22 Microscopy image of hepatic spheroids sandwiched between a glass slide and a porous membrane (Scalebar = 100 µm).* [105]

A study by Gunness and coworkers [106] also used the commercially available (GravityPLUS plates – InSphero) hanging drop method to culture HepaRG spheroids and compare the metabolizing capabilities to cells cultured in monolayer (collagen-coated 24 and 96 well-plates). Paracetamol, troglitazone and rosiglitazone were used in varying concentrations for 24 hours on day 4 and day 21 and the viability of the spheroids were determined using an ATP

assay. Using 2 x $10^3$ cells / spheroid the $EC_{50}$ value determined for Paracetamol was 10 and 3-fold lower in the spheroids compared to the monolayered cultures, on day 5 and 22, respectively. The expression of CYP2E1 was also compared between the spheroids and the monolayered cultures (Figure 2.23) through LC-MS by the conversion of chlorzoxazone to its hydroxylated metabolite, (OH-chlorzoxazone). Their results indicate that the spheroids had actively expression of the CYP2E1 protein.

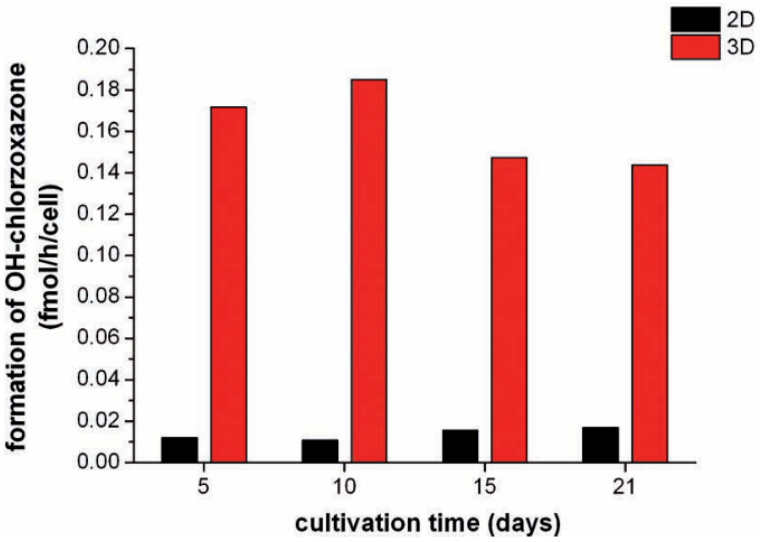


*Figure 2.23 Graph indicating the formation of OH-chlorzoxazone of hepatic spheroids (3D) compared to monolayer (2D) cultures.* [106]

In summary it has been shown that spheroids are at least as (if not more) metabolically active as sandwich cultures. Culturing cells as spheroids have the advantage of increasing the amount of individual data points that can be generated compared to most other 3D structures (e.g. cords or layered configurations) by using less cells to form functioning culture units. Most commonly a few hundred to thousand cells are used to create a single function spheroid, depending on cell source or method employed. Some methods

involve multiple steps to generate spheroids which inherently increases cost and opportunities for errors to occur; or alternatively rely heavily on the skill of the user. Very little information is available on the effect of using low cell numbers to generate functional hepatic spheroids.

## 2.6 Objectives

The aim of this thesis is to investigate the integration of microfluidic and 3D culture techniques to assess the metabolizing capabilities of liver spheroids. The novelty of this thesis is in exploring how miniaturised 3D liver assays can be obtained to retain full metabolic activity using LC-MS.

# Chapter 3. Methods and Materials

## 3.1 Introduction

This chapter will detail the methods and materials used to complete the experiments described in the thesis for both the preliminary experiments using HepG2 cells and the subsequent experiments using primary rat hepatocytes. A list of materials and equipment used can be found in the Appendix.

## 3.2 Device fabrication

This section will introduce the processes involved in fabricating the microfluidic platforms.

### 3.2.1 Droplet-based platform

The wafers used to cast the droplet microfluidic platforms used in these experiments were fabricated by myself using photo-lithography and soft-lithography. The wafers for the multi-array and single array platforms were made by colleagues (T Christ and G Robertson). The droplet-based microfluidic platform design (Figure 3.1) used was modified from a platform kindly provided by Dr Michele Zagnoni; with a few minor alterations to address cell-specific issues identified during the start of this research project. These alterations included shortening of the cell inlet (Figure 3.1 (B)) to minimize cell aggregating in the channel and increasing the length of the outlet (Figure 3.1 (E)). The latter was increased as it was noted that air could be introduced from the outlet when removing the tubing from the inlets. The longer outlet channel

increased the volume and served to reduce the chance of the air reaching the trap closest to the outlet. The microfluidic designs were created using CorelDRAW X5 and sent for printing (JD photo tools, UK) on acetate photomasks. Topological features in the x and y-axis were created this way, while the z-axis was controlled by the thickness of the photoresist after spin-coating during the fabrication process.

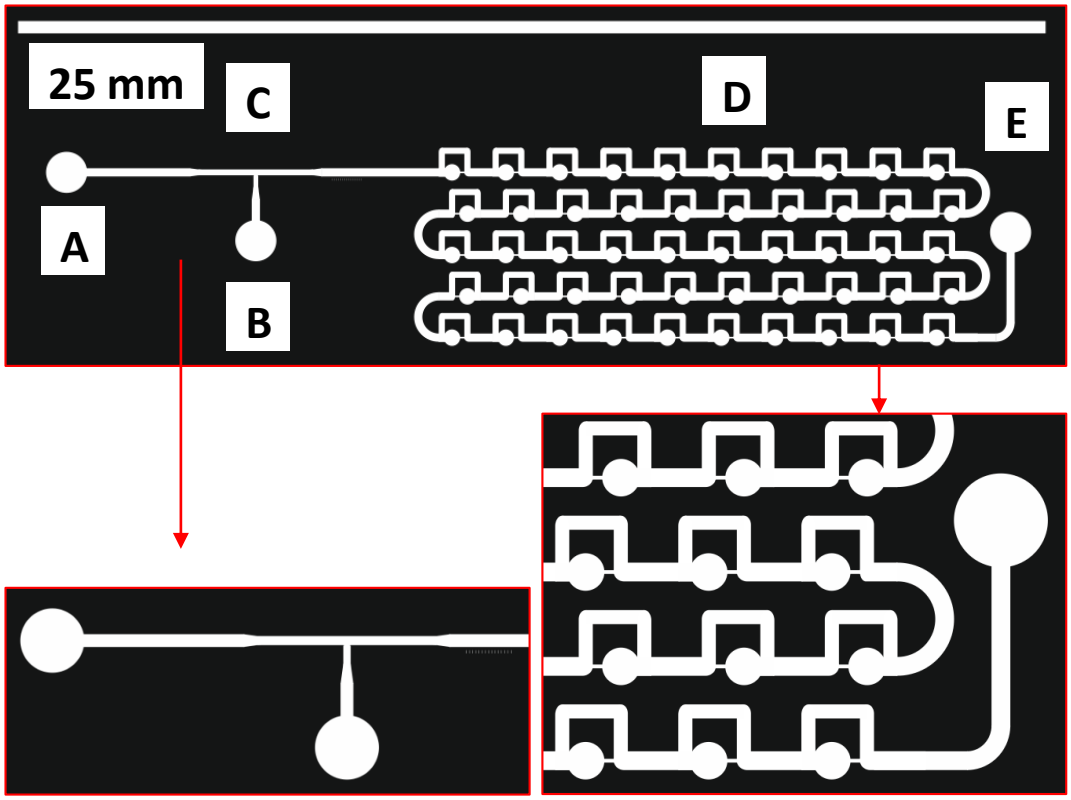


*Figure 3.1 (Top) Schematic of the droplet-based platform (White bar = 25 mm): (A) The oil and surfactant inlet (continuous phase), (B) the cell inlet (aqueous phase), (C) the T-junction where the droplets are generated, (D) the droplet parking network where the droplets are stored and (E) the outlet. (Bottom left and right) Magnified image of the inlets and T-junction and the parking network and outlet. Images created in CoralDRAW X5.*

A silicon wafer (University Wafer, USA) was cleaned using three solvents in sequence (acetone, methanol, isopropanol) for 3 minutes each in a sonic bath

and dried at the end using compressed nitrogen. The wafer was placed on a hot plate at >200 °C for a minimum of 1 hour to dehydrate, before being allowed to cool to room temperature. Subsequently, SU 3035 photoresist (MicroChem, Newton, MA) was poured onto the wafer and spin coated to produce an evenly distributed layer. The thickness of the coating was controlled by the spin rate, based on the manufacturer's recommendation for the specific photoresist. Wafers coated with a thickness near 100 µm were allowed to rest for 15 minutes before being placed on a hot plate at 95 °C for 20 minutes. The wafer was rotated approximately every 5 minutes during this "soft-baking" process and once off the hotplate allowed to cool to room temperature. Next the acetate photomask was placed over the wafer and exposed to collimated UV light (150 – 200 mJ/cm$^2$) for 40 – 135 seconds, depending on the photoresist thickness. Afterwards, the wafer went through a "post-bake" stage on a hot plate (1 minute at 65 °C, then 7 minutes at 95 °C), then was taken off the hotplate and allowed to cool to room temperature before development. The wafer was immersed in MicroPosit EC solvent and gently agitated, removing any unlinked SU8. A soft plastic pipette was used to direct developer between features if needed. The wafer was removed and gently rinsed with IPA before being dried using a stream of nitrogen. The wafer finally went through a "hard-bake" stage on a hot plate with an initial temperature of 95 °C, ramped up in increments to a maximum of 210 °C over approximately 30 minutes. For designs which required a thickness larger than 100 µm an additional photoresist coating and "*soft-bake*" step was carried out before the UV exposure step.

After fabricating the master wafer (Figure 3.2), silinization was carried out to prevent adhesion of the poly(dimethyl siloxane) (PDMS) to the wafer used to cast the platform. The wafer was exposed to oxygen plasma (below 0.4 mbar) for 2 minutes at 200 W and placed in a vacuum with 50µl of 1H, 1H, 2H, 2H-perfluorooctyl-trichlorosilane in a weighing boat for 45 minutes. Wafers patterned and silanized this way allowed multiple casts to be obtained using soft-lithography and could be reused multiple times. The wafer was placed inside a tin foil covered petri dish to act as the mould. Liquid PDMS (Sylgard 184 Silicone Elastomer, Dow Corning, USA) was mixed with a curing agent in a 10:1 ratio and poured into the mould to an approximate thickness of 5 mm. The mould was placed in a desiccator and degassed for 40 minutes to remove any air bubbles that have been introduced during mixing. The PDMS was set in an oven at 80 °C for a minimum of 2 hours. The cured PDMS was cut from the mould using a scalpel and divided into individual platforms. Inlets and outlets were created by punching a hole over the features using a 1 mm biopsy punch.

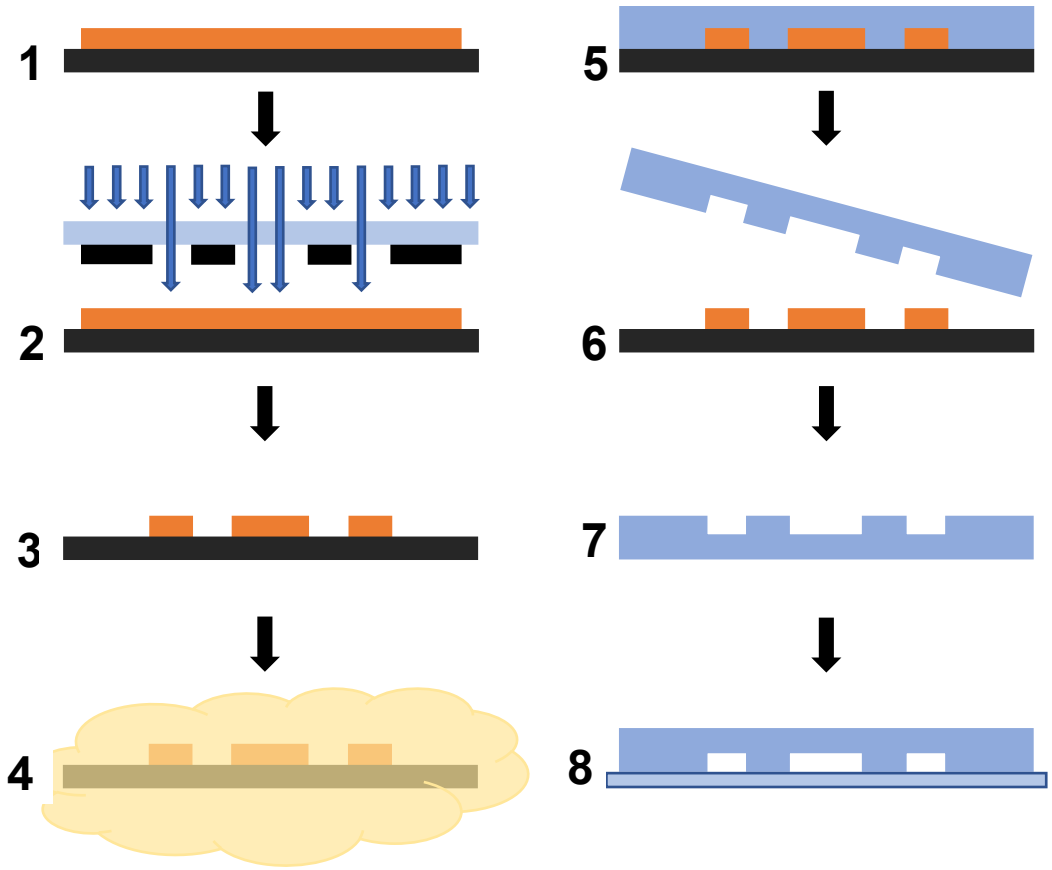


*Figure 3.2 Diagram of the fabrication process: (1) SU 3035 is spin coated on a cleaned wafer to produce an even thickness, (2) An acetate mask is placed over the wafer which is exposed to UV which cures the uncovered SU 3035, (3) The uncured SU 3035 is removed and the wafer is (4) silanized, (5) PDMS is poured onto the wafer and allowed to set before being (6) removed, (7) the PDMS is then (8) bonded to a cleaned glass slide.*

Prior to bonding to a glass slide, the PDMS sections were cleaned of debris using Scotch tape (810), which was applied to the surfaces and removed. Co-workers(Dr. G Robertson) [107] (and others [108][109]) have found previously that this process does not interfere with bonding the PDMS to the glass slide. Another method to clean the PDMS would be to use a solvent in a sonic bath, but this process is more time consuming and produces additional solvent waste. Bonding was carried out by treating the PDMS to oxygen plasma below 0.3 mbar for 6 seconds at 100 W. This process results in a change of the –O-

$Si(CH_3)_2$ groups on the PDMS surface to (SiOH) groups, forming irreversible covalent Si-O-Si bonds when the PDMS and glass comes into contact. Light pressure was applied to the PDMS to ensure no air was trapped between the bonded surfaces. The platforms were placed in an oven (80 °C) and left overnight to increase the strength of the bond. On the morning of loading, the inner channels of the droplet-based devices were treated with Aquapel, to increase the hydrophobicity of the channels, for approximately 30 seconds. Using a 1 ml syringe placed over an inlet, Aquapel solution was injected and later displaced using air from an empty 1 ml syringe. The platform was moved under a microscope and primed for loading.

### 3.2.2 Microwell array platforms

Two alternative microfluidic platforms (Figure 3.3 and 3.4) were kindly provided by Dr Zagnoni based on their ability to trap cells using “gravity-driven” microwell arrays. The first platform was composed of two bonded layers of PDMS. The top layer consisted of 2 reservoirs connected by a straight channel. The bottom layer possessed four microwell arrays, each made up of 8 x 8 square individual wells (150 x 150 µm). When the top and bottom layers have been aligned the arrays and the channel (connecting the two reservoirs) form a culturing environment capable of holding in excess of 1500 individual spheroids / platform [110].

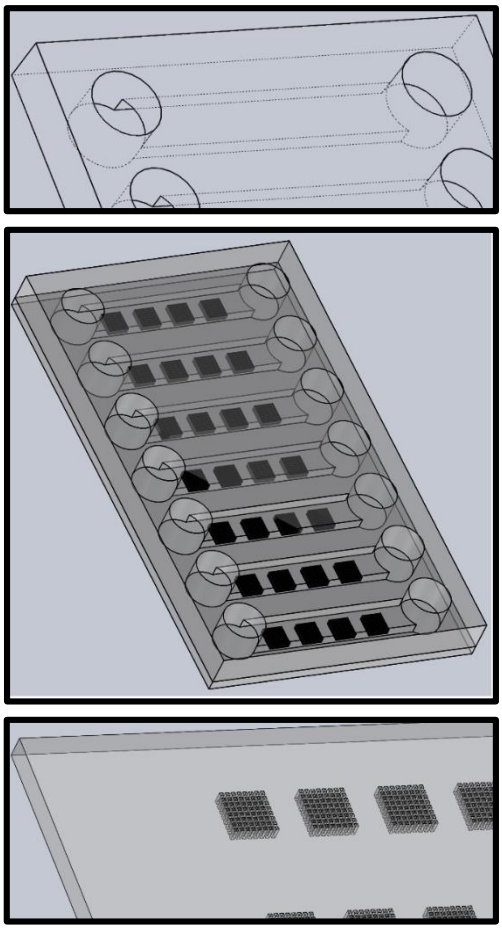

*Figure 3.3 A SolidWorks drawing of the multi-array platform provided by Dr Zagnoni. (Top) The top layer (wire frame view) showing the two reservoirs connected by a straight channel, (Middle) the complete platform and (Bottom) the bottom player indicating the 4 microwell arrays. (Dimensions not to scale)*

The inner surface of the platform had to be treated with a synperonic solution a day before loading cells. To treat the platform, the already bonded devices were exposed to oxygen plasma (200 W for 2 min). Afterwards the reservoirs were filled with a 0.1 % (w/v) synperonic solution (in $dH_2O$). The platforms were stored in a plastic container, with a PBS filled weighing boat in the incubator overnight. The following morning the platforms were gently flushed twice using a 1 ml syringe filled with PBS (covering one reservoir) and an empty 1 ml syringe (covering the other), alternating between withdrawing and producing

flow. The reason a syringe was used instead of a pipette was to remove as much of the synperonic as possible, as this has the potential to damage the HPLC column or affect the results during LC-MS analysis. Lastly the platforms were filled with medium and placed in the incubator (minimum 1 hour) to be retrieved just before seeding the hepatocytes.

Near the end of this project an even smaller platform (Figure 3.4) was kindly provided by Dr Zagnoni. This platform also used microwells to capture cells but consisted of a single 4 x 4 array per channel.

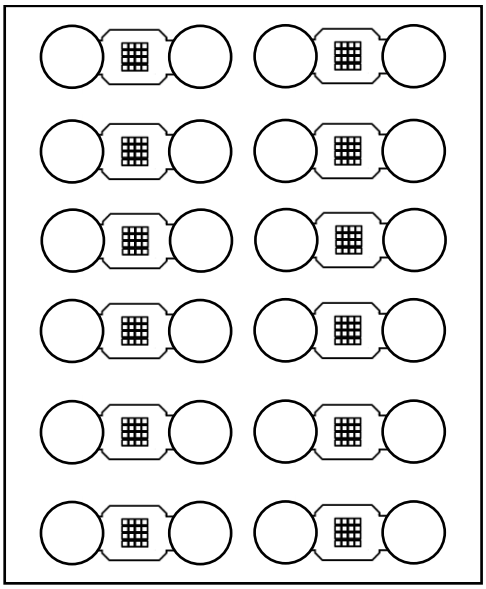

*Figure 3.4 Diagram of the single array platform provided by Dr Zagnoni. A single platform contained 12 channels, each enclosing a 4 x 4 microwell array. (Dimensions not to scale)*

## 3.3 HepG2 and Primary Rat Hepatocyte culture

All protocol used are in accordance with standard University of Strathclyde operating procedure unless stated otherwise.

### 3.3.1 HepG2 culture

*Stock solutions*

Versene (EDTA) in PBS (pH 7.2) – Made with NaCl (12 g), KCl (0.30 g), $Na_2HPO_4$ (1.73 g), $KH_2PO_4$ (0.30 g) and 2.25 ml Phenol red 1 % (w/v) dissolved in 1.5 L distilled water and autoclaved. Stock solutions were aliquoted in 20 ml universal containers and stored at room temperature.

Tris buffered saline for Trypsin stock – Made with NaCl (4.00 g), $Na_2HPO_4$ (0.05 g), Tris (1.500 g), KCl (0.19 g) and 1.5 ml Phenol red 0.5 % (w/v) dissolved in 500 ml distilled water and autoclaved.

Trypsin in Versene – Trypsin in Tris buffered solution is diluted in Versene (1:5) to make a 0.05 % working concentration.

*HepG2 maintenance*

HepG2 cells were purchased from Sigma Aldrich, thawed and seeded into a 75 $cm^2$ culture flask. The cells were maintained in Dulbecco's Modified Eagle Medium (DMEM) supplemented with 10% Foetal bovine serum (FBS), 1% Penicillin / Streptomycin, 1% non-essential amino acids, 1% L-glutamine and 1% Amphotericin B. Cells were allowed to proliferate to between 60 – 80 % confluency before being passaged (usually twice a week). To passage the cells the flasks were washed twice with 5 ml of warm Versene, before 2 ml of Trypsin in Versene is added and left for 5 minutes in the laminar hood at room temperature. Flasks were checked under a microscope to confirm detachment of cells. The Trypsin was neutralized by adding 8 ml of Dulbecco's Modified Eagle Medium (DMEM) to the flask. The cell concentration and viability were

determined using a Trypan blue exclusion dye. Two hundred µL of the cell suspension was added to an equal volume of Trypan Blue (0.4 % w/v in PBS, pH 7.4, 0.2 µm filtered) and counted in a haemocytometer. All experiments were concluded using cells below passage 90 (from receipt).

### 3.3.2 Perfusion and isolation of primary rat hepatocytes

*Stock solutions for perfusion*

Hanks buffer solution (10x) – Made in a 1 litre volumetric flask containing NaCl (80.0 g), KCl (4.0 g), $MgSO_4 7H_2O$ (2.0 g), $Na_2HPO_4 2H_2O$ (0.6 g) and $KH_2PO_4$ (0.6 g) dissolved in distilled water and stored at 4 °C until use.

Krebs-Henseleit buffer solution (2x) – Made in a 2 litre brown bottle containing distilled water (785 ml), 16.09 % (w/v) NaCl (200 ml), 1.10 % (w/v) KCl (150 ml), 0.22 M $KH_2PO_4$ (25 ml), 2.74 % (w/v) $MgSO_4.7H_2O$ (50 ml) and 0.12 M $CaCl_2.6H_2O$ (100 ml) which is bubbled for 10 minutes (5 % $CO_2$, 95 % $O_2$). At the same time $NaHCO_3$ (9.71 g) is dissolved in distilled water (1 L) which is bubbled for 10 minutes (5 % $CO_2$, 95 % $O_2$) before being added to the brown bottle.

*Perfusion solutions*

Hank's I buffer – Made in a 500 ml flask, 50 ml of Hank's (10x) buffer was added to $NaHCO_3$ (1.05 g), N-[2-hydroxyethyl]piperazine-N'-[2-ethanesulphonoic](Hepes) (1.50 g), Bovine Serum Albumin (BSA) (3.33 g) and Ethylene glycol-bis-(β-amino-ethylether)N'N'tetraacetic acid (EGTA) (114 mg).

The pH was adjusted to 7.4 using 5 M NaOH and the volume made up to 500 ml using distilled water.

Hank's II buffer – Made in a 500 ml flask with 50 ml of Hank's (10x) buffer with $NaHCO_3$ (1.05 g), N-[2-hydroxyethyl]piperazine-N'-[2-ethanesulphonoic](Hepes) (1.50 g), $CaCl_2.2H_2O$ (147 mg). The pH was adjusted to 7.4 and the volume made up to 500 ml using distilled water.

Krebs-HEPES buffer solution (KH) – Made in a 500 ml flask with 250 ml of Krebs-Henseleit buffer (2x) and Hepes (1.5 g) where the pH was adjusted to 7.4 using 5 M NaOH and the volume made up to 500 ml using distilled water.

Krebs-Albumin buffer (KA) – Made in a 500 ml flask using 250 ml of Krebs-Henseleit buffer (2x) which was added to N-[2-hydroxyethyl]piperazine-N'-[2-ethanesulphonoic](Hepes) (1.5 g) and BSA (5.0 g). After the pH was adjusted to 7.4 the volume was made up to 500 ml using distilled water.

*Procedure to isolate the hepatocytes*

The whole isolation procedure was carried out by a qualified technician following University guidelines. All solutions were bubbled with 5 % $CO_2$, 95 % $O_2$ at 37 °C. Adult male Sprague-Dawley rats (180 – 220 grams) were anaesthetised using a lethal injection of sodium pentobarbital (30 mg / ml). Seven rats were used in total, three for the cultures exposed to Paracetamol, three for the cultures exposed to Diclofenac and 4'-Hydroxydiclofenac and one for the single array platform. The number of rats that could be used was based on the schedule of the technician, the ethical weight and the time needed to perform a single experiment. The liver perfusion was carried out [111],

following a two-step collagenase protocol. The unconscious rats were placed in a laminar flow cabinet on their backs and with their abdomen exposed. The surgical area was cleaned with 70 % (v/v) alcohol and the peritoneal cavity was opened by a midline incision from the sternum to the pubis. Heparin (0.1 ml, 1000 IU / ml) in PBS (pH 7.4) was injected into the hepatic vein. A steel cannula containing Hanks' I buffer was inserted into the liver through the portal vein and clipped into place. The liver was dissected from the body and placed into a 250 ml beaker containing the Hanks' I buffer for 10 min. The liver was then relocated into a second beaker containing 150 ml of Hanks' II buffer and perfused with 78 mg collagenase for 10 – 20 min until the liver changed to a pale brown colour. All perfusion solutions were bubbled with oxygen and carbon dioxide (95:5 %) and kept at 37 °C during the procedure.

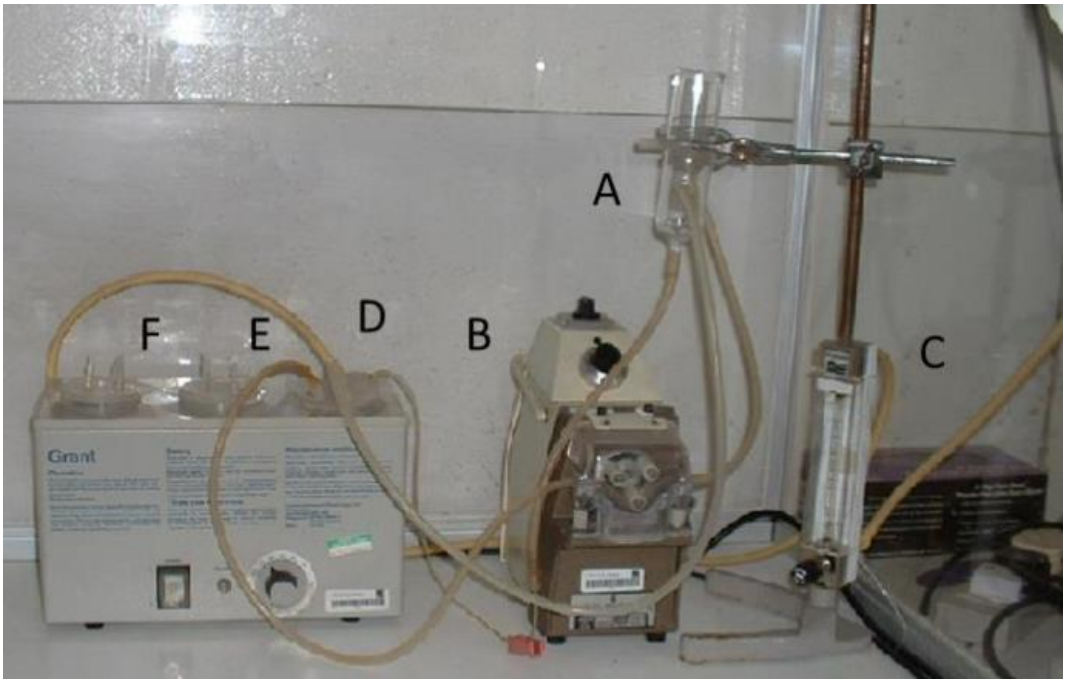


*Figure 3.5 Rat perfusion equipment: (A) Reservoir, (B) pump, (C) gas regulator, (D) $Ca^{2+}$ free perfusion solution, (E) collagenase solution, (F) BSA containing buffer.* [111]

After the digestion period the cells were gently dispersed using forceps into a petri dish containing 100 ml of KA buffer (warmed to 37 °C). To remove any connective tissue and undigested fragments the suspension was filtered through a cell strainer (Sigma Aldrich – 280 µm pore size) into a 100 ml bottle and kept on ice. Once the cells settled under gravity the KA buffer was carefully removed and the cells were washed by adding 50 ml of KH buffer and allowed to settle. Finally, the KH buffer was removed and the viability of the cells was determined.

The viability of the cells was determined using Trypan blue exclusion test. This was achieved by adding 10 µl of the cell suspension to 990 µl of Trypan Blue (0.1 % w / v in PBS, pH 7.4, 0.2 µm filtered) and counted in a haemocytometer. All nine squares on each side were counted totalling eighteen sections and the viability was calculated using the following equations:

$$\%\ viability = \frac{No\ of\ live\ cells}{Total\ no\ of\ cells} \times 100$$

*Equation 3.1 Calculating the total percentage of viable cells.*

$$Total\ viable\ cell\ concentration = \frac{No\ of\ live\ cells}{18} \times 10^4 \times 100$$

*Equation 3.2 Calculating the total number of viable cells / ml.*

Where 18 is the number of sections in the haemocytometer, $10^4$ is the conversion factor to compensate for the volume in the haemocytometer and 100 is the initial dilution factor. The hepatocytes were resuspended at a

concentration of 3 x $10^6$ / ml. Only perfusions with a viability greater than 80% was used in the subsequent experiments.

Primary rat hepatocytes were maintained in suspension in Williams's medium E culture medium supplemented with Insulin-transferrin-selenium solution (1%), L-glutamine (1%), Foetal bovine serum (5%), Penicillin / Streptomycin (1%), Amphotericin B (1%) and 1 µM Dexamethasone in ethanol (final ethanol concentration 0.1%).

## 3.4 Loading and maintenance of the microfluidic platforms

### 3.4.1 Droplet-based microfluidic platform (HepG2 cells only)

The droplet-based platforms were primed with a 0.1 % block copolymer fluorosurfactant in oil (w/v) solution using a micropump fitted with a glass syringe connected to Inlet A (Figure 3.1) via tubing. Once no air could be observed in the platform the desired flow rate was set (0.9 µl / min) and the platform given time to equilibrate (minimum 5 minutes) before the cells were introduced via the cell inlet (Figure 3.1 (B)).

HepG2 cells were resuspended to a concentration of 3 x $10^6$ / ml and 500 µl transferred to a 2 ml Eppendorf. At this concentration, if all cells are dispersed in the same density in the solution, it should result in approximately 40 to 70 cells / droplet depending on the size of the trap. A micropump fitted with a 1 ml glass syringe filled with warm DMEM and connected with tubing was inserted into the Eppendorf and the suspension was slowly withdrawn (0.4 µl / min). Once an adequate amount of suspension was withdrawn in the tubing, the flow was reversed (0.8 µl / min). The end of the tubing was gently inserted

into the cell inlet (Figure 3.1 (B)). Newly formed droplets were sequentially trapped filling the array (Figure 3.6).

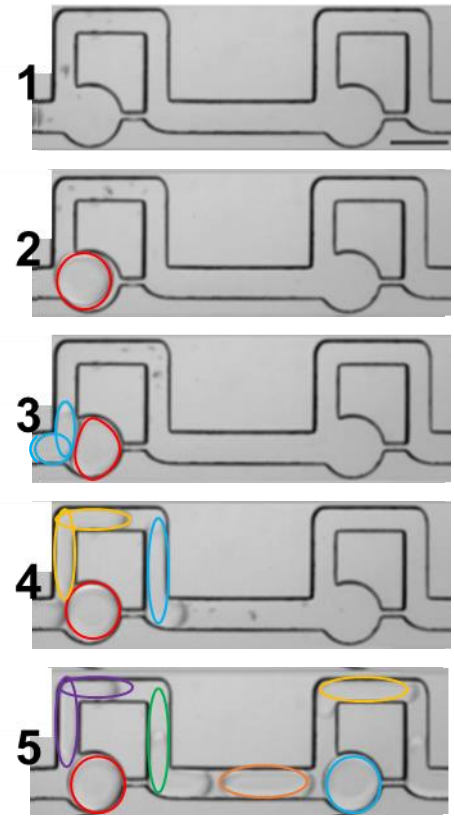
1
2
3
4
5

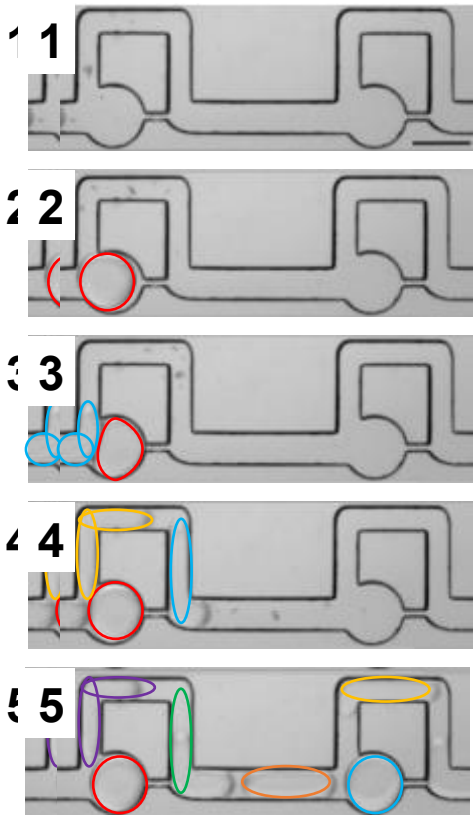
1
2
3
4
5

*Figure 3.6 Microscopic image of droplets sequentially filling the traps: (1) Empty traps, (2) first droplet (red) enters trap effectively, (3) second droplet (blue) follows the bypass channel and flows (4) towards the second trap and (5) enters the second trap, followed by the next droplet (yellow). This process continues until all traps are filled.* [79]

Once all the traps were filled the flow from the cell inlet was stopped. The flow from the continuous phase inlet was allowed to continue to clear the platform of any un-trapped droplets remaining in the main channel. The tubing was slowly removed allowing the continuous phase to clear the cell inlet. Finally, the flow from the continuous phase inlet was stopped and allowed to equilibrate (minimum 5 minutes) before the tubing was gently removed. Platforms were stored in the incubator (37 °C) in containers with plastic weigh boats containing DMEM to aid in retaining humidity. Cells trapped in the droplets (Figure 3.7) aggregated overnight.

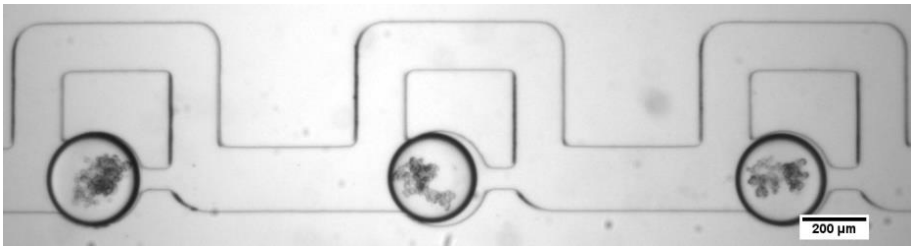


*Figure 3.7 HepG2 cells in droplets directly after seeding (day 0). (x 5 objective)*

The following day the surfactant in oil solution (continuous phase) was displaced by pumping warm DMEM through the platform (0.3 µl / min). Some time (< 1 minute) after the medium encounters the droplets in the traps the interface between the two coalesce, allowing the exchange of nutrients and waste. After all the surfactant in oil solution has been displaced the flow is

switched off and allowed to equilibrate (minimum 5 minutes), before the platform is returned to the incubator. Medium was replaced every 2 days by micropump-driven flow for 15 minutes at a rate of 0.3 µl / min.

### 3.4.2 The multi-array microfluidic platform

To load cells in the multi-array platform the media in the reservoirs were removed using a pipette. Five µl of medium containing the stock cell suspension of 1.5 x $10^6$ cells / ml was introduced into the left-hand reservoir, totalling approximately 7500 cells. Due to a combination of capillary forces and surface tension, a flow was induced, drawing cells into the channel (Figure 3.8) where they sedimented into the microwells. The wells were filled to different degrees, with the highest number of cells / well closest to the reservoir. A total of 20 microlitre was added to each channel, alternating between reservoirs at 5 min intervals. The intervals allowed the flow in the channel to reach equilibrium before new cells were introduced. Un-trapped cells were washed out and removed at the reservoirs.

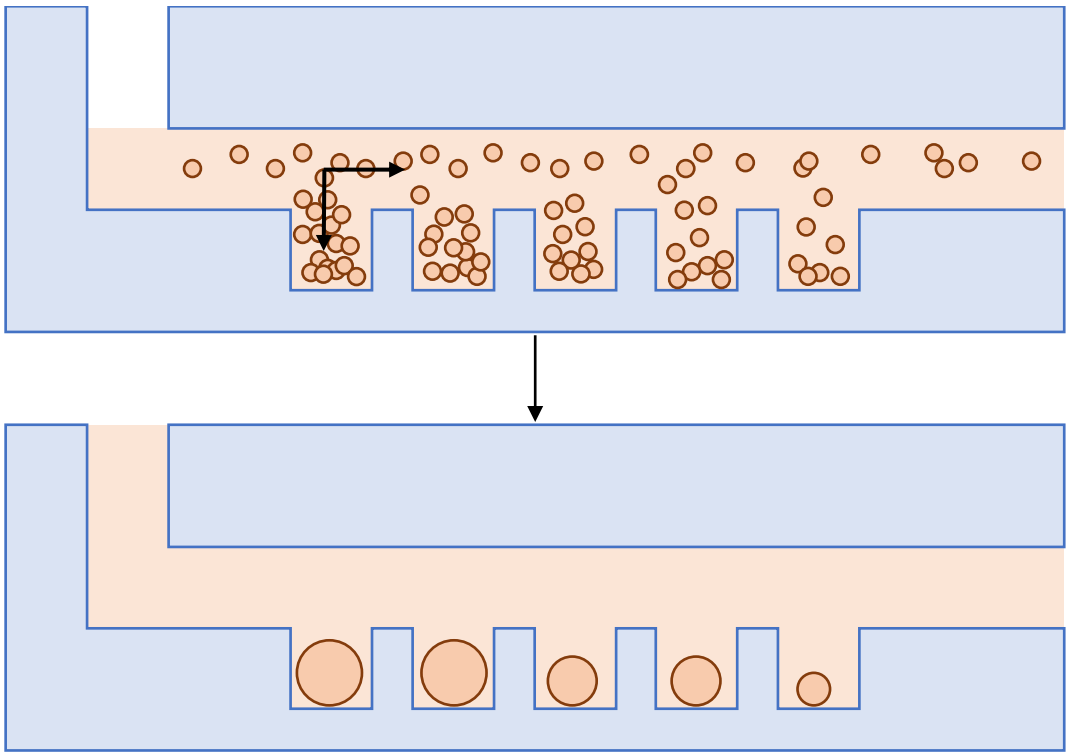

*Figure 3.8 (Top) Illustration of a side view of the microwell platform with arrows indicating the direction of motion of the cells and (Bottom) the formation of spheroids of varying sizes.*

Next the reservoirs were filled slowly and simultaneously using 25 µl to a total volume of 50 µl each. The platforms were returned to the incubator and medium was replaced every two days for the HepG2 cell cultures and daily for the primary rat hepatocyte cultures. To replace the medium the reservoirs were simultaneously and carefully emptied (25 µl at a time). Five µl was added to the reservoir and after 5 minutes both reservoirs were carefully refilled.

For the single array platform (Figure 3.4) a total of 4 µl of primary rat hepatocyte suspension (3 x $10^6$ cell / ml) was introduced to accommodate the smaller culturing area. This was repeated from the other reservoir after 5 min to ensure equal distribution of cells in the microwells. Un-trapped cells in the reservoirs were removed using a 10 µl pipette and re-introduced to increase

trapping efficiency. After the wells were filled the last remaining un-trapped cells in the reservoirs were removed and the reservoirs filled with 8 µl (each) medium containing foetal bovine serum. This theoretically resulted in a cell / medium ratio of approximately 750 cells / µl, compared to the 300 cells / µl in the multi-array platform. All microfluidic platforms were kept in plastic containers with a plastic weighing boat containing medium alongside to minimize evaporation inside the incubator. Medium was replenished daily.

## 3.5 Culturing of primary rat hepatocytes in a collagen sandwich configuration in 24 – and 6 well-plates

To assemble the collagen sandwich configuration a 0.3 % collagen type I gel solution was prepared with the following materials: 1ml mixture of 10× DMEM and 0.4M NaOH (2:1); 4.615 ml collagen solution (6.5 mg / ml); 1:1000 acetic acid up to 10ml total (per batch) and kept on ice. For the collagen to set, the pH of the solution had to be adjusted to 8 - 8.5 though the drop-wise addition of 1 M NaOH until the solution containing phenol red turned a pale pink. For the 24 well-plates 450 µl of the collagen solution were pipetted into the wells and gently swirled to distribute evenly. The well-plates were allowed to set at room temperature for a minimum of 2 hours in a laminar flow cabinet and washed twice with PBS. A total of 450 µl medium was added to the wells which were left in the incubator for an additional 20 – 30 minutes. Before seeding the cells, the medium was removed and 100 µl of fresh medium was added to the 24 well-plates. Next the cell suspension was added to the plates, resulting in 200 µl medium total, with 3 x $10^5$ cells / well. The plates were gently swirled to

distribute the cells evenly. After cells were left to adhere to the collagen layer for a minimum of 2 hours, the wells were washed twice with PBS and 400 µl medium added (cell / medium ratio of 750 cells / µl), before being returned to the incubator. The following day (day 1 of experiment) a second layer of 0.1 % collagen solution (made following the same protocol as for the bottom layer) was added to each well to complete the sandwich configuration. For the top layer 150 µl was used to minimise the depth of the top collagen layer. The plates were gently swirled to provide an even distribution and allowed to set in the incubator for a minimum of 1 hour. The wells were washed once with PBS, before having the medium replaced and being returned to the incubator. For the intracellular LC-MS analysis (Chapter 5), 6 well-plates were also constructed following the same protocols, with some alterations due to the larger culturing area. The bottom layer of collagen was made using 1 ml of the 0.3 % collagen solution; 1.5 x $10^6$ PRH were seeded and allowed to adhere (2 hours) before the medium was exchanged with 2 ml of medium containing FBS. The top layer was added the following day using 450 µl of 0.1 % collagen solution. The final configuration for the 24 well-plates was 450 µl 0.3 % collagen (bottom layer), 3 x $10^5$ hepatocytes, 150 µl 0.1 % collagen (top layer) and 400 µl medium. The final configuration for the 6 well-plates was 1 ml of 0.3 % collagen, 1.5 x $10^6$ hepatocytes, 450 µl 0.1 % collagen and 1.5 ml of culture medium (cell / medium ratio of 1000 cell / µl).

## 3.6 Immunofluorescence of hepatic cultures in the microfluidic platforms and collagen sandwich configurations

To mix the staining solution 10 ml of serum-free medium was supplemented with 100 µl PI and either 16 µl FDA (for the microfluidic platforms) or 3.3 µl Hoechst (for the collagen sandwich configuration). The staining solutions were protected from light. Different solutions had to be used between the microfluidic platforms and the collagen sandwich configurations. It was observed during early experiments that using an FDA / PI stain did not allow for quantification of individual viable cells in the collagen sandwich cultures. When multiple cells were in contact with each other it was impossible to count individual cells, as the fluorescent FDA signal from overlapping cells merge into a single, solid shape (when viewed). For this reason, Hoechst was used instead, as only the nucleus provided a fluorescent signal, making counting individual cells possible.

### 3.6.1 Hepatic spheroids

Before the staining solution was introduced into the droplet-based platform the channels and traps were gently flushed with serum-free medium (0.3 µl / min for a minimum 10 minutes). Next, the staining solution was introduced at a flowrate of 0.3 µl / min for 15 minutes. After the flow was stopped and had adequate time to equilibrate, the platforms were returned to the incubator for 10 minutes. Next the solution was flushed out using PBS at the same flowrate for the same length of time.

For the multi-array (and single array) platform the medium was removed, and the staining solution introduced using a pipette. The platforms were placed in

an incubator for 10 minutes before the solution was gently washed out using PBS. Finally, the images could be recorded using fluorescent microscopy.

Accurately determining viability of a 3D object using a 2D image is challenging. The “viable fraction” (Equation 3.3), defined as the area of living cells (FDA area) over the total area of the spheroid (BF area) the day prior, was utilized (Figure 3.10). A low viable fraction would indicate significant cell death in the spheroid, while a fraction closer to 1 (or over if cells continue to proliferate) would indicate a healthy spheroid.

$$V_f = \frac{FDA\ area}{BF\ area}$$

*Equation 3.3 Calculating the viable fraction ($V_f$). FDA area is the area of cells producing a fluorescent signal (viable cells), BF area is the brightfield (total) area of the spheroid.*

The area of the spheroids was determined using an in-house MatLab code developed by Dr Zagnoni.

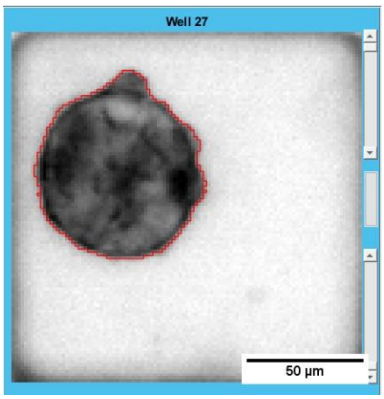


*Figure 3.9 Image of a segment of the interface used to calculate the area of a hepatic spheroid. The red line indicating the detected area of the spheroid.*

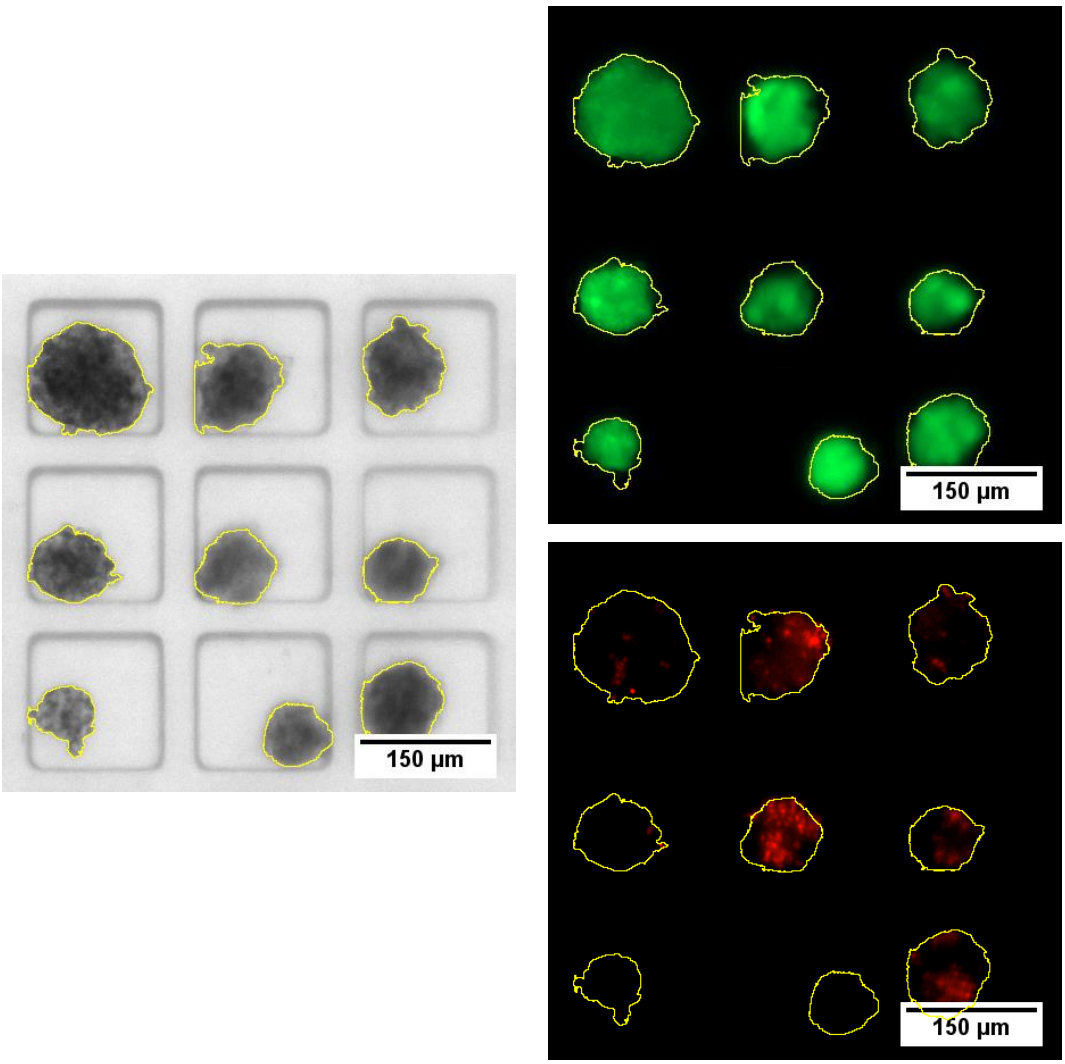


*Figure 3.10 (Left) Brightfield image and (Top) FDA and (Bottom) PI counterstain. The fraction of the area of the spheroid recorded in the brightfield image (the day before staining) and the FDA area is used as an indicator of spheroid health.*

Images taken are adjusted to remove any background fluorescence and converted to .TIFF format using the commercially available Zen2 (Blue edition ZEISS). All graphs were created using OriginPro (2018).

The mean viable fraction ($\bar{V}_f$) of the spheroids for a microfluidic platform was calculated by using the outer well array (8 x 8) in each channel (condition), on three different devices per condition.

$$Mean\ viable\ fraction\ (\bar{V}_f) = \frac{V_{f1} + \cdots + V_{fn}}{n}$$

*Equation 3.4 Calculating the mean viable fraction for the microfluidic platform. Where $V_f$ = individual viable fraction of spheroids in a channel (per platform) and n is the number of platforms.*

*Fixation of hepatic spheroids*

Hepatocytes were also fixed and stained for the presence of tight junctions. Cells were washed 3 times using PBS, before being fixed with a 1:1 acetone and methanol solution and stored in the freezer for 10 minutes. Cultures were then washed and refilled with PBS and stored in the fridge for another 10 minutes. Cultures were exposed to a 10 % solution of goat serum in PBS at room temperature for an hour before being washed with PBS (3 times). A 1:100 dilution of primary rabbit-anti-ZO-1 in bovine serum albumin (BSA) was added to the cultures and left at room temperature for an hour. Finally, the cultures were washed with PBS and a 1:400 solution of Alexa fluor 594 labelled goat anti-rabbit IgG in BSA was added for 45 minutes at room temperature. Lastly, the cultures were washed with PBS and stored in the fridge or imaged later in the day.

### 3.6.2 Collagen sandwich configurations

Before adding the staining solution, each well was washed three times with PBS. Four hundred µl of staining solution was added for the 24 well-plate and 1 ml for the 6 well-plate, respectively. The well-plates were then returned to

the incubator for 10 minutes before the solution was removed by washing each well three times with PBS. The plates could then be taken for fluorescent imaging.

The viable ratio ($\overline{V_r}$) of the cells cultured in the collagen sandwich configuration was assessed by staining using Hoechst and PI. Hoechst is a nuclear stain which binds to the DNA in all cells in the culture, while PI will only permeate cells and bind to DNA in which the membranes have been damaged. The latter is an indicator of cell death. To determine the viable ratio, the fluorescent images were converted to a .TIFF format and opened in ImageJ (FIJI plug-in). Three randomly selected square sections on the image of a single 24 well-plate were enlarged. The total number of blue (Hoechst stained) and red (PI stained) stained cells from all three areas were counted and added up. The number of viable cells was divided by the total number of cells. The viable ratio of the collagen sandwich configurations per condition was calculated using three 24-well plates.

$$Viable\ ratio\ (\overline{V_r}) = \frac{V_1 + V_2 + V_3}{(V_1 + D_1) + (V_2 + D_3) + (V_3 + D_3)}$$

*Equation 3.5 Calculating the viable ratio for the collagen sandwich configuration. Where V = total number of viable cells (in three segments / well) and D = total number of dead cells (in three segments / well). The mean viable ratio was calculated using 3 separate 24 well-plates.*

The decline in viability was calculated by dividing the viable ratio (collagen sandwich configurations) or viable fraction (microfluidic platforms) per

concentration by their respective control group means. This was carried out in order to quantify the difference in the response on a test condition versus no exposure. This difference was compared between the two systems.

$$Decline\ in\ viability = \bar{x}\ of\ \frac{Viability\ per\ condition_{ratio\ or\ fraction}}{Mean\ viability\ of\ controls_{ratio\ or\ fraction}}$$

*Equation 3.6 Calculating the normalised decline in viability for both systems.*

## 3.7 Induced hepatotoxicity in the microfluidic platforms and collagen sandwich configurations

Diclofenac sodium salt (318.13 g / mol) was weighed out and dissolved in 100% DMSO for a maximum stock concentration of 500mM. Paracetamol (151.12 g / mol) was prepared to a stock solution of 7.5 M. The drug solutions were placed in an incubator, and removed at regular interval and shaken, to aid the dissolving process. Only once the drugs were completely dissolved were the solutions filtered (0.2 µm nylon filter). The stock solutions were serially diluted in filtered DMSO (0. 2 µm nylon filter) resulting in 31.25 mM, 62.50 mM, 125.00 mM, 250.00 mM and 500.00 mM for Diclofenac and 0.47 M, 0.94 M, 1.88 M, 3.75 M and 7.50 M for Paracetamol. The serial dilutions were added to serum-free medium, resulting in dilution factor of a thousand (final DMSO concentration 0.1 %).

A stock solution of Hydroxy-Diclofenac in DMSO to a concentration of 5 mM was prepared using the same method and stored in 50 µl aliquots in a freezer at – 20 °C until use. All cultures were exposed to a compound for 24 hours before the viability was determined. Cultures exposed to Diclofenac or

Paracetamol were cultured for an additional 24 hours in serum-free medium, referred to as the recovery period, before being stained for viability. These drugs were chosen as they are known to lead to the production of toxic metabolites at supra-therapeutic concentrations. The enzymes involved in the production of the toxic metabolites (CYP3A4 and CYP2E1) are responsible for over 40 % of all orally taken drug metabolism.

## 3.8 Preparation of solutions for LC-MS analysis of primary rat hepatocyte supernatant and cell lysate

### 3.8.1 LC-MS Solutions

The mobile phase consisted of two different solutions. Mobile phase (A) was composed of 0.01 % acetic acid in water and phase (B) of 0.01 % acetic acid in acetonitrile.

The quenching solution, which is used to disrupt further metabolic processes, was composed of acetonitrile, methanol and water in a 5:3:2 ratio (0.2 µm nylon filtered) and stored at – 20 °C in a 150 ml glass bottle with parafilm wrapped around the lid. The quenching solution was aliquoted and stored at – 20 °C which was stored on ice during use.

### 3.8.2 Collection and storage of primary rat hepatocyte samples for LC-MS analysis

*Detection of metabolites in cell culture media*

The samples used for metabolite detection from the 24 well-plates were collected by taking 150 µl each from three wells (per condition) for Diclofenac and Paracetamol (as well as 4'-Hydroxydiclofenac) and stored in Eppendorfs. An equal volume of ice-cold quenching solution was added to the samples. Pooled samples, which included small equal volumes from multiple conditions and both systems, were also collected this way. The pooled samples were used as a reference to identify any drift in the chromatogram or change in absorbance during LC-MS analysis. This protocol was also followed for the samples collected from the 6 well-plates.

*Detection of metabolites in cell lysate*

Cells were taken from the 6 well-plates using a cell-scraper. The wells were emptied and washed with PBS (pH 7.4), before 1 ml quenching solution was added. The collagen sandwich cultures were carefully mashed using a cell scraper until the large lumps were broken apart. A pipette with a cut tip was used to collect the sample including the mashed collagen containing the rat hepatocytes.

For the multi-array microfluidic platform 60 µl was taken from each channel (condition) per device. For the single array platform only 10 µl per channel could be taken (12 channels / device). The same method of quenching was used for the microfluidic platforms as with the collagen sandwich configurations. To collect cells for LC-MS analysis, the microfluidic channels were carefully cut into separate sections. One end of the channel was cut using a scalpel and held over an Eppendorf, while the other end was plugged with a

syringe containing 250 µl quenching solution. The plunger on the syringe was gently pushed down. Due to the angle the platform was held at and the flow generated by the syringe the spheroids were forced out of the wells into the Eppendorf. All LC-MS samples were stored at – 80 °C until analysis.

After a period of storage and before being analyzed, the samples were allowed to defrost at room temperature. To remove proteins and other potential interference the samples were centrifuged at 13,5000 rpm for 10 minutes in a temperature controlled (kept at 4 °C) benchtop centrifuge. After this the fluid portion (supernatant) of each sample was transferred to a new Eppendorf and stored at – 80 °C until analysis.

To monitor the accuracy of the experiment the samples were loaded into the LC-MS in consistent order. The initial sample contained acetonitrile (to clean the column), the second a standard of either Diclofenac, Paracetamol or 4'-Hydroxydiclofenac, in medium to check the elution time. The next 3 samples were in the following order; Standard in medium (of condition), 6 well-plate samples, 24 well-plate samples and microfluidic platform samples. This process was first done for the cultures exposed for 24 hours, and then 24 hours exposure followed by 24 hours recovery. This "set" was then repeated for each condition (starting with a sample containing acetonitrile) for each experiment. A pooled sample for each experiment was loaded intermittently between the other samples to monitor retention time drift or absorbance change. The samples containing the cell lysate were run at the end of each "set" (6 well-plate and then the multi-array microfluidic platform samples). A diagram (Figure 3.11) represents the timeline of the primary rat hepatocyte cultures.

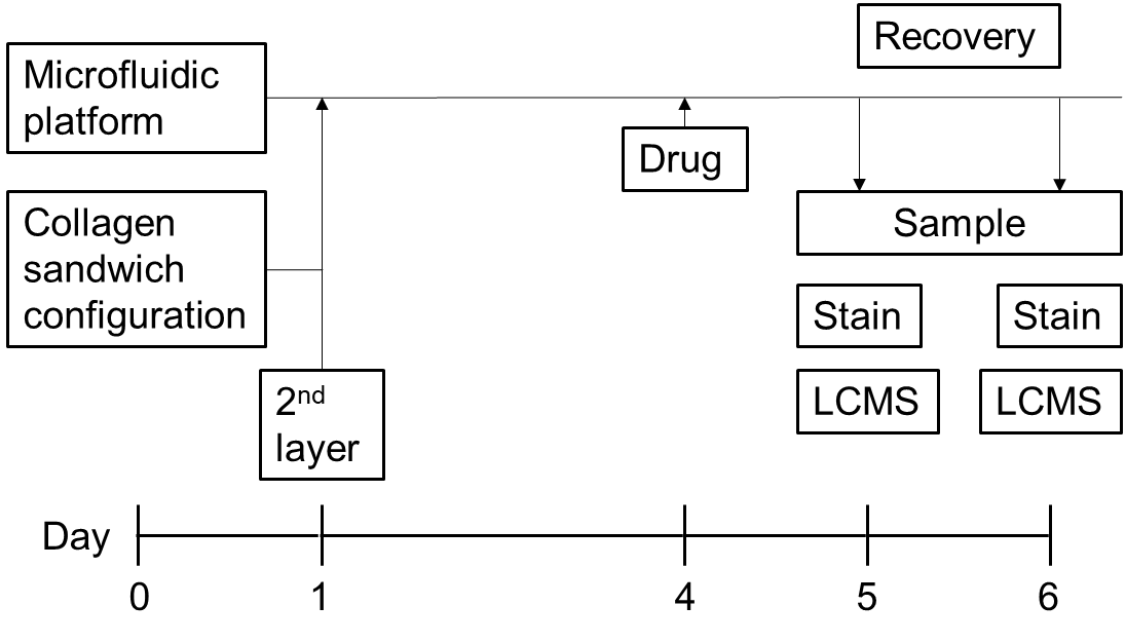


*Figure 3.11 Experimental protocol when culturing primary rat hepatocytes. Cells are isolated on day 0 and seeded into both systems and on day 1 the second collagen layer is added. Medium is replaced every day and the cultures are exposed to a drug on day 4 for 24 hours. Cultures are stained and samples (cell lysate and supernatant) are taken for LC-MS analysis on day 5. Parallel cultures are then allowed to recover in serum-free medium for 24 hours before being stained and additional samples are taken for LC-MS analysis.*

## 3.9 Separation and identification of components using LC-MS

Separation of the different components was performed using a Dionex HPLC connected to an Exactive Orbitrap MS. The mobile phase used was composed of an isocratic elution of 60 % (A) and 40 % (B) for 20 minutes. Ten µl of each sample was injected and pumped into the system at a flowrate of 0.4 ml/min. The stationary phase was an C18-AR (C18 chain with integrated phenyl phase) column (dimensions, 150mm x 4.6 mm). The column was chosen as it is highly suited to separate samples where a difference in polarity is expected. The aromatic ring (AR) functionality is recommended for components containing aromatic rings, as it aids in separation.

The HPLC was connected to an Exactive Orbitrap (ThermoFisher) and the ionization was carried out using Electron spray Ionization (ESI). Switching was achieved between negative and positive mode using a voltage of 4.5 kV each and a capillary temperature of 320 °C. Nitrogen was used for nebulization at a sheath gas flow of 50 and an AUX gas flow of 17 (arbitrary units). The total ion chromatogram (TIC) was scanned between the *m/z* range of 75 – 1200 and the data viewed using Xcalibur software (version 2.0) and MZmine (version 2.31). Quantification was carried out using both these programs.

### 3.9.1 Data processing

*Xcalibur*

The TIC and mass spectra could be visualised in Xcalibur and were used to measure the peak area by scanning for the specific m/z ratios for each compound of interest. The mass spectral data was used for identification of

the molecules present in the peak. To achieve this the software calculates the most likely molecular structure of the compound based on the m/z value (5 ppm tolerance), the fragmentation patterns and isotope ratios.

*MZmine*

The processing followed the instructions provided by the developer with the following settings: Mass detector set at “Centroid” for negative polarity; Chromatogram builder “Min height” at 1 x $10^4$, *m/z* tolerance of 0.001 (*m/z*) or 5 ppm; Chromatogram deconvolution set “Wavelets”; Isotope “retention time tolerance” set at 0.5 min and “max charge” = 2; Peak alignment and gap filling was set with the same tolerance as the chromatogram builder; next, complexes were identified using the “[M – H] –“ Ionization method (same m/z tolerance as the chromatogram builder).

*Statistics*

Two-way ANOVA with a Tukey’s test (95% confidence interval) was used to compare the mean viability and relative abundance of the total ion chromatogram between the test groups.

# Chapter 4. Cultured HepG2 and Primary rat hepatocytes in the microfluidic platform and the collagen sandwich configuration.

This chapter outlines the initial results of culturing the carcinoma cell line, HepG2, in two different microfluidic platforms, followed by the discussion and motivation for the following sections.

## 4.1 Preliminary results of culturing HepG2 cells in a droplet-based microfluidic platform

As mentioned in Chapter 2, *in vitro* investigation of drug-induced hepatotoxicity is ideally performed using freshly obtained primary human hepatocytes. Primary hepatocytes contain higher levels of metabolizing enzymes, but are limited in availability, high cost and instability in culture. This has prompted scientists to investigate alternative sources to use in their place. Established cell lines provide the advantages of being robust and readily available, at a relatively low cost.

The HepaRG cell line has been extensively investigated for their use in hepatotoxicity screening [112]. This cell line differentiates into two distinct cell types, hepatic-like and biliary-like cells [113]. A study by Yokoyama and co-workers [114] investigated the drug metabolizing capabilities of HepaRG cells, HepG2 cells and cryopreserved human hepatocytes. By exposing the various cell types cultured in collagen-coated 96 well-plates to a variety of substrates for CYP450 metabolizing enzymes (e.g. Midazolam for CYP3A4); they

concluded that the enzymatic activities in the HepaRG cultures were “almost equal to or higher” than those recorded in the cryopreserved human hepatocytes and significantly higher than HepG2 cells (except for the Phase II sulfation enzyme).

The carcinoma cell line, HepG2, is an immortal hepatic cell line that has been thoroughly characterized as well [115] [48]. This cell line possesses some Phase II metabolizing enzymes at a similar concentration to human hepatocytes, but unfortunately has very limited Phase I metabolizing capabilities (specifically CYP450). A study by Wilkening [116] compared the expression of some of these metabolizing genes through RT-PCR. They could not detect the CYP3A4 gene in HepG2 cells cultured in a collagen sandwich configuration. This is an important consideration when conducting hepatotoxicity assays as the CYP3A4 gene is responsible for roughly 50% of all first-pass oxidative xenobiotic metabolism [117]. This makes HepG2 cells potentially suitable for only testing the toxicity of a compound that does not require Phase I activation. However, they do have the advantage of being a whole cell-based model. There are also some morphological differences between HepG2 and primary hepatocytes. HepG2 cells represent an epithelial-like morphology and contain only a single nucleus. Primary hepatocytes (and HepaRG) are typically more cube-like in appearance and are multi-nucleate [118].

Although HepG2 cells lack key Phase I metabolizing enzymes, they are useful as a preliminary tool to assess how primary hepatic cells might respond to being cultured in a microfluidic platform. Additionally, culturing primary

hepatocytes in a 3D configuration leads to increased, or at least prolonged, functionality regarding their metabolizing capabilities (Chapter 2). The same principle appears to apply to cell-lines [48].

This section will present the results obtained from culturing HepG2 cells in the microfluidic platforms. The aim of these experiments was to evaluate if the platforms provide a suitable environment for sustained hepatic cell culture and evaluate the response to hepatotoxicity.

### 4.1.1 Cellular aggregation and spheroid formation

The HepG2 cells aggregated quickly to form spheroids within 1 to 2 days in the droplet-based platform (Figure 4.1). The platforms were imaged daily, and the area of each spheroid was measured using ImageJ.

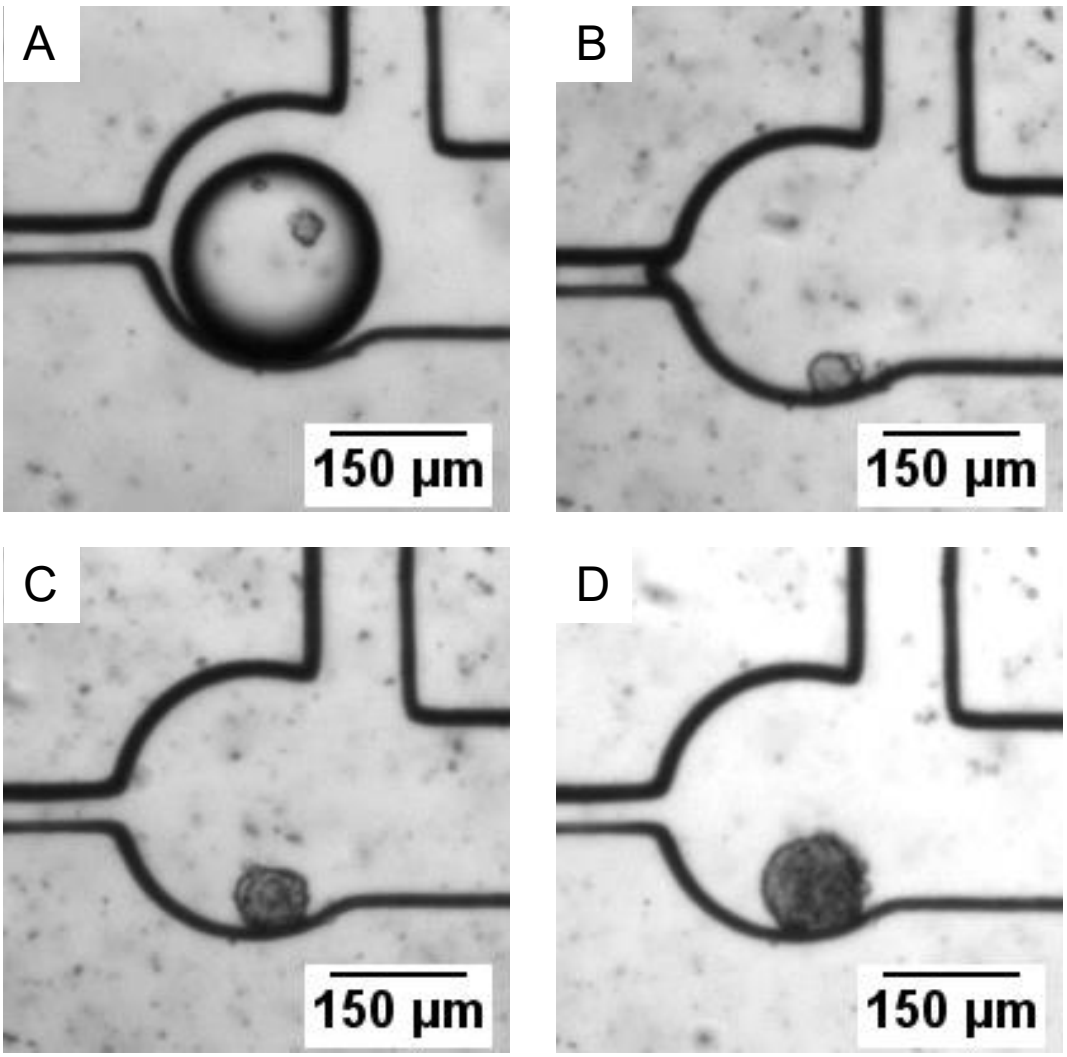


*Figure 4.1 Brightfield images of HepG2 cells in the droplet-based platform on (A) day 1, (B), day 3, (C) day 5 and (D) day 7. (x 5 objective)*

The mean cell count in a droplet (± standard deviation) at the seeding density of 3 x $10^6$ cell / ml was found to be 30 ± 14 cells / droplet using FIJI (ImageJ). In some droplets multiple small aggregates were present. These droplets regularly resulted in multiple spheroids forming in a single trap. Irrespective of seeding density there appeared to be no difference in spheroid size on day 3 or day 5. The results however do show an increase in the rate of the area (from day 7 to day 13).

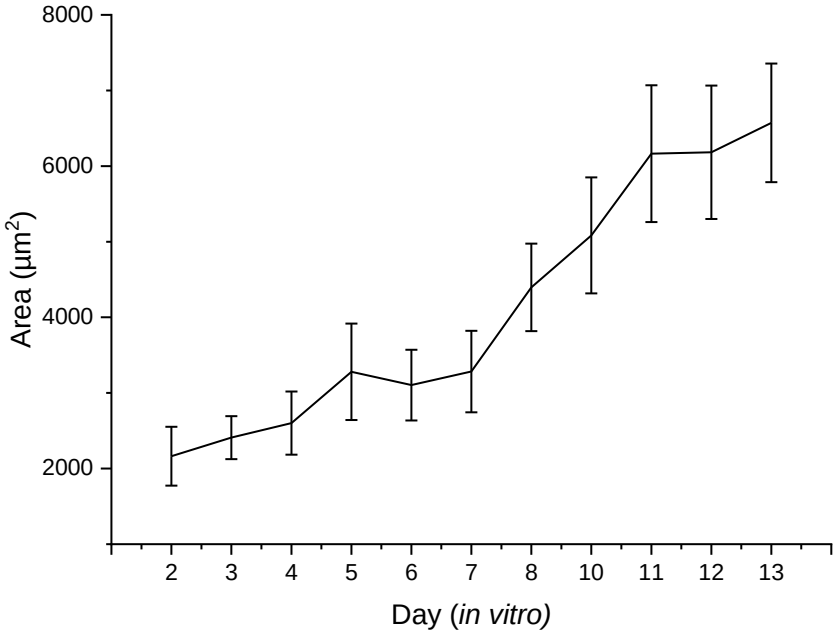


*Figure 4.2 Mean (± standard error) area of HepG2 spheroids cultured in the droplet-based platforms over 13 days. (Results from 6 platforms, 35 spheroids)*

HepG2 spheroids were stained using FDA and PI (10 min incubation) as an indicator of spheroid health using the in-house MatLab code (Figure 4.3).

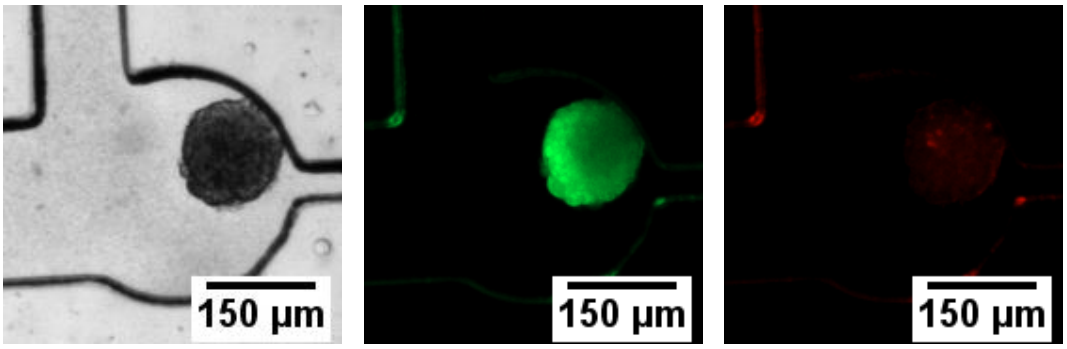


*Figure 4.3 Brightfield image (Left), FDA staining indicating viable cells in green (Middle) and PI staining indicating dead cells in red (Right) of a single HepG2 spheroid on day 9. (x 5 objective)*

*Microfluidic platform*

HepG2 cells were also cultured in the multi-array microfluidic platform for 8 days and images acquired daily. The HepG2 cells quickly aggregated to form spheroids in the wells in 1 – 2 days (Figure 4.4). The average number of cells / well (Figure 4.6) was found to be 14 ± 10 cells / well. Due to the large variation in the number of cells in the wells, the formed spheroids ranged in size (Figure 4.5), so they were separated into 3 categories; Small spheroids are under 50 µm in diameter, Medium spheroids between 50 and 100 µm and Large spheroids over 100 µm. The platform was intentionally designed to produce spheroids of different sizes as it was originally intended for culturing cancer tumours, not primary hepatocytes. By analysing the different sized spheroids information can be gathered regarding the impact of size on the response of the spheroid to the external stimulant.

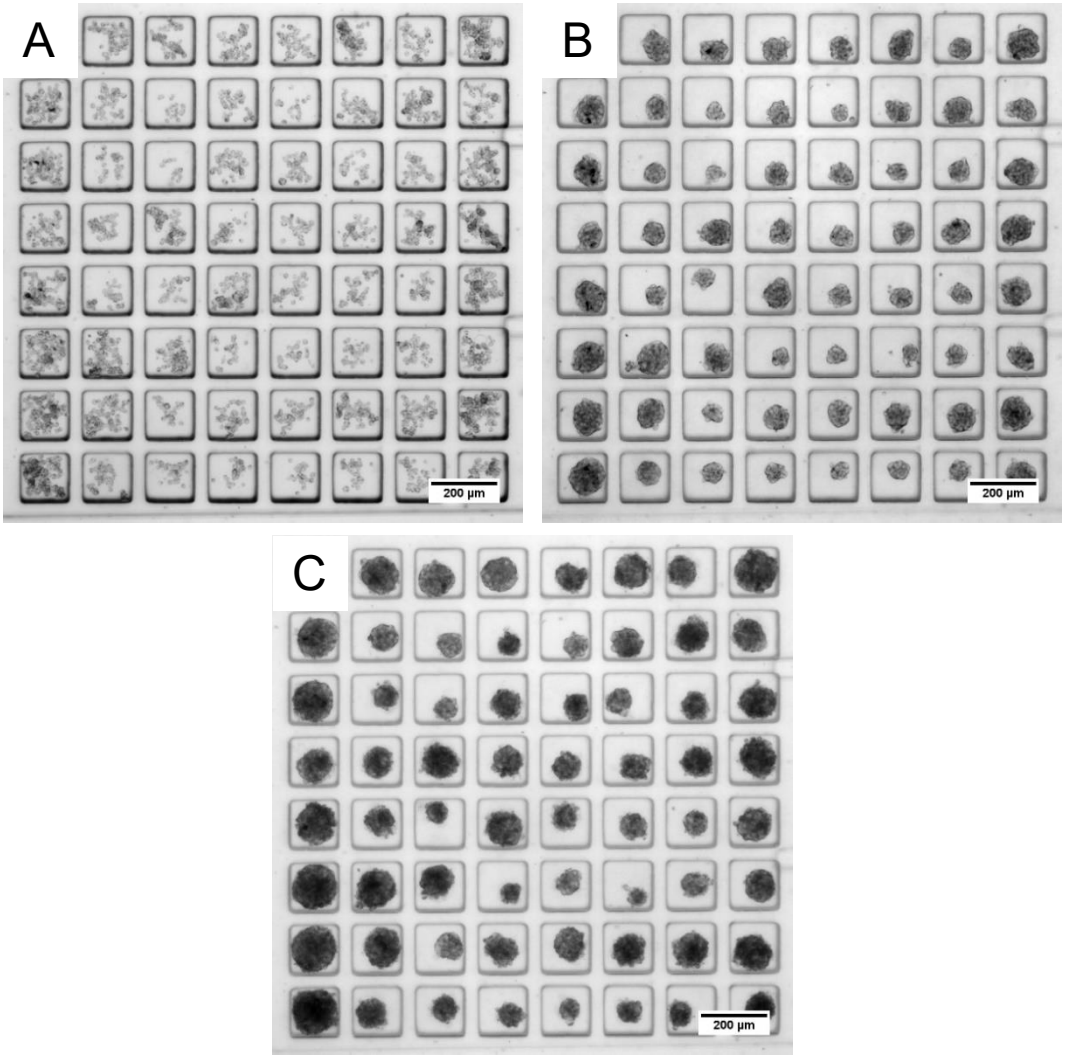


*Figure 4.4 HepG2 cells in the multi-array platform on day 0, (B) day 3 and (C) day 5. (x 5 objective)*

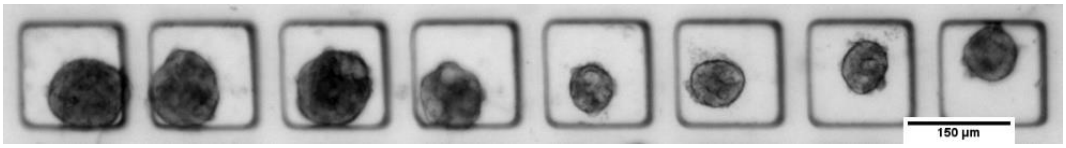


*Figure 4.5 Brightfield image of HepG2 spheroids varying in size (Day 5) in the multi-array platform. (x 5 objective)*

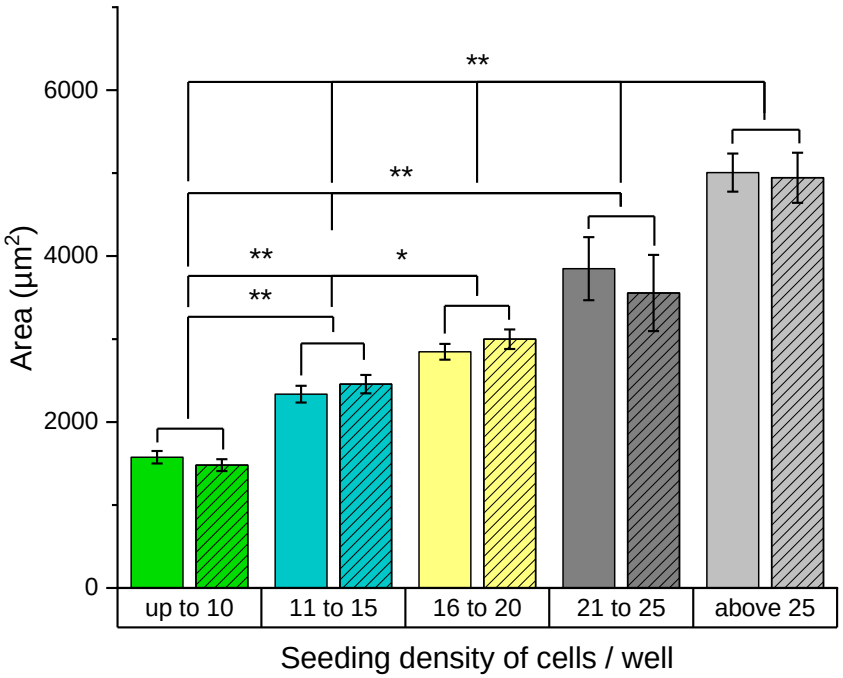


*Figure 4.6 Mean (± standard error) number of HepG2 cells / well in the multi-array platform and the recorded area on day 3 (solid) and day 5 (striped). (based on >160 spheroids over 3 platforms; * = p < 0.05, ** = p < 0.01)*

Figure 4.7 shows the mean area (± standard error) of three categories of spheroids in the outer well array. Unlike the HepG2 spheroids in the droplet-based platform, the area of the spheroids in the multi-array platform does not rapidly increase but remains relatively stable throughout the experiment. The potential reasons for this will be addressed in the discussion.

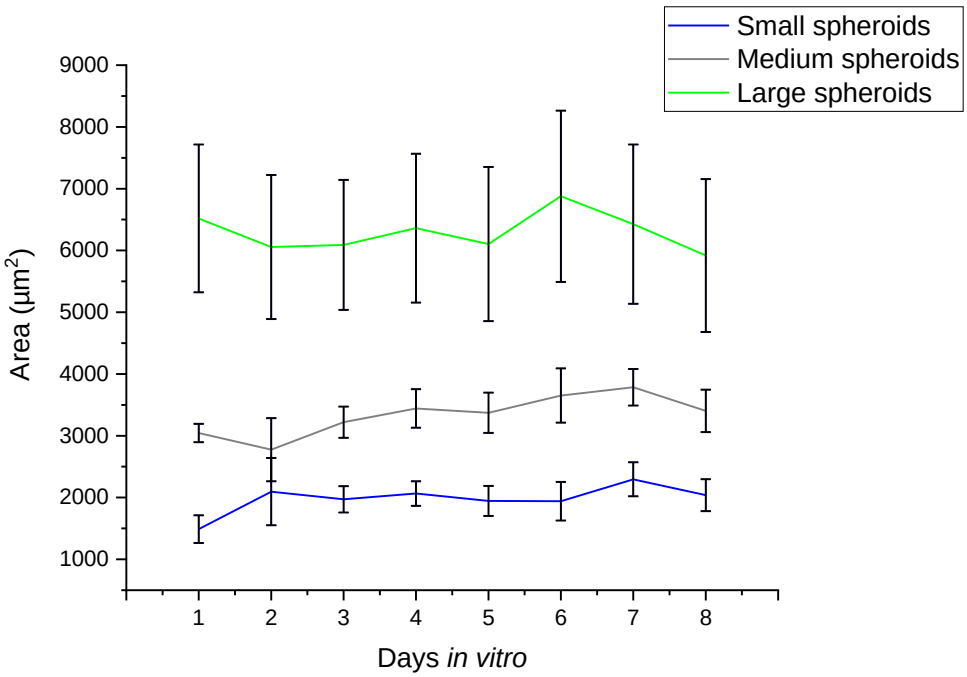


*Figure 4.7 Mean (± standard error) area of HepG2 spheroids (determined by FIJI) cultured in the multi-array platform over 8 days. (n = 1 platform, repeated in triplicate)*

### 4.1.2 Diclofenac induced hepatotoxicity in HepG2 spheroids in the microfluidic platforms

The HepG2 spheroids were exposed to Diclofenac sodium salt for 24 hours in serum-free medium on day 5. Diclofenac was chosen since HepG2 cells lack most major Phase I metabolizing enzymes but they do express detectable levels of the CYP2C9 enzyme [119] responsible for Diclofenac hydroxylation. It has also been suggested that Diclofenac has some direct toxicity through direct mitochondrial impairment [31]. Representative images of the HepG2 spheroids after Diclofenac exposure are shown in Figure 4.8. Regrettably, most spheroids were periodically lost during insertion and removal of the tubing used to refresh the medium. The displacement of fluid through removal

/ insertion of the tube resulted in spheroids being forced out of the traps. This resulted in too few remaining spheroids to accurately determine the decline in viability after Diclofenac exposure.

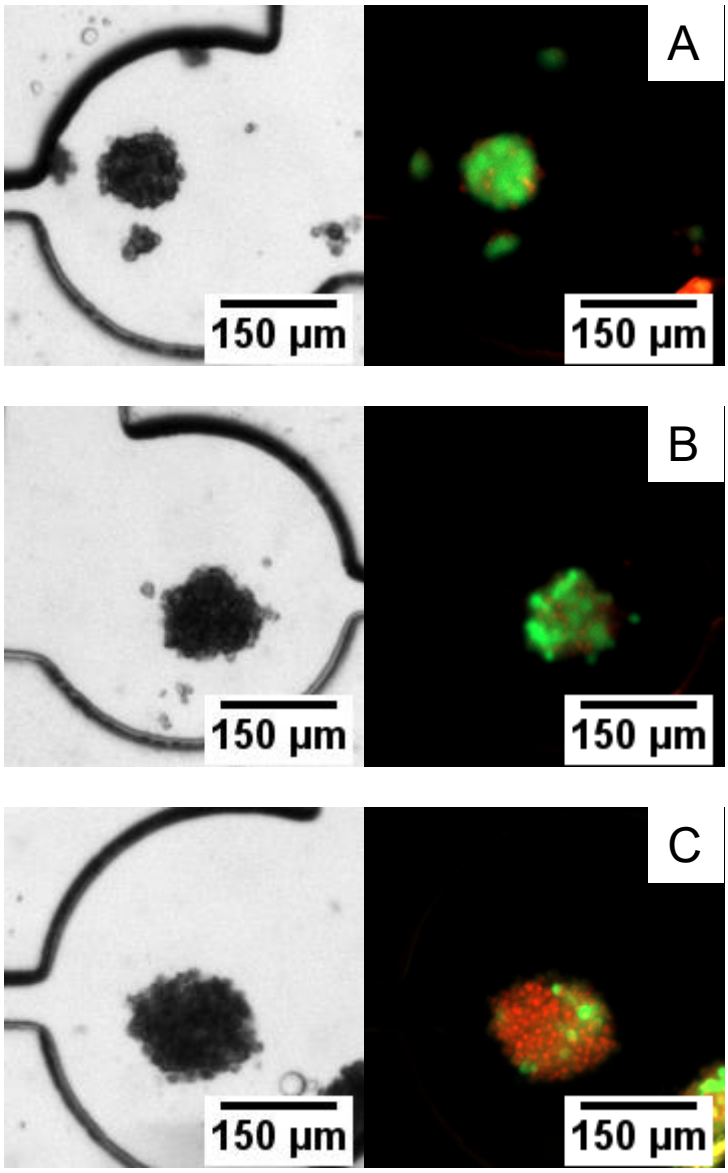


*Figure 4.8 FDA (green) and PI (red) staining of HepG2 spheroids on day 6 after 24 hours exposure to Diclofenac in the droplet-based platform. (A) Control, (B) 0 µM (vehicle control) and (C) 500 µM. Viable cells are green and dead cells are red.*

The HepG2 spheroids in the multi-array platform were exposed to the same range of concentrations of Diclofenac (as the droplet-based platform) for 24 hours. On every platform a single channel was dedicated as the control group, where spheroids were not exposed to Diclofenac but cultured in serum-free medium for 24 hours. Serum-free media was chosen to more closely mimic the conditions of the test groups as drug exposure was done using serum-free media. A second channel was the vehicle control group (0 µM) containing spheroids exposed to 0.1% DMSO only (serum-free media).

The results (Figure 4.9) show a weak decline in the viable ratio as the concentration increases, determined by the decrease in FDA fluorescent area produced by the spheroids. Counter staining with PI confirmed an increasing number of cells with permeated membranes, indicating cell death. The viable fraction for the control and 0 µM (vehicle control) groups were 1.12 ± 0.02 and 1.09 ± 0.02, respectively, compared to 0.96 ± 0.03 for the highest concentration of Diclofenac (500 µM).

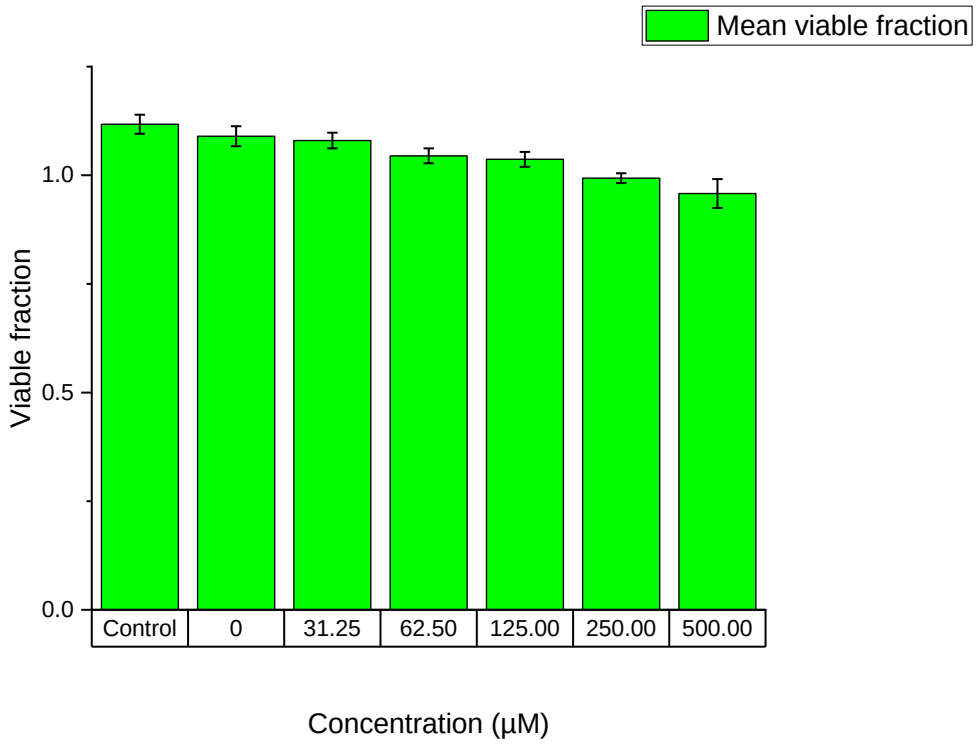


*Figure 4.9 Mean (± standard error) viable fraction of HepG2 spheroids on day 6 cultured in the multi-array platform after 24 hours exposure to Diclofenac determined using FDA / PI staining. (n = 1, repeated in triplicate).*

## 4.2 Results of culturing primary rat hepatocytes

The systems described in the previous section demonstrated that the multi-array platform was able to facilitate the culture of the HepG2 cell line, was more “user-friendly” and had a higher throughput than the droplet-based platform. Spheroids remained viable for over 10 days and after exposing them to Diclofenac (at day 5) a non-significant but steady decline in viability was observed. The slight decline is likely due to the fact that HepG2 cells do not possess high enough levels of the CYP450 enzymes resulting in the production of toxic metabolites [116]. Primary human hepatocytes are considered the gold standard for hepatotoxicity screening as they express an almost complete set of Phase I and Phase II metabolizing enzymes, but are limited in availability and costly [112]. An alternative to using primary human hepatocytes to investigate xenobiotic metabolism is using primary animal hepatocytes. Primary rat hepatocytes (PRH) are more accessible than human hepatocytes and have been shown to be a valuable source of information [124].

The advantage sought from this research is to generate functional hepatic spheroids using lower cell numbers than what is currently available [66], thereby reducing resources and indirectly increasing throughput. This section will describe the results of using primary rat hepatocytes to evaluate the metabolizing capabilities of spheroids constructed in the platforms. Hepatocytes are cultured for 4 days to allow the cells to aggregate into spheroids before being exposed to Diclofenac or Paracetamol, as both these compounds are known to induce metabolism-related hepatotoxicity [6] [12].

The expression of the Phase I metabolizing enzymes has already been shown to be stable during this length of culture in a 3D configuration using primary rat hepatocytes [127].

### 4.2.1 Preliminary results of the primary rat hepatocytes cultured in the microfluidic platforms and on the collagen sandwich configurations

Primary rat hepatocytes took an average of 1 – 2 days to form aggregates and formed smooth, compact spheroids in the microfluidic platforms by day 3 (Figure 4.10).

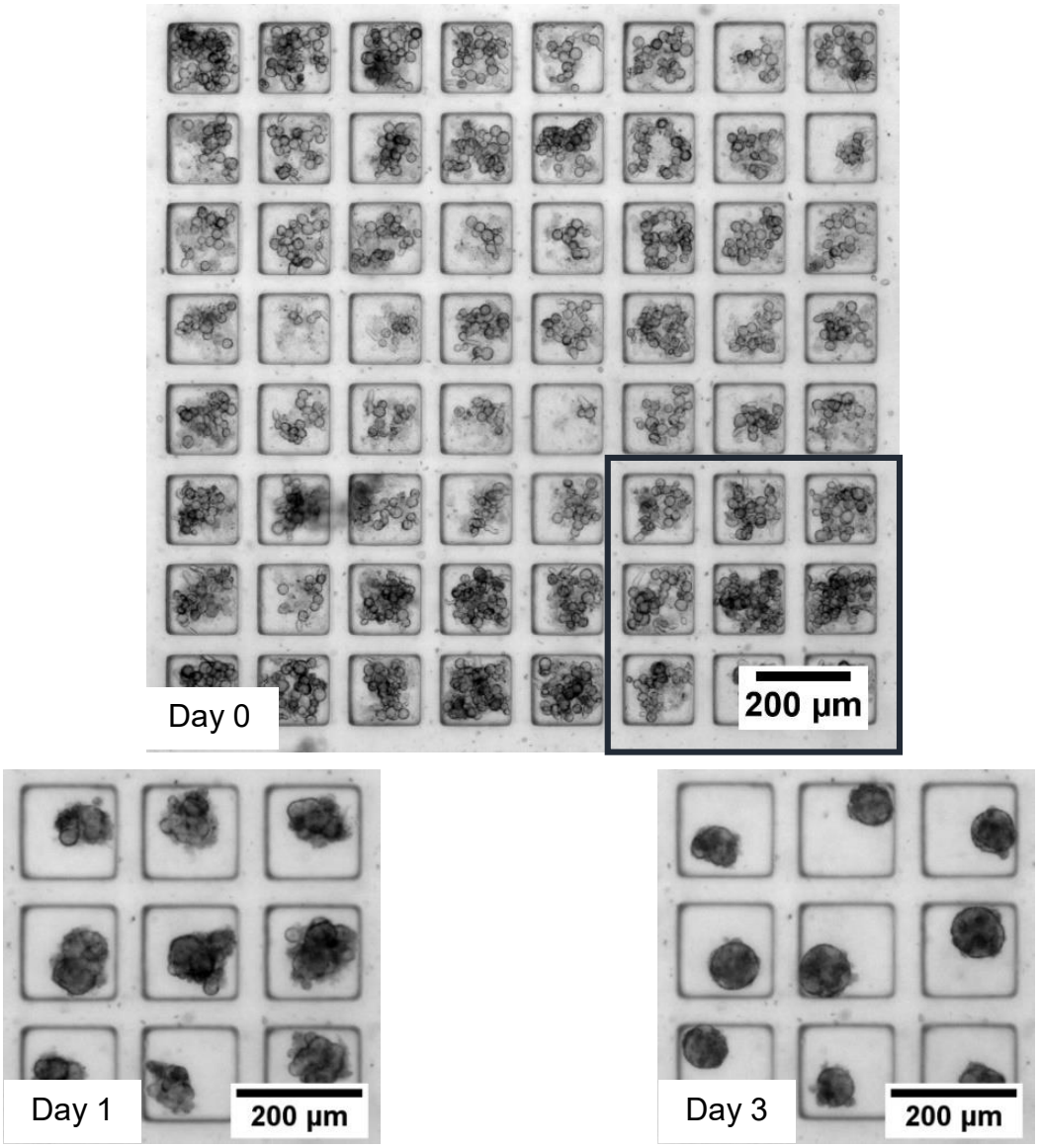


*Figure 4.10 Microscopic image of primary rat hepatocytes perfused from a male Sprague Dawley rat in the multi-array platform on the day of seeding (Day 0) at a concentration of 3 x $10^6$ cells / ml. Inserts of the bottom right-hand corner on Day 1 and Day 3 showing the aggregation and formation of smooth spheroids. (x 5 objective)*

The mean number of cells per microwell was found to be 21 ± 9 cells / well in the arrays closest to the reservoirs. This resulted in a significant difference in spheroid size by day 3 and day 5 (Figure 4.11).

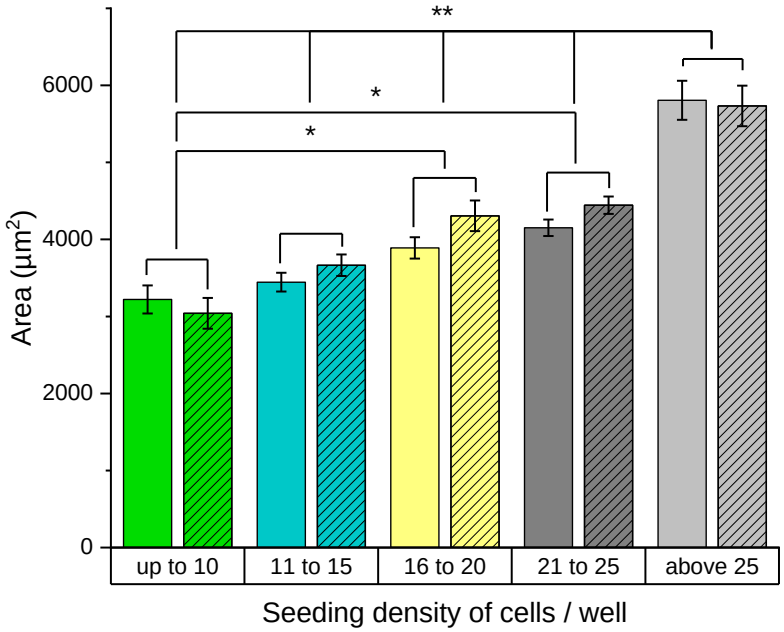


*Figure 4.11 Seeding density of primary rat hepatocytes in the multi-array platform and the mean (± standard error) area of the formed spheroids on day 3 (solid) and day 5 (striped). (based on 164 individual spheroids over 3 platforms; * = p <0.05, ** = p < 0.01)*

PRH cultured in the collagen sandwich configurations were imaged (ZEISS) on day 5 (Figure 4.12) and showed refractile white borders between neighbouring cells (blue arrow), suggestive of bile canaliculi formation. Of note is the many cells that possess multiple nuclei (red arrow).

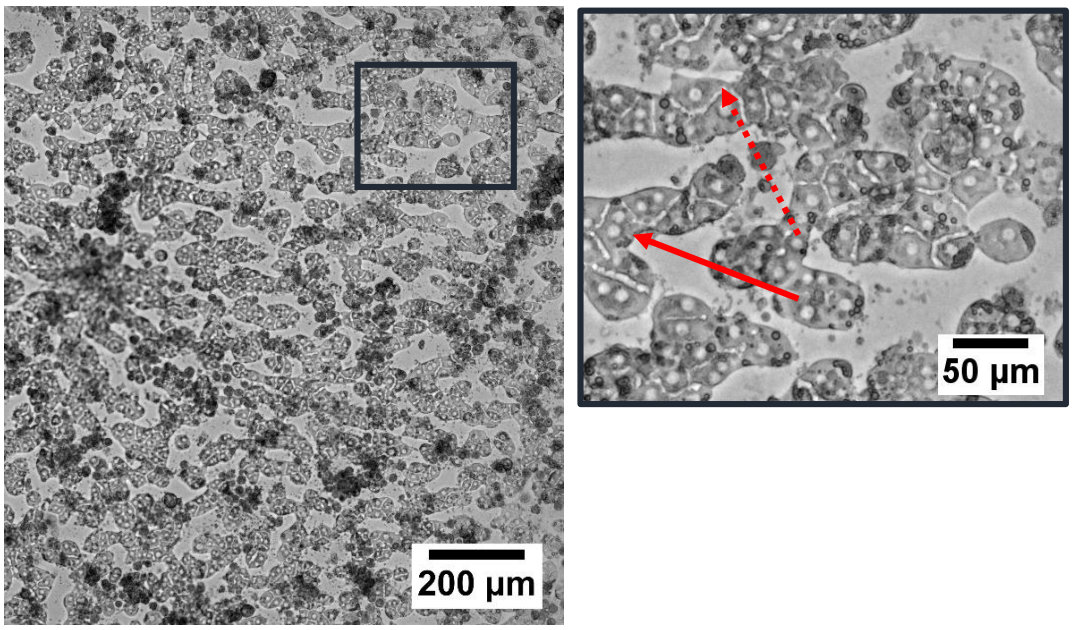


*Figure 4.12 Primary rat hepatocytes cultured in a collagen sandwich configuration for 5 days imaged using phase contrast microscopy. Insert is an enlarged image of the collagen sandwich configuration where the solid arrow indicates multi-nuclear cells and the dashed arrow indicates bright, refractile cell borders, suggesting the presence of bile canaliculi. (x 10 objective)*

### 4.2.2 Viability of primary rat hepatocytes cultured in the microfluidic platform

In a preliminary experiment, parallel cultures of PRH were maintained in the platform and their mean viable fraction calculated on different days. To obtain a viable fraction for day 1 the *brightfield image on the day of staining* was used, instead of the brightfield image taken the day before (day 0) (Chapter 3, section 3.6). On day 0 the cells had not aggregated enough to be considered spheroids. For all other days the brightfield image from the day before staining

was used. The mean viable fraction was 0.93 ± 0.02 on day 1 and declined to 0.81 ± 0.01 on day 7.

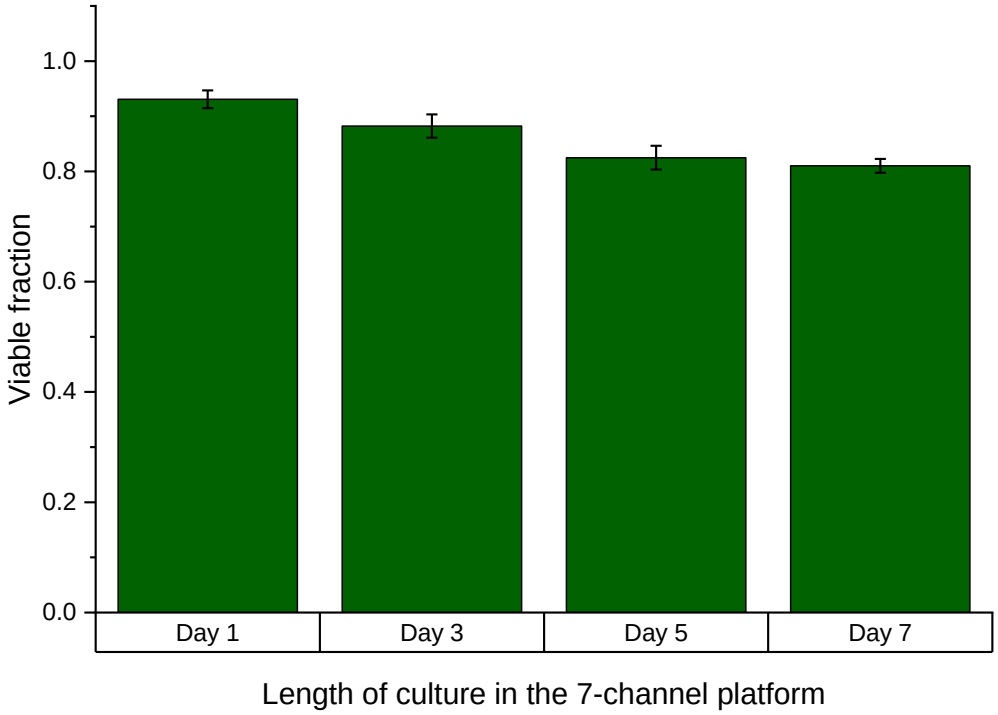


*Figure 4.13 Mean (± standard deviation) daily viable fraction of primary rat hepatic spheroids cultured in the multi-array platforms determined by FDA / PI staining using a single liver perfusion (n = 1 liver perfusion, replicated in triplicate) acquired from a male Sprague Dawley rat; 30 000 cells used.*

Hepatocytes are some of the few cells in the body that exhibit polarity (i.e. have a specific orientation). If neighbouring cells in a culture environment are in the correct orientation, they form tight junctions between the cell membranes which are an important component of the bile canaliculi network used for excretion and an indicator of the functional integrity of the culture. PRH

cultured in the multi-array platform were fixed and stained (Figure 4.14) using a fluorescent anti-body. Localisation of the ZO-1 stain at the cell boundaries is indicative of the formation of tight-junctions; and DAPI was used as a counter stain for the nuclei of the cells.

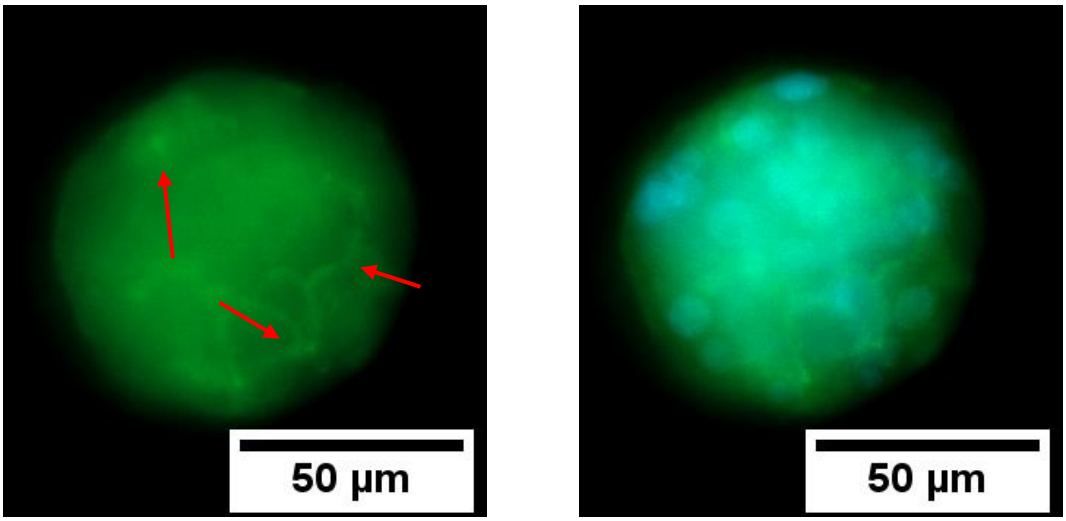


*Figure 4.14 (Left) Four day old primary rat hepatic spheroid stained for the formation of tight junctions, indicated by the localization of the ZO-1 stain (red arrows) and (Right) DAPI counter stain illustrating the nuclei in the spheroid. (x 10 objective taken with an Apotome attachment)*

The same staining protocol was used for the PRH in the collagen sandwich configuration but did not allow definitive identification of features as non-specific binding occurred.

### 4.2.3 Induced hepatotoxicity in primary rat hepatocytes cultured in the collagen sandwich configuration versus the microfluidic platform

PRH cultured in both systems were exposed to a range of different concentrations of Diclofenac (0 – 500 µM) and Paracetamol (0 – 7.5 mM), since both are known to be hepatotoxic at high concentrations. The $IC_{50}$ (concentration that inhibits cellular function of 50 % of the population) for Diclofenac and hepatocytes is approximately 330 – 500 µM [31], although this value varies greatly in the literature depending on the culture method / length or media additives. The $IC_{50}$ for Paracetamol has been reported to vary between 0.1 – 1 mM [118]. For this project, cultures were stained to assess viability at 24 – and 48 hours post-exposure. The cultures stained at 48 hours had 24 hours of recovery in serum-free medium. Figure 4.15 and 4.16 show a representative set of images of the collagen sandwich configurations and the multi-array platforms. A concentration-dependent decrease in viability is observed in both systems. For the collagen sandwich configurations this decline is illustrated as an increase in the number of nuclei stained with PI and for the multi-array platform it is observed as a decrease in the area of the spheroid stained with FDA (and an increase in PI). FDA was not used to stain the collagen sandwich configurations as this did not allow identification of single cells, thus Hoechst was used instead. The decrease is more noticeable, in both systems, at the maximum concentration used and at 48 hours post-exposure.

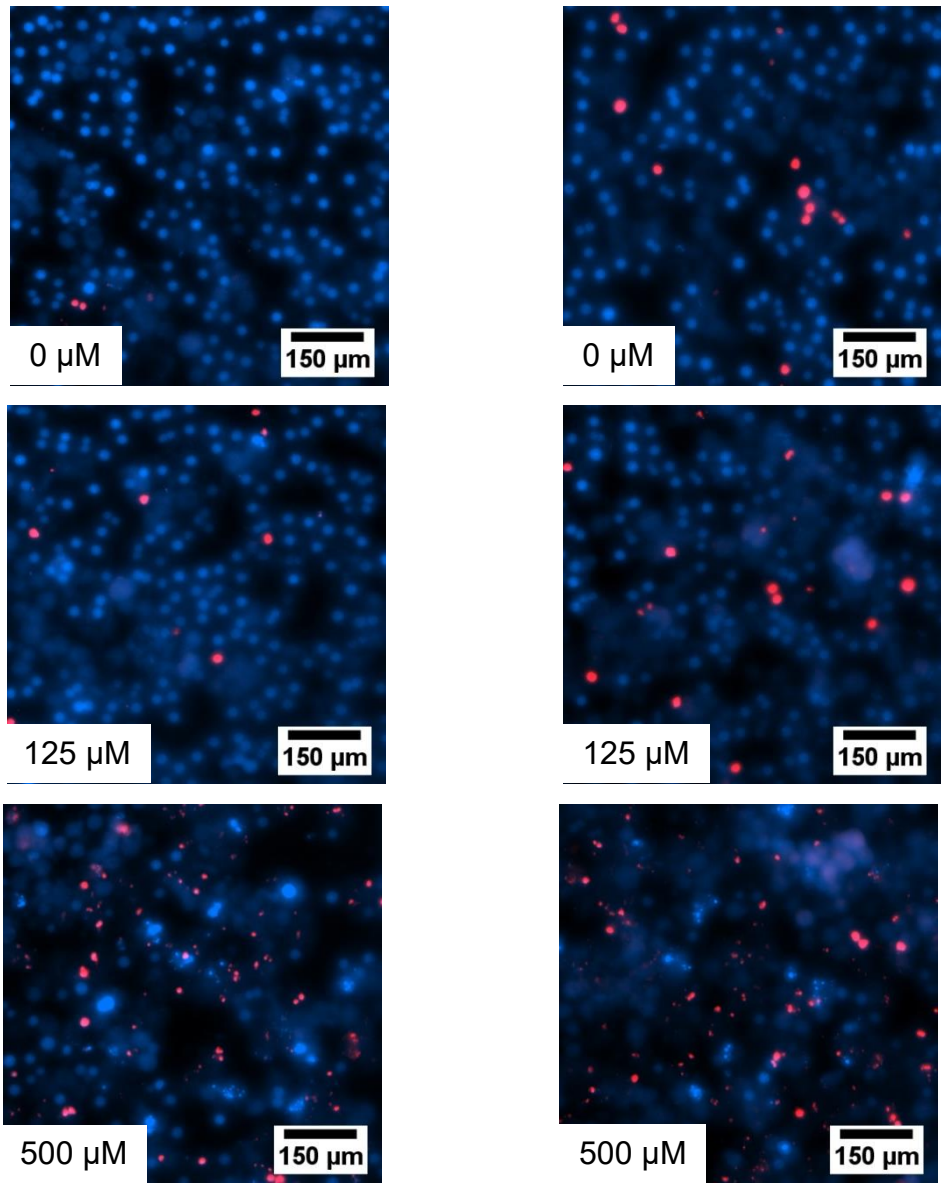


*Figure 4.15 Staining of primary rat hepatocytes perfused from a male Sprague Dawley rat cultured for 4 days in a collagen sandwich configuration after being exposed to Diclofenac for (left) 24 hours and (right) 24 hours followed by 24 hours recovery in serum-free medium. Hoechst (blue) stained all nuclei and PI (red) stained only nuclei of cells that have damaged membranes, indicating cell death. (x 10 objective)*

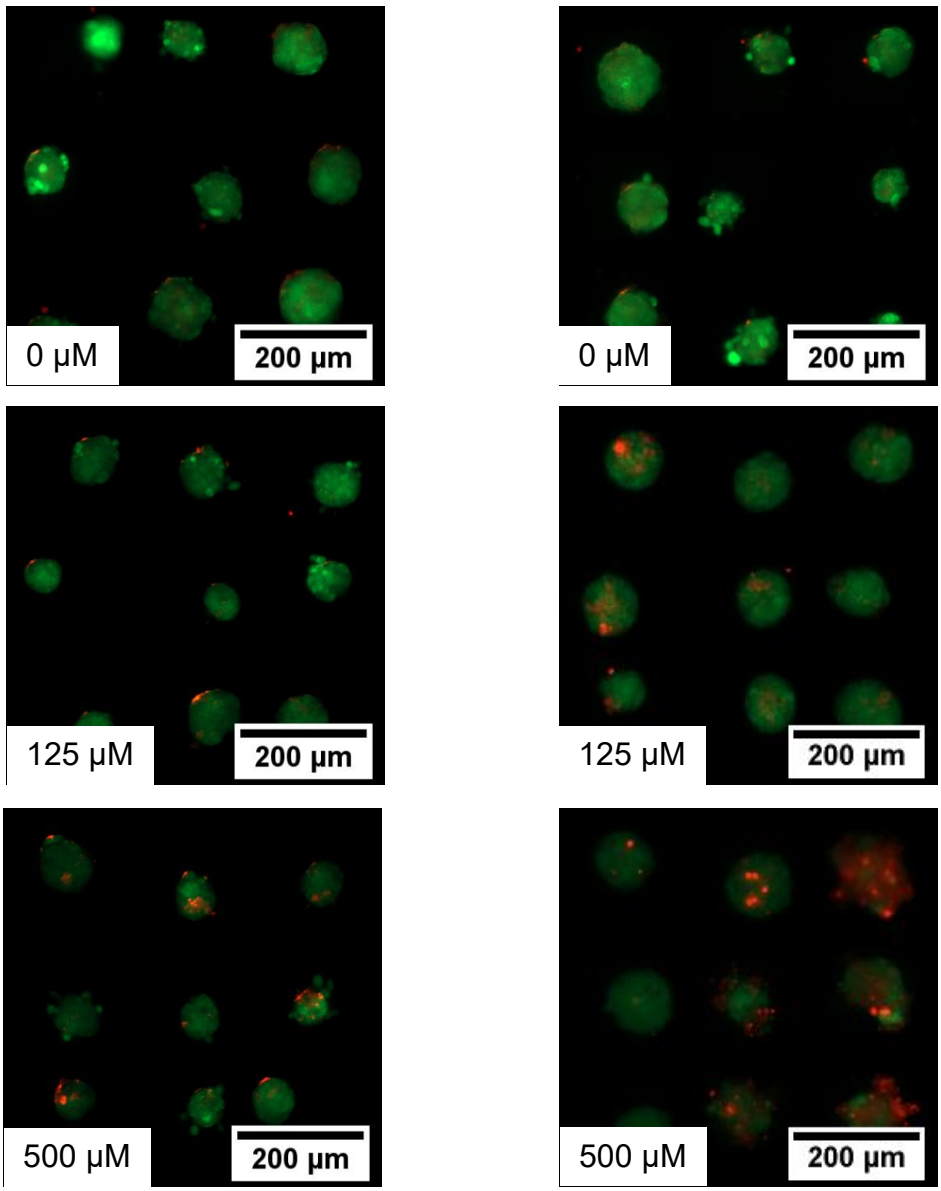


*Figure 4.16 Staining of primary rat hepatic spheroids perfused from a male Sprague Dawley rat in the multi-array platform after being exposed to Diclofenac for (left) 24 hours (day 5) and (right) 24 hours followed by 24 hours recovery (day 6) in serum-free medium. Viable cells are stained using FDA (green) and dead cells are stained using PI (red). (x 5 objective)*

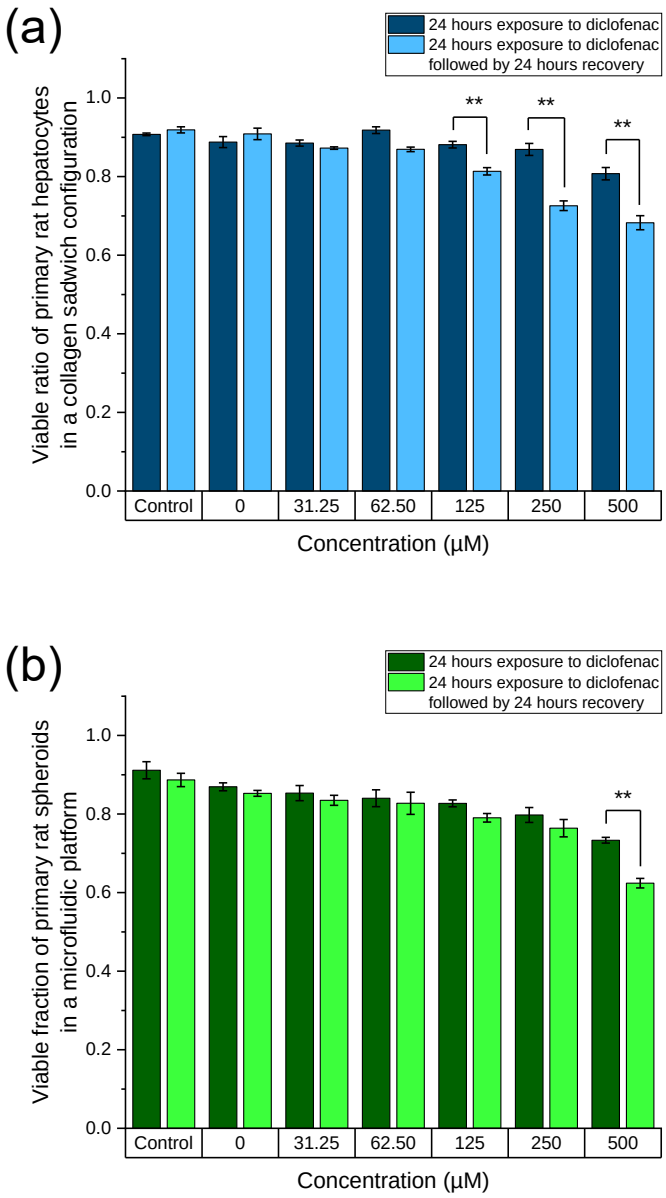


*Figure 4.17 (a) Mean (± standard error) viable ratio for the collagen sandwich configurations and (b) viable fraction for multi-array platforms of primary rat hepatocyte cultures (acquired from perfusing a liver of a male Sprague Dawley rat liver) exposed to Diclofenac after 24 and 48 hours determined by Hoechst / PI (a) and FDA / PI (b) staining (n = 3 liver perfusions, replicated in triplicate;* = $p < 0.05$, ** = $p < 0.01$).*

Figure 4.17 (a) illustrates a significant difference when applying a two-way ANOVA test for the three highest concentrations of Diclofenac (125 µM, 250 µM and 500 µM) after 24 hours exposure compared to 48 hours post-exposure in the collagen sandwich configurations. When comparing the viable ratio for the 24-hour exposure group only, the highest concentration (500 µM) was significantly different ($p < 0.05$ for 250 µM and $p < 0.01$ for control, 0, 31.25, 62.50 and 125 µM) to all other concentrations. For the 24-hour exposure followed by 24-hour recovery group the cultures exposed to 125 µM was significantly different to the control and 0 µM group ($p < 0.01$) and the cultures exposed to 31.25 µM and 62.50 µM ($p < 0.05$). Hepatocytes exposed to 250 µM was significantly different compared with all lower concentrations ($p < 0.01$) and the cultures exposed to 500 µM was significantly different compared with all lower concentrations ($p < 0.01$) except those exposed to 250 µM.

Figure 4.17 (b) shows that the spheroids in the multi-array platforms after 24 hours exposure to Diclofenac is significantly different at the highest concentration (500 µM) only when compared to 48 hours post-exposure.

When comparing the viable fraction of cultures after 24-hours exposure those exposed to 250 µM were significantly different ($p < 0.01$) to the control group, while the cultures exposed to 500 µM was significantly different ($p < 0.05$ for 125 µM and $p < 0.01$ for control, 0, 31.25 and 62.5 µM) to all lower concentrations except from those exposed to 250 µM.

For the cultures exposed for 24 hours, followed by 24 hours recovery, the 125 µM concentration was significantly different ($p < 0.05$) to the control group and the 250 µM was significantly different to the control and 0 µM concentration (p

< 0.01 and p < 0.05, respectively). At 500 µM there was a significant difference (p <0.01) to all lower concentrations.

The hydroxylated metabolite of Diclofenac, 4'-Hydroxydiclofenac (4'-OHDIC), was used to test the Phase II metabolizing capabilities of the primary rat hepatocyte cultures. This toxic metabolite (4'-OHDIC) undergoes Phase II metabolism and consequently gets detoxified through conjugation to glutathione. Due to time constraints only a single experiment (one animal) was conducted. Representative images are shown in Figure 4.18.

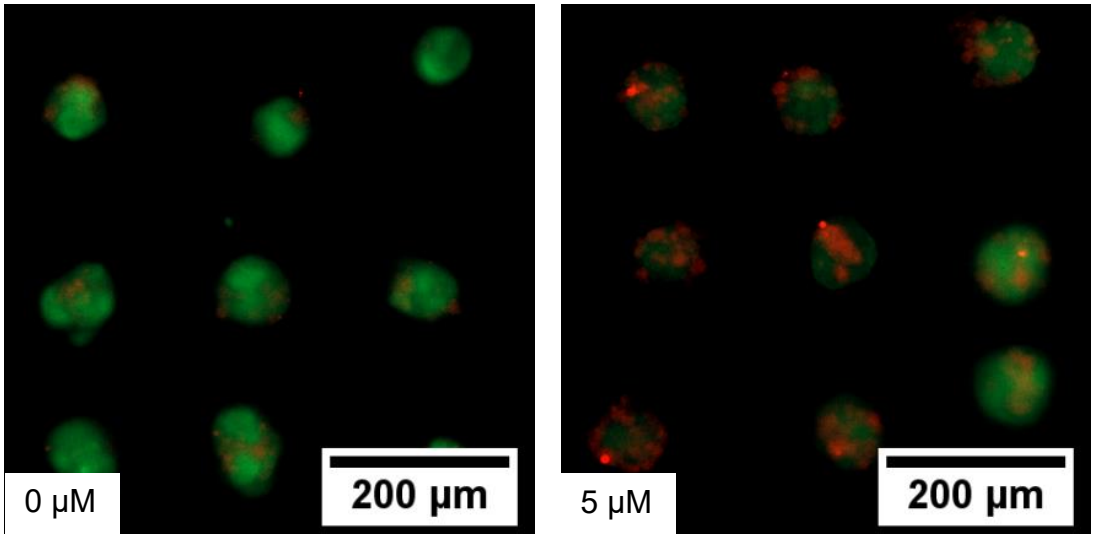


*Figure 4.18 Staining of primary rat hepatic spheroids in the multi-array platform after being exposed to 4'-Hydroxydiclofenac for 24 hours. Viable cells are stained using FDA (green) and dead cells are stained using PI (red). (x 5 objective)*

To compare the collagen sandwich configurations and the multi-array platforms the viable fraction and viable ratio had to be normalised (Figure 4.19). This was carried out because of the difference in starting viability of the

control groups between the two culturing methods. To normalise the data the control viability was set to 1 and each condition was adjusted according to this ratio.

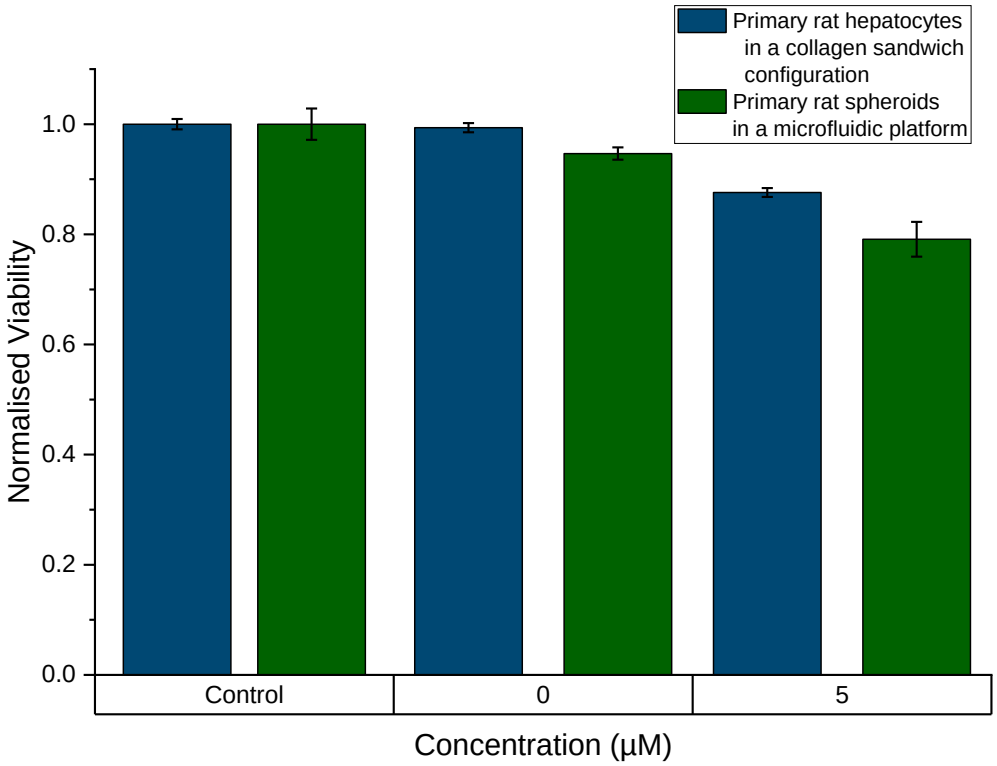


*Figure 4.19 Mean (± standard error) normalised viability for the collagen sandwich configurations (blue) and the multi-array platforms (green) of primary rat hepatocyte cultures exposed to 4-Hydroxydiclofenac for 24 hours determined by Hoechst / PI (blue) and FDA /PI (green) staining (n = 1 animal perfusions, replicated in triplicate).*

Primary rat hepatocyte cultures were also exposed to Paracetamol and the viable ratio and viable fraction was determined following the same protocol as for the cultures exposed to Diclofenac.

*Paracetamol cultures*

When comparing the viable ratio (Figure 4.20 a) between the 24 hours and 48 hours post-exposure groups there is a significant difference ($p < 0.01$) at the 0.94, 1.88, 3.75 and 7.50 mM concentrations. For the 24 hours post-exposure groups there was a significant difference ($p < 0.01$) between the 3.75 mM concentration and all lower concentrations used. This was also true for the 7.5 mM concentration except there was no significant difference between that and the 3.75 mM concentration.

For the 48 hours post-exposure cultures there was a significant difference ($p < 0.01$) between the 1.88 mM concentration and all lower concentrations, which was also true for the cultures exposed to 3.75 mM and 7.5 mM.

*Primary rat hepatocytes : Viable fraction*

For the primary rat spheroids (Figure 4.20 b) there is a significant difference ($p < 0.01$) between the 24 hours and 48 hours post-exposure cultures at the highest concentration of 7.5 mM only.

When comparing the cultures of the 24 hours post-exposure there was a significant difference ($p < 0.01$) between the 7.5 mM concentration and all lower concentrations. This was also true for the 7.5 mM concentration in the 48 hours post-exposure cultures.

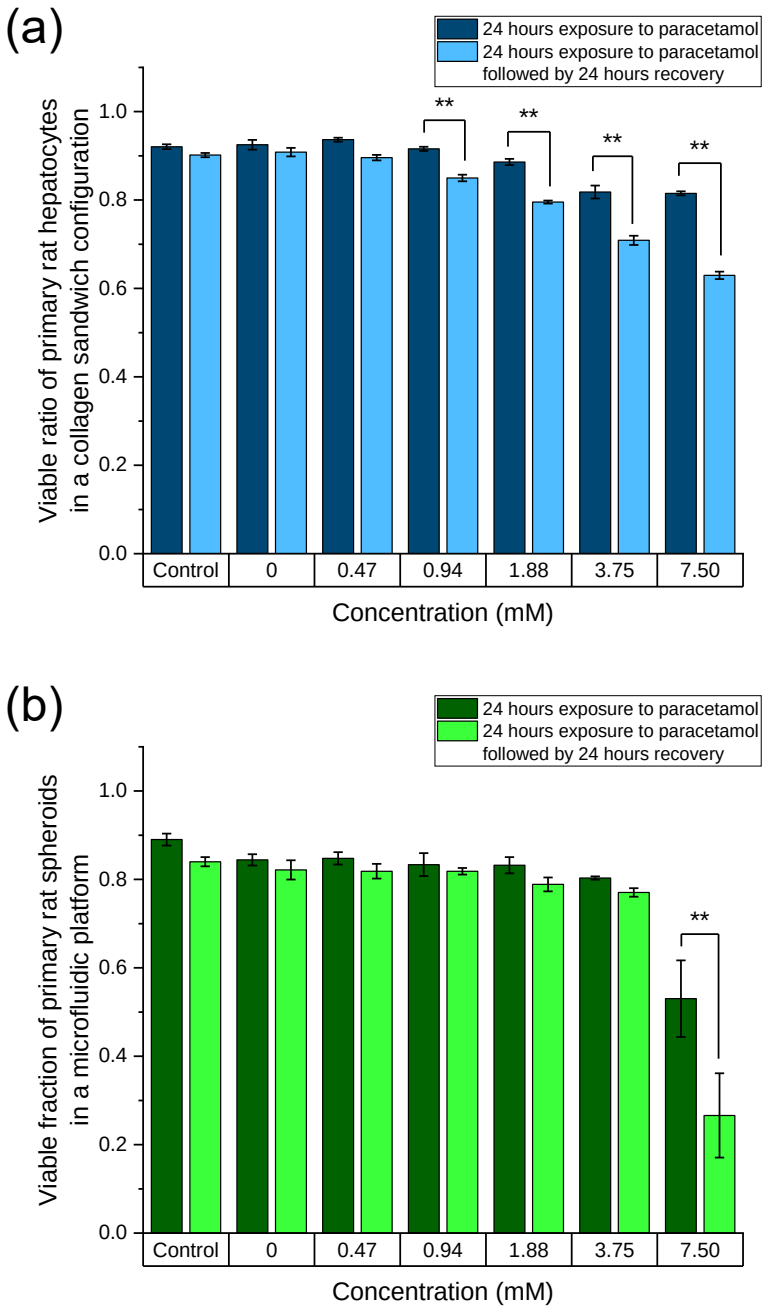


*Figure 4.20 Mean (± standard error) viable ratio for the collagen sandwich configurations (a) and viable fraction for multi-array platforms (b) of primary rat hepatocyte cultures exposed to Paracetamol after 24 – and 48 hours determined by Hoechst / PI (a) and FDA / PI (b) staining (n = 3 animal perfusions, replicated in triplicate; * = p < 0.05, ** = p < 0.01).*

To compare the different culturing methods and illustrate the decline in viability (compared to the control groups) the data were normalised following the same protocol as for the data from the 4'-Hydroxydiclofenac experiments. Figure 4.21 displays the decline for the cultures exposed to Diclofenac at 24 – and 48 hours post-exposure. At 24 hours post-exposure (Figure 4.21 a) the decline is more obvious in the multi-array platforms compared to the collagen sandwich configurations. At 48 hours post-exposure (Figure 4.21 b) the decline in viability is obvious for both culturing methods.

Figure 4.22 illustrates the decline in viability for the cultures exposed to Paracetamol after 24 hours and 48 hours post-exposure. The largest decline in viability can be observed in the multi-array platform at the 7.5 mM concentration after 24 hours (Figure 4.22 a) post-exposure and is the same for the cultures at 48 hours (Figure 4.22 b) post-exposure. It can be observed however, that there is a more obvious trend in the decline in viability for the collagen sandwich configurations starting from the 1.88 mM concentration through to the 7.5 mM concentration.

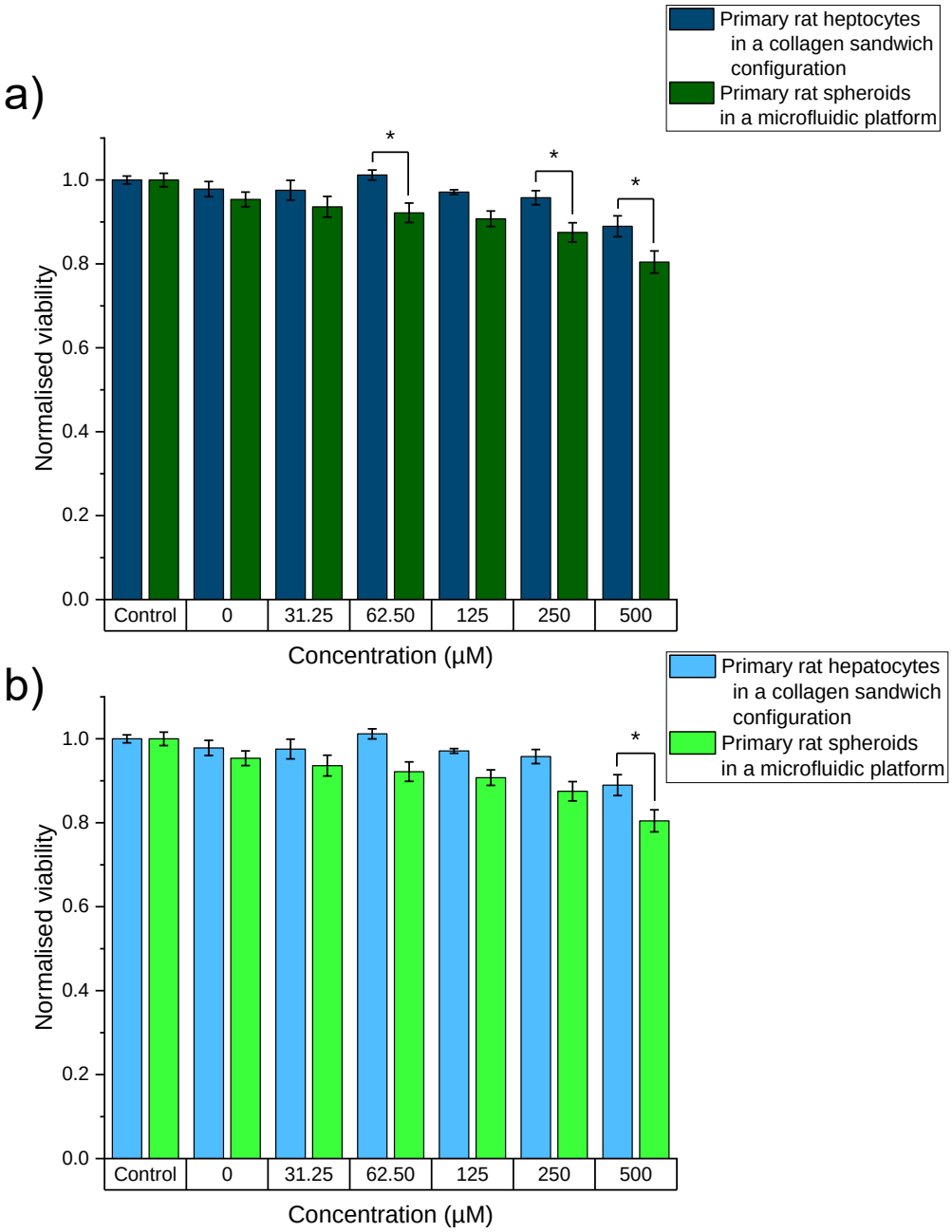


*Figure 4.21 Mean (± standard error) normalised viability of primary rat hepatocytes cultured in a collagen sandwich configuration (blue) and the multi-array microfluidic platform (green) after 24 hours (a) and 48 hours (b) post-exposure to Diclofenac determined by Hoechst / PI (blue) and FDA / PI (green) staining (n = 3 animal perfusions, replicated in triplicate; * = $p < 0.05$).*

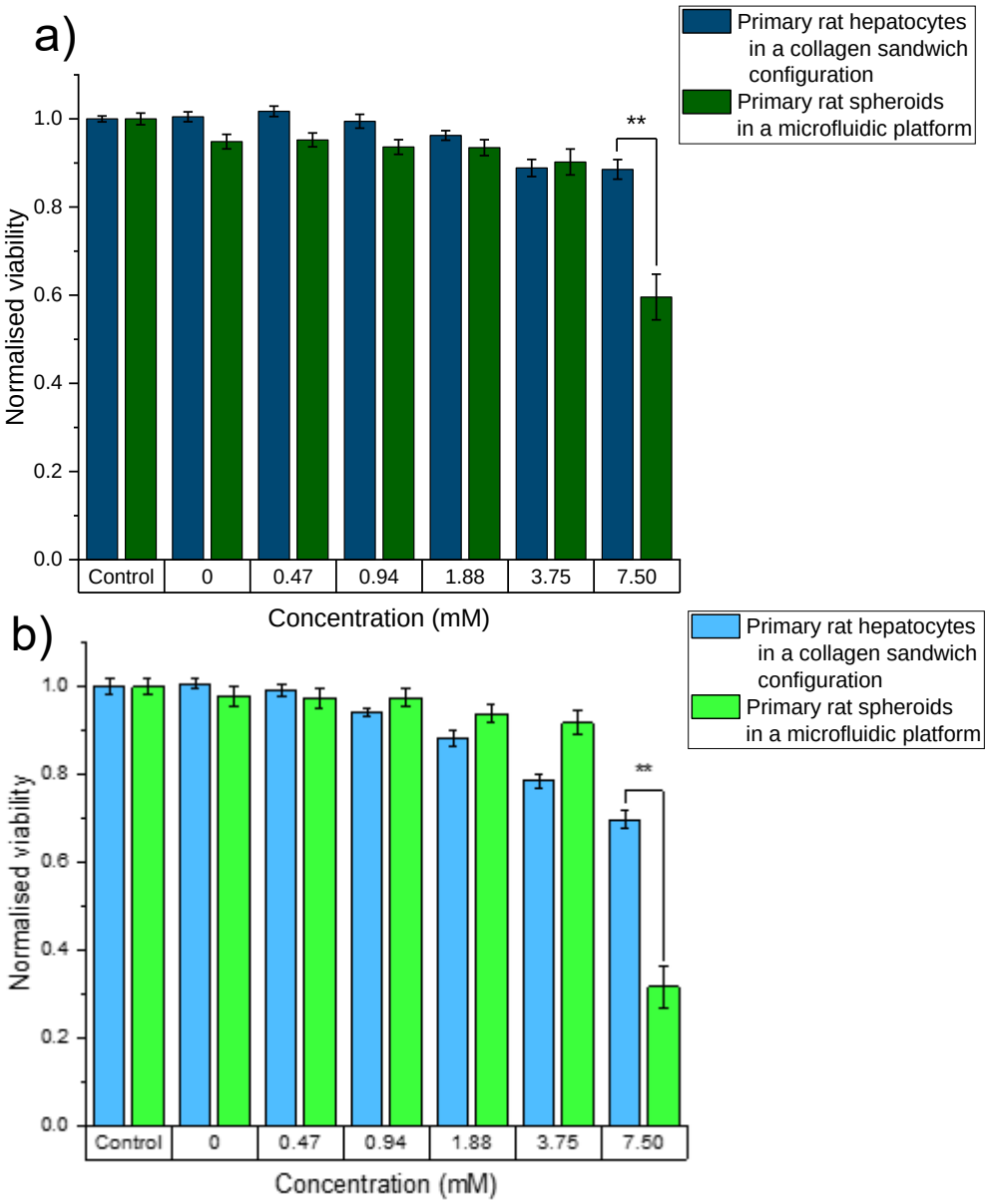


*Figure 4.22 Mean (± standard error) normalised viability of primary rat hepatocytes cultured in a collagen sandwich configuration (blue) and the multi-array microfluidic platform (green) after 24 hours (a) and 48 hours (b) post-exposure to Paracetamol determined by Hoechst / PI (blue) and FDA / PI (green) staining (n = 3 animal perfusions, replicated in triplicate; * = $p < 0.05$, ** = $p < 0.01$).*

Of note are the large error bars for the cultures in the multi-array platforms, particularly at the 7.5 mM concentration. During staining it was observed that some spheroids were completely dead (Figure 4.23) while neighbouring spheroids remained significantly more viable. The potential cause of the variation is addressed in the discussion section.

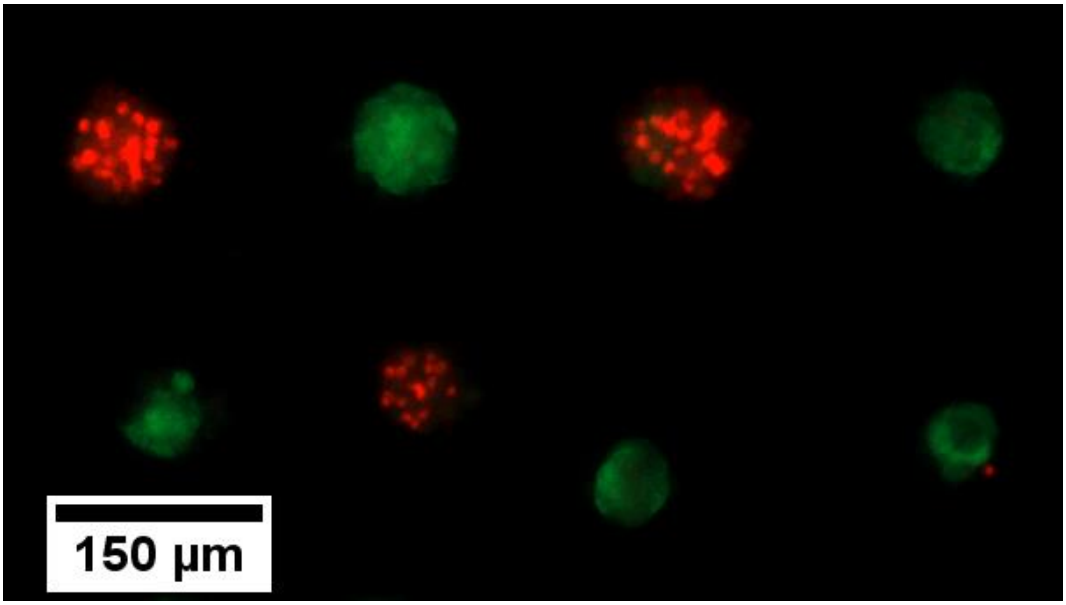


*Figure 4.23 Primary rat hepatic spheroids after being exposed to 7.50 mM Paracetamol for 24 hours. Note the difference in viable cells stained with FDA (green) and dead cells stained with PI (red) between neighbouring spheroids. (x 5 objective)*

### 4.2.4 Viability of the single array microfluidic platform after Diclofenac exposure

Primart rat hepatocytes were cultured in the single array platform for 4 days and exposed to 500 µM Diclofenac for 24 hours. The number of cells / well was

found to be 60 ± 18 (mean ± standard deviation). This platform was used to determine whether a lower number of spheroids cultured would still be metabolically active. Due to time constraints only a single experiment was completed. The representative images of sections of the single well array and the mean viable fraction can be found in Figure 4.24 and 4.25, respectively.

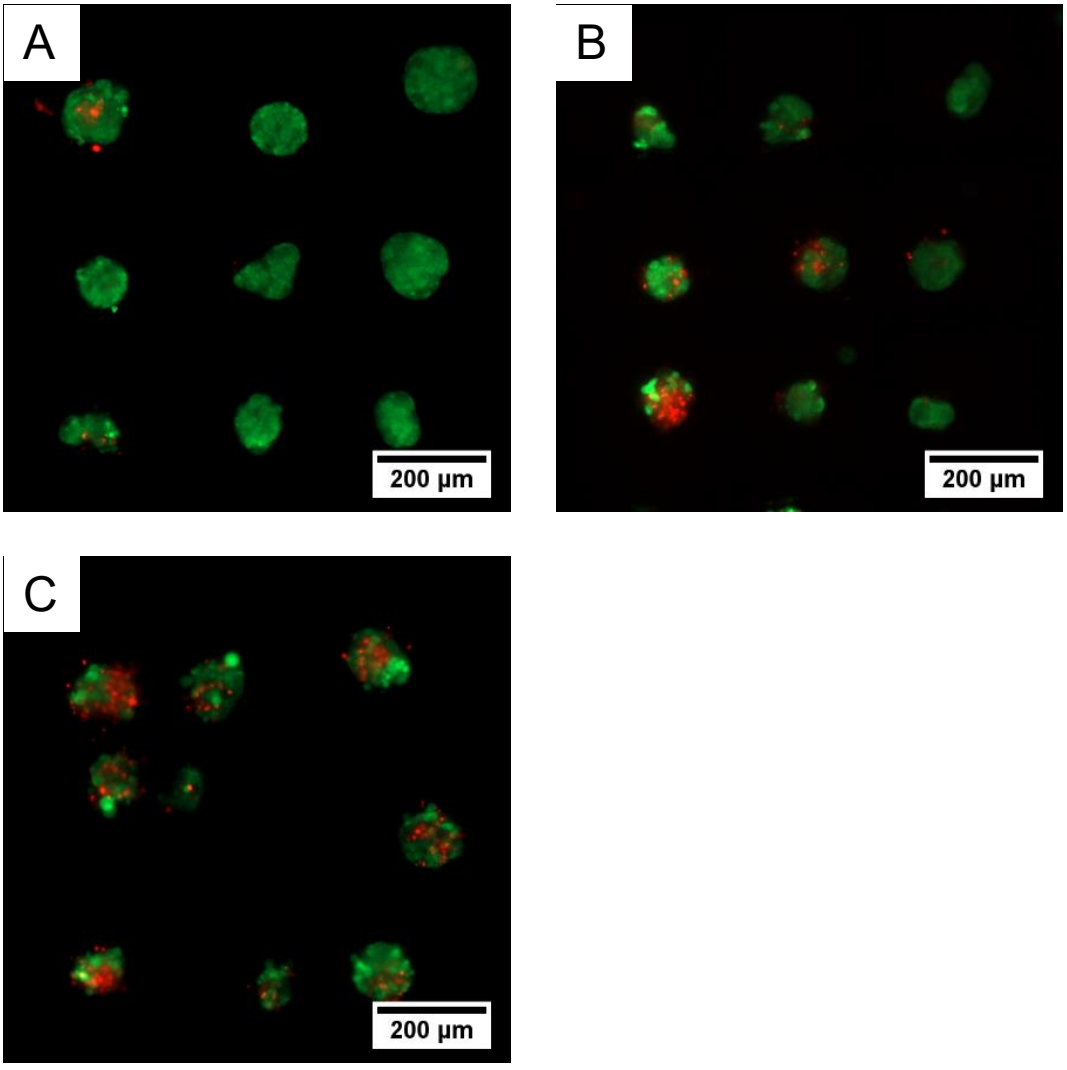


*Figure 4.24 Primary rat hepatocyte spheroids in the single array platform on day 5 after 24 hours exposure to (A) control (serum-free medium), (B) 0 µM and (C) 500 µM of Diclofenac. (x 5 objective)*

Due to the low number of repeats no statistical analysis could be completed, however the trend is the same as for the multi-array platform, showing a decline in the viable fraction. The mean viable fraction for the control and the 0 µM (vehicle control) was 0.81 ± 0.02 and 0.68 ± 0.04, respectively, compared to 0.53 ± 0.03 for 500 µM Diclofenac. This was lower than the 0.73 ± 0.01 recorded in the multi-array platform.

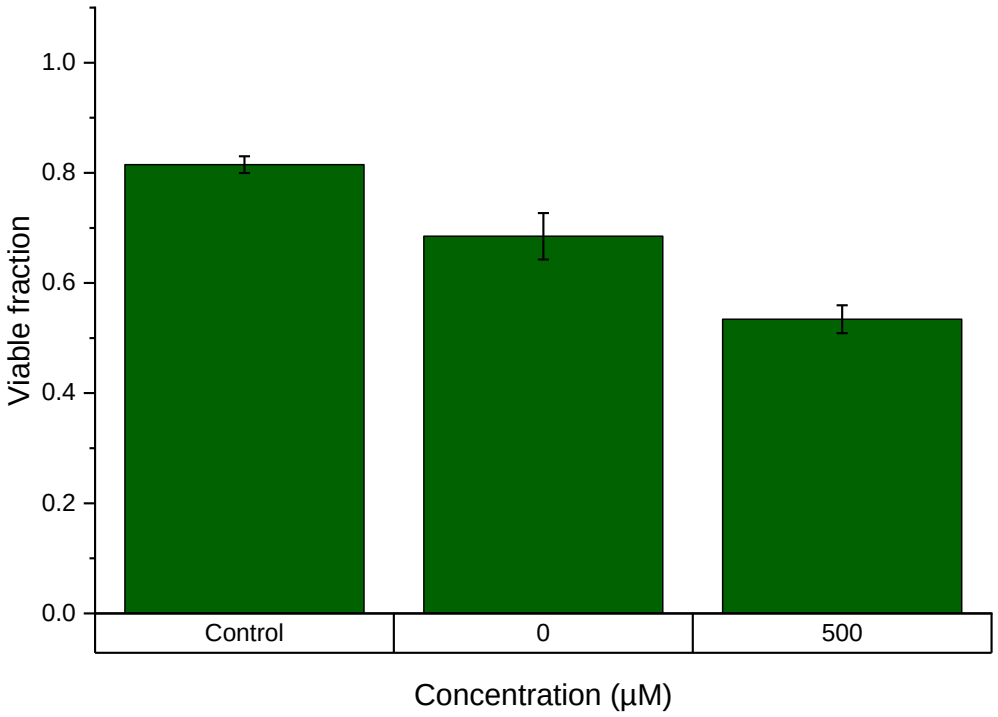


*Figure 4.25 Mean (± standard deviation) viable fraction of primary rat hepatocyte spheroids cultured in the single array platform for 4 days before being exposed to Diclofenac for 24 hours determined using FDA / PI staining. (n = 1 rat liver perfusion, replicated in triplicate)*

## 4.3 Discussion and conclusion on the droplet-based vs multi-array platforms using the HepG2 cell line

### 4.3.1 Platform operation and maintenance

*Droplet-based platform*

The droplet-based platform allows up to 50 individual spheroids to be cultured on a single device smaller than a standard microscope slide. Filling of traps in the platform is quick (< 1 minute) and the whole procedure takes approximately 20–30 minutes to complete (including priming of device). Replacement of medium takes approximately 15 minutes, but insertion and removal of the tubing connected to the inlets remains challenging as this could force the HepG2 spheroids out of the traps and into the channel. The efficiency of maintaining spheroids in the trap during the culturing period is heavily dependent on the skill of the user. The total volume of the medium in the platform is between 7 to 9 µl. However, a disadvantage is the small volume relatively to large surface area of the channels in the platform; this makes the platform sensitive to evaporation. This is true for most microfluidic platforms and to limit this problem, PDMS reservoirs can be built around the inlets of the platforms, which reduces the impact of evaporation.

*Multi-array platform*

The multi-array platform can accommodate up to 1700 individual spheroid cultures simultaneously. The total volume of medium in the platform is approximately 100 µl / channel, providing a higher surface area to volume ratio and making it less vulnerable to evaporation. Provided the flow rate inside the

channel is kept low the HepG2 spheroids are not forced out of the wells making this platform more robust. To keep the flow rate below the critical velocity which will displace the spheroids, the difference in hydrostatic pressure, between the two reservoirs at each end of the channel, is kept to a minimum.

The spheroid aggregation in the two platforms (droplet-based and multi-array) showed that HepG2 cells will form into spheroids given a wide range of starting cell numbers. This agrees with work from Miyamoto and coworkers [120], who cultured HepG2 cells at different densities corresponding to 100, 500 and 1000 cells / well in a microwell array placed in a 6 well-plate. They found >85% spheroid formation efficiency for all starting cell densities used. The droplet-based platform only needed approximately 30 cells to form a compact spheroid, with less in the multi-array platform. Unfortunately no LC-MS analysis was performed using the droplet-based platform.

### 4.3.2 Culturing HepG2 spheroids in the droplet-based and multi-array microfluidic platforms

The HepG2 cells quickly aggregated to form spheroids in both systems. Figure 4.2 shows that the area of the spheroids in the droplet-based platform steadily increased up to day 7 but then increased at a faster rate up to day 13. HepG2 cells are an immortalised carcinoma cell line that lack contact inhibition (in 2D cultures) and will continue to proliferate *in vitro*. The large increase in the slope is more likely the result of a large number of traps containing multiple spheroids that eventually fused into a larger single spheroid. This is opposite to what is seen in Figure 4.7 for the mean area of the spheroids in the multi-array

platform. These wells nearly always contained a single spheroid. Passage number may play an important role in the difference between proliferation rates observed between the two platforms. The HepG2 cells used in the multi-array platform were at a much higher passage number than those used in the droplet-based platform. As the passage number increases the doubling time (proliferation) of the cells decrease, due to a change in phenotype or genotype over time.

HepG2 cell have poor Phase I metabolizing capabilities. Diclofenac has been shown to have some direct toxic affect (Figure 4.8), but it is the toxic intermediate produced by hydroxylation through the CYP2C9 enzyme that is primarily associated with hepatic injury. At the highest Diclofenac concentration of 500 µM the spheroids had a viability higher than 90 %. This indicates that HepG2 cells are relatively insensitive to Diclofenac and agrees with what Fey and co-workers [118] reported in 2012 using HepG2 spheroids. They cultured HepG2 cells in Aggrewell plates after centrifugation overnight. The Aggrewell plates provide a non-adherent surface with microwells patterned on a 24 well-plate format. These cells quickly formed spheroids and were maintained in a bioreactor for 21 days before being exposed to six compounds, one being Diclofenac. They calculated a $LC_{50}$ (concentration required to kill 50 % of the population) to be 2.6 mM based on the cells ability to produce ATP. Estimating an $LC_{50}$ value on the viable fractions determined in the droplet-based platform experiment would not provide a reliable curve due to the small decline. A commonly used equation to calculate a 50 %

response curve is the 4-parameter logistic model (Equation 4.1), with describes a sigmoid-shaped response [121].

$$Y = \frac{a - d}{1 + (\frac{X}{c})^b} + d$$

*Equation 4.1 The 4-PL model equation to calculate a 50 % inhibitory effect. Y is the response at X concentration; Lower asymptote is a; upper asymptote is d, c corresponds to midway between a and d. Steepness of the linear portion is described by slope factor, b.*

It is generally recommended to have data points somewhere in the middle of the curve (between 30 – 60 % viable) and when the spheroids are nearly completely dead to calculate an accurate curve [122]. The HepG2 spheroids that were exposed to Diclofenac showed a small concentration dependent response (Figure 4.9). This suggest that the HepG2 spheroids cultured in the multi-array platform may be negatively impacted by the addition of the Diclofenac. This response, combined with the viability during the experiment, proves that the platforms are suitable for generating hepatic spheroids; and they may be useful for detection of hepatotoxicity if more metabolically active cells are used.

### 4.3.3 Conclusion

Both microfluidic platforms have been shown to provide an efficient environment to culture HepG2 spheroids. Both platforms have the advantage of physically constraining the size of the spheroids. A large spheroid (diameter exceeding 500 µm) would develop a necrotic core [123] due to the lack of oxygen in the inner cells of the spheroid. The multi-array platform can generate

over 250 individual spheroids in a single channel and was shown to be more robust compared to the droplet device. The multi-array platform also proved to be less susceptible to evaporation. An important consideration was the sample volume produced by both systems, as one part of this research project was to evaluate the effect of the miniaturization process on detection of induced hepatotoxicity. Although a decline in viability can be seen (Figure 4.9) no test to confirm this decline was due to metabolism-related toxicity was conducted using the HepG2 cells. As the platform has been shown to facilitate the culture of a hepatic cell line, primary hepatic cells are used in all future experiments. As detailed in Chapter 2 (section 2.2.2) and at the beginning of this chapter, primary hepatocytes are preferred to cell lines when conducting drug-induced toxicity assays as primary hepatocytes have higher levels of the major Phase I and Phase II metabolizing enzymes. Both these enzyme groups are important when evaluating drug toxicity since it is crucial to evaluate the whole metabolic process. Samples of culture media containing different Phase I and II metabolites generated by the cells can be sent for identification and quantification by LC-MS analysis. (Chapter 5).

## 4.4 Discussion of primary rat hepatocytes toxicity experiments

This section will discuss the results obtained from the primary rat hepatocyte experiments. Cells were cultured in the microfluidic platforms (multi-array platform and the single array platform) or in a collagen sandwich configuration (24 well-plate only).

### 4.4.1 Functional assessment of microfluidic platform

*Multi-array and Single array platforms*

The cells quickly formed smooth spheroids for the duration of the experiment. Based on the results from Figure 4.13 the difference in the viable fraction differs by approximately 10 % between day 1 and day 7. The small decline demonstrates that the platforms provide a suitable culturing environment for primary rat hepatocytes. The average diameter (± standard deviation) of the spheroids ranged between 73 ± 12 and 82 ± 13 µm, far below the size of 200 µm that would cause cells inside the spheroid to become necrotic due to a lack of oxygen [128]. It is likely the slight decline is due to a combination of factors. The isolation process is known to cause some stress / damage to cells, which may be introduced into the platform following seeding. If a cell sustains damage it will initially try to repair itself [128], and if not, may undergo programmed cell death. The method for evaluating the viable fraction of the spheroid is also not ideal. Analysing a 3D structure using a 2D image could lead to over / under estimation of the signal being produced. The intensity of the fluorescent signal is (in part) proportional to the amount of FDA that has accumulated inside the cell [129]. If this signal is found in a cell on the top of the spheroid and provides an intense enough fluorescence signal, it may in fact be hiding dead cells in the centre or bottom.

An important *in vivo* hepatic function is the transport of bile through the bile canaliculi between neighbouring cells. To achieve this, polarity in the cells needs to be established *in vitro* so the bile canaliculi can form. This network-like structures are sealed by tight-junctions formed of multiprotein complexes,

including ZO-1 [130]. Spheroids were stained with anti-ZO-1 fluorescent anti bodies (Figure 4.14), where the localization of the stain between neighbouring cells can be seen [131]. This is an indicator that cells in the spheroids have re-established polarity, which is important, as hepatocytes that retain their polarity have been shown to retain other liver-specific functions, such as metabolism of xenobiotics.

The phase-contrast images (Figure 4.12) of the refractile border between some neighbouring cells suggest the formation of bile canaliculi [132]. It was found that using the same anti body staining protocol with the collagen sandwich configuration resulted in the image being over-saturated. This was due to the staining protocol not suited for the sandwich configuration. Time limitations prevented re-evaluation. No obvious structures could be identified using either DAPI or ZO-1 stain. The results do however demonstrate that functional bile canaliculi have developed, which could suggest the presence of active ATP-binding cassette (ABC) transporters. Some of which are active in the movement of Diclofenac and Paracetamol metabolites (etc. ABCC2 and ABCG2) [133].

### 4.4.2 Drug-induced toxicity in collagen sandwich configuration versus the microfluidic platform

PRH spheroids and collagen sandwich configurations were exposed to drugs that are known to induce hepatotoxicity at high concentrations.

*Diclofenac*

The first drug was Diclofenac, is a nonsteroidal anti-inflammatory drug (NSAID) used to treat patients suffering from osteo- or rheumatoid-arthritis [32]. Diclofenac can undergo two potentially toxic metabolizing pathways in human and rat livers [134]. The first Phase I pathway is ring hydroxylation by CYP2C9 resulting in 4'-Hydroxydiclofenac, with a minor contribution from CYP3A4 resulting in 5'-Hydroxydiclofenac [135]. Both metabolites can be further oxidized to form quinone imines [136], which are electrophilic in nature and can undergo binding to non-proteins (e.g. glutathione) or proteins containing sulfhydryl groups, leading to cellular dysfunction. These compounds have also been implicated in redox cycling and production of oxidative stress [137]. The second Phase II pathway is glucuronidation involving the UGT2B7 enzyme in humans (UGT2B1 in rats), resulting in Diclofenac 1-O-β-acyl glucuronide [138]. These acyl glucuronides can covalently bind to proteins, via transacylation, affecting protein function or eliciting an immune response [136].

*Collagen sandwich configuration*

Examining Figure 4.17 for the cells exposed to varying concentrations of Diclofenac for 24 hours it is clear that there is no significant difference between the two time points until the 125 µM Diclofenac challenge in the collagen sandwich configuration. This is not surprising as it has been shown [139] that rat hepatocytes incubated for 24 hours with Diclofenac had an Inhibitory Concentration ($IC_{50}$) of 263 ± 43.1 µM for Diclofenac. This value was calculated by the ability of the cells to metabolize amounts of a tetrazolium salt (WST-1)

that could be quantified on a plate reader. Lauer and coworkers [137] also found the $TC_{50}$ value be to 138 ± 29 µM for rat hepatocytes after 24 hours exposure based on ATP content. Kawase et al [135] cultured primary rat hepatocytes in a collagen sandwich configuration and showed an increase of approximately 20% in LDH leakage after 24-hour exposure to 600 µM Diclofenac when compared to the control. This suggest a large range of values published for $IC_{50}$ (Inhibitory concentration), $LC_{50}$ (Lethal concentration) and $TC_{50}$ (Threshold concentration) values for Diclofenac when using primary rat hepatocytes. This is likely due to differences in culturing techniques, length of exposure, day of exposure and species differences. The length of culture ranges from a few hours to over a week which will affect the gene expression in the cells responsible for metabolism [140]; the culturing method include: Monolayers, cells cultured in a non-adherent wells, sandwich configurations in collagen / Matrigel, or spheroids. A significant difference ($p<0.01$) is shown in the three highest concentrations of Diclofenac used (> 125 µM) between the 24 hour post-exposure and 48 hour post-exposure collagen sandwich configuration groups (Figure 4.17). This suggests that the viability of the cultures continue to decline even though the drug has been removed.

*Multi-array platforms*

For the hepatocyte spheroids in the microfluidic platform, the differences between the two time points were not significant until the highest concentration. The microfluidic platform displayed a similar trend of declining viable fraction as the concentration increased. The difference between the two

time points was less obvious than in the collagen sandwich configuration. The non-significant decline in viable fraction between the two time points in the microfluidic platform might be attributed to the large variation of viable fractions measured. An example of this variation can be seen in Figure 4.23.

Xu and coworkers [115] found that hepatic spheroids exposed for 24 hours to Diclofenac at varying concentrations only had a significant response at the maximum dose (1mM) when comparing LDH leakage. This agrees with the finding from this research, as the decline in viable fraction at the highest concentration was less than 20 % (0.73 ± 0.01 and 0.62 ± 0.01 on day 5 and day 6, respectively – Figure 4.17b).

There is no significant difference in viability in either culture model at the low concentration range. This suggests the drug had no impact on cellular health. Overall, the differences in both systems are more pronounced at the 48-hour time point. It is not uncommon for DILI to present itself a few hours after initial exposure, which could explain the continued decline in the cultures. Alternatively, any drug still left in the cultures during the recovery period could also contribute to the results observed. This will be addressed in Chapter 5.

When comparing the decline in viability after 24 hours in both systems it can be seen that the decline is more noticeable for the microfluidic platform, suggesting that the spheroids are more sensitive to the lower concentrations than the collagen sandwich configuration. Alternatively, the top layer of collagen in the collagen sandwich configurations could be shielding the cells from the drug. It may only initially act as a barrier to the diffusion of the Diclofenac from the medium to the cells. The larger decline in viability is seen

in the collagen sandwich configurations 48 hours post-exposure. During the recovery period the cultures were incubated in serum-free medium only for 24 hours. It is possible that not all the Diclofenac could be completely removed prior the recovery stage. At high concentrations of electrophilic metabolites the GSH stocks inside the cells get depleted [141] [1]. If the cultures are under continuous exposure to Diclofenac this would result in some cells dying during the recovery period.

*Paracetamol*

Paracetamol was the second drug chosen for this experiment. While safe in moderation, shockingly, Paracetamol overdose accounts for roughly 48% of all poisoning admissions to hospitals across the UK [142]. The majority of Paracetamol is metabolized by the glucuronidation and sulfation pathways, with a minor portion being oxidized to a toxic intermediate metabolite known as N-acetyl-p-benzoquinone imine (NAPQI) by the CYP2E1 and CYP1A2 enzymes. Although highly reactive, at low concentrations NAPQI is detoxified by conjugation with the sulfhydryl group of glutathione (GSH) and excreted through bile. At high concentrations of Paracetamol as occurs in overdose, the sulfation pathway gets saturated, resulting in more production of NAQPI. This leads to rapid depletion of GSH stores in the liver resulting in the binding of NAPQI to the cysteine groups of proteins forming adducts and leading to mitochondrial dysfunction. During mitochondrial dysfunction key components are affected, such as the electron transport chain and ATP synthesis, which

leads to the production of reactive oxygen species (ROS) and eventual cell death.

Cultures in the multi-array platforms exposed to 7.5 mM Paracetamol showed a large variability in viability between neighbouring primary rat hepatocyte spheroids (Figure 4.20b &Figure 4.23. This may be related to the original location of the primary rat cells in the liver, referred to as zonation. There are three zones in the liver (Zone 1, Zone 2 and Zone 3) [143]. The hepatocytes in Zone 1 are smaller and highly efficient at Phase II metabolism like glutathione conjugation. Zone 3 are larger and are where most of the xenobiotic metabolism occurs. Zone 2 is an intermediate zone and has no specific boundaries [144]. Due to the higher Phase II detoxifying capabilities of the Zone 1 hepatocytes [10], they may be more resistant to the high Paracetamol concentration than the Zone 3 hepatocytes. If a large proportion of cells from either Zone landed in a single well the viability of the spheroid would be affected.

The normalized viability (Figure 4.22) for both systems shows that after 24 hours exposure the spheroids in the microfluidic platform were more sensitive than the collagen sandwich configuration at the highest concentration. After 48 hours exposure the decline in viability was more noticeable for both systems, but the largest difference was seen in the microfluidic platform again.

As mentioned earlier, the top layer of collagen used to complete the sandwich configuration may affect the drug exposure to the hepatocytes. The material or substrate of the systems used to culture the hepatocytes also varied, i.e. hepatocytes in the well-plates are surrounded by collagen, while the spheroids

in the microfluidic platforms are in contact with PDMS. PDMS can also trap some small hydrophobic molecules [145]. Paracetamol and Diclofenac are both hydrophobic compounds so the PDMS may influence the actual concentration of the drug the spheroids are exposed to. As a final note, the concentration gradient of the drugs across the spheroid is unknown. It is likely that cells inside the spheroids could be more protected from direct exposure than those on the surface.

### 4.4.3 Toxicity of the Phase I metabolite, Hydroxy-diclofenac

To test if the hepatocytes in both systems were capable of Phase II detoxification the cultures were exposed to a 5 µM 4'-Hydroxydiclofenac for 24 hours. A single concentration was used due to the limited amount of the compound available. As shown in Figure 4.19, viability remains stable for the control groups and there is a decline in the viability for the group exposed to the metabolite. Castell et al., [31] used 30 µM of 4'-Hydroxydiclofenac on hepatocytes and found approximately a 30 % decrease in mitochondrial ATP. This suggests that the concentration used in this experiment may have been too low to cause cell death. LC-MS analysis did not detect the GSH conjugated metabolite (Chapter 5).

### 4.4.4 Drug-induced toxicity of primary rat hepatocytes in the single array platform

The viable fraction in Figure 4.25 from the single array platform shows a decline between the control groups and the maximum concentration of

Diclofenac, based on 3 separate platforms. As mentioned earlier only a single experiment was completed, so it is not possible to make statistically-based conclusions about the platform. It should be stated that the viable fraction of the controls and 0 µM groups (vehicle controls) was lower than those in the multi-array platforms and in the collagen sandwich configuration.

The viability was still above 80 %, which is considered an acceptable threshold to use when screening potential hepatotoxins.

The decline in the single array platform could be due to metabolism-related toxicity, which would suggest that the spheroids are functionally active even when far fewer spheroids (compared to the multi-array platform) are able to communicate with each other. These spheroids were generated using, on average, more cells / well, compared to the multi-array platform.

# Chapter 5. Liquid chromatography-mass spectroscopy analysis of primary rat hepatocytes cultured in the microfluidic platform

It is shown in Chapter 4 that the multi-array microfluidic platform provided a suitable environment for culturing hepatic spheroids, using HepG2 cells and primary rat hepatocytes. The primary rat cultures were exposed to 2 different drugs, Diclofenac and Paracetamol, chosen because they are known to produce toxic Phase I metabolites. The results show a concentration-dependent decline in the viability for both culturing systems. To confirm the decline in viability was due to metabolism-related toxicity, samples of culture medium and cell lysate were collected at 24- and 48-hours post exposure and analyzed using LC-MS. This allowed the effect of the miniaturisation process, more precisely the effect of using low cell numbers to generate spheroids, to be explored and compared to a conventional 3D culturing method. The latter method requires a larger amount of resources in terms of cell numbers, medium and the compounds to be tested. The reduction in resources needed and the increased acquisition of data from the microfluidic platforms is beneficial as primary cells are scare, unstable in culture, expensive to acquire, and raise ethical considerations.

## 5.1 Introduction – detection of metabolites

As discussed in Chapter 4, Diclofenac is metabolized into several hydroxylated forms (3'-, 4'- and 5'-) and a highly reactive acyl glucuronide. Paracetamol is

metabolized into a toxic intermediate NAPQI, but most of the Paracetamol is metabolized through the sulfation – and glucuronidation pathways leading to the generation of Paracetamol sulfate and Paracetamol glucuronide, which are non-toxic. Excessive production of the oxidized metabolites (Hydroxydiclofenac and NAPQI) can lead to cell death if not detoxified by conjugation to GSH.

Using liquid chromatography and mass spectrometry, individual components in a sample may be separated and identified as described in Chapter 2. As mentioned in Chapter 2 (section 2.4) there are several separation techniques, some being more suitable than others depending on the desired outcome and the sample composition. If a high difference in affinity between the components of interest and the polar mobile phase and the non-polar stationary phase is expected reverse-phase HPLC is well-suited. The end product of metabolism is normally the conversion of a compound into a more hydrophilic one, thus facilitating excretion and resulting in a difference in affinity between the parent compound and the metabolites produced. Identification is achieved through mass spectral analysis after separation. Mass spectrometers are highly-specific but also sensitive, the components from a complex sample are normally separated before ionization. Separation greatly decreases interference and improves the quality of the data.

The m/z ratio of Diclofenac in negative ion mode is 294.010; after hydroxylation the m/z shifts to 310.005, due to the addition of the -OH group while acyl glucuronidation results in a shift to a m/z of 470.042 (Figure 5.1).

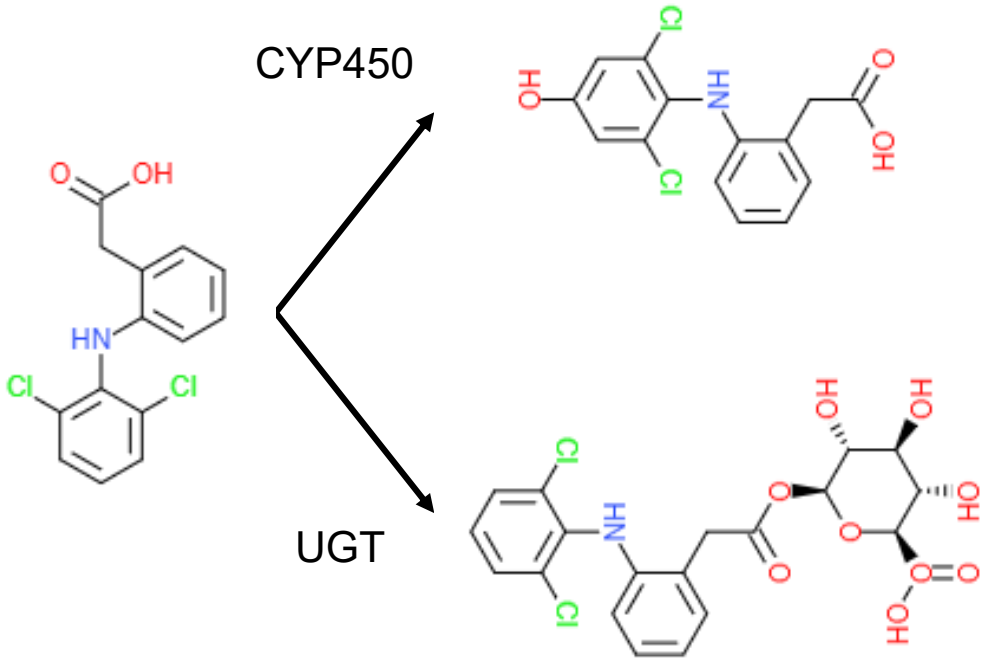


*Figure 5.1 Diclofenac and its two major toxic metabolites, catalyzed by the CYP450 family (CYP2C) into the hydroxylated form (top) and the acyl glucuronide (bottom) catalysed by the UGT enzymes (UGT2B7).*

Paracetamol (m/z = 150.056) produces a larger variety of metabolites (Figure 5.2) which were identified using LC-MS. The sulfated (m/z = 230.013) and glucuronidation (m/z = 326.088) metabolites would be expected to be present. If a portion of the Paracetamol was metabolized to the toxic NAPQI the GSH conjugated metabolite (m/z = 455.125) would also be present. Thus formation of NAPQI correlates with formation of the toxic species.

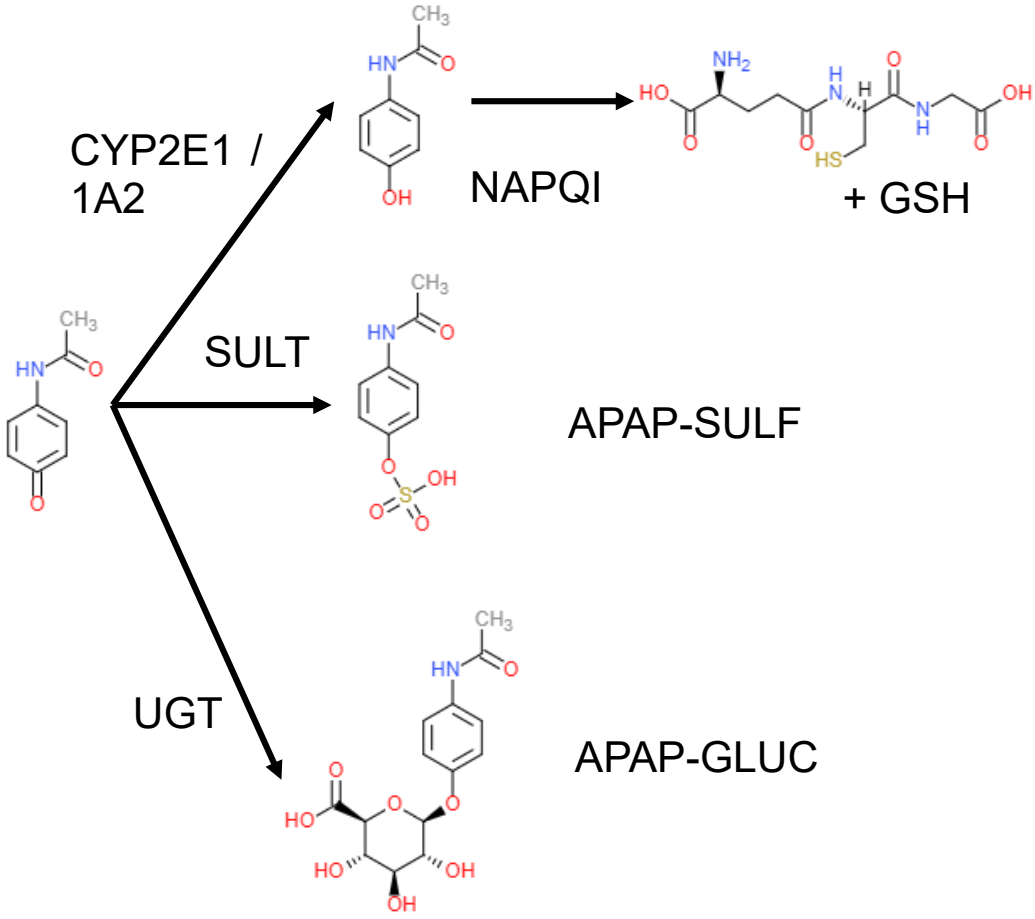


*Figure 5.2 Paracetamol metabolism: potential metabolic pathways, the CYP2E1 and CYP1A2 producing a toxic metabolite, NAPQI (top) which is detoxified by conjugation to GSH; The sulfation (SULT) pathway (middle) and the glucuronidation (UGT) pathway (bottom), both producing non-toxic metabolites.*

## 5.2 LC-MS experiment results

Data were collected and processed using Xcalibur and MZmine and formatted in OriginPro.

### 5.2.1 LC-MS raw data

Data recorded in Xcalibur are presented as a TIC with mass spectral scans. Identification of a compound was performed by searching for specific *m/z* values (from literature) that are expected to be found if metabolites are present in the sample (Table 5.1).

*Table 5.1: Mass-to-charge ratio's identified using XCalibur and available literature.*

| Compounds | *m/z* | Xcalibur chemical composition (Negative ion mode) |
|---|---|---|
| Diclofenac (standard) | 294.010 | $C_{14}H_{10}O_2NCL$ |
| '-hydroxydiclofenac (standard) | 310.005 | $C_{14}H_{10}Cl_2NO_3$ |
| Diclofenac acyl glucuronide | 470.042 | $C_{20}H_{18}O_8NCl_2$ |
| Paracetamol (standard) | 150.056 | $C_8H_8O_2N$ |
| Paracetamol-sulfate | 230.013 | $C_8H_8O_5NS$ |
| Paracetamol glucuronide | 326.088 | $C_{14}H_{16}O_8N$ |
| Paracetamol GSH | 455.125 | $C_{18}H_{23}O_8N_4S$ |

The fragmentation pattern and retention time of the peaks were used to aid identification between the drug standards and the samples. Using Xcalibur the chemical composition could be identified. The retention time of the Peak areas recorded from the TIC where the compound is present can be used to monitor drift between samples. The baseline was determined by the average abundance recorded over 30 sec in the control group samples at the respective retention times. Figure 5.3 shows a representative result obtained using Xcalibur displaying the TIC (top) and mass spectra (bottom) for a Diclofenac standard. More representative figures can be found in the Appendix.

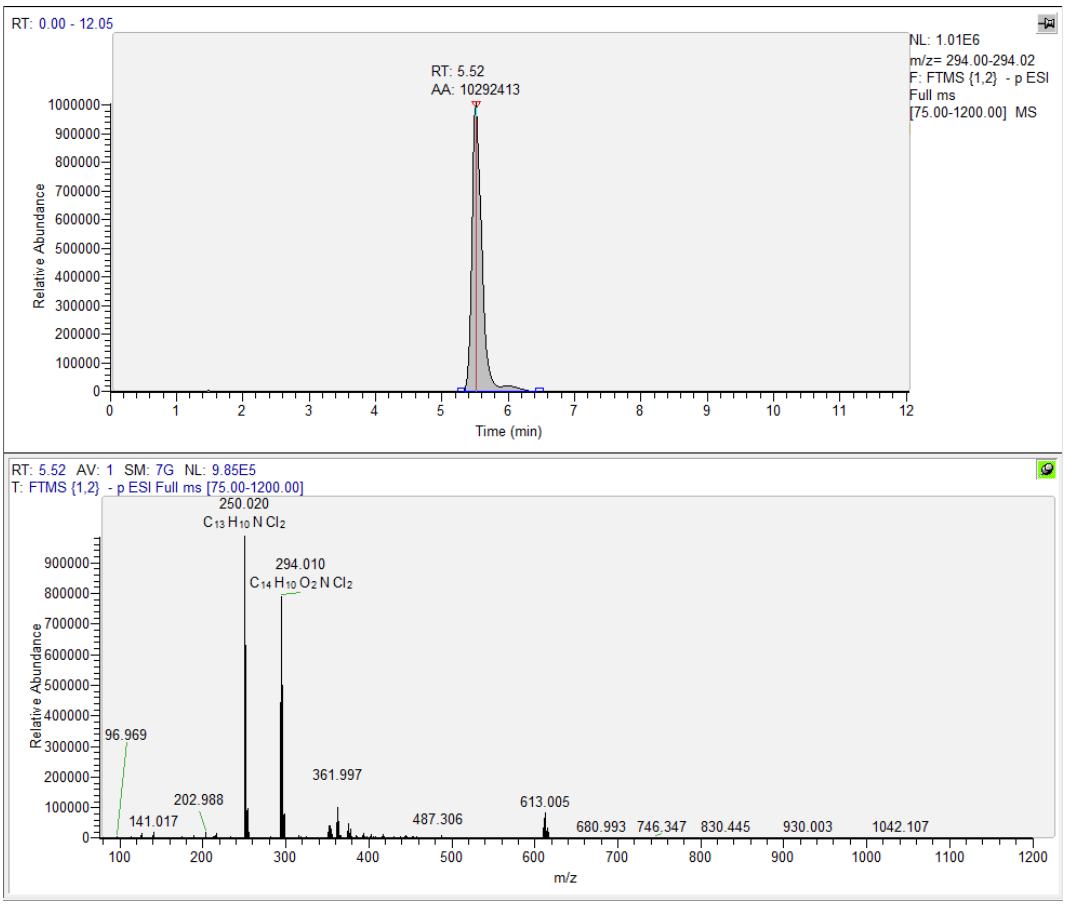


*Figure 5.3 (Top) Total ion chromatogram of Diclofenac with retention time (RT) and peak area (AA). (Bottom) Mass spectral data with chemical composition, the larger peak (m/z = 250.025) is a fragment of the parent (Diclofenac) compounds (m/z = 294.010).*

*MZmine data*

Once the metabolites have been identified and the Peak areas recorded (with the baseline subtracted) the raw data is separated into positive and negative scans for quantification. Where positive identification of the metabolite using Xcalibur occurred the ion intensities in the mass spectral data were recorded. This was used to determine the ratio of the ion intensity of the compound of

interest over the total of all the ion intensities recorded in the scan (Equation 5.1).

$$Ion\ intensity\ ratio_{Parent\ ion} = \frac{Ion\ intensity_{Target}}{Total\ ion\ intensity_{All\ ions}}$$

*Equation 5.1 Calculating the Ion intensity ratio to minimize background noise, defined as the ion intensity of the target over the total intensity of all the ions in the scan.*

Due to the complex nature of the samples ion intensity readings not related to the metabolite would also be recorded. To find a more accurate representation of the relative abundance of the metabolites in a detected peak, the Peak area was multiplied by the Ion intensity ratio (Equation 5.2).

$$Relative\ abundance = Ion\ intensity\ ratio_{Parent\ ion} \times TIC\ peak\ area$$

*Equation 5.2 Calculating the Relative abundance, defined as the ion intensity ratio multiplied by the peak area recorded in the TIC.*

### 5.2.2 Collagen sandwich configuration vs Microfluidic Platform

To compare the results between the different culturing models the data were normalized and presented as the relative abundance produced per 1000 cells / µl. Although no standard was available for some of the metabolites to provide full and accurate quantification this normalisation allows comparison between systems irrespective of medium volume or cell count. The following figures show the results comparing the primary rat hepatocytes from both culturing systems based on their metabolic capabilities. Culture medium was taken from the 6 and 24 well-plates (collagens sandwich configurations) and the

microfluidic platforms (multi-array and single array). The amount of the parent compound remaining after the initial 24 hours exposure is shown in Figure 5.4 and Figure 5.10 (for Diclofenac and Paracetamol, respectively); there is no significant difference between the platforms for either parent drug but on average more of the parent drug was recovered after 24 hours in the microfluidic platforms compared to the collagen sandwich configurations.

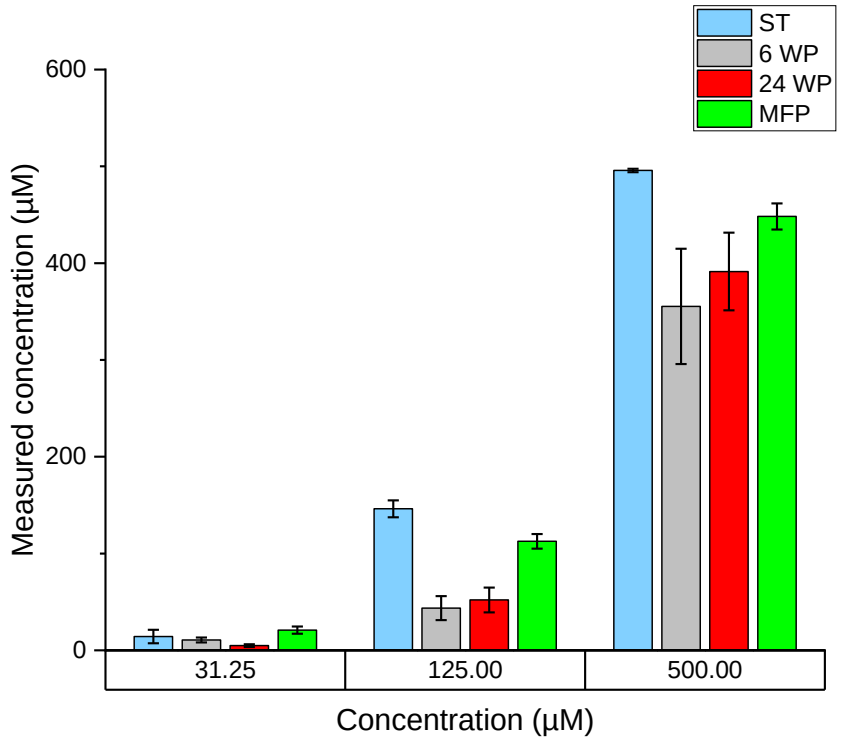


*Figure 5.4 Mean (± standard error) concentration of leftover Diclofenac detected in primary rat hepatocyte cultures in 6 well collagen-coated plates (6 WP), 24 well-plates (24 WP) and the multi-array platforms (MFP) after 24 hours exposure to different concentrations compared to a freshly prepared standard at the same concentration (ST). (n = 3 animal perfusions, pooled from triplicate samples)*

Next, Phase I and II metabolites for Diclofenac were compared. Hydroxylated and acyl glucuronide metabolites of Diclofenac were detected and can be seen

in Figure 5.5 and 5.6, respectively. A standard was prepared using 4'-Hydroxydiclofenac, but it was noted that the absorbance values measured resulted in a non-linear calibration curve; although the retention time remained constant, it was decided to not include a standard (ST) for Figure 5.5. A decrease in absorbance was noted by monitoring the pooled samples. The potential reasons for this sensitivity change and the consequences will be addressed in the discussion. With no standard available for the acyl glucuronide metabolite, statistical analysis showed no significant difference between the two culturing systems. On average more of the hydroxylated metabolite (Figure 5.5) was measured in the collagen sandwich configurations than in the microfluidic platforms. This was also true for the acyl glucuronide metabolite (Figure 5.6) except at the highest concentration of Diclofenac.

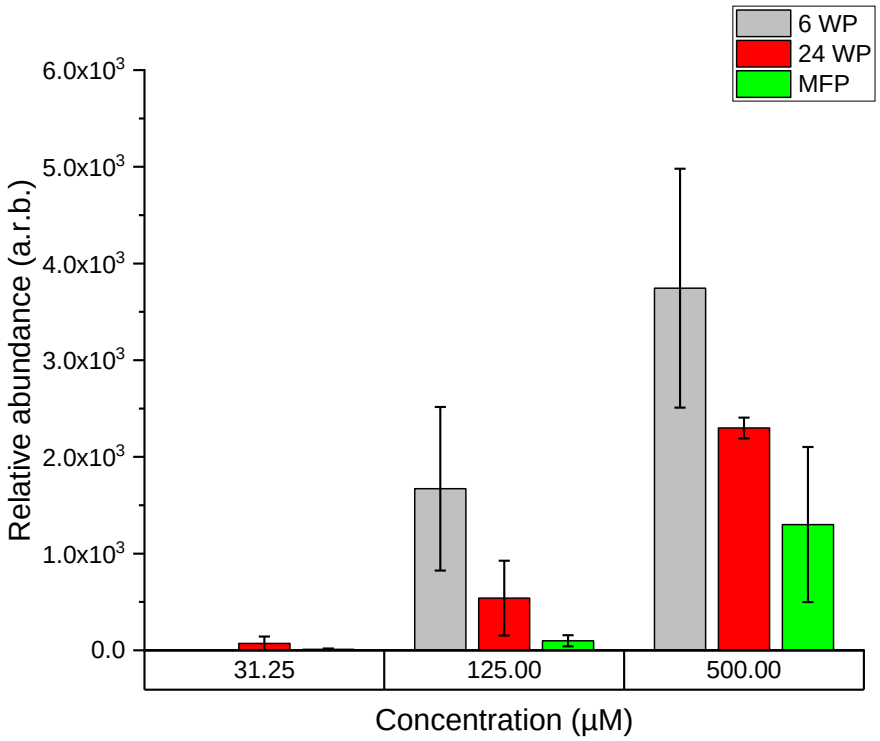


*Figure 5.5 Phase I metabolites: Mean (± standard error) relative abundance of a Hydroxylated Diclofenac metabolite detected in primary rat hepatocyte cultures in 6 well-plates (6 WP), 24 well-plates (24 WP) and the multi-array platforms (MFP) after 24 hours exposure to different concentrations of Diclofenac. (n = 3 animal perfusions, pooled from triplicate samples)*

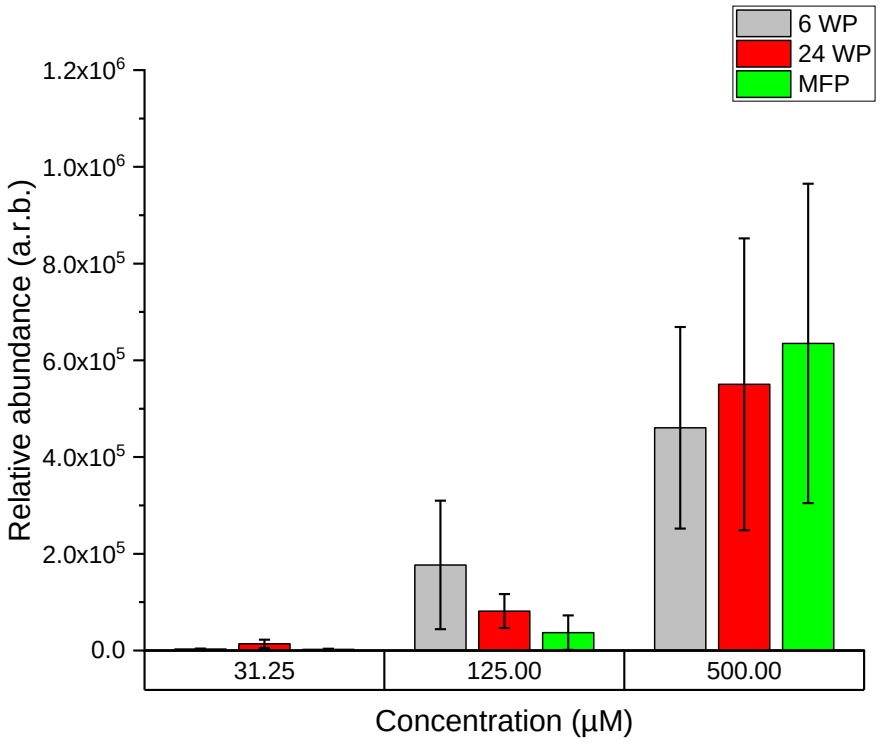


*Figure 5.6 Mean (± standard error) relative abundance of an Acyl Glucuronide Diclofenac metabolite detected in primary rat hepatocyte cultures in 6 well-plates (6 WP), 24 well-plates (24 WP) and the multi-array platforms (MFP) after 24 hours exposure to different concentrations of Diclofenac. (n = 3 animal perfusions, pooled from triplicate samples)*

Primary rat hepatic cell lysates in the culturing systems were also analyzed by lysing the cells with the quenching solution. After 24 hours exposure to 500 µM Diclofenac very little remained of the parent compound, as observed in Figure 5.7.

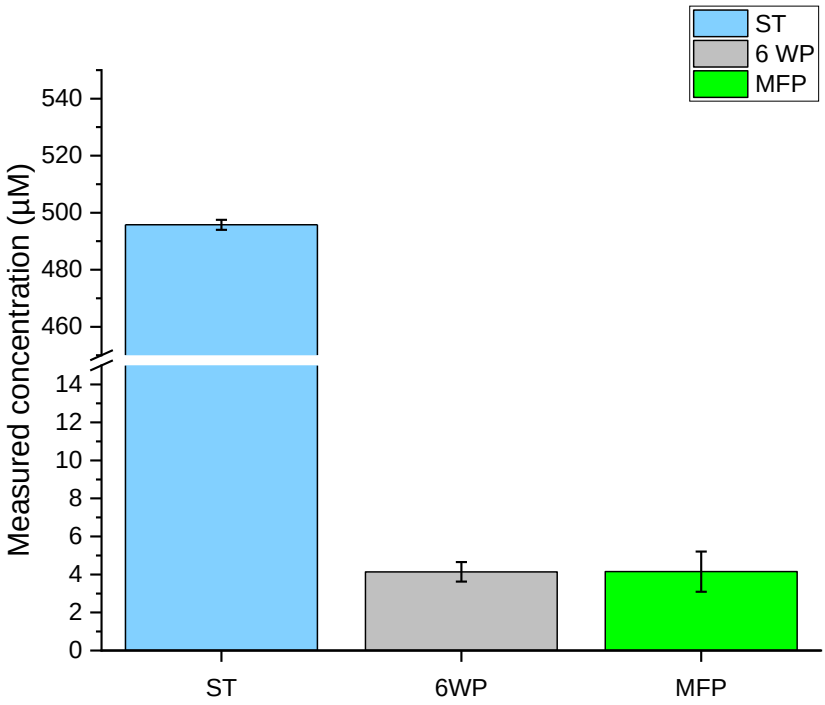


*Figure 5.7 Mean (± standard error) concentration of leftover Diclofenac detected in primary rat hepatocyte lysate from cultures in 6 well collagen-coated plates (6 WP) and the multi-array platforms (MFP) after 24 hours exposure compared to a 500 µM Diclofenac standard (ST). (n = 3 animal perfusions, pooled from triplicate samples)*

Both the hydroxylated and acyl glucuronide metabolites were found in the cell lysate. There is a significant difference in both the amount of the hydroxylated form (Figure 5.8) and the acyl glucuronide form (Figure 5.9).

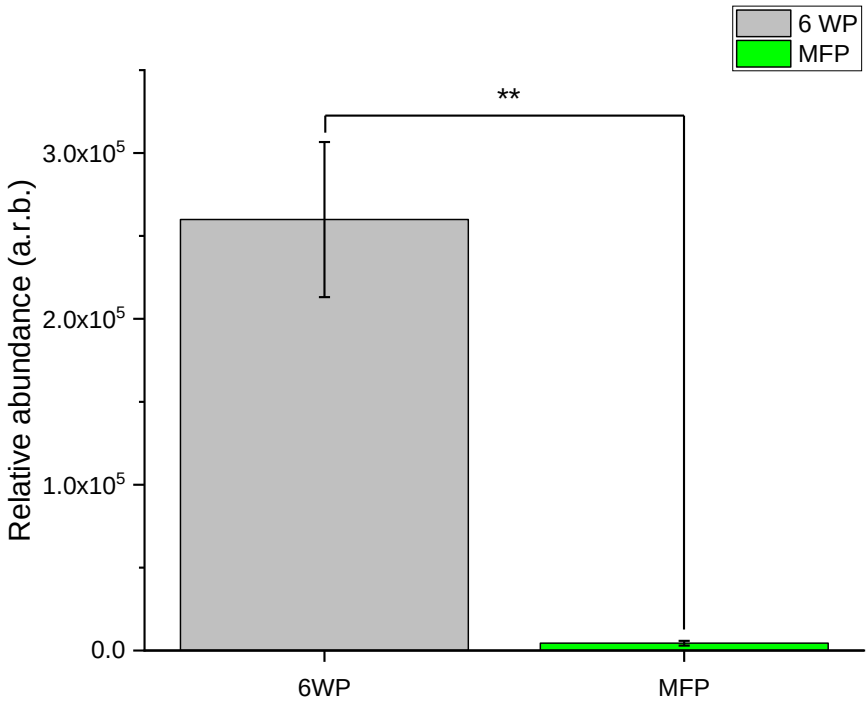


*Figure 5.8 Mean (± standard error) relative abundance of a Hydroxylated Diclofenac metabolite detected in primary rat hepatocyte lysate from cultures in 6 well collagen-coated plates (6 WP) and the multi-array platforms (MFP) after 24 hours exposure to 500 µM Diclofenac. n = 3 animal perfusions, pooled from triplicate samples; ** = p < 0.01)*

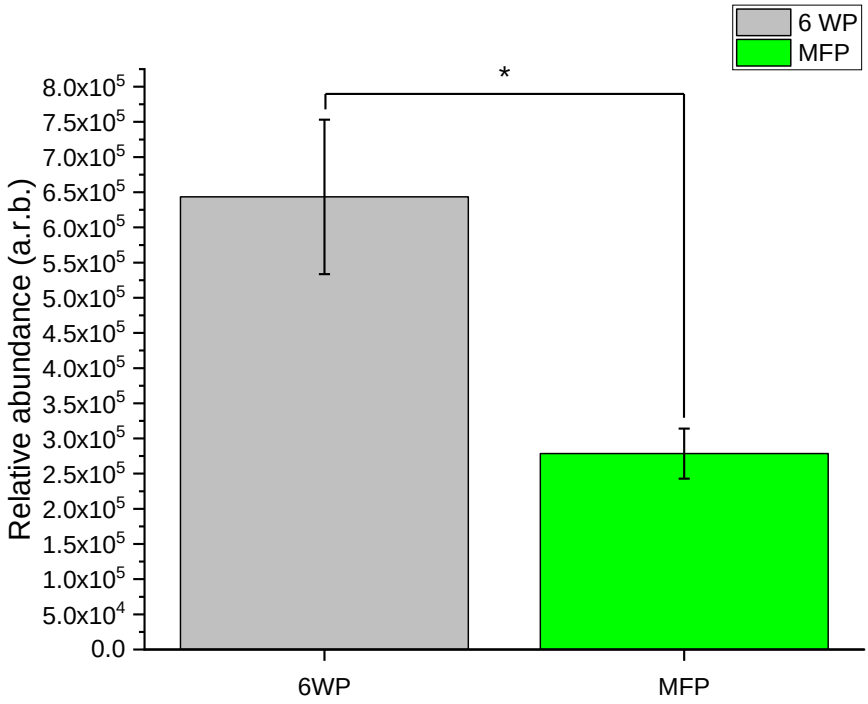


*Figure 5.9 Mean (± standard error) relative abundance of an Acyl Glucuronide Diclofenac metabolite detected in primary rat hepatocyte lysate from cultures in 6 well-plates (6 WP) and the multi-array platforms (MFP) after 24 hours exposure to 500 µM Diclofenac. (n = 3 animal perfusions, pooled from triplicate samples; * = p < 0.05)*

The cultures exposed to Paracetamol produced a larger variety of metabolites that were detected. The amount of unmetabolized parent drug was compared to the corresponding standard in Figure 5.10. There was no significant difference between the remaining concentration of Paracetamol between the two culturing systems.

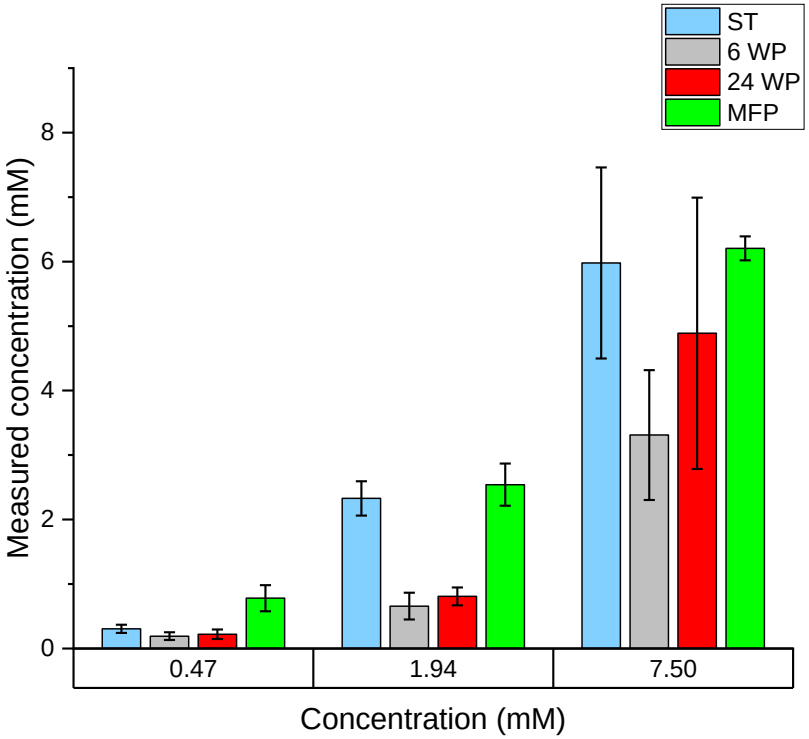


*Figure 5.10 Mean (± standard error) concentration of Paracetamol detected in primary rat hepatocyte cultures in 6 well-plates (6 WP), 24 well-plates (24 WP) and the multi-array platforms (MFP) after 24 hours exposure to different concentrations compared to a standard (ST). (n = 3 animal perfusions, pooled from triplicate samples)*

A sulfated metabolite of Paracetamol (Figure 5.11) was detected in both systems at all concentrations. No significant difference between the systems was found or between the concentrations.

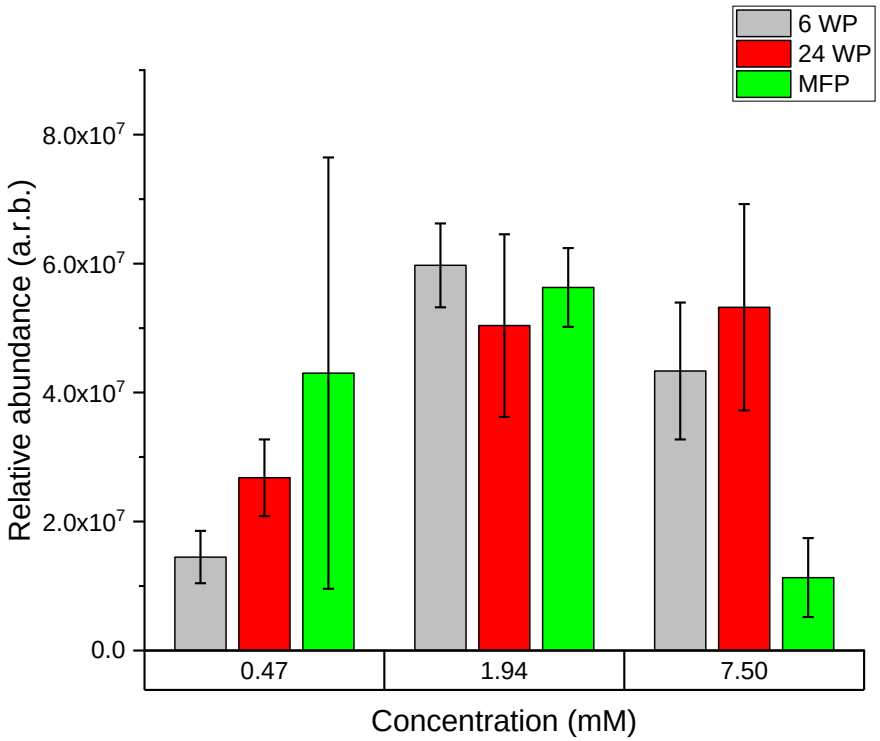


*Figure 5.11 Mean (± standard error) relative abundance of a Sulfated Paracetamol metabolite detected in primary rat hepatocyte cultures in 6 well-plates (6 WP), 24 well-plates (24 WP) and the multi-array platforms (MFP) after 24 hours exposure to different concentrations of Paracetamol. (n = 3 animal perfusions, pooled from triplicate samples)*

The glucuronidated APAP metabolite (Figure 5.12) was also detected in both systems, with no significant difference observed. Interestingly the mean amount detected in the microfluidic platforms was larger than that found in the collagen sandwich configurations, except at the highest concentration of 7.5 mM.

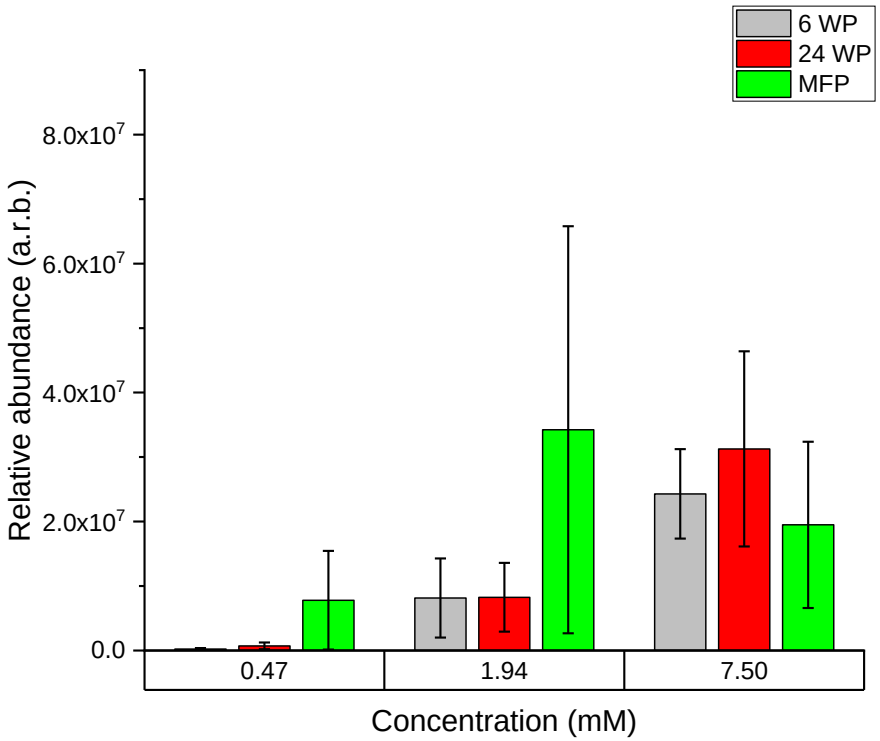


*Figure 5.12 Mean (± standard error) relative abundance of a Glucuronidated Paracetamol metabolite detected in primary rat hepatocyte cultures in 6 well-plates (6 WP), 24 well-plates (24 WP) and the multi-array platforms (MFP) after 24 hours exposure to different concentrations of Paracetamol. (n = 3 animal perfusions, pooled from triplicate samples).*

At high concentrations Paracetamol gets metabolized into a toxic intermediate, NAPQI, which needs to be detoxified by GSH. This conjugated GSH metabolite (Figure 5.13) was also found in both systems. Peaks were observed in the TIC corresponding to a GSH conjugated component, however the signal-to-noise in the mass spectra made quantification unreliable at the lowest Paracetamol concentration.

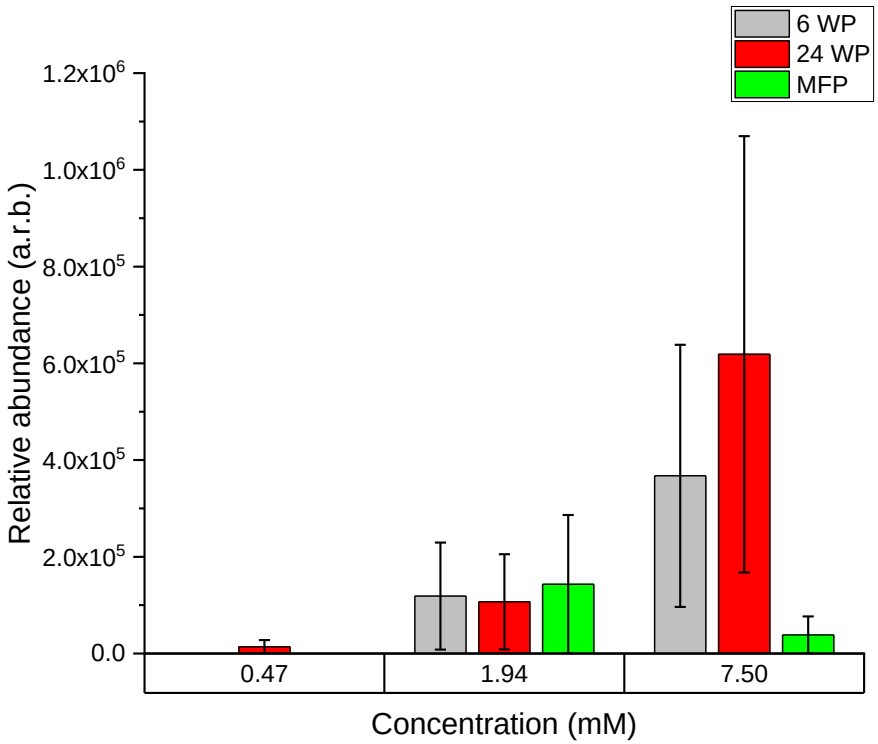


*Figure 5.13 Mean (± standard error) relative abundance of a GSH conjugated Paracetamol metabolite detected in primary rat hepatocyte cultures in 6 well-plates (6 WP), 24 well-plates (24 WP) and the multi-array platforms (MFP) after 24 hours exposure to different concentrations of Paracetamol. (n = 3 animal perfusions, pooled from triplicate samples)*

The samples were lysed and the amount of parent drug was compared to the standard (Figure 5.14).

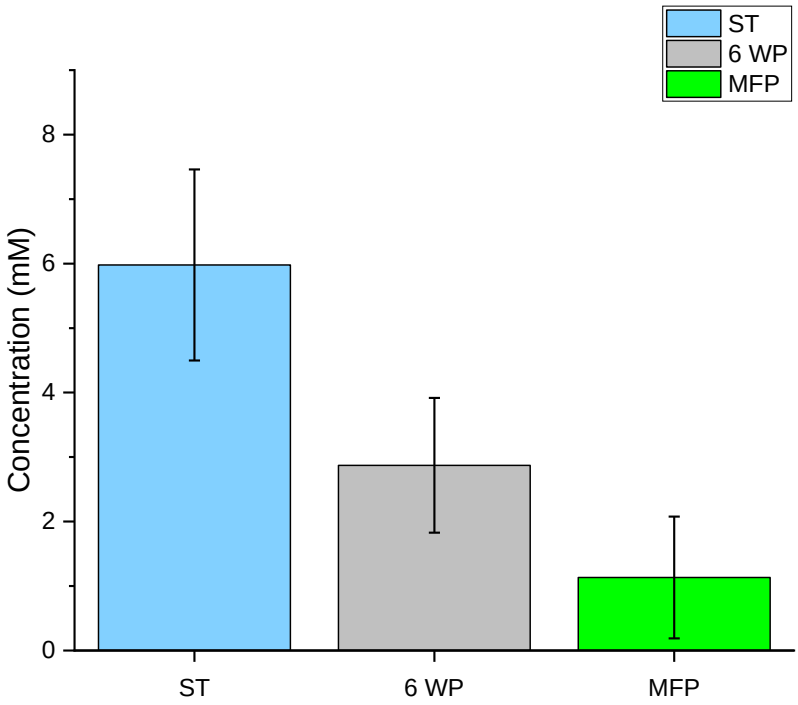


*Figure 5.14 Mean (± standard error) concentration of Paracetamol detected in primary rat hepatocyte lysate from cultures in 6 well-plates (6 WP) and the multi-array platforms (MFP) after 24 hours exposure compared to a 7.5 mM Paracetamol standard (ST). (n = 3 animal perfusions, pooled from triplicate samples)*

The other three metabolites, (Figure 5.15 to 5.17) were also detected in the lysed samples of the 6 well collagen sandwich configurations, but barely in the microfluidic platforms.

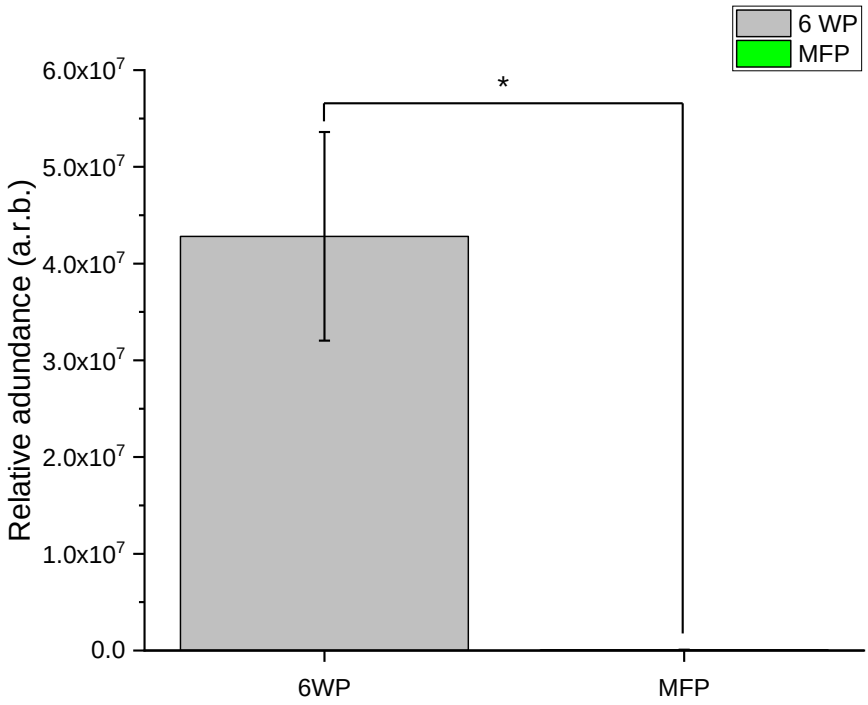


*Figure 5.15 Mean (± standard error) relative abundance of a Sulfated Paracetamol metabolite detected in primary rat hepatocyte lysate from cultures in 6 well-plates (6 WP) and the multi-array platforms (MFP) after 24 hours exposure to 7.5 mM Paracetamol. (n = 3 animal perfusions, pooled from triplicate samples; * = $p < 0.05$)*

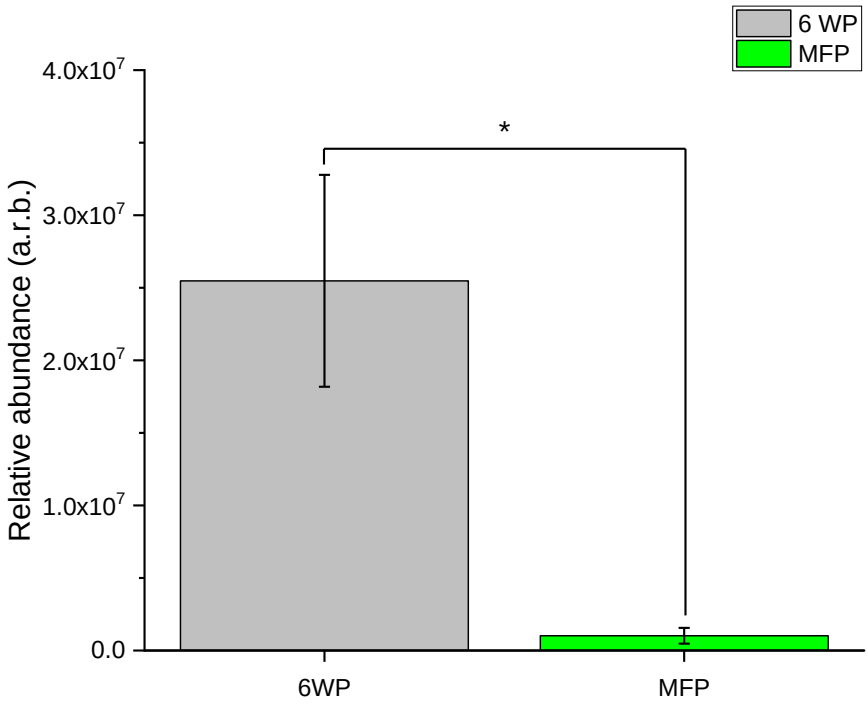


*Figure 5.16 Mean (± standard error) relative abundance of a Glucuronidated Paracetamol metabolite detected in primary rat hepatocyte lysate from cultures in 6 well-plates (6 WP) and the multi-array platforms (MFP) after 24 hours exposure to 7.5 mM Paracetamol. (n = 3 animal perfusions, pooled from triplicate samples; * = p < 0.05)*

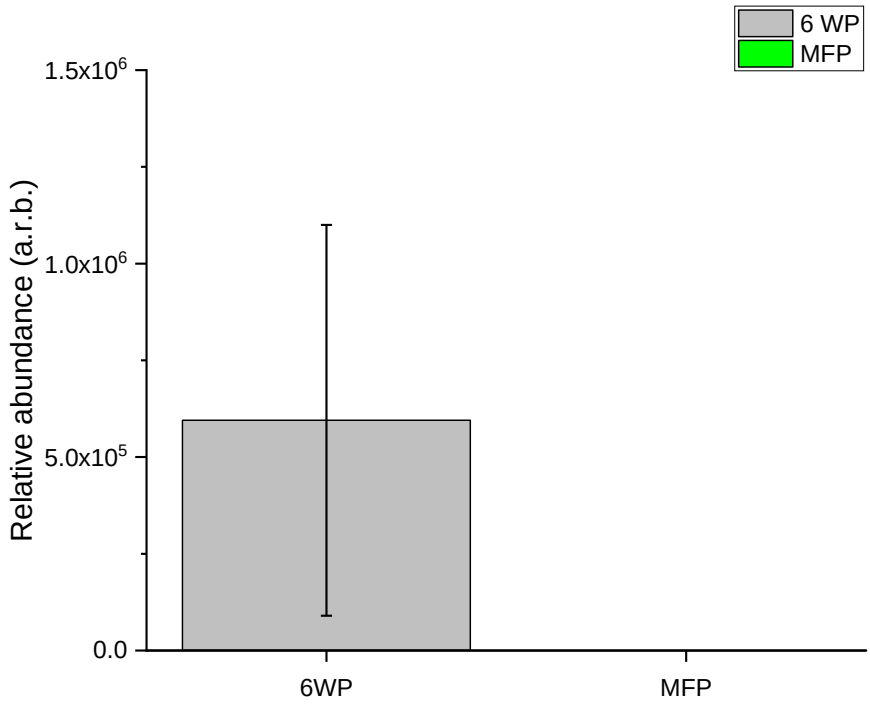


*Figure 5.17 Mean (± standard error) relative abundance of a GSH conjugated Paracetamol metabolite detected in primary rat hepatocyte lysate from cultures in 6 well-plates (6 WP), and the multi-array platforms (MFP) after 24 hours exposure to 7.5 mM Paracetamol. (n = 3 animal perfusions, pooled from triplicate samples)*

*Paracetamol cultures in the single array platform*

The medium from parallel cultures that were exposed to the parent drug for 24 hours and then allowed to recover in serum-free medium for 24 hours was also analyzed. In most of the samples the quantity of metabolites produced by the cultures exposed to Diclofenac could not be accurately determined which will be addressed in the discussion. More reliable data was found in the cultures

exposed to Paracetamol. Figure 5.18 displays the concentration of the parent compound left 48 hours after initial exposure. There is no significant difference between the two culture systems, but the mean concentration of metabolites found was higher in the collagen sandwich configurations than in the microfluidic platforms.

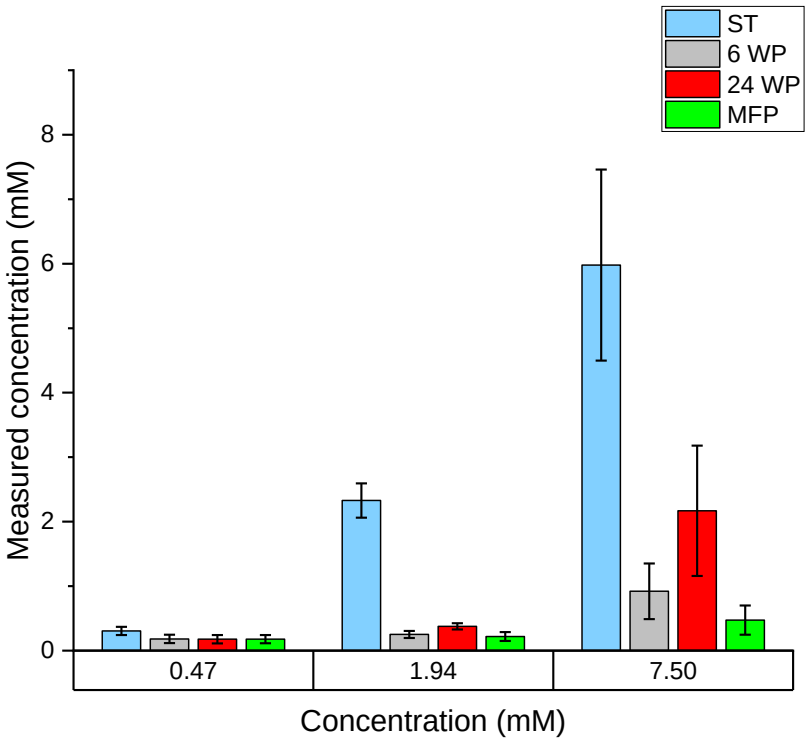


*Figure 5.18 Mean (± standard error) concentration of Paracetamol detected in primary rat hepatocyte cultures in 6 well-plates (6 WP), 24 well-plates (24 WP) and the multi-array platforms (MFP) after 24 hours exposure to different concentrations of Paracetamol followed by 24 hours recovery compared to a standard (ST). (n = 3 animal perfusions, pooled from triplicate samples)*

The sulfated and glucuronidated metabolites were also detected (Figure 5.19 and Figure 5.20) 48 hours after initial exposure, with the largest amount found in the collagen sandwich configurations. The GSH conjugated data proved to be too inconsistent to gather a reliable representation of the amount present.

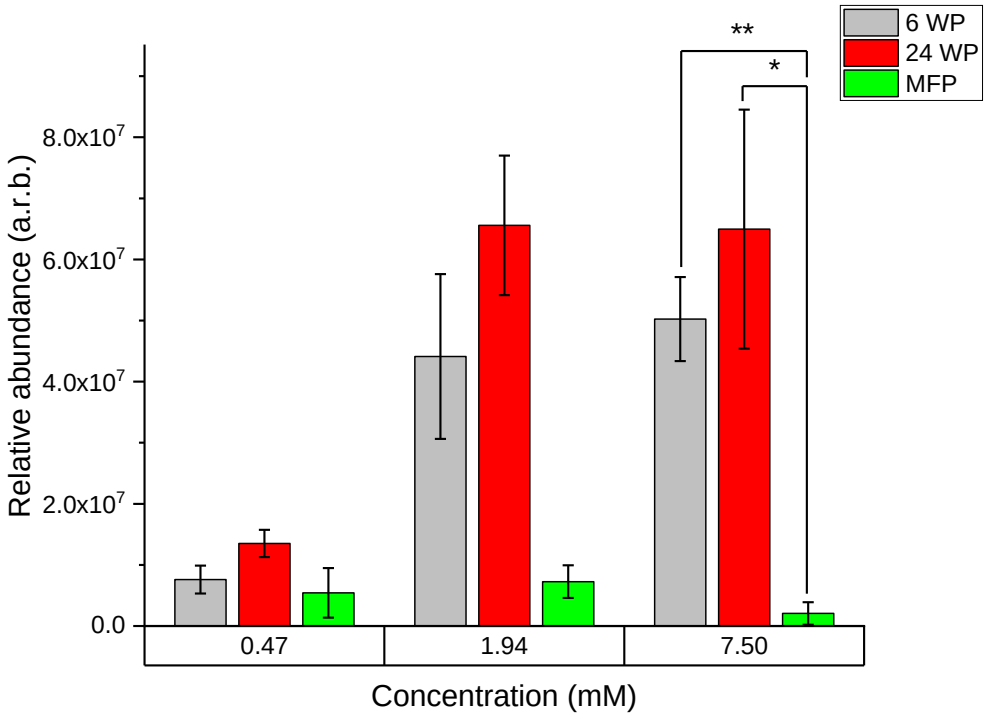


*Figure 5.19 Mean (± standard error) relative abundance of a Sulfated Paracetamol metabolite detected in primary rat hepatocyte cultures in 6 well-plates (6 WP), 24 well-plates (24 WP) and the multi-array platforms (MFP) after 24 hours exposure to different concentrations of Paracetamol followed by 24 hours recovery. (n = 3 animal perfusions, pooled from triplicate samples; * = p < 0.05, ** = p < 0.01).*

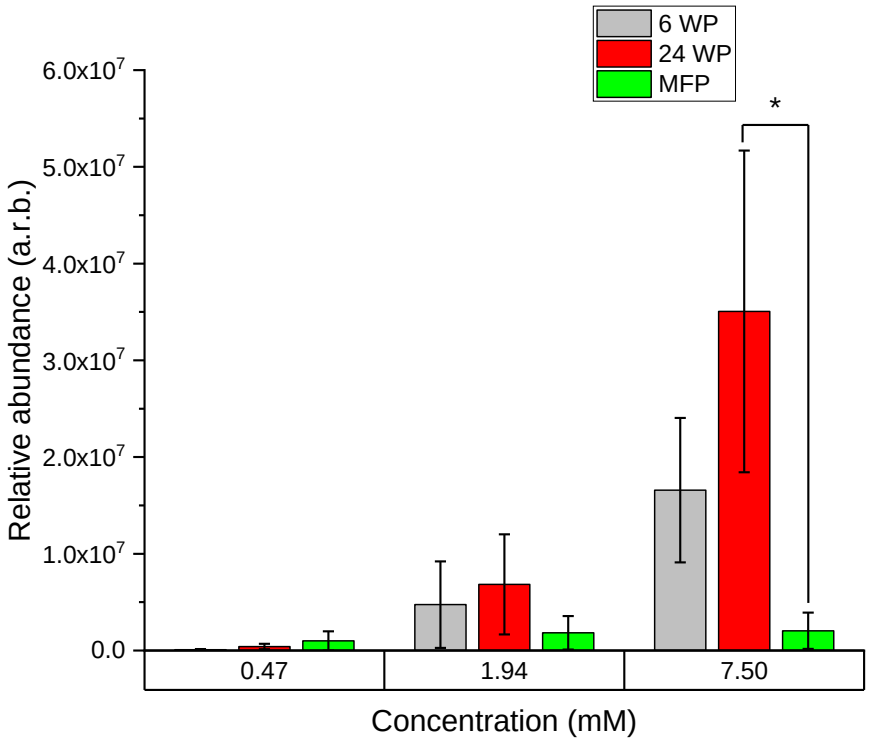


*Figure 5.20 Mean (± standard error) relative abundance of a Glucuronidated Paracetamol metabolite detected in primary rat hepatocyte cultures in 6 well-plates (6 WP), 24 well-plates (24 WP) and the multi-array platforms (MFP) after 24 hours exposure to different concentrations of Paracetamol followed by 24 hours recovery. (n = 3 animal perfusions, pooled from triplicate samples; * = p < 0.05).*

### 5.2.3 Single array platform

To further evaluate the effect of miniaturisation on metabolite detection using LC-MS samples from the single array platform were analyzed using the same protocols. For the single array platform Diclofenac and two metabolites were detected. Figure 5.21 shows the concentration of Diclofenac in the collagen

sandwich configuration, the multi-array microfluidic platform and the single array platform after 24 hours. This was carried out to determine if even fewer spheroids can be used to effectively detect metabolism-related hepatotoxicity.

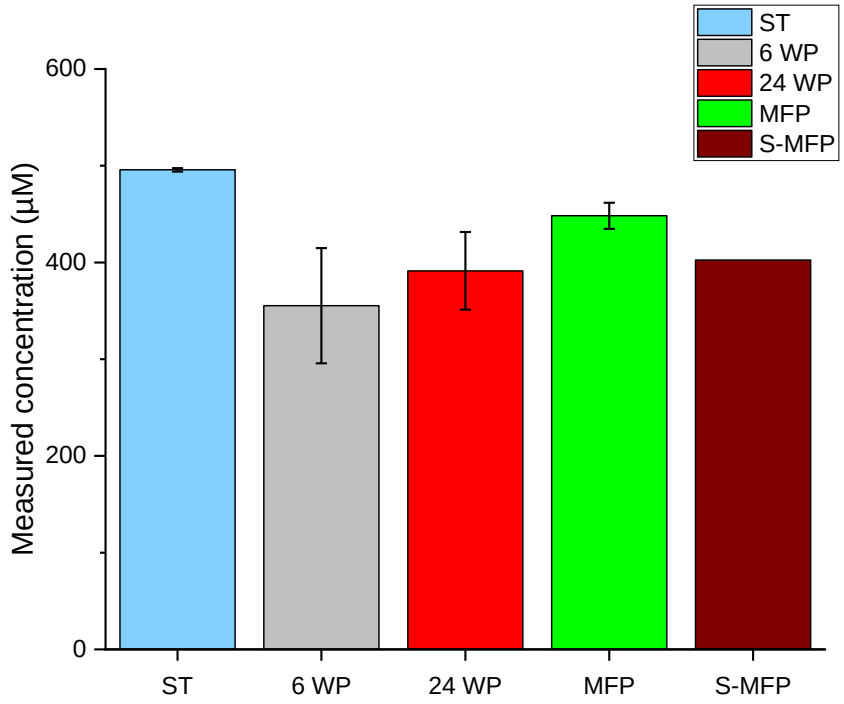


*Figure 5.21 Mean (± standard error) concentration of Diclofenac detected in primary rat hepatocyte (cultures) in 6 well-plates (6 WP), 24 well-plates (24 WP), the multi-array platforms (MFP) and the single array platforms (S-MFP) after 24 hours exposure compared to a 500 µM Diclofenac standard (ST). (n = 3 liver perfusions, pooled from triplicate samples for all systems apart from the S-MFP, which is from a single experiment (n = 1 liver perfusion), using 12 channels)*

The hydroxylated and glucuronide (Figure 5.22a and b) metabolites were also detected in the single array microfluidic platform.

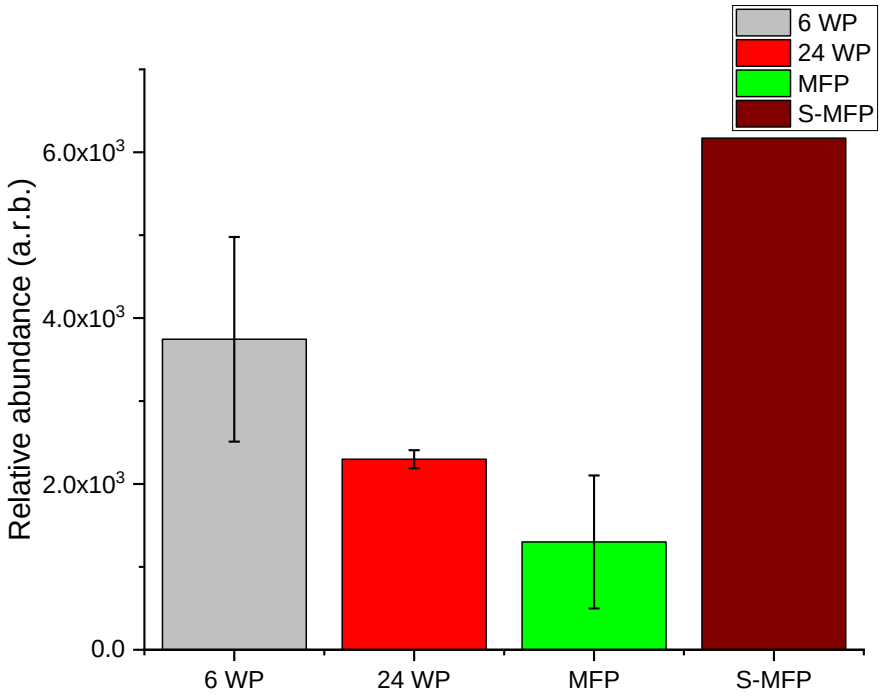


*Figure 5.22a Mean (± standard error) relative abundance of a Hydroxylated Diclofenac metabolite detected in primary rat hepatocyte cultures in 6 well-plates (6 WP), 24 well-plates (24 WP), the multi-array platforms (MFP) and the single array platforms (S-MFP) after 24 hours exposure to a 500 µM Diclofenac. (n = 3 animal perfusions, pooled from triplicate samples for all systems apart from the S-MFP, which is n = 1 animal perfusion, using 12 channels)*

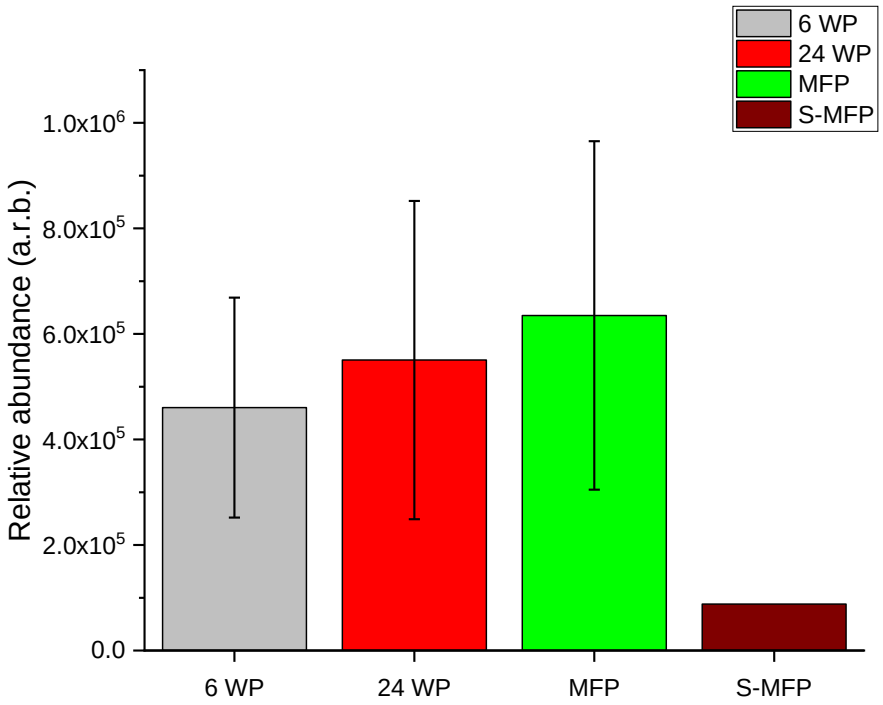


*Figure 5.22b Mean (± standard error) relative abundance of an Acyl Glucuronide Diclofenac metabolite detected in primary rat hepatocyte cultures in 6 well-plates (6 WP), 24 well-plates (24 WP), the multi-array platforms (MFP) and the single array platforms (S-MFP) after 24 hours exposure to a 500 µM Diclofenac. (n = 3 animal perfusions, pooled from triplicate samples for all systems apart from the S-MFP, which is n = 1 animal perfusion, using 12 channels)*

## 5.3 Discussion

The aim was to investigate if it was possible to construct metabolically active spheroids using a lower starting cell number (per spheroid) than has been described in literature and compare the activity of metabolism to conventional collagen sandwich configurations (in well-plates). The 6 well-plates contained $1.5 \times 10^6$ cells / well, the 24 well-plates contained $3 \times 10^5$ cells / well, while the multi-array microfluidic platform only contained $3 \times 10^4$ cells / channel generating over 250 individual spheroids (averaging 120 cells / spheroid) and lastly, the single array platform contained $1.2 \times 10^4$ cells / channel generating 16 individual spheroids (averaging 750 cells / spheroid). These values were based on the assumption that all cells loaded into the channels were trapped and distributed evenly. This is not the case in practise for the multi-array microfluidic platform, as explained in Chapter 3 (a higher cell density is found in wells near the reservoirs).

### 5.3.1 Drug metabolism

*Parent compound (Diclofenac and Paracetamol)*

The concentration remaining of the parent compounds Diclofenac (Figure 5.4) and Paracetamol (Figure 5.10) after 24 hours were compared to freshly made standards. Results show a small decrease of the parent in the cultures, suggesting the parent has been metabolized or undergone binding to proteins in the culture medium [146]. Milligan and coworkers [147] found the mean percentage of Paracetamol bound to plasma proteins was 24.1 %. This value could be higher in the experiments conducted in this project due to the

presence of collagen. The samples from the cultures that were washed with PBS and lysed after 24 hours also contained the parent compounds. For Diclofenac the concentrations found in the lysed samples (Figure 5.7) were negligible (below 10%), but for the Paracetamol cultures (Figure 5.14) there appears to be considerably more. For the 6 well-plates nearly half of the parent compound could be recovered and close to a quarter for the microfluidic platforms. The variation in the relative abundance (represented by the large standard error bars) in the cultures containing Paracetamol was larger than those of Diclofenac, but less noticeable at the lower concentrations. The reason for this larger variation at the highest concentration may be that the column and / or the detector became saturated.

*Metabolites detected*

*Hydroxy-diclofenac (Phase I)*

At the lowest concentration (Figure 5.5) of Diclofenac the hydroxylated metabolite (OHDIC) could only be quantified in a single sample using medium from primary rat hepatocyte cultures (24 well-plate). The relative abundance of the hydroxylated form was identified in the other cultures (6 well-plate and the multi-array microfluidic platform) based on the mass spectral data but were not statistically significant (ion intensity ratio) after quantification. This is not surprising as only a minor portion of the parent drug is expected to undergo Phase I metabolism. The relative abundance detected increases with concentration, with the 6 well-plates, consistently producing more OHDIC compared with the 24 well-plates and microfluidic platforms. Significantly more

OHDIC (Figure 5.8) and AGDIC (Figure 5.9) were detected in the lysed samples of the collagen sandwich configurations compared to the multi-array platform. The reason for this is unknown, but cell numbers may play a role. If the number of cells is near the minimum threshold for the LC-MS to detect any disruption of sample preparation could be detrimental to the data acquired.

The GSH-conjugated form of the hydroxylated diclofenac metabolite was not positively identified for certain. A peak with a m/z ratio of 616 was detected while scanning, which corresponds to the m/z ratio of a GSH conjugated metabolite in literature [24], but the low intensity made identification unreliable. The cultures exposed to 5 µM 4-Hydroxydiclofenac also did not produce a reliable peak. Wang and coworkers [148] found that the hydroxylated metabolites of Diclofenac were only stable for a short period when incubated with medium without cells (<96 hours). The results show this GSH-conjugated metabolite can be successfully detected, indicating that the hepatic spheroids and collagen sandwich cultures still possess some Phase I metabolizing capabilities after 5 day *in vitro*.

*Acyl glucuronide (Phase II)*

Cells in both culturing systems produced the acyl glucuronide metabolite (AGDIC) at all concentrations of Diclofenac. Without a standard it is difficult to determine the actual amount produced, but literature suggests that direct glucuronidation of Diclofenac is the major metabolic clearance pathway (~75 %) [138]. As with the hydroxylated metabolite the collagen sandwich configurations produced more than the microfluidic platforms (except at 500

μM) on average when analysing the medium and the cell lysate (6 well-plates and 7 channel microfluidic platforms). Unlike other Phase II metabolites, acyl glucuronides are highly reactive and electrophilic and can form covalent bonds with molecules containing many electrons [135] [149]. Critical cellular functions that depend on “macro-molecules”, including proteins and DNA, are targets of these acyl glucuronides [150] [151]. At the highest concentration of Diclofenac (500 μM) all systems produced comparable amount of the metabolite (Figure 5.6). Acyl glucuronides are excreted through the bile [138] and from Chapter 4 (Figure 4.14) it was shown that the spheroids had a bile canaliculi system established through ZO-1 anti-body staining. The results show evidence that the cultures are capable of Phase II glucuronidation.

*Paracetamol Phase II metabolism: Sulfation, glucuronidation and conjugation*

The first metabolite identified was produced through the sulfation pathway, catalysed by the cytosolic sulfotransferase enzymes. As mentioned briefly in Chapter 4 the sulfation pathway gets saturated at high concentrations [152]. There is limited literature on the concentration at which this saturation occurs, but *in vivo* experiments suggest a dose of more than 4 g / kg / day is sufficient in humans. The results (Figure 5.11) show no significant increase in the relative abundance of the sulphated metabolite detected between the two largest concentrations (1.94 mM and 7.50 mM) of Paracetamol, strengthening the hypothesis that the pathway has been saturated. Interestingly a decline in sulfation of Paracetamol at the highest concentration of Paracetamol can be observed for the microfluidic platforms. It is observed in the viability data

(Figure 4.22) that the spheroids have a lower viability at the highest concentration of PAR, which could be impacting their ability to metabolize the drug through sulfation.

The second metabolite found was catalysed by the UDP-glucuronosyl transferase (UGT) enzyme, which is responsible for metabolizing between 50 – 70 % of Paracetamol at therapeutic doses (*in vivo*) [153]. It can be seen in Figure 5.12 that the relative abundance of detected glucuronide metabolite increases with the concentration of which is likely due to a combination of more parent drug available and the saturated sulfation pathway.

The final metabolite detected was the GSH-conjugated from of the Phase I metabolite NAPQI. Only a minor proportion of the parent compound gets metabolized by the CYP450 family into NAPQI (approximately 5%) and at therapeutic levels this gets detoxified through GSH. Not surprisingly detection and quantification at the lowest concentration of Paracetamol proved difficult. The amount detected increased with the concentration of the parent compound; however, it can be seen from Figure 5.13 that the microfluidic platforms produced less compared to the collagen sandwich configurations. This could be a result of the spheroids having a lower viability (Figure 4.22) compared to the collagen sandwich configurations. The large error bars are due to some samples having non-significant amounts of metabolites, making quantification difficult and affecting the ANOVA results.

The sulfate and glucuronide metabolites (Figure 5.15 to 5.17) were also detected in the cell-lysed samples, again with the 6 well-plates producing significantly more compared to the microfluidic platforms.

Media samples (from the 6 well-plates and multi-array microfluidic platform) were also taken 48 hours post exposure. No metabolites were detected after 48 hours in the cultures exposed to Diclofenac, for either system. This may be attributed to the difference in magnitude between the concentrations for Diclofenac and Paracetamol drugs (µM vs mM). In the cultures exposed to Paracetamol there is a more obvious difference in the detected metabolites between the culturing systems after 48 hours (Figure 5.19 and 5.20). Interestingly a relatively higher initial concentration of Paracetamol was found in the collagen sandwich configurations compared to the microfluidic platform (Figure 5.18) and may contribute to the increased metabolite production.

The difference in the abundance of metabolites detected could be related to the different architecture between the culturing systems and not the metabolic activity of the cells. In the collagen sandwich configurations, a larger number of cells could be directly exposed to the parent drug (disc shape), compared to the cells in the microfluidic platform. It is assumed that cells on the outside of the spheroids are more exposed to the parent drugs compared to the inner cells.

Another contributing factor could be the number of cells successfully trapped in the microfluidic platforms; Although all effort was made to trap as many cells as possible, approximately a third of the cells did not end up in the well arrays in the multi-array platform, lowering the total number of cells. A similar argument can be made with the collagen sandwich configurations. The freshly isolated rat hepatocytes were plated and left to adhere for a minimum of 1 hour (maximum 2 hours) in an incubator before being washed and refilled with fresh

medium. It was observed that not all cells attached to the bottom collagen layer after removing the seeding medium. After checking viability using a Trypan blue exclusion test (counting both living and dead cells) the cell concentration is calculated on only the viable cells, therefor some dead cells will be introduced during the seeding process. The cultures from the collagen sandwich configurations and the microfluidic platforms, were able to produce Phase I and Phase II metabolites in detectable quantities, implying that the rat hepatocytes were still metabolically active.

### 5.3.2 Single array platform

The primary rat spheroids in the single array platform were exposed to 500 µM Diclofenac for 24 hours. All results are based on a single experiment due to time constraints and therefore no statistical analysis was conducted, although data was compared to the collagen sandwich configurations and the multi-array platform (Figure 5.21 and 5.22a and b). The main limiting factor was that the single array was only fabricated at the end of the studentship. The platform was intended for use in research related to cancer screening, however the potential for hepatoxicity screening could not be ignored. Using a minimal number of primary hepatocytes (12000 cells / channel) and approximately 10 µl (per channel), metabolites were successfully detected using LC-MS. It was observed during culture that the single array platforms were slightly more susceptible to evaporation (compared to the multi-array microfluidic platform). This may have had an impact on the quantity of the metabolites detected, potentially increasing the concentration. An advantage the single array

platform has over the other culturing systems (including the multi-array platform) is the number of platforms that can be loaded simultaneously. Due to the shorter channel length the time required for the induced flow to reach equilibrium is reduced, shortening overall loading time. This has an impact on the “static” time where cells in the suspension could begin to aggregate, which is unwanted as large aggregates could block the channels. Regularly after these “static” intervals, the cells have to be disaggregated using a needle which could have a negative impact on the cells.

The total number of cells loaded into the single array platform was 12000 cells / per channel. As with the multi-array platform it was observed that not all cells ended up being trapped as some settled in the channel and others ended up in the opposite reservoir. Repeated emptying and re-introduction of the cell suspension increased the number of cells trapped but could only be carried out a limited number of times to reduce the time spent out of the incubator. This would also impact the concentration of metabolites found in the single array platform after normalizing (taking cell number and medium into consideration).

The results gathered from the primary rat spheroids in the multi-array and single array microfluidic platforms demonstrate that the cells exhibit functionality, similarly to conventional 3D culturing methods, such as a collagen-sandwich configuration; whose implications will be summarized in Chapter 6. The main limitation of this study is that only a single experiment (from 12 channels / condition) using the single array platform could be

completed and thus more experiments need to be carried out in order to draw more concrete conclusions.

### 5.3.3 Sample preparation and LC-MS considerations

Samples (from medium) were taken at 48 hours after initial drug exposure using Diclofenac or Paracetamol. These samples were prepared following the same protocol as those collected at 24 hours (post-initial exposure), however no data could be gathered from the cultures exposed to Diclofenac. It was observed that in most samples the recorded peak from the TIC was too small and positive identification proved to be difficult. This was not the case for the cultures exposed to Paracetamol as the parent drug and some of the metabolites were still detectable and quantifiable. The GSH-conjugated metabolite of Paracetamol was less stable and harder to detect after 48 hours (post-exposure). The Phase I metabolite, reactive metabolic species comes from the addition of an -OH functional group. Since the hydroxylated metabolite from Diclofenac could not be detected (at 48 hours) and the results were inconsistent for the Paracetamol cultures, the instability may be related to the reactivity of the NAPQI metabolite [154]. It is widely accepted that these hydroxylated metabolites are highly reactive and will bind to proteins unless adequate levels of GSH are available in the cell. The results from Chapter 4 show a concentration-dependent decline in viability for both cultures, with the largest decline after 48 hours at the highest concentration of each drug. This decline has been shown to be related to the production of the toxic metabolites that deplete GSH stocks before inducing cell death. This would fit with the

hypothesis that these highly reactive metabolites (NAPQI) were not detected due to binding to proteins most of which is removed during the sample preparation process (centrifugation).

As mentioned briefly the GSH-conjugated metabolites were not found in the samples exposed to Diclofenac but were detected in samples exposed to Paracetamol. The concentration of the parent drug used varied greatly (µM vs. mM), and assuming the cultures behaved similarly between the two test compounds; this might contribute to a larger quantifiable formation of conjugated metabolites.

Another consideration was the use of the quenching solution. The temperature of the solution impacts the stability of the sample and it should be as cold as possible. Instead of storing small volumes of the solution on ice a potentially more effective method would be to store the solution in a glass contained in a dish filled with dry ice and methanol. This mixture reaches a temperature below freezing, keeping the quenching solution colder than normal. Samples had to be transported between departments, from storage to analysis. Ideally this would be carried out using dry-ice to maintain the temperature as low as possible, since samples were stored at - 80°C. Transport of the dry-ice across the different departments within the University campus was deemed too high a risk and this method could not be employed for this project.

As mentioned in Chapter 3 the results from Xcalibur had to be split between positive and negative ion mode. Originally this is done to reduce computational time and interference between the two modes when using MZmine. The positive ion mode results did not provide reliable data. It appeared that the

separation failed as no individual peaks could be seen when viewing the TIC. The mass spectral data showed that the detector appeared saturated as all the ion intensities were of similar value. A potential cause of this phenomenon could be that the column was not adequately cleaned before, resulting in interference from a previous sample. This is however unlikely as the negative ion mode provided consistent results. This may be related to the voltage switching of the ionization equipment. Not only was a drift noticed by monitoring the pooled samples; but a large change in absorbance between the first and final experiments was also recorded. While calibrating the standards this change was obvious, but each standard still provided a linear calibration curve for the concentrations used. This was the main cause for the large standard error bars seen between samples. More modern LC-MS equipment are less prone to these problems.

Finally, the internal surfaces of the microfluidic platforms had to be treated with a surfactant. Surfactants can damage the column in the HPLC and affect the separation of the components of interest, decreasing the detected amount. Although all effort was made to remove any unbound surfactant from the platforms before seeding, some traces may remain.

Chapter 6 will combine all the results and conclusions from Chapter 4 and 5.

# Chapter 6. Conclusion for the use of microfluidics and LC-MS for detection of drug induced hepatotoxicity

In this Chapter the results from Chapter 4 and 5 will be summarised and combined to provide a broader understanding on how the aims of this thesis have been met.

## 6.1 Introduction

The objective of this project was to investigate the effect of miniaturisation of the culturing method on the capacity of liver spheroids for metabolism. The aims were to culture primary hepatocytes for a time period long enough for the cells to establish some degree of *in vivo* architecture (i.e. bile canaliculi formation); expose these cultures to compounds known to induce metabolism-related toxicity and measure their response, using LC-MS of intracellular content and culture media.

## 6.2 HepG2 spheroids in a microfluidic platform

In Chapter 4 two distinctly different microfluidic platforms were compared on parameters considered practical for later combination with LC-MS. These included:

- Time needed to seed the platform
- Stability of the platform throughout the culturing period
- Number of different conditions that could be tested
- Number of individual structures for data extraction (throughput)
- Volume of media collected for LC-MS analysis

Both microfluidic platforms were able to produce a large number of individual spheroids using the hepatic cell line, HepG2. Evaporation and the potential to displace spheroids in the droplet-based platform were the main causes of instability of the platform, however, these disadvantages can be negated through the use of robotics and steps taken to reduce evaporation. The multi-array microfluidic platform proved more suitable due to the increased reliability during culture and the larger number of spheroids that can be generated. The advantage of conducting multiple experiments (different conditions / channel) on a single chip was an attractive feature of this platform. It is seen in the data that the HepG2 spheroids have different growth rates between the two platforms. The size of the spheroids increased in the droplet-based platform but remained stable in the multi-array platform. The results from the droplet-based platform were based on a much lower number of individual spheroids across multiple platforms; and may be different if more experiments are completed. The difference could also be related to the passage number of the HepG2 cells used in the droplet-based platform and the multi-array platform, varying between roughly 50 passages.

Lastly, on many droplet-based platforms multiple spheroids trapped in a single droplet merged during the culture. Viability was monitored during the

experiments by fluorescence microscopy (FDA and PI staining). The area of viable cells was divided by the total area of the spheroid from the day before, resulting in the viable fraction. This method showed a slight concentration-dependent decline in the HepG2 spheroids after 24 hours exposure to Diclofenac, which has low non-metabolic toxicity. It is not surprising that only a small decline is observed, as HepG2 cells express less of the Phase I metabolizing enzymes needed to induce metabolism-related toxicity. The main limitation using this method for quantification of viability was extracting information from a 2D image of a 3D structure. Cells on the top of the spheroid that are viable, thus producing a fluorescent signal, might be covering those below which are not. Confocal microscopes can provide a more reliable 3D image of the whole spheroid but would dramatically increase the time needed to analyse a single spheroid, effecting throughput.

Overall the preliminary results demonstrated that the multi-array platform was more robust and suited for combining LC-MS analysis. This was based on:

- The ability to generate more individual spheroids
- Larger volume of media samples for LC-MS analysis
- The platform was more robust and less sensitive to the skill of the user

## 6.3 Drug-induced response in primary hepatic spheroids and a collagen sandwich configuration

The multi-array microfluidic platform was able to sustain primary rat hepatocytes that retained / established polarity after assembling into

spheroids. That was demonstrated by ZO-1 anti-body staining. The cells assembled rapidly (< 2 days) into spheroids and remained viable for the duration of the experiments (6 days). From literature, spheroids cultured in well-plates can take up to 7 days to form [155], depending on the methods used to influence aggregation. Centrifugation speeds up the process of aggregation compared to static culturing. The size of the well and cell starting number also impacts on the rate of spheroid formation. In each channel 3 x $10^4$ cells were seeded, forming potentially over 250 spheroids of varying sizes. The size distribution was due to the decreasing flowrate in the channel as it tended to equilibrium. The wells contained 22 cells on average based on 164 individual spheroids over three separate experiments. Due to the method of loading there is an uneven distribution of cells in each well. The wells nearest the reservoirs contained the most cells, with the highest numbers ranging between 40 – 50 cells / well. The wells furthest away could contain as few as 5 – 15 cells / well.

Spheroids were exposed to two drugs, Diclofenac and Paracetamol, known to induce metabolism-related hepatotoxicity at high concentrations for 24 hours and compared with a conventional 3D culturing method (collagen-sandwich configuration). The responses to the drugs were recorded after 24 hours exposure and at 48 hours after exposure (these samples were allowed to recover in serum-free medium for 24 hours) using fluorescence microscopy. Again, a concentration-dependent response was observed, which was more noticeable after 48 hours, indicating that the cultures continue to decline after the parent drugs have been removed. This is not surprising as the onset of

drug-induced hepatotoxicity can be delayed after exposure, depending on the mechanism of toxicity. A smaller microfluidic platform (the single array platform) was also used to culture the primary rat hepatocytes into spheroids which were exposed to Diclofenac for 24 hours. As with the collagen sandwich configurations and multi-array microfluidic platforms the single array platform also provided a concentration-dependent response, however the results were based on a single experiment (12 channels) per condition. The decline in viability for all culturing systems is likely due to metabolism-related hepatotoxicity, which was confirmed in Chapter 5 using LC-MS analysis of the culture media and cells lysate.

The results from this chapter showed that spheroids generated using a low starting cell number (per well) can still form into smooth spheroids and respond to hepatotoxins similarly to a collagen sandwich configuration containing a higher number of cells.

## 6.4 Intra- and extracellular metabolic analysis of primary hepatic spheroids and collagen sandwich configurations using LC-MS

The final phase of this research project was to determine the metabolic capabilities of the primary hepatocytes, when compared to the gold standard sandwich configuration. The results from Chapter 5 show that toxic metabolites were produced in both systems, confirming the presence of Phase I and Phase II metabolizing enzymes which is an indicator of hepatocyte function. The cultures exposed to Diclofenac produced a hydroxylated metabolite. Either 3-, 4- or 5-Hydroxydiclofenac can be produced, but 4-Hydroxydiclofenac is the

most abundant *in vivo* (human urine) [30] compared to the other two. Further identification of which hydroxylated metabolites are present can be carried out using nuclear magnetic resonance imaging technology. Additionally, glucuronidation of Diclofenac could also be detected in the microfluidic platforms and collagen sandwich configurations. The cultures exposed to Paracetamol also produced a toxic metabolite, likely NAPQI, which was confirmed by the presence of the GSH conjugated metabolite. As mentioned GSH conjugation is a result of the liver's attempt to detoxify electrophilic metabolites that would otherwise bind to proteins, disrupting normal cellular function. Sulfation and glucuronidation of Paracetamol was also detected in the samples from both culturing systems, confirming activity of a wide range of Phase I and II metabolizing enzymes. The levels detected are in agreement with the known metabolic pathway of Paracetamol, indicated by the slight increase of sulfation when the concentration is increased 4-fold. The saturated sulfation pathway allows for more NAPQI production, leading to increased levels of the GSH conjugate being detected.

Metabolites were also detected in the single array microfluidic platform after 24 hours Diclofenac exposure using even less resources than the multi-array microfluidic platform. In total, for the 6 well-plates (used for extra- and intracellular metabolic analysis) $1.5 \times 10^6$ cells were seeded / well, the 24 well-plates (extracellular analysis) were seeded at $3 \times 10^5$ cells / well and the multi-array platforms (extra- and intracellular analysis) were seeded at $3 \times 10^4$ cells / channel. The single array platforms (extracellular analysis) were only seeded with $12 \times 10^3$ cells / channel. The difference in media needed to seed and

maintain the cultures were also hugely different. Well-plates needed 400 µl and 1500 µl / well for the 24 and 6 well-plates, respectively. The platforms only needed 100 µl and 16 µl of medium for the multi-array and single array platform, respectively.

The conclusion formed from the results from this chapter demonstrated that the spheroids were still able to metabolize drugs through different, recognised pathways. The results also demonstrated that the spheroids produced comparable levels of metabolites.

## 6.5 Conclusions

The combined results from Chapter 4 and 5 show that the multi-array and single-array microfluidic platforms can sustain primary rat hepatocyte cultures long enough (6 days) to carry out detection of metabolism-induced toxicity. The primary outcome of this research was to evaluate the metabolic functionality and the effect of using 10 or 100 times less cells and media, than in a conventional 3D culturing method. Other studies using spheroids have suffered from drawbacks such as needing multiple steps or platforms to produce / store spheroids; or using hundreds (or thousands) of cells to generate a single spheroid. Alternative 3D structures, such as cords, have the disadvantage of producing less data as the structure is much larger and requires more cells than when culturing spheroids. Additionally, some platforms do not allow individual spheroids to communicate through a shared medium.

The spheroids generated and stored in the microfluidic platforms used in these experiments behaved in a similar manner to the hepatocytes in the collagen sandwich configurations when comparing the concentration-dependent viability decline using fluorescent microscopy. The spheroids were also able to produce detectable and quantifiable amounts of both Phase I (CYP2E1, CYP1A2, CYP2C9 and CYP3A4) [30] and Phase II (SULF, GLUC, GSH) generated metabolites, in both the multi-array and single array microfluidic platforms, although at a lower relative abundance.

Additions to the platform can be made to improve its efficiency, such as adding a gradient generator or altering the traps to allow retrieval of individual spheroids; or introduction of continuous perfusion. These additions could improve the level of data that is acquired, demonstrating the utility of using a microfluidic platform. This could be beneficial to the pharmacology industry by increasing throughput while reducing the required resources (compared to conventional collagen sandwich configurations) and may reduce the associated cost of developing a new drug. For example, hepatocytes isolated from a small liver biopsy tends to yield roughly $1 \times 10^7$ cells / gram [156]. A sandwich culture in a standard 96 well-plate requires a cell seeding density of roughly $0.6 – 0.8 \times 10^6$ cells / well to generate a single result. Using 20 – 50 cells to generate a single spheroid, or in this thesis $3 \times 10^4$ cells to generate over 250 individual data points is a large increase in efficacy.

The platforms could be useful for early detection of metabolism related toxicity during the preclinical stages of drug development. The initial stages of identifying target genes or proteins associated with a disease, through to lead

identification and optimisation accounts for roughly 80 – 90 % of animals used in the development process [157]. Increasing throughput using cell-based models could reduce the number of animals used, reducing cost. Primary human cells are limited in availability, thus by reducing the number of resource (i.e. cells needed to generate a metabolically active spheroid), would have a positive impact on the efficacy of using these cells. If compounds which induce hepatotoxicity can be detected earlier, the development length of the preclinical phase can be reduced and the success rates of development phases down the pipeline could potentially benefit as well. DiMasi (2002) suggested a 5 % reduction in the preclinical stage would lead to a 0.5 % reduction in the total costs associated with that stage [1]. This amount may seem small, but considering this reduction in the preclinical stage applies to nearly half of the total cost associated with the whole development process [158].

The results of this project relate closely to the 3 Rs (replacement, reduction and refinement) in drug development, albeit less related to the first R (replacement) since this technology can mainly be utilized in the early stages of drug development. To reduce the resources needed to effectively detect drug candidates that can cause drug induced liver injury has been demonstrated by using less than 100 cells to form a functional spheroid. Using 3D culture techniques, with microfluidics and LC-MS analysis encompasses refinement. All 3 aspects should continuously be advanced in a never-ending quest to improve the efficacy of drug development. In summary these experiments showed that spheroids can be generated using far fewer cells

than previously described in literature [159] [128]. These spheroids are metabolically active and can remain viable for long enough to conduct hepatotoxicity testing. Lastly, LC-MS analysis can be conducted using the supernatant and cell lysate from these spheroids generated using low cell numbers.

## 6.6 Future work

There are two main areas which could be investigated in future, environmental and resources. Environmental is defined here as the external factors that can influence the cell culture, such as material or design of the platform. PDMS is used as it allows for inexpensive mass fabrication of microfluidic platforms, allows gas exchange and is bio-inert, however it can also absorb test compounds or metabolites that have been produced. Hard plastics, such as COP or polystyrene (PS) are biocompatible and will absorb less test compounds / metabolites, at the cost of less gas exchange. Lastly, a more accurate method to control the introduction of the cells into the chip would be beneficial. Regarding the design of the platform, a method to introduce continuous perfusion will represent a more in vivo-like environment. As for the resources, the use of primary human hepatocytes should be considered, as they possess nearly all the metabolic enzymes found in vivo. Including non-parenchymal cells native to the liver, such as Kupffer or Stellate cells, could improve the metabolic capabilities of the cells. Finally, even less cells could be used to determine the lower limit of metabolically active spheroid formation.

# References


[1] J. A. DiMasi, “The value of improving the productivity of the drug development process: Faster Times and Better Decisions,” *Pharmacoeconomics*, vol. 20, no. SUPPL. 3, pp. 1–10, 2002.

[2] T. Denayer, T. Stöhrn, and M. Van Roy, “Animal models in translational medicine: Validation and prediction,” *New Horizons Transl. Med.*, vol. 2, no. 1, pp. 5–11, 2014.

[3] J. Pourahmad, P. J. O’Brien, P. Eftekhari, J. Pourahmada, and P. J. O’Brien, “Application of Cell-Based Assay Systems for the Early Screening of Human Drug Hepatotoxicity in the Discovery Phase of Drug Development,” *Iran. J. Pharm. Res.*, vol. 4, no. August, pp. 191–204, 2005.

[4] J. J. Xu, D. Diaz, and P. J. O’Brien, “Applications of cytotoxicity assays and pre-lethal mechanistic assays for assessment of human hepatotoxicity potential,” *Chem. Biol. Interact.*, vol. 150, no. 1, pp. 115–128, 2004.

[5] A. Zorn, “Liver development,” *StemBook, ed. Stem Cell Res. Community*, pp. 1–26, 2008.

[6] E.-M. Materne, A. G. Tonevitsky, and U. Marx, “Chip-based liver equivalents for toxicity testing--organotypicalness versus cost-efficient high throughput.,” *Lab Chip*, vol. 13, no. 18, pp. 3481–95, 2013.

[7] P. J. De Bleser *et al.*, “Cell biology of liver endothelial and Kupffer cells,” *Gut*, vol. 35, no. 11, pp. 1509–1516, 1994.

[8] F. Winau, C. Quack, A. Darmoise, and S. H. Kaufmann, “Starring stellate

cells in liver immunology," *Curr. Opin. Immunol.*, vol. 20, no. 1, pp. 68–74, 2008.

[9] H. Reynaert, M. G. Thompson, T. Thomas, and A. Geerts, "Hepatic stellate cells: Role in microcirculation and pathophysiology of portal hypertension," *Gut*, vol. 50, no. 4, pp. 571–581, 2002.

[10] O. B. Usta *et al.*, "Microengineered cell and tissue systems for drug screening and toxicology applications: Evolution of in-vitro liver technologies," *Technol. (World Sci.*, vol. 3, no. 1, pp. 1–26, 2015.

[11] W. C. Zhou, Q. B. Zhang, and L. Qiao, "Pathogenesis of liver cirrhosis," *World J. Gastroenterol.*, vol. 20, no. 23, pp. 7312–7324, 2014.

[12] B. R. Ware and S. R. Khetani, "Engineered Liver Platforms for Different Phases of Drug Development," *Trends Biotechnol.*, vol. 35, no. 2, pp. 172–183, 2017.

[13] P. Godoy *et al.*, "Recent advances in 2D and 3D in vitro systems using primary hepatocytes, alternative hepatocyte sources and non-parenchymal liver cells and their use in investigating mechanisms of hepatotoxicity, cell signaling and ADME," *Arch. Toxicol.*, vol. 87, no. 8, pp. 1315–1530, 2013.

[14] A. S. Kalgutkar *et al.*, "A Comprehensive Listing of Bioactivation Pathways of Organic Functional Groups," *Curr. Drug Metab.*, vol. 6, no. 3, pp. 161–225, 2005.

[15] R. Roškar and T. T. Lušin, "Analytical Methods for Quantification of Drug Metabolites in Biological Samples," in *Analytical Methods for Quantification of Drug Metabolites in Biological Samples,*

*Chromatography - The Most Versatile Method of Chemical Analysis*, 2012, pp. 79–126.

[16] W. E. Evans and M. V. Relling, “Pharmacogenomics: Translating functional genomics into rational therapeutics,” *Science (80-. ).*, vol. 286, no. 5439, pp. 487–491, 1999.

[17] P. Jancova, P. Anzenbacher, and E. Anzenbacherova, “Phase II drug metabolizing enzymes,” *Biomed. Pap.*, vol. 154, no. 2, pp. 103–116, 2010.

[18] A. Forman, Henry Jay, Zhang, Hongqiao, Rinna, “Glutathione: Overview of its protective roles, measurement, and biosynthesis,” *Mol. Aspects Med.*, vol. 30, no. 1–2, pp. 1–12, 2009.

[19] K. Levsen *et al.*, “Structure elucidation of phase II metabolites by tandem mass spectrometry : an overview,” *J. Chromatogr. A*, vol. 1067, no. 1–2, pp. 55–72, 2005.

[20] N. J. Thatcher and S. Murray, “Analysis of the glutathione conjugate of paracetamol in human liver microsomal fraction by liquid chromatography mass spectrometry,” *Biomed. Chromatogr.*, vol. 15, no. 6, pp. 374–378, 2001.

[21] A. Allameh, M. Farahani, and A. Zarghi, “Kinetic studies of aflatoxin B1-glutathione conjugate formation in liver and kidneys of adult and weanling rats,” *Mech. Ageing Dev.*, vol. 115, no. 1–2, pp. 73–83, 2000.

[22] S. Shen, M. R. Marchick, M. R. Davis, G. A. Doss, and L. R. Pohl, “Metabolic activation of diclofenac by human cytochrome P450 3A4: Role of 5-hydroxydiclofenac,” *Chem. Res. Toxicol.*, vol. 12, no. 2, pp.

214–222, 1999.

[23] T. J. Monks, M. W. Anders, W. Dekant, J. L. Stevens, S. S. Lau, and P. J. van Bladeren, “Glutathione conjugate mediated toxicities,” *Toxicol. Appl. Pharmacol.*, vol. 106, no. 1, pp. 1–19, 1990.

[24] S. Dragovic, J. S. Boerma, N. P. E. Vermeulen, and J. N. M. Commandeur, “Effect of human glutathione S-transferases on glutathione-dependent inactivation of cytochrome P450-dependent reactive intermediates of diclofenac.,” *Chem. Res. Toxicol.*, vol. 26, no. 11, pp. 1632–41, 2013.

[25] H. Dong, R. L. Haining, K. E. Thummel, A. E. Rettie, and S. D. Nelson, “Involvement of Human Cytochrome P450 2D6 in the Bioactivation of Acetaminophen,” *Drug Metab. Dispos.*, vol. 28, no. 12, pp. 1397–1400, Dec. 2000.

[26] J. E. Laine, S. Auriola, M. Pasanen, and R. O. Juvonen, “Acetaminophen bioactivation by human cytochrome P450 enzymes and animal microsomes,” *Xenobiotica*, vol. 39, no. 1, pp. 11–21, Jan. 2009.

[27] H. Ye, L. J. Nelson, M. G. Del Moral, E. Martínez-Naves, and F. J. Cubero, “Dissecting the molecular pathophysiology of drug-induced liver injury,” *World J. Gastroenterol.*, vol. 24, no. 13, pp. 1373–1385, 2018.

[28] L. J. Nelson *et al.*, “Acetaminophen cytotoxicity is ameliorated in a human liver organotypic co-culture model,” *Sci. Rep.*, vol. 5, no. 17455, pp. 1–12, 2015.

[29] M. W. den Braver, S. P. den Braver-Sewradj, N. P. E. Vermeulen, and J. N. M. Commandeur, “Characterization of cytochrome P450 isoforms

involved in sequential two-step bioactivation of diclofenac to reactive p-benzoquinone imines," *Toxicol. Lett.*, vol. 253, pp. 46–54, 2016.

[30] R. Bort, K. Macé, A. Boobis, M. J. Gómez-Lechón, A. Pfeifer, and J. Castell, "Hepatic metabolism of diclofenac: Role of human CYP in the minor oxidative pathways," *Biochem. Pharmacol.*, vol. 58, no. 5, pp. 787–796, 1999.

[31] R. Bort, X. Ponsoda, R. Jover, M. Jose, M. J. Gómez-Lechón, and J. V Castell, "Diclofenac toxicity to hepatocytes: a role for drug metabolism in cell toxicity," *J. Pharmacol. Exp. Ther.*, vol. 288, no. 1, pp. 65–72, 1999.

[32] M. J. Gómez-Lechón, X. Ponsoda, E. O'Connor, T. Donato, R. Jover, and J. V. Castell, "Diclofenac induces apoptosis in hepatocytes," *Toxicol. Vitr.*, vol. 17, no. 5–6, pp. 675–680, 2003.

[33] P. A. C. 'T Hoen, M. K. Bijsterbosch, T. J. C. Van Berkel, N. P. E. Vermeulen, and J. N. M. Commandeur, "Midazolam is a phenobarbital-like cytochrome P450 inducer in rats," *J. Pharmacol. Exp. Ther.*, vol. 299, no. 3, pp. 921–927, 2001.

[34] J. T. Backman, K. T. Olkkola, and P. J. Neuvonen, "Rifampin drastically reduces plasma concentrations and effects of oral midazolam," *Clin. Pharmacol. Ther.*, vol. 59, no. 1, pp. 7–13, 1996.

[35] V. Adams, Christopher Paul, Vu Brantner, "Spending on new drug development," *Health Econ.*, vol. 19, no. 2, pp. 130–141, 2010.

[36] V. Y. Soldatow, E. L. LeCluyse, L. G. Griffith, and I. Rusyn, "In vitro models for liver toxicity testing," *Toxicol. Res. (Camb).*, vol. 2, no. 1, pp. 23–39, 2013.

[37] D. Zhang, G. Luo, X. Ding, and C. Lu, “Preclinical experimental models of drug metabolism and disposition in drug discovery and development,” *Acta Pharm. Sin. B*, vol. 2, no. 6, pp. 549–561, 2012.

[38] A. B. Lennernas, H, “The Biopharmaceutics Classification System,” in *Comprehensive Medicinal Chemistry II*, vol. 5, 2007, pp. 971–988.

[39] R. Vrbanac, J, Slauter, “ADME in drug discovery,” in *A Comprehensive Guide to Toxicology in Nonclinical Drug Development*, 2nd ed., vol. I, Elsevier Inc., 2017, pp. 39–67.

[40] J. Liu, G. J. Tawa, and A. Wallqvist, “Identifying cytochrome P450 functional networks and their allosteric regulatory elements,” *PLoS One*, vol. 8, no. 12, pp. 1–11, 2013.

[41] S. J. Richardson, A. Bai, A. A. Kulkarni, and M. F. Moghaddam, “Efficiency in Drug Discovery: Liver S9 Fraction Assay As a Screen for Metabolic Stability,” *Drug Metab. Lett.*, vol. 10, no. 2, pp. 83–90, 2016.

[42] R. Gebhardt *et al.*, “New hepatocyte in vitro systems for drug metabolism: Metabolic capacity and recommendations for application in basic research and drug development, standard operation procedures,” *Drug Metab. Rev.*, vol. 35, no. 2–3, pp. 145–213, 2003.

[43] A. Dash and W. R. Proctor, “Hepatic microphysiological systems: Current and future applications in drug discovery and development,” in *Microfluidic Cell Culture Systems*, 2nd ed., Elsevier Inc., 2019, pp. 159–186.

[44] A. P. Li, “Primary hepatocyte cultures as an in vitro experimental model for xenobiotic metabolism and toxicology,” in *Advances in*

*Pharmacology*, vol. 43, 1997, pp. 103–130.

[45] K. L. Swift, B, Pfeifer, N D, Brouwer, “Sandwich-Cultured Hepatocytes: An In Vitro Model to Evaluate Hepatobiliary Transporter-Based Drug Interactions and Hepatotoxicity,” *Drug Metab. Rev.*, vol. 42, no. 3, pp. 446–471, 2010.

[46] R. Kostadinova *et al.*, “A long-term three dimensional liver co-culture system for improved prediction of clinically relevant drug-induced hepatotoxicity,” *Toxicol. Appl. Pharmacol.*, vol. 268, no. 1, pp. 1–16, 2013.

[47] Y. Luo *et al.*, “Three-dimensional hydrogel culture conditions promote the differentiation of human induced pluripotent stem cells into hepatocytes,” *Cytotherapy*, vol. 20, no. 1, pp. 95–107, 2018.

[48] S. C. Ramaiahgari *et al.*, “A 3D in vitro model of differentiated HepG2 cell spheroids with improved liver-like properties for repeated dose high-throughput toxicity studies,” *Arch. Toxicol.*, vol. 88, no. 5, pp. 1083–1095, 2014.

[49] J. Landry, D. Bernier, C. Ouellet, R. Goyette, and N. Marceau, “Spheroidal aggregate culture of rat liver cells: Histotypic reorganization, biomatrix deposition, and maintenance of functional activities,” *J. Cell Biol.*, vol. 101, no. 3, pp. 914–923, 1985.

[50] Y. Du, S. Chia, R. Han, S. Chang, H. Tang, and H. Yu, “3D hepatocyte monolayer on hybrid RGD/galactose substratum,” *Biomaterials*, vol. 27, no. 33, pp. 5669–5680, 2006.

[51] I. Maschmeyer *et al.*, “A four-organ-chip for interconnected long-term co-

culture of human intestine, liver, skin and kidney equivalents," *Lab Chip*, vol. 15, no. 12, pp. 2688–2699, 2015.

[52] C.-Y. Fu, S.-Y. Tseng, S.-M. Yang, L. Hsu, C.-H. Liu, and H.-Y. Chang, "A microfluidic chip with a U-shaped microstructure array for multicellular spheroid formation, culturing and analysis," *Biofabrication*, vol. 6, no. 1, pp. 1–9, 2014.

[53] L. W. Klassen *et al.*, "An in vitro method of alcoholic liver injury using precision-cut liver slices from rats," *Biochem. Pharmacol.*, vol. 76, no. 3, pp. 426–436, 2008.

[54] M. G. Soars, D. F. McGinnity, K. Grime, and R. J. Riley, "The pivotal role of hepatocytes in drug discovery," *Chem. Biol. Interact.*, vol. 168, no. 1, pp. 2–15, 2007.

[55] A. Guillouzo, "Liver cell models in in vitro toxicology," *Environ. Health Perspect.*, vol. 106, no. SUPPL. 2, pp. 511–532, 1998.

[56] C. Macdonald, M. Vass, B. Willett, A. Scott, and H. Grant, "Expression of liver functions in immortalised rat hepatocyte cell lines," *Hum. Exp. Toxicol.*, vol. 13, no. 6, pp. 439–444, 1994.

[57] P. Sancho-Bru *et al.*, "Directed differentiation of murine-induced pluripotent stem cells to functional hepatocyte-like cells," *J. Hepatol.*, vol. 54, no. 1, pp. 98–107, 2011.

[58] E. L. LeCluyse, "Human hepatocyte culture systems for the in vitro evaluation of cytochrome P450 expression and regulation," *Eur. J. Pharm. Sci.*, vol. 13, no. 4, pp. 343–368, 2001.

[59] S. J. Griffin and J. B. Houston, "Prediction of in vitro intrinsic clearance

from hepatocytes: Comparison of suspensions and monolayer cultures," *Drug Metab. Dispos.*, vol. 33, no. 1, pp. 115–120, 2005.

[60] N. J. Hewitt *et al.*, "Primary Hepatocytes: Current Understanding of the Regulation of Metabolic Enzymes and Transporter Proteins, and Pharmaceutical Practice for the Use of Hepatocytes in Metabolism, Enzyme Induction, Transporter, Clearance, and Hepatotoxicity Studies," *Drug Metab. Rev.*, vol. 39, no. 1, pp. 159–234, Jan. 2007.

[61] R. T. Mingoia, D. L. Nabb, C. H. Yang, and X. Han, "Primary culture of rat hepatocytes in 96-well plates: Effects of extracellular matrix configuration on cytochrome P450 enzyme activity and inducibility, and its application in in vitro cytotoxicity screening," *Toxicol. Vitr.*, vol. 21, no. 1, pp. 165–173, 2007.

[62] Q. Meng, "Three-dimensional culture of hepatocytes for prediction of drug-induced hepatotoxicity," *Expert Opin. Drug Metab. Toxicol.*, vol. 6, no. 6, pp. 733–746, Jun. 2010.

[63] C. Lerche-Langrand and H. J. Toutain, "Precision-cut liver slices: Characteristics and use for in vitro pharmaco-toxicology," *Toxicology*, vol. 153, no. 1–3, pp. 221–253, 2000.

[64] E. Hashemi, C. Till, and C. Ioannides, "Stability of phase II conjugation systems in cultured precision-cut rat hepatic slices," *Toxicol. Vitr.*, vol. 13, no. 3, pp. 459–466, 1999.

[65] H. Gaskell, P. Sharma, H. E. Colley, C. Murdoch, D. P. Williams, and S. D. Webb, "Characterization of a functional C3A liver spheroid model," *Toxicol. Res. (Camb).*, vol. 5, no. 4, pp. 1053–1065, 2016.

[66] C. C. Bell *et al.*, “Characterization of primary human hepatocyte spheroids as a model system for drug-induced liver injury, liver function and disease,” *Sci. Rep.*, vol. 6, no. May, pp. 1–13, 2016.

[67] C. C. Bell *et al.*, “Comparison of hepatic 2D sandwich cultures and 3d spheroids for long-term toxicity applications: A multicenter study,” *Toxicol. Sci.*, vol. 162, no. 2, pp. 655–666, 2018.

[68] H. Boukellal, E. Selimović, Y. Jia, G. Cristobal, and S. Fraden, “Simple, robust storage of drops and fluids in a microfluidic device,” *Lab Chip*, vol. 9, no. 2, pp. 331–338, 2009.

[69] J. R. Petrulis, G. Chen, S. Benn, J. Lamarre, and N. J. Bunce, “Application of the ethoxyresorufin-O-deethylase (EROD) assay to mixtures of halogenated aromatic compounds,” *Environ. Toxicol.*, vol. 16, no. 2, pp. 177–184, 2001.

[70] N. Murayama, T. Usui, N. Slawny, C. Chesné, and H. Yamazaki, “Human HepaRG Cells can be Cultured in Hanging-drop Plates for Cytochrome P450 Induction and Function Assays,” *Drug Metab. Lett.*, vol. 9, no. 1, pp. 3–7, 2015.

[71] J. C. Mcdonald *et al.*, “Fabrication of microfluidic systems in poly(dimethylsiloxane),” *Electrophoresis*, vol. 21, no. 1, pp. 27–40, 2000.

[72] T. Thorsen, R. W. Roberts, F. H. Arnold, and S. R. Quake, “Dynamic pattern formation in a vesicle-generating microfluidic device,” *Phys. Rev. Lett.*, vol. 86, no. 18, pp. 4163–4166, 2001.

[73] S. L. Anna, N. Bontoux, and H. A. Stone, “Formation of dispersions using ‘flow focusing’ in microchannels,” *Appl. Phys. Lett.*, vol. 82, no. 3, pp.

364–366, 2003.

[74] R. Seemann, M. Brinkmann, T. Pfohl, and S. Herminghaus, “Droplet based microfluidics,” *Reports Prog. Phys.*, vol. 75, no. 1, pp. 1–41, 2012.

[75] H. Liu and Y. Zhang, “Droplet formation in a T-shaped microfluidic junction,” *J. Appl. Phys.*, vol. 106, no. 3, pp. 1–8, 2009.

[76] A. B. Theberge *et al.*, “Microdroplets in microfluidics: An evolving platform for discoveries in chemistry and biology,” *Angew. Chemie - Int. Ed.*, vol. 49, no. 34, pp. 5846–5868, 2010.

[77] S. S. Bithi, W. S. Wang, M. Sun, J. Blawzdziewicz, and S. A. Vanapalli, “Coalescing drops in microfluidic parking networks: A multifunctional platform for drop-based microfluidics,” *Biomicrofluidics*, vol. 8, no. 3, pp. 1–13, 2014.

[78] S. S. Bithi and S. a Vanapalli, “Behavior of a train of droplets in a fluidic network with hydrodynamic traps.,” *Biomicrofluidics*, vol. 4, no. 4, p. 44110, 2010.

[79] K. S. Mcmillan, “Engineering Development of a Microfluidic Platform for Multicellular Tumour Spheroid Assays,” The University of Strahclyde, 2016.

[80] Y. Sakai *et al.*, “Effect of microwell chip structure on cell microsphere production of various animal cells,” *J. Biosci. Bioeng.*, vol. 110, no. 2, pp. 223–229, 2010.

[81] H. C. Moeller, M. K. Mian, S. Shrivastava, B. G. Chung, and A. Khademhosseini, “A microwell array system for stem cell culture,” *Biomaterials*, vol. 29, no. 6, pp. 752–763, 2008.

[82] H. Chen, J. Li, H. Zhang, M. Li, G. Rosengarten, and R. E. Nordon, “Microwell perfusion array for high-throughput, long-term imaging of clonal growth,” *Biomicrofluidics*, vol. 5, no. 4, pp. 1–13, 2011.

[83] W. Lim and S. Park, “A microfluidic spheroid culture device with a concentration gradient generator for high-throughput screening of drug efficacy,” *Molecules*, vol. 23, no. 12, pp. 1–10, 2018.

[84] K. Ziółkowska, A. Stelmachowska, R. Kwapiszewski, M. Chudy, A. Dybko, and Z. Brzózka, “Long-term three-dimensional cell culture and anticancer drug activity evaluation in a microfluidic chip,” *Biosens. Bioelectron.*, vol. 40, no. 1, pp. 68–74, 2013.

[85] Y. Chen, D. Gao, H. Liu, S. Lin, and Y. Jiang, “Drug cytotoxicity and signaling pathway analysis with three-dimensional tumor spheroids in a microwell-based microfluidic chip for drug screening,” *Anal. Chim. Acta*, vol. 898, pp. 85–92, 2015.

[86] B. Corrado, V. De Gregorio, G. Imparato, C. Attanasio, F. Urciuolo, and P. A. Netti, “A three-dimensional microfluidized liver system to assess hepatic drug metabolism and hepatotoxicity,” *Biotechnol. Bioeng.*, vol. 116, no. 5, pp. 1152–1163, 2018.

[87] M. Yamada *et al.*, “Cell-sized condensed collagen microparticles for preparing microengineered composite spheroids of primary hepatocytes,” *Lab Chip*, vol. 15, no. 19, pp. 3941–3951, 2015.

[88] C. Y. Li, K. R. Stevens, R. E. Schwartz, B. S. Alejandro, J. H. Huang, and S. N. Bhatia, “Micropatterned cell-cell interactions enable functional encapsulation of primary hepatocytes in hydrogel microtissues,” *Tissue*

*Eng. - Part A*, vol. 20, no. 15–16, pp. 2200–2212, 2014.

[89] S. R. Caliari and J. A. Burdick, “A Practical Guide to Hydrogels for Cell Culture,” *Nat Methods*, vol. 13, no. 5, pp. 405–414, 2016.

[90] A. M. Kloxin, A. M. Kasko, C. N. Salinas, and K. S. Anseth, “Photodegradable hydrogels for dynamic tuning of physical and chemical properties,” *Science (80-. ).*, vol. 324, no. 5923, pp. 59–63, 2009.

[91] J. J. Moon *et al.*, “Biomimetic hydrogels with pro-angiogenic properties,” *Biomaterials*, vol. 31, no. 14, pp. 3840–3847, 2010.

[92] S. F. Wong, D. Y. No, Y. Y. Choi, D. S. Kim, B. G. Chung, and S. H. Lee, “Concave microwell based size-controllable hepatosphere as a three-dimensional liver tissue model,” *Biomaterials*, vol. 32, no. 32, pp. 8087–8096, 2011.

[93] Y. Y. Choi, J. Kim, S.-H. Lee, and D.-S. Kim, “Lab on a chip-based hepatic sinusoidal system simulator for optimal primary hepatocyte culture,” *Biomed. Microdevices*, vol. 18, no. 4, p. 58, 2016.

[94] S. A. Lee, D. Y. No, E. Kang, J. Ju, D. S. Kim, and S. H. Lee, “Spheroid-based three-dimensional liver-on-a-chip to investigate hepatocyte-hepatic stellate cell interactions and flow effects,” *Lab Chip*, vol. 13, no. 18, pp. 3529–3537, 2013.

[95] Y.-C. Toh, T. C. Lim, D. Tai, G. Xiao, D. van Noort, and H. Yu, “A microfluidic 3D hepatocyte chip for drug toxicity testing.,” *Lab Chip*, vol. 9, no. 14, pp. 2026–2035, 2009.

[96] Y. Nakao, H. Kimura, Y. Sakai, and T. Fujii, “Bile canaliculi formation by

aligning rat primary hepatocytes in a microfluidic device," *Biomicrofluidics*, vol. 5, no. 2, 2011.

[97] Q. Chen, S. Utech, D. Chen, R. M. Prodanovic, J.-M. Lin, and D. A. Weitz, "Controlled Assembly of Heterotypic cells in a Core-Shell Scaffold: Organ in a Droplet," *Lab Chip*, vol. 16, no. 8, pp. 1346–1349, 2016.

[98] C. Siltanen *et al.*, "One step fabrication of hydrogel microcapsules with hollow core for assembly and cultivation of hepatocyte spheroids," *Acta Biomater.*, vol. 50, pp. 428–436, 2017.

[99] T. Okuyama, H. Yamazoe, N. Mochizuki, A. Khademhosseini, H. Suzuki, and J. Fukuda, "Preparation of arrays of cell spheroids and spheroid-monolayer cocultures within a microfluidic device," *J. Biosci. Bioeng.*, vol. 110, no. 5, pp. 572–576, 2010.

[100] B. Patra, C. C. Peng, W. H. Liao, C. H. Lee, and Y. C. Tung, "Drug testing and flow cytometry analysis on a large number of uniform sized tumor spheroids using a microfluidic device," *Sci. Rep.*, vol. 6, no. 21061, pp. 1–12, 2016.

[101] R. D. Mittal, "Tandem Mass Spectroscopy in Diagnosis and Clinical Research," *Indian J. Clin. Biochem.*, vol. 30, no. 2, pp. 121–123, 2015.

[102] A. El-Aneed, A. Cohen, and J. Banoub, "Mass spectrometry, review of the basics: Electrospray, MALDI, and commonly used mass analyzers," *Appl. Spectrosc. Rev.*, vol. 44, no. 3, pp. 210–230, 2009.

[103] A. Makarov and M. Scigelova, "Coupling liquid chromatography to Orbitrap mass spectrometry," *J. Chromatogr. A*, vol. 1217, no. 25, pp.

3938–3945, 2010.

[104] K. Rennert *et al.*, “A microfluidically perfused three dimensional human liver model,” *Biomaterials*, vol. 71, pp. 119–131, 2015.

[105] F. Yu *et al.*, “A perfusion incubator liver chip for 3D cell culture with application on chronic hepatotoxicity testing,” *Sci. Rep.*, vol. 7, no. 1, pp. 1–16, 2017.

[106] P. Gunness, D. Mueller, V. Shevchenko, E. Heinzle, M. Ingelman-Sundberg, and F. Noor, “3D organotypic cultures of human heparg cells: A tool for in vitro toxicity studies,” *Toxicol. Sci.*, vol. 133, no. 1, pp. 67–78, 2013.

[107] G. Robertson, “Development of Microfluidic Systems for Studying Functional Connectivity Between In Vitro Neuronal Co-Cultures,” The University of Strahclyde, 2015.

[108] N. L. Harris, Joseph, Lee, Hyuna, Vahidi, Behrad, Tu, Cristina, Cribbs, David, Cotman, Carl, Jeon, “Non-plasma Bonding of PDMS for Inexpensive Fabrication of Microfluidic Devices,” *J. Vis. Exp.*, no. 9, p. 410, 2007.

[109] S. Shin, Yoojin, Han, Sweoon, Jeon, Jessie S, Yamamoto, Kyoko, Zervantonakis, Ioannis K, Sudo, Ryo, Kamm, Roger D, Chung, “Microfluidic assay for simultaneous culture of multiple cell types on surfaces or within hydrogels,” *Nat. Protoc.*, vol. 7, no. 7, pp. 1247–1259, 2012.

[110] T. Mulholland *et al.*, “Drug screening of biopsy-derived spheroids using a self-generated microfluidic concentration gradient,” *Sci. Rep.*, vol. 8,

no. 1, pp. 1–12, 2018.

[111] O. I. G. Khreit, “Developing methods for profiling of cathinone derivatives and elucidation of their metabolites formed in rat and human hepatocytes,” The University of Strathclyde, 2013.

[112] H. H. J. Gerets *et al.*, “Characterization of primary human hepatocytes, HepG2 cells, and HepaRG cells at the mRNA level and CYP activity in response to inducers and their predictivity for the detection of human hepatotoxins,” *Cell Biol. Toxicol.*, vol. 28, no. 2, pp. 69–87, 2012.

[113] D. Marion, Marie-Jeanne, Hantz, Oliver, Durantel, “The HepaRG Cell Line: Biological Properties and Relevance as a Tool for Cell Biology, Drug Metabolism, and Virology Studies,” *Methods Mol. Biol.*, vol. 640, pp. 261–272, 2010.

[114] Y. Yokoyama *et al.*, “Comparison of drug metabolism and its related hepatotoxic effects in heparg, cryopreserved human hepatocytes, and HepG2 cell cultures,” *Biol. Pharm. Bull.*, vol. 41, no. 5, pp. 722–732, 2018.

[115] J. Xu, M. Ma, and W. M. Purcell, “Characterisation of some cytotoxic endpoints using rat liver and HepG2 spheroids as in vitro models and their application in hepatotoxicity studies. II. Spheroid cell spreading inhibition as a new cytotoxic marker,” *Toxicol. Appl. Pharmacol.*, vol. 189, no. 2, pp. 112–119, 2003.

[116] S. Wilkening, F. Stahl, and A. Bader, “Comparison of primary human hepatocytes and hepatoma cell line Hepg2 With Regard To Their Biotransformation Properties,” *Drug Metab. Dispos.*, vol. 31, no. 8, pp.

1035–1042, 2003.

[117] J. L. C. M. Dorne, K. Walton, and A. G. Renwick, “Human variability in CYP3A4 metabolism and CYP3A4-related uncertainty factors for risk assessment,” *Food Chem. Toxicol.*, vol. 41, no. 2, pp. 201–224, 2003.

[118] S. J. Fey and K. Wrzesinski, “Determination of drug toxicity using 3D spheroids constructed from an immortal human hepatocyte cell line,” *Toxicol. Sci.*, vol. 127, no. 2, pp. 403–411, 2012.

[119] W. M. A. Westerink and W. G. E. J. Schoonen, “Cytochrome P450 enzyme levels in HepG2 cells and cryopreserved primary human hepatocytes and their induction in HepG2 cells,” *Toxicol. Vitr.*, vol. 21, no. 8, pp. 1581–1591, 2007.

[120] Y. Miyamoto, M. Ikeuchi, H. Noguchi, T. Yagi, and S. Hayashi, “Spheroid Formation and Evaluation of Hepatic Cells in a Three-Dimensional Culture Device,” *Cell Med.*, vol. 8, no. 1–2, pp. 47–56, 2015.

[121] J. L. Sebaugh, “Guidelines for accurate EC50/IC50 estimation,” *Pharm. Stat.*, vol. 10, no. 2, pp. 128–134, 2010.

[122] Z. A. Noel, J. Wang, and M. I. Chilvers, “Significant Influence of EC 50 Estimation by Model Choice and EC 50 Type,” *Plant Dis.*, vol. 102, no. 4, pp. 708–714, 2018.

[123] J. Fukuda *et al.*, “Efficacy of a polyurethane foam/spheroid artificial liver by using human hepatoblastoma cell line (Hep G2),” *Cell Transplant.*, vol. 12, no. 1, pp. 51–58, 2003.

[124] X. Ponsoda, R. Jover, C. Nunez, M. Royo, J. V. Castell, and M. J. Gomez-Lechon, “Evaluation of the cytotoxicity of 10 chemicals in human

and rat hepatocytes and in cell lines: Correlation between in vitro data and human lethal concentration," *Toxicol. Vitr.*, vol. 9, no. 6, pp. 959–966, 1995.

[125] A. Kawase, R. Hashimoto, M. Shibata, H. Shimada, and M. Iwaki, "Involvement of Reactive Metabolites of Diclofenac in Cytotoxicity in Sandwich-Cultured Rat Hepatocytes," *Int. J. Toxicol.*, vol. 36, no. 3, pp. 260–267, 2017.

[126] A. Ramachandran and H. Jaeschke, "Acetaminophen toxicity: Novel insights into mechanisms and future perspectives," *Gene Expr.*, vol. 18, no. 1, pp. 19–30, 2018.

[127] S. Wilkening and A. Bader, "Influence of culture time on the expression of drug-metabolizing enzymes in primary human hepatocytes and hepatoma cell line HepG2," *J. Biochem. Mol. Toxicol.*, vol. 17, no. 4, pp. 207–213, 2003.

[128] R. Glicklis, J. C. Merchuk, and S. Cohen, "Modeling mass transfer in hepatocyte spheroids via cell viability, spheroid size, and hepatocellular functions," *Biotechnol. Bioeng.*, vol. 86, no. 6, pp. 672–680, 2004.

[129] H. Itagaki, *Fluorescence Spectroscopy*, 1st ed. San Diego: Academic press, 2000.

[130] P. Gissen and I. M. Arias, "Structural and functional hepatocyte polarity and liver disease," *J. Hepatol.*, vol. 63, no. 4, pp. 1023–1037, 2015.

[131] H. Meerschaert, Kris, Tun, Moe Phyu, Remue, Eline, De Ganck, Ariane, Boucherie, Ciska, Vanloo, Berlinda, Degest, Gisele, Vandekerckhove, Cho, Wonhwa, Gettemans, Jan Zimmermann, Pascale, Bhardwaj, Nitin,

Lu, “The PDZ2 domain of zonula occludens-1 and -2 is a phosphoinositide binding domain,” *Cell. Mol. Life Sci.*, vol. 66, no. 24, pp. 3951–3966, 2009.

[132] G. Tuschl and S. O. Mueller, “Effects of cell culture conditions on primary rat hepatocytes - Cell morphology and differential gene expression,” *Toxicology*, vol. 218, no. 2–3, pp. 205–215, 2006.

[133] J. S. Lagas, R. W. Sparidans, E. Wagenaar, J. H. Beijnen, and A. H. Schinkel, “Hepatic clearance of reactive glucuronide metabolites of diclofenac in the mouse is dependent on multiple ATP-binding cassette efflux transporters,” *Mol. Pharmacol.*, vol. 77, no. 4, pp. 687–694, 2010.

[134] M. Syed, C. Skonberg, and S. Honoré, “Mitochondrial toxicity of selective COX-2 inhibitors via inhibition of oxidative phosphorylation ( ATP synthesis ) in rat liver mitochondria,” *Toxicol. Vitr.*, vol. 32, pp. 26–40, 2016.

[135] A. Kawase, R. Hashimoto, M. Shibata, H. Shimada, and M. Iwaki, “Involvement of Reactive Metabolites of Diclofenac in Cytotoxicity in Sandwich-Cultured Rat Hepatocytes,” *Int. J. Toxicol.*, vol. 36, no. 3, pp. 260–267, 2017.

[136] U. A. Boelsterli, “Diclofenac-induced liver injury: A paradigm of idiosyncratic drug toxicity,” *Toxicol. Appl. Pharmacol.*, vol. 192, no. 3, pp. 307–322, 2003.

[137] B. Lauer, G. Tuschl, M. Kling, and S. O. Mueller, “Species-specific toxicity of diclofenac and troglitazone in primary human and rat hepatocytes,” *Chem. Biol. Interact.*, vol. 179, no. 1, pp. 17–24, 2009.

[138] Y. Zhang *et al.*, “Diclofenac and Its Acyl Glucuronide: Determination of in Vivo Exposure in Human Subjects and Characterization as Human Drug Transporter Substrates in Vitro,” *Drug Metab. Dispos.*, vol. 44, no. 3, pp. 320–328, 2015.

[139] K. Wang, H. Shindoh, T. Inoue, and I. Horii, “Advantages of in vitro cytotoxicity testing by using primary rat hepatocytes in comparison with established cell lines,” *J. Toxicol. Sci.*, vol. 27, no. 3, pp. 229–237, 2002.

[140] S. Cassim, V. A. Raymond, P. Lapierre, and M. Bilodeau, “From in vivo to in vitro: Major metabolic alterations take place in hepatocytes during and following isolation,” *PLoS One*, vol. 12, no. 12, pp. 1–14, 2017.

[141] M. P. Grillo, F. Hua, C. G. Knutson, J. A. Ware, and C. Li, “Mechanistic studies on the bioactivation of diclofenac: identification of diclofenac-S-acyl-glutathione in vitro in incubations with rat and human hepatocytes,” *Chem. Res. Toxicol.*, vol. 16, no. 11, pp. 1410–1417, 2003.

[142] C. I. Wallace, P. I. Dargan, and A. L. Jones, “Paracetamol overdose: an evidence based flowchart to guide,” *Emerg. Med.*, vol. 19, no. 3, pp. 202–205, 2002.

[143] S. Ben-Moshe, Y. Shapira, A. E. Moor, K. B. Halpern, and S. Itzkovitz, “Spatial sorting enables comprehensive characterization of liver zonation,” *Nat. Metab.*, vol. 1, pp. 899–911, 2019.

[144] J. J. Gumucio and D. L. Miller, “Functional implications of liver cell heterogeneity,” *Gastroenterology*, vol. 80, no. 2, pp. 393–403, 1981.

[145] M. W. Toepke and D. J. Beebe, “PDMS absorption of small molecules and consequences in microfluidic applications,” *Lab Chip*, vol. 6, no. 12,

pp. 1484–1486, 2006.

[146] U. Sarkar *et al.*, “Integrated assessment of diclofenac biotransformation, pharmacokinetics, and omics-based toxicity in a three-dimensional human liver-immunocompetent coculture system,” *Drug Metab. Dispos.*, vol. 45, no. 7, pp. 855–866, 2017.

[147] T. P. Milligan, H. C. Morris, P. M. Hammond, and C. P. Price, “Studies on paracetamol binding to serum proteins,” *Ann. Clin. Biochem.*, vol. 31, no. 5, pp. 492–496, 1994.

[148] A. G. Wang *et al.*, “Effects of phenobarbital on metabolism and toxicity of diclofenac sodium in rat hepatocytes in vitro,” *Food Chem. Toxicol.*, vol. 42, no. 10, pp. 1647–1653, 2004.

[149] M. Syed, C. Skonberg, and S. Honoré, “Toxicology in Vitro Mitochondrial toxicity of diclofenac and its metabolites via inhibition of oxidative phosphorylation ( ATP synthesis ) in rat liver mitochondria : Possible role in drug induced liver injury ( DILI ),” *Toxicol. Vitr.*, vol. 31, pp. 93–102, 2016.

[150] T. R. Van Vleet, H. Liu, A. Lee, and E. A. G. Blomme, “Acyl glucuronide metabolites: Implications for drug safety assessment,” *Toxicol. Lett.*, vol. 272, pp. 1–7, 2017.

[151] A. Iwamura, M. Nakajima, S. Oda, and T. Yokoi, “Toxicological potential of acyl glucuronides and its assessment,” *Drug Metab. Pharmacokinet.*, vol. 32, no. 1, pp. 2–11, 2017.

[152] T. E. Mazaleuskaya, Liudmila L, Sangkuhl, Katrin, Thorn, Caroline F, FitzGerald, Garret A, Altman, Russ B, Klein, “PharmGKB summary:

Pathways of acetaminophen metabolism at the therapeutic versus toxic doses," *Pharmacogenet. Genomics*, vol. 25, no. 8, pp. 416–426, 2015.

[153] H. Ramachandran, Anup, Jaeschke, "Mechanisms of acetaminophen hepatotoxicity and their translation to the human pathophysiology," *J. Clin. Transl. Res.*, vol. 3, no. Suppl 1, pp. 157–169, 2017.

[154] M. P. Grillo, C. G. Knutson, P. E. Sanders, D. J. Waldon, F. Hua, and J. A. Ware, "Studies on the chemical reactivity of diclofenac acyl glucuronide with glutathione: Identification of diclofenac-S-acyl-glutathione in rat bile," *Drug Metab. Dispos.*, vol. 31, no. 11, pp. 1327–1336, 2003.

[155] C. M. Brophy *et al.*, "Rat hepatocyte spheroids formed by rocked technique maintain differentiated hepatocyte gene expression and function," *Hepatology*, vol. 49, no. 2, pp. 578–586, 2009.

[156] O. Hwan-Mook, KIM, Sang-bae, HAN, Byung-Hwa, HYUN, Chang-Joon, AHN, Young-Nam, CHA, Kyu-Shik, JEONG, Goo-Taeg, "Functional Human Hepatocytes: Isolation from small liver biopsy samples and primary cultivation with liver-specific functions," *Jounral Toxicol. Sci.*, vol. 20, no. 5, pp. 565–578, 1995.

[157] D. K. Badyal and C. Desai, "Animal use in pharmacology education and research: the changing scenario," *Indian J. Pharmacol.*, vol. 46, no. 3, pp. 257–265, 2014.

[158] J. A. DiMasi, R. W. Hansen, and H. G. Grabowski, "The price of innovation: New estimates of drug development costs," *J. Health Econ.*, vol. 22, no. 2, pp. 151–185, 2003.

[159] S. F. Abu-Absi, J. R. Friend, L. K. Hansen, and W. S. Hu, “Structural polarity and functional bile canaliculi in rat hepatocyte spheroids,” *Exp. Cell Res.*, vol. 274, no. 1, pp. 56–67, 2002.

# Appendix

## Reagents and Equipment

### Chemicals and reagents

*Reagents used in the fabrication of the master wafer and the Microfluidic platforms*

Acetone – Fisher Scientific, UK

Methanol – Fisher Scientific, UK

Isopropanol – Fisher Scientific, UK

Poly(dimethyl siloxane) – Dow Corning Sylgard 184 Silicone Elastomer kit

SU3035 photoresist – MicroChem, MA, USA

MicroPosit EC solvent – MicroChem, MA, USA

1H, 1H, 2H, 2H-perfluorooctyl-trichlolosilane – Sigma Aldrich, UK

Aquapel glass treatment – PPG industries Inc, Pittsburgh, USA

Fluorinated oil (FC-40) – Sigma Aldrich, UK

Block copolymer fluorosurfactants – RAN technologies, USA

Synperonic F108 surfactant – Sigma Aldrich, UK

*Reagents used in the culturing of the HepG2 cells*

Dulbecco’s Modified Eagle Medium – Lonza, UK

Penicillin / Streptomycin – Life Technologies, UK

Amphotericin B – Life Technologies, UK

Foetal bovine serum – Life Technologies, UK

Non-essential amino acids (NEAA) – Lonza, UK

Trypsin – Sigma Aldrich, UK

*Reagents used in the culturing of the Primary rat hepatocytes*

Williams's medium E culture medium – (Invitrogen) ThermoFisher, UK

Insulin-transferrin-selenium solution – (Invitrogen) ThermoFisher, UK

L-glutamine – Life Technologies, UK

Dexamethasone – Sigma Aldrich, UK

Ethanol – Sigma Aldrich, UK

*Reagents used in the construction of the collagen sandwich configuration*

Collagen type I solution in acetic acid (extracted from rat tails)

Dulbecco's Modified Eagle's Medium 10 x – Sigma Aldrich, UK

Sodium Hydroxide (NaOH) – Sigma Aldrich, UK

Acetic acid – Sigma Aldrich, UK

Distilled water

*Reagents used in the toxicity assays*

Dimethyl sulfoxide – Sigma Aldrich, UK

Diclofenac sodium salt – Sigma Aldrich, UK

4-Acetaminophenol – Sigma Aldrich, UK

4'-Hydroxydiclofenac – Sigma Aldrich, UK

*Reagents used in the Immunofluorescence assays*

Fluorescein diacetate – Sigma Aldrich, UK

Propidium Iodide – Sigma Aldrich, UK

Trypan Blue solution – ThermoFisher, UK

Hoechst 33342 solution (20mM) – ThermoFisher, UK

DAPI – Sigma Aldrich, UK

Primary rabbit anti-ZO1 antibody – ThermoFisher, UK

Alexa fluor 594 labelled goat anti-rabbit IgG – ThermoFisher, UK

*Reagents used in the liquid chromatography-mass spectrometry analysis*

Acetonitrile (HPLC grade) – Sigma Aldrich, UK

Methanol (HPLC grade) – Sigma Aldrich, UK

Water (HPLC grade) – Sigma Aldrich, UK

Acetic acid (HPLC grade) – Sigma Aldrich, UK

## Equipment

*Consumables and equipment used during cell culture*

Microscope: Axio inverted A1 – ZEISS

Haemocytometer – Fisher Scientific, UK

Glass slides – Fisher Scientific, UK

4 well dish with lid – Thermo Scientific, UK

*Equipment used with the microfluidic platforms*

Syringe pump: Aladdin 1000 – World Precision Instruments, UK

Glass syringes – Hamilton Company, USA

Acetate photomask – JD Photo-Tools, UK

PTFE Tubing – Cole Palmer

Biopsy punch (1 mm and 4 mm) – Stiefel, SmithKleine Beecham Ltd, UK

Oxygen plasma asher – Pico A, Diener Electronic, Germany

0.2 Nylon filter – Sigma Aldrich, UK

*Liquid chromatography-mass spectrometry equipment*

Dionex High Performance Liquid Chromatograph

Exactive Orbitrap mass spectrometer

C18-AR column (dimensions, 150mm x 4.6 mm) – VWR, UK

## LC-MS representative figures

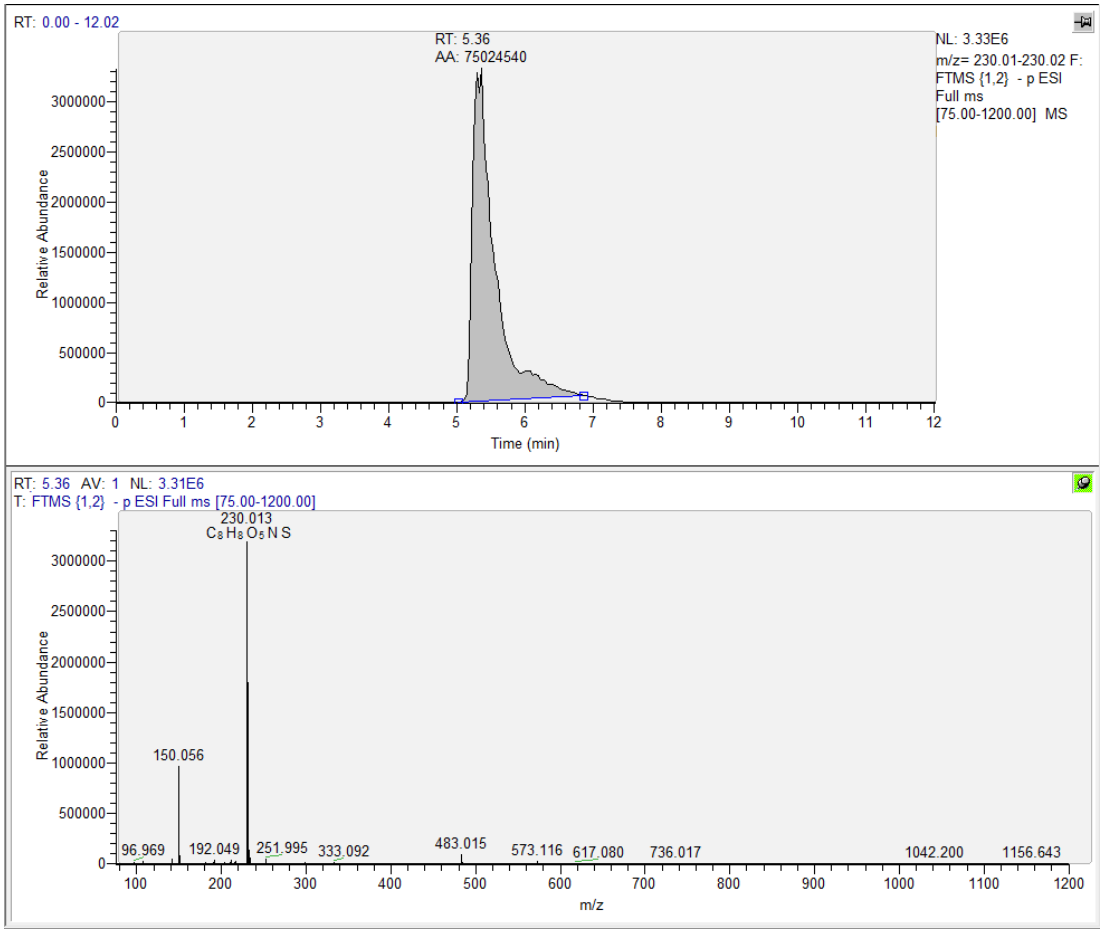


*Figure A.1: Representative LC-MS image (TIC above and mass spectra below) the APAP-SUL (m/z ratio 230) metabolite detected using primary rat hepatocytes cultured in a collagen sandwich configuration (4 days) and exposed to 0.47 mM APAP for 24 hours.*

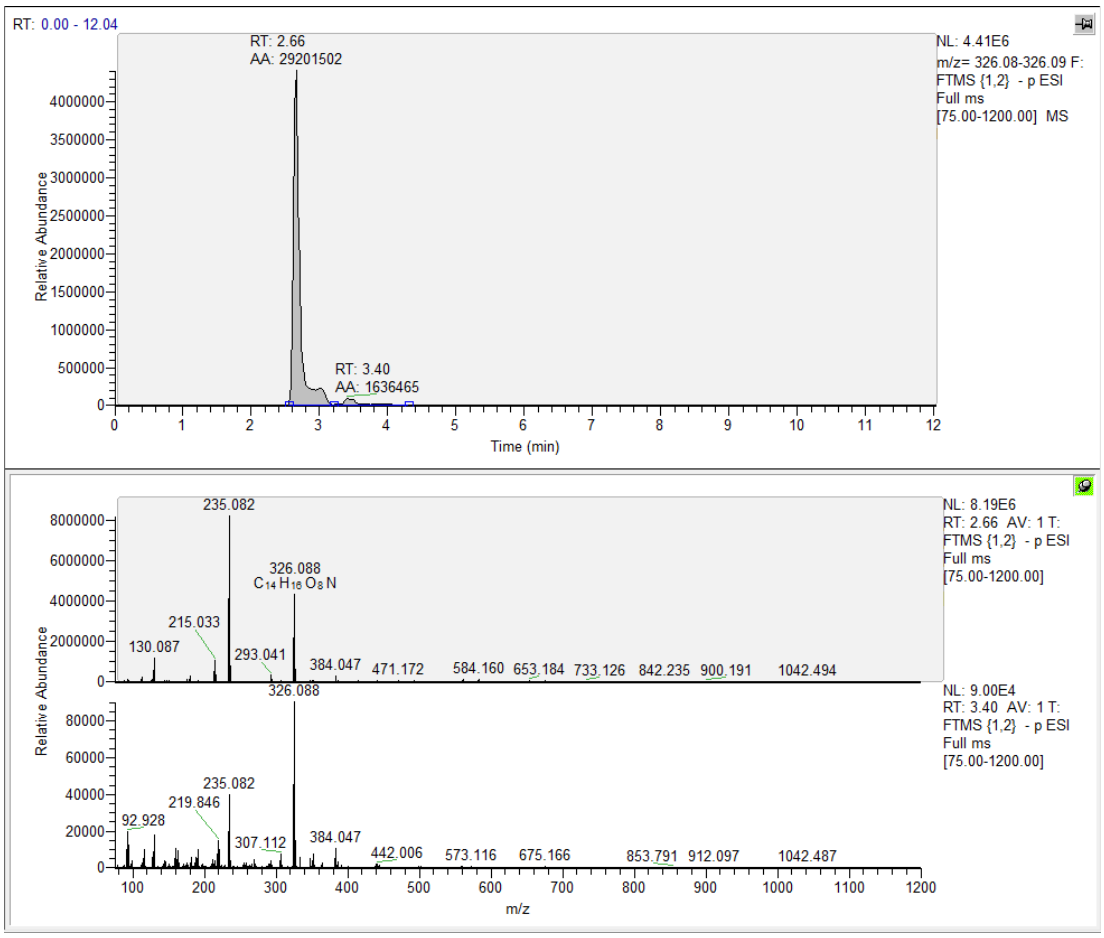


*Figure A.2 Representative LC-MS image (TIC above and mass spectra below) the APAP-GLUC metabolite (m/z ratio 328) detected using primary rat hepatocytes cultured in a collagen sandwich configuration (4 days) and exposed to 1.94 mM APAP for 24 hours. Peak splitting can be observed*

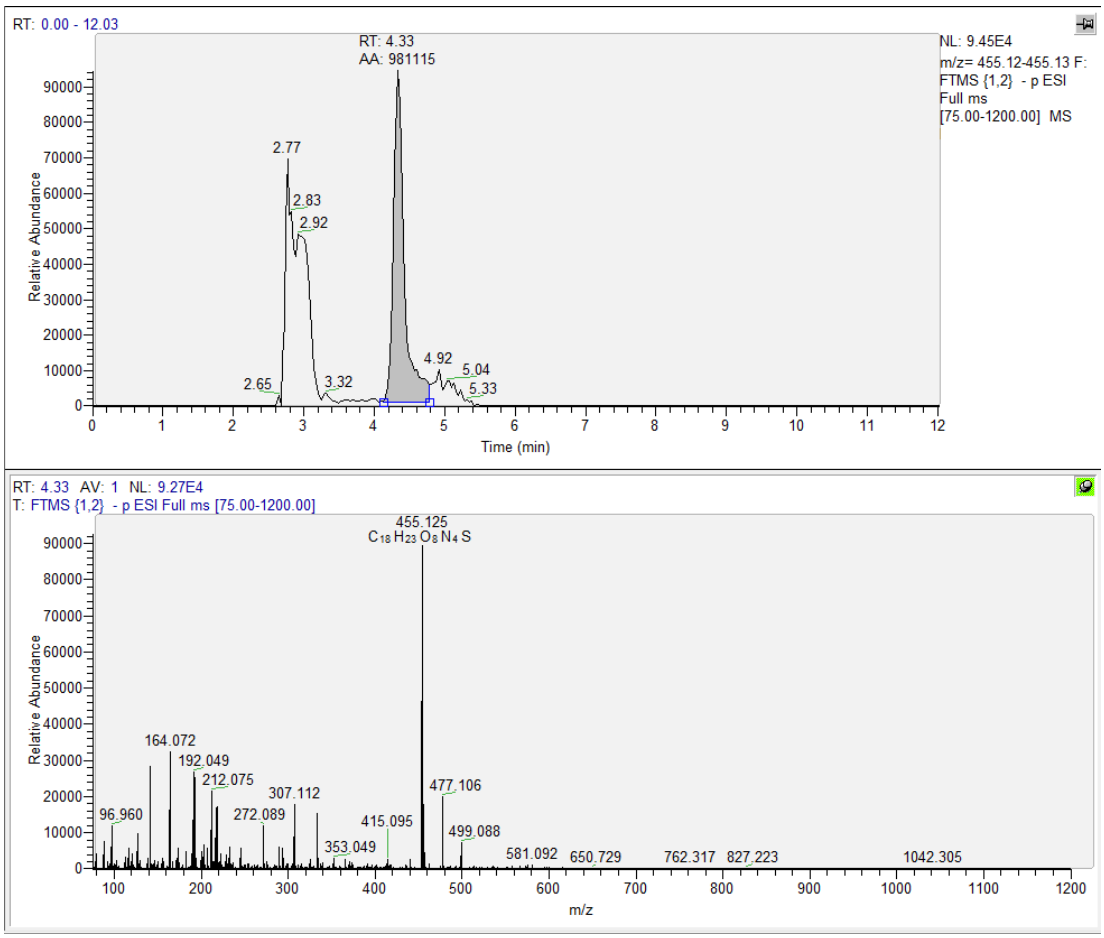


*Figure A.3 Representative LC-MS image (TIC above and mass spectra below) the APAP-GSH metabolite (m/z ratio 455) detected using primary rat hepatocytes cultured in a collagen sandwich configuration (4 days) and exposed to 7.50 mM APAP for 24 hours.*

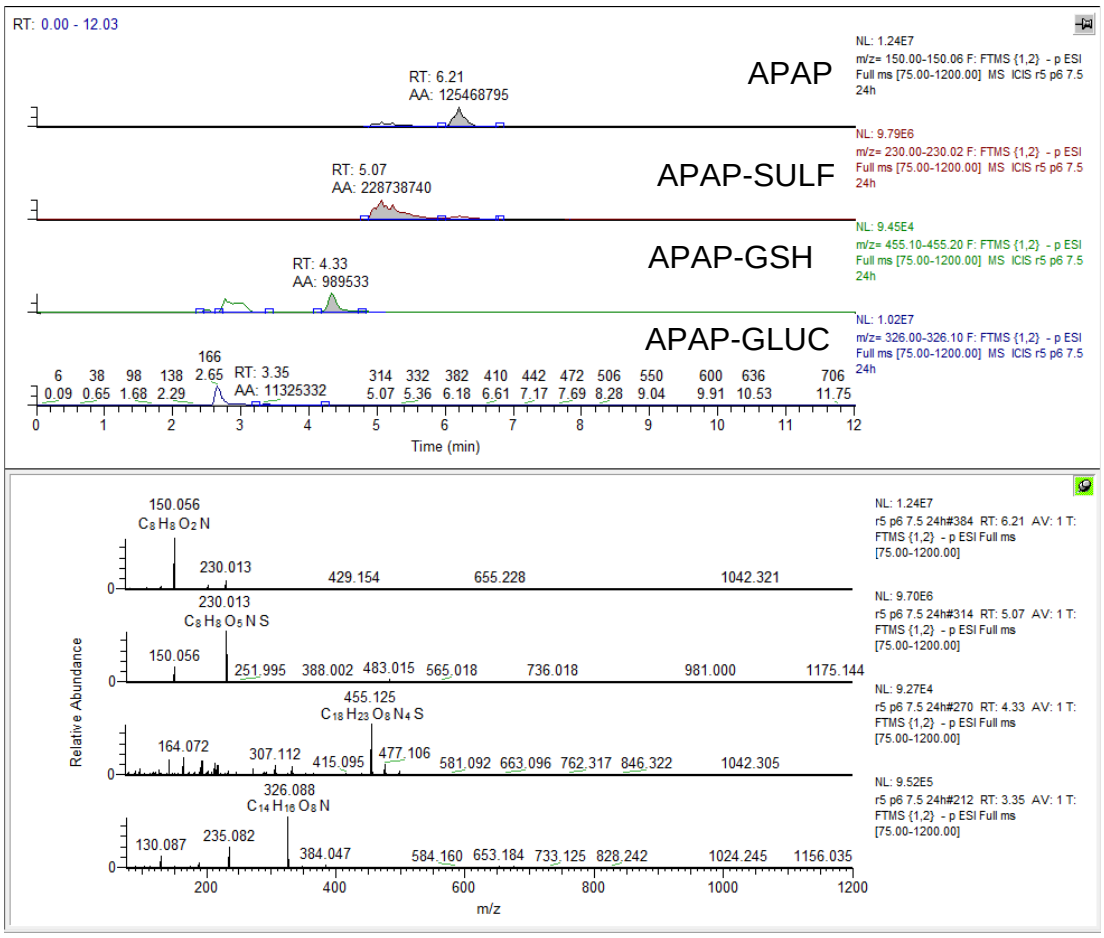


*Figure A.4 Representative LC-MS image (TIC above and mass spectra below) of APAP and all the metabolites detected using primary rat hepatocytes cultured in a collagen sandwich configuration (4 days) and exposed to 7.50 mM APAP for 24 hours.*